

UNIVERSITA' VITA-SALUTE SAN RAFFAELE

**CORSO DI DOTTORATO DI RICERCA
INTERNAZIONALE IN MEDICINA MOLECOLARE**

**Curriculum in
Basic and Applied Immunology and Oncology**

IFN-alpha by in vivo-engineered macrophages
abates liver metastases and triggers counter
regulatory responses limiting efficacy



DoS: Prof. Luigi Naldini & Dr. Mario Leonardo Squadrito

Second Supervisor: Prof. Jo Van Genderacher

Tesi di DOTTORATO di RICERCA di Thomas Kerzel

matr. 014293

Ciclo di dottorato XXXIV

SSD: MED/06; MED/46; BIO/11; BIO/13; BIO/18

Anno Accademico 2020/21

CONSULTAZIONE TESI DI DOTTORATO DI RICERCA

Il/la sottoscritto/I	Thomas Kerzel
Matricola / <i>registration number</i>	014293
nato a/ <i>born at</i>	Munich
il/on	14/05/1992

autore della tesi di Dottorato di ricerca dal titolo / *author of the PhD Thesis titled*
IFN-alpha by in vivo-engineered macrophages abates liver metastases and triggers
counter regulatory responses limiting efficacy

- AUTORIZZA la Consultazione della tesi / *AUTHORIZES the public release of the thesis*
- NON AUTORIZZA la Consultazione della tesi per 12 mesi / *DOES NOT AUTHORIZE the public release of the thesis for 12 months*

a partire dalla data di conseguimento del titolo e precisamente / *from the PhD thesis date, specifically*

Dal / *from* 04/04/2022 Al / *to* 03/04/2023

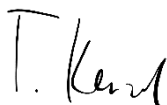
Poiché / *because*:

l'intera ricerca o parti di essa sono potenzialmente soggette a brevettabilità/ *The whole project or part of it might be subject to patentability;*

ci sono parti di tesi che sono già state sottoposte a un editore o sono in attesa di pubblicazione/ *Parts of the thesis have been or are being submitted to a publisher or are in press;*

la tesi è finanziata da enti esterni che vantano dei diritti su di esse e sulla loro pubblicazione/ *the thesis project is financed by external bodies that have rights over it and on its publication.*

E' fatto divieto di riprodurre, in tutto o in parte, quanto in essa contenuto / *Copyright the contents of the thesis in whole or in part is forbidden*



Data / *Date* 07/03/2022 Firma / *Signature*

Declaration

This thesis has been composed by myself and has not been used in any previous application for a degree. Throughout the text I use both 'I' and 'We' interchangeably.

All the results presented here were obtained by myself, except for:

- 1) The ALT and AST quantification (Results, chapter 4.2.1.2, Figure 7f) was done by Michele Raso (Ospedale San Raffaele Mouse Clinic)
- 2) The quantification of autoreactive antibodies in the serum of mice (Results, chapter 4.2.1.2, Figure 8) was performed by the UTSW Microarray Core facility (University of Texas, Southwestern Medical Center).
- 3) The histopathologic evaluation of different organs (Results, chapter 4.2.1.2, Figure 9) as well as human and murine liver metastasis (Results, chapter 4.3.1, Figure 13b) was performed at the GLP SR-TIGET Pathology department by Francesca Sanvito and Patrizia Cristofori
- 4) MRI analysis was performed at the Ospedale San Raffaele Preclinical imaging Facility by Tamara Canu
- 5) The library preparation for the scRNA-seq (Results, chapter 4.5) was performed with the help of Marco Genua (Genomics of the innate immune system Unit, San Raffaele Telethon Institute for Gene and Cell Therapy)
- 6) Bioinformatical analysis of the scRNA-seq data (Results, chapter 4.5) as well as the spatial transcriptomic data (Results, chapter 4.6) was performed with the help of Stefano Beretta (Gene transfer technology and new gene therapy strategies Unit, San Raffaele Telethon Institute for Gene and Cell Therapy)

All sources of information are acknowledged by means of reference.

Acknowledgements and dedications

This PhD-project has been a large team effort and would not have been possible without the support of many people involved. Therefore, I would like to take the opportunity to thank all my supervisors, colleagues and friends, that accompanied me along the way.

First of all, I am extremely grateful to my supervisors Prof. Naldini and Mario Squadrino for giving me the opportunity to participate in an exciting and innovative project involving a wide palette of different techniques. Especially, the trust you had in me and the room you gave me to explore let me grow as a scientist. I learned and keep learning a lot under your supervision.

I would like to extend my sincere gratitude to all the lab members that accompanied and supported me in this project. First, I would like to thank Eloise, who supported me in virtually every experiment with her experience and technical expertise. Without you, this project would not have been possible. Federica and Giovanna, two very talented master students in the lab with whom I had the chance to closely work, I like to thank you for your precious help and dedication to the project, even though it sometimes involved long nights. I thank the other members of the Squadrino team, Chiara, Marco and Gabrielle. I think we really have a great atmosphere in the lab not only scientifically speaking, but also with a lot of fun and support for each other. This does not just account for the Squadrino team, but for the entire Naldini lab. I really appreciate how you immediately included me and made me feel welcome once I arrived here.

I would like to thank Tiziana Plati, Tiziano Di Tomaso and Lucia Sergi Sergi, who keep the lab running with their organization skills and technical expertise.

I am grateful to Prof. Ginderachter for serving as my external supervisor. He was always available for interesting scientific discussions and always handy with some good advice.

Even though a PhD is full of opportunities and positive experiences, it is also a demanding time with challenges. I think good friends are one of the most important things to get through difficult times. Therefore, I would like to thank Francesco and Chiara as well as Filippo, Matteo and Federico. During this time, you have not only been dear

colleagues, but you have grown to be good friends. Hopefully, for a lifetime. Also outside the lab, I was lucky to be surrounded by good friends, Luca, Cise, Elli and Stefano, who supported me throughout the past years. Thank you for the fun memories, without you I would not have enjoyed this period as much as I did.

My parents and my siblings played a major role not only throughout this PhD but throughout my entire educational career. You always kept supporting me in every step and allowed me to follow my path, even though it sometimes led me far away. Thank you for always being there for me.

Lastly, I would like to thank Jenita. You supported me in taking this opportunity, even though it meant some challenges for us. Thank you for all the hours you spend in busses, trains and airplanes to visit me. Thank you for all the time you spend listening to my science problems, you surely deserve a PhD for this as well. But most importantly, thank you for making me happy, I am lucky to have you by my side.

Abstract

The liver hosts an immune suppressive environment, favoring metastatic seeding and proliferation of cancer cells. Pharmacological treatments, including immunotherapies, fail in the presence of liver metastases (LMS). Therefore, identifying new interventional tools and key targetable players involved in the immunosuppressive environment is of pivotal importance.

Vesicular stomatitis virus G protein-pseudotyped lentiviral vectors (LVs) delivered systemically to mice and non-human primates efficiently transduce liver cells, including resident macrophages, termed Kupffer cells (KCs). Building on these findings, we developed a novel LV-based platform, termed KC-LV, to selectively engineer KCs in vivo with the goal of delivering bio-therapeutics specifically to LMS. To this aim, the KC-LV design exploits a reconstituted mannose receptor c type 1 (MRC1) promoter, active in macrophages, including KCs. To further fine-tune KC specificity, the KC-LV also includes microRNA target (miRT) sequences that prohibit off-target transgene expression in liver sinusoidal endothelial cells (LSECs) and hepatocytes. Upon systemic delivery of the KC-LV, we observed selective transgene expression in KCs which was enhanced in areas surrounding LMS.

We then equipped the KC-LV with an IFN α -coding sequence, a cytokine with pleiotropic immune effects. Long-term analysis in mice showed LV dose-dependent, sustained and well-tolerated IFN α expression.

To investigate the therapeutic efficacy, we employed different murine models of colorectal carcinoma (CRC)-derived liver metastasis (LMS) including a CRC organoid-based syngeneic mouse model of LMS containing molecular and histopathological hallmarks of the human disease. IFN α LV treatment significantly delayed LMS growth in all tested models reaching a complete response in up to 50 % of treated animals.

Single cell omics of LMS from IFN α LV-treated mice showed upregulation of IFN α -responsive genes, macrophage skewing to an antigen presenting (M1-like) polarization state, and expansion as well as reduced exhaustion of LMS-associated antigen specific CD8 T cells. Employing spatial transcriptomics, we found that the interface between LMS and liver parenchymal tissue was the major site of IFN α action, which was associated with enhanced immune activation and antigen presentation.

When comparing LMS of treatment responsive to resistant mice, we found accumulation of activated CD8 T-cells in responsive lesions and instead a high number of immunosuppressive T regulatory type 1 (TR1)-like cells in resistant mice. Molecular analyses suggest that TR1-like cell infiltration was associated with increased IL10 signaling in resistant LMS.

In summary, we developed an innovative gene-based platform that upon a single well-tolerated intravenous LV infusion rapidly promotes a protective therapeutic response against LMS through enabling immune activation. However, we also found that TR1-like cells might promote tumor immune evasion in presence of IFN α signaling in this setting, suggesting targeting of TR1-like cells when facing resistance to cancer immunotherapies that trigger IFN α signaling.

Table of Contents

1	Introduction	15
1.1	Liver Structure and function	15
1.1.1	Kupffer cells – a population of liver resident macrophages	16
1.1.2	The immune suppressive environment in the liver.....	18
1.2	Liver metastasis in colorectal carcinoma, an unmet medical need	19
1.2.1	Frequency and characteristics of colorectal carcinoma	19
1.2.2	High frequency of liver metastasis in colorectal carcinoma.....	22
1.2.3	Formation of liver metastasis	22
1.2.4	Effective treatment options of metastatic CRC, an unmet clinical need	25
1.3	Preclinical models of CRC-LMS	26
1.4	Identification and targeting of Hallmarks of cancer biology	30
1.5	Antitumor immunity and immune evasion mechanisms	34
1.5.1	Cancer immunity cycle	35
1.5.2	Antigenic variations.....	35
1.5.3	Loss of immunogenicity	36
1.5.4	Suppression of immune response by modulation of the tumor microenvironment	37
1.6	Cancer Immunotherapy, a new promising strategy for cancer treatment	46
1.6.1	Checkpoint inhibitors	47
1.6.2	Reshaping the cytokine composition in the tumor microenvironment..	50
1.6.3	IFN α -based therapies in oncology	51
1.7	Gene therapy	55
1.7.1	Lentiviral vectors allow stable gene transfer in dividing and non-dividing cells.....	56
1.7.2	Regulatory elements in gene therapy.....	59

1.8	Gene therapy approaches in oncology.....	60
1.8.1	CAR T cell therapy	61
1.8.2	Tie2.IFN α -based gene therapy	62
1.9	Liver directed <i>in vivo</i> gene therapy	63
1.9.1	Lentiviral vector-based liver targeting	64
2	Aim of this work.....	66
3	Results.....	68
3.1	Development of a KC specific <i>in vivo</i> gene delivery platform	68
3.1.1	Engagement and characterization of the MRC1 promotor	68
3.1.2	In vivo bio distribution analysis of the MRC1 LV	70
3.1.3	Integration of miRT sites fine-tunes transgene expression to Kupffer cells	71
3.1.4	Transgene expression is enhanced in close proximity to liver metastasis	74
3.2	IFN α delivery to LMS leveraging the KC LV	77
3.2.1	Dynamics and long-term systemic effects of <i>in vivo</i> IFN α deliver.....	77
3.2.2	Therapeutic intervention leads to reduced tumor growth in an MC38 based murine tumor model.....	82
3.3	Evaluation of therapeutic effect in a more relevant tumor model	88
3.3.1	Organoid based tumor model closely resembles human disease	88
3.3.2	Enhanced tumor infiltration of transgene expressing cells in the organoid based tumor model.....	91
3.3.3	<i>Mrc1</i> .IFN α .miRT LV substantially inhibits tumor growth.....	92
3.4	Enhanced IFN α signaling in treated LMS leads to substantial reprogramming of the TME	94
3.4.1	Upregulation of IFN α responsive genes confirms activity of the treatment in LMS.....	95

3.4.2	Effective reprogramming of the TME in cellular composition and spatial distribution	96
3.5	Single cell omics gives mechanistic insight into therapeutic effect and reveals a compensatory mechanism	97
3.5.1	Strong reprogramming of the APC compartment upon IFN α treatment	99
3.5.2	Composition of T and NK cell compartment determines antitumoral immune response.....	103
3.6	Spatial transcriptomics analysis reveals importance of the tumor border ..	108
3.6.1	Unbiased determination of spatial zones with regards to the tumor....	108
3.6.2	Multiple comparison of the zones by GSEA	111
4	Discussion	115
5	Material and Methods.....	126
5.1	Molecular Biology	126
5.1.1	Plasmid design, cloning and amplification.....	126
5.2	Cell culture.....	127
5.2.1	Human embryonic kidney 293T (HEK-293T) cells.....	127
5.2.2	MC38 cells.....	128
5.2.3	AKTPF Organoids.....	128
5.2.4	Bone marrow derived macrophages	129
5.2.5	LV-Production	129
5.3	ddPCR for vector copy determination and gene expression analysis	131
5.3.1	Vector copy number determination	131
5.3.2	Gene expression.....	132
5.4	Flow cytometry analysis and fluorescence activated cell sorting	132
5.5	In-vivo methods	133
5.5.1	Mouse strains.....	133

5.5.2	LV Injection	133
5.5.3	Intrahepatic injection of MC38 cells.....	133
5.5.4	Subcutaneous injection of MC38 cells.....	133
5.5.5	Intrasplenic injection of AKTPF organoids	134
5.5.6	Blood collection and analysis.....	134
5.5.7	Magnetic resonance imaging analysis for liver metastasis volume assessment.....	136
5.5.8	Endpoint analysis	136
5.5.9	Processing of organs for flow cytometry analysis	137
5.5.10	Processing of organs for IF analysis.....	139
5.5.11	Processing of organs for VCN and gene expression analysis	142
5.6	Single-cell RNA sequencing	142
5.6.1	Sample processing and fluorescence activated cell sorting	142
5.6.2	Library preparation.....	142
5.6.3	scRNA-seq analysis	142
5.6.4	scRNA-seq analysis – data handling.....	142
5.7	Spatial transcriptomic analysis	144
5.7.1	Sample processing for spatial transcriptomics	144
5.7.2	Library preparation for Visium	145
5.7.3	Spatial transcriptomic sample analysis	145
6	References.....	147

Acronyms and Abbreviation

Table 1: Abbreviations

Abbreviation	Word/Phrase
AAV	adeno associated viral vectors
Ahr	Aryl hydrocarbon receptors
ALT	alanine aminotransferase
APC	antigen presenting cells
BMDMs	bone marrow-derived macrophages
BRAF	B-Raf proto-oncogene serine/threonine kinase
CAF	cancer associated fibroblasts
CAR	Chimeric antigen receptor
CAR T cells	Chimeric antigen receptor expressing T cells
CCL	C_C motif chemokine ligand
CRC	colorectal carcinoma
CTLA4	T lymphocyte-associated protein 4
CXCL	C-X-C motif chemokine ligand
DCPs	dendritic cell progenitors
DCs	dendritic cells
ddPCR	digital droplet PCR
dLNGFR	truncated low affinity nerve growth factor receptor
E	embryonic day
EGFR	epidermal growth factor receptor
EMT	epithelial-mesenchymal-transition
EOMES	Eomesodermin
FACS	fluorescence activated cell sorting
FasL	Fas ligand
FBS	fetal bovine serum
<i>Fbxw7</i>	f-box and wd-40 domain-containing protein 7 gene
FDA	U.S. Food and Drug Administration
FoxP3	forkhead box p3
Gag	group-specific antigen sequence
gd NKT	gamma-delta NKT cells
GFP	Green fluorescent protein
GM-CSF	granulocyte-macrophage colony stimulating factor
GSEA	gene set enrichment analysis
GZMA	granzyme K
GZMB	granzyme B
HEK-293T	Human embryonic kidney 293T
HIV	Human Immunodeficiency 1
HLA	human leukocyte antigen
HSCs	hepatic stellate cells
HSPCs	hematopoietic stem and progenitor cells

IFNα	interferon alpha
IFNαR	IFN α receptor
IFNγ	interferon gamma
IL	interleukin
ILCs	innate lymphocytic cells
IMDM	Dulbecco's Modified Eagle Medium
iNKT	invariant NKT cells
ISGs	IFN α -stimulated genes
JAK/STAT	enhanced Janus kinase and signal transduced and activator of transcription
KCs	Kupffer cells
kDa	kilo Dalton
KRAS	Kirsten rat sarcoma virus gene
LAG3	lymphocyte-activation gene 3
LB	Luria-Bertani
LMS	liver metastasis
LPS	lipopolysaccharides from Escherichia coli O55:B5
LSECs	liver sinusoidal endothelial cells
LVs	lentiviral vectors
MDSCs	myeloid-derived suppressor cells
MHC	major histocompatibility complex
miRNA	mircoRNA
miRT	miRNA target sites
Mo DCs	monocyte dendritic cells
MRC1	mannose receptor C-type 1
mRNA	messenger RNA
MRT	magnetic resonance imaging
NES	normalised enrichment score
NK	natural killer
NKT	natural killer T
OVA	antigen chicken ovalbumin
PBS	Phosphate Buffered Saline
PCs	principal components
PD1	programmed cell death protein 1
PDL1	programmed death-ligand 1
Pol	DNA polymerase sequence
rmEGF	murine epidermal growth factor
rpm	rotations per minute
scFv	specific single-chain variable fragments
scRNA-seq	single-cell RNA sequencing
SCTransform	Variance Stabilizing Transformations
TAMs	tumor associated macrophages
TAP	transported associated with antigen processing protein

TAs	Tumor antigens
TCR	T cell receptor
TEMs	Tie2-expressing monocytes
TGFb	tumor growth factor beta
<i>Tgfr2</i>	tumor growth factor receptor 2 gene
TIM3	T cell immunoglobulin and mucin protein 3
TME	tumor microenvironment
TNFa	tumor necrosis factor alpha
TR1s	type1 regulatory T cells
Tregs	FoxP3 dependent regulatory T cells
TU	transducing units
VCN	Vector copy number
VEGF	vascular endothelial growth factor
VSVG	vesicular stomatitis virus glycoprotein
WBCs	white blood cells
WPRE	woodchuck hepatitis virus posttranscriptional regulatory element

List of Figures and Tables

Figures

<i>Figure 1: Anatomical structure of the human liver at different resolution level.....</i>	<i>15</i>
<i>Figure 2: Hallmarks of cancer.</i>	<i>31</i>
<i>Figure 3: Characterization of the Mrc1 promotor.</i>	<i>69</i>
<i>Figure 4: In vivo biodistribution analysis of the MRC1 LV</i>	<i>70</i>
<i>Figure 5: Screening of miRT sites</i>	<i>73</i>
<i>Figure 6: Biodistribution analysis of the Mrc1.GFP.miRT LV in the presence of MC38-based LMS.....</i>	<i>76</i>
<i>Figure 7: Assessment of the long-term dynamics IFNα expression and adverse events in the blood parameters and liver enzymes.....</i>	<i>79</i>
<i>Figure 8: No induction of autoreactive antibodies in treated mice.....</i>	<i>80</i>
<i>Figure 9: Hostopathologic assessment of adverse events in different organs collected during endpoint analysis.....</i>	<i>81</i>
<i>Figure 10: Therapeutic efficacy of the Mrc1.IFNα.miRT LV treatment in a murine MC38 cell-based tumor model.....</i>	<i>83</i>
<i>Figure 11: Re-challenge shows partial protection of complete responding mice</i>	<i>85</i>
<i>Figure 12: Remodelling of the TME upon treatment in MC38-OVA derived LMS.....</i>	<i>87</i>
<i>Figure 13: Characterisation of the AKTPF organoid-based murin tumor model in C57Bl6 mice.....</i>	<i>90</i>
<i>Figure 14: Biodistribution of transgene expression of the Mrc1.GFP.miRT LV</i>	<i>92</i>
<i>Figure 15: Therapeutic efficacy of the Mrc1.IFNα.miRT LV in the AKTPF organoid-based tumor model.....</i>	<i>93</i>
<i>Figure 16: Remodeling of the TME in AKTPF organoid derived LMS upon Mrc1.IFNα.miRT LV treatment.....</i>	<i>95</i>
<i>Figure 17: Analysis of the reprogramming of the TME by scRNA-seq.</i>	<i>98</i>
<i>Figure 18: Detailed analysis of the scRNA-seq data for the APC compartment</i>	<i>102</i>
<i>Figure 19: Subclustering of the T and NK cell population in scRNA-seq data.....</i>	<i>104</i>
<i>Figure 20: Focused analysis of the T and NK cell compartment in the scRNA-seq data</i>	<i>107</i>
<i>Figure 21: Development of a method to determine zones based on distance to the tumor-liver interface in spatial transcriptomic analysis</i>	<i>110</i>

Figure 22: Spatial transcriptomics differential analysis of the previously defined zones
..... 114

Figure 23: Gating strategy for sorting of all viable cells processed for scRNA-seq..... 142

Tables

Table 1: Abbreviations..... 10

Table 2: Restriction enzymes..... 127

Table 3: Antibodies used for flow cytometry analysis..... 129

Table 4: TaqManTM Gene Expression Assays used in this project..... 132

Table 5: Flow cytometry antibodies used for blood analysis..... 135

Table 6: Antibodies used for flow cytometry analysis on murine organs..... 138

Table 7: Antibodies and antibody combinations used for immunofluorescence staining.
..... 141

Table 8: Parameters used for the DoubletFinder v3. 143

1 Introduction

1.1 Liver Structure and function

With an average weight of 1.5 kg, the liver is one of the biggest organs in the human body playing a central role in metabolic turnover as well as detoxification. Structurally, the liver is divided into 50.000 to 100.000 lobules. As depicted in figure 1, each lobule is composed of a central vein in the center and six portal veins which are located at the interface between different lobules giving each lobule a hexagon-like form. The connection between central vein and portal vein is composed of sinusoids, small blood vessels with an average diameter of about 10 to 15 μm . Thereby, the blood from the digestive tract enters the liver through the portal vein, drains through the sinusoids, where it mixes with arterial blood, and is collected in the central vein. Then, the blood exits the liver by the hepatic vein. With about 80 % of the total cellular population, hepatocytes are the most abundant cell types in the liver (Schulze *et al*, 2019). With high secretory and internalizing activity, hepatocytes are addressed to as the workhorses of the liver and play a central role in several biological processes as metabolism, detoxification and protein synthesis (Zhou *et al*, 2016; Friedman, 1997; Schulze *et al*, 2019).

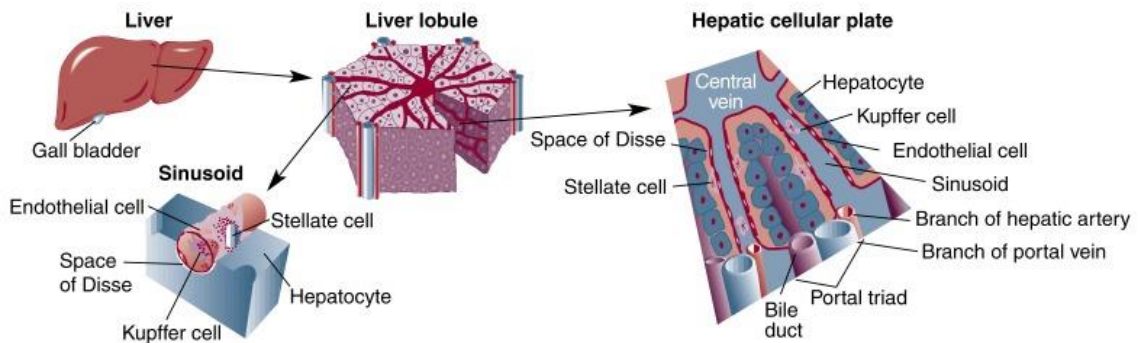


Figure 1: Anatomical structure of the human liver at different resolution level. Upper left: overall structure of the liver and the gall bladder. Center: Structure of a liver lobule. Right: anatomical arrangement of a portal vein and a central vein connected by liver sinusoids. Lower left: cellular composition of a liver sinusoid (Friedman, 1997).

In order to exert their function in detoxification and protein secretion, hepatocytes require a close connection to the bloodstream. This is provided by the particular structure of the sinusoidal wall, composed of LSECs. This wall contains a high density of open pores and fenestrae, which do not contain any physical barrier, hence allow a direct access from the bloodstream to hepatocytes. Nutrients as well as potentially toxic material, which enter the blood stream in the digestive tract and drain into the liver by the portal

vein, can be internalized and metabolized by hepatocytes. Metabolites can then be stored or released into the bloodstream, upon requirement (Zhou *et al*, 2016; Friedman, 1997). Furthermore, hepatocytes produce bile, a cocktail in which the main components are cholesterol, bilirubin and bile salts and plays a crucial role in digestion of fats in the small intestine (Ticho *et al*, 2019). Thereby, bile is collected in the bile ducts, which are located in close proximity to the portal vein, and drained into the gall bladder.

This liver has an astonishingly high potential for self-renewal. Studies in mice have shown that after removal of two thirds of the liver complete regeneration is observed with the liver reaching its original weight after 10 days (Gilgenkrantz & Collin de l'Hortet, 2018). Accordingly, in human patients undergoing partial hepatectomy a remaining volume of disease-free liver tissue of 25 % has been described as sufficient for full recovery of the patient (Vauthey *et al*, 2000). The high regenerative potential of the liver may be required to compensate eventual hepatic injury caused by exposure to toxic material.

1.1.1 Kupffer cells – a population of liver resident macrophages

Kupffer cells are an abundant population of liver-resident macrophages. With about 80 % they compose the biggest fraction of tissue resident macrophages in the whole human body (Kakinuma *et al*, 2017). As shown in Figure 1, they are located in the space of Disse, which describes the area between the epithelium of sinusoids and hepatocytes, and therefore are closely associated to LSECs. KCs were discovered in 1876 by Karl Wilhelm von Kupffer who addressed to them as stellate cells due to their morphology (Kupffer, 1876). Together with LSECs and liver-resident dendritic cells (DCs), KCs constitute the reticulo-endothelial system. Based on the expression of pattern recognition receptors and other scavenger receptors, these cells recognize pathogen-associated molecular patterns leading to phagocytosis of viral and bacterial moieties, antigens and other toxins derived from the sinusoidal blood (Nguyen-Lefebvre & Horuzsko, 2015).

KCs are established during embryogenesis. They develop after embryonic day (E) 12.5 originating from late yolk sac-derived erythro-myeloid progenitors (van de Laar *et al*, 2016). Their life span and potential to self-renew however is controversially debated. Some studies predicted an estimated life span of 3.8 days while donor derived KCs in liver transplanted patients can be detected for up to one year after transplantation (Naito

et al, 2004). There are two models proposed for KC homeostasis in healthy conditions. In one, the KC compartment is renewed from bone marrow-derived monocytes, whereas in the other KCs are capable of self-renewal independently from bone-marrow derived cells (van Furth, 1980; Zigmond *et al*, 2014). However, independently of the origin and self-renewal capacity of KCs under homeostatic conditions, it is clear, that bone marrow-derived monocytes can repopulate the liver displaying a KC phenotype in case of KC depletion. Mouse studies have shown that the liver is repopulated within 14 days (Yamamoto *et al*, 1996; Diesselhoff-den Dulk *et al*, 1979).

1.1.1.1 Mannose receptor C-type 1, a marker of M2-like macrophages

One of the scavenger receptors highly expressed by KCs is the mannose receptor C-type 1 (MRC1). MRC1 is a 166 kilo Dalton (kDa) type 1 transmembrane protein. It is expressed by a variety of myeloid cells, including monocytes, some dendritic cells and tissue resident macrophages as KCs, as well as LSECs. Upon binding of mannose- and fucose-based glycol structures, MRC1 mediates endocytosis and cellular trafficking of glycoproteins present on the surface of viral and bacterial pathogens (Feinberg *et al*, 2021). Interestingly, MRC1 is highly upregulated on alternatively activated (M2-like) macrophages (Orecchioni *et al*, 2019a). This phenotype is predominantly present in tumor associated macrophages (TAMs) (Scodeller *et al*, 2017; Squadrito *et al*, 2012). Indeed, studies have shown that the expression of MRC1 is regulated by the presence of inflammatory signals in the circulation. Inflammation enhancing molecules such as interferon gamma (IFN γ) and lipopolysaccharide (LPS) led to a downregulation of MRC1 expression, while dexamethasone, a molecule with immunosuppressive effect, induced upregulation of MRC1 expression (Shepherd *et al*, 1990; Alan *et al*, 1986; Shepherd *et al*, 1985). Therefore, MRC1 is downregulated in the initial phase of inflammatory reaction allowing robust immune reactions to be established. At later stages, MRC1 is upregulated and involved in the removal of inflammatory signaling molecules. This finding in combination with the results of studies on MRC1 deficient mice by Nussenzweig and collaborators suggests a general involvement of MRC1 in the homeostasis and remodeling of the landscape of endogenous glycosylated proteins (Lee *et al*, 2002).

1.1.2 The immune suppressive environment in the liver

The liver is characterized by an immunosuppressive and tolerogenic environment. This is required since the healthy liver is continuously exposed to endotoxins and bacterial products originating from the digestive tract, which can induce inflammatory responses. In order to prevent a chronic hepatic inflammation, a tolerogenic behavior towards these potentially immune stimulatory signals is required (Robinson *et al*, 2016). The tolerogenic potential of the liver is strikingly evident in the field of solid-organ transplantation. For example, the occurrence of cardiac rejection events in patients following heart transplantation is increased compared to patients undergoing a combination of heart and liver transplantation (Raichlin *et al*, 2009). Furthermore, while most of patients undergoing any type of solid organ transplantation require life-long immune-suppressive regimens and experience a high number of acute rejection events, immunosuppressive regimen can be completely abrogated in about 20 % of patients with liver transplantation (Londoño *et al*, 2013).

KCs play a fundamental role in the maintenance of the tolerogenic microenvironment and suppression of inflammations in the liver. Equally to other macrophage populations, KCs are considered antigen presenting cells (APCs) hence are capable of cross presenting antigens in a MHCII dependent manner in order to induce antigen specific immune reactions. Interestingly, also LSECs and hepatocytes have been described to contain antigen presenting functions (Bénéchet *et al*, 2019; Knolle & Wohlleber, 2016). The expression level of MHCII on KCs and other liver resident APCs as DCs are decreased compared to APC-populations outside the liver, which reduces the potential to effectively induce immune reactions (AYALA, 1992; Nguyen-Lefebvre & Horuzsko, 2015). As discussed above, KCs are the cells that encounter the most with antigens arriving in the liver due to their positioning in the sinusoids and their potential to actively recognize and phagocyte pathogen by pattern recognition receptors (Kakinuma *et al*, 2017). In most myeloid cells, engagement of pattern recognition receptors activates a number of intracellular signaling cascades such as NF- κ B signaling, JAK/STAT signaling and MyD88 dependent pathways leading to expression and secretion of a variety of pro-inflammatory molecules. This includes Type-1 Interferons, Tumor necrosis factor alpha (TNF α) and others which are crucial to mount an effective inflammatory response (Lee & Kim, 2007). In contrast to that, KCs respond to sensing of bacterial endotoxins with

secretion of anti-inflammatory cytokines such as interleukin (IL)-10, tumor growth factor beta (TGF β) and prostaglandins (Knoll *et al*, 1995; Callery *et al*, 1991; Roth *et al*, 1998). This leads to a reduced expression of costimulatory molecules in other APCs such as DCs hence preventing the engagement of the adoptive immune system (Cilenti *et al*, 2021). Furthermore, increased levels of IL-10 lead to a recruitment of different regulatory T cell populations as FoxP3 dependent regulatory T cells (Tregs) and type1 regulatory T cells (TR1s) (Knolle *et al*, 1998; Roncarolo *et al*, 2018a). Furthermore, the hepatic environment is also characterized by the presence of large numbers of myeloid derived suppressor cells (MDSCs). MDSCs describe a population of bone marrow-derived myeloid progenitor cells with a substantial immunosuppressive potential which will be addressed in section 1.5.4.2 (Weston *et al*, 2019).

Due to the tolerogenic capacity of the liver, several studies attempt to take advantage of this environment in order to generate antigen-specific tolerance. However, limited success has been achieved so far (Doherty, 2019; Richardson *et al*, 2020).

Despite the immunosuppressive hepatic environment in homeostatic conditions, the liver is nevertheless capable of mounting effective immune reactions under certain circumstances. Iannacone and coworkers have shown that hepatic priming under normal conditions leads to generation of dysfunctional antigen-specific CD8 T cells. Upon additional treatment with IL-2 that T cell phenotype was at least partially rescued. This confirms that the hepatic environment could be a promising target for vaccination approaches due to the high number of APCs present (Bénéchet *et al*, 2019).

1.2 Liver metastasis in colorectal carcinoma, an unmet medical need

1.2.1 Frequency and characteristics of colorectal carcinoma

With an incidence of more than 1.9 million newly diagnosed cases and 935.000 fatal cases in 2020 worldwide, colorectal carcinoma is ranked as the third most common type of malignancy but second in terms of mortality (Sung *et al*, 2021). Hereby, the age-standardized incidence rate is substantially increased in man compared to woman with incidence between 23.6 and 16.3 cases per 100.000 individuals per year, respectively (Abancens *et al*, 2020). A similar pattern for the mortality has been observed confirming the higher risk of CRC for male individuals. Furthermore, incidence rates increase rapidly with age. Accordingly, in the United States from 2012 until 2016 the incidents rates of

CRC per 100.000 individuals in age groups below 44 years of age remained below 20 cases but increased up to 198 cases in the group of age 75 -79 years (Siegel *et al*, 2020). Next to gender and age dependent differences, an unequal global distribution of CRC incidences has been detected. Interestingly, there is a positive correlation between the human development index, a measure for gross national income, life expectants and educational attainment, and the incidence rate of CRC (Fidler *et al*, 2016). This supports the hypothesis of the risk for developing CRC to be highly dependent on the lifestyle (Sung *et al*, 2021). In accordance, major risk factors associated with an increased CRC incidence are low physical activity, obesity, a diet based on animal-sourced food, heavy alcohol consumption and smoking (Siegel *et al*, 2020; Abar *et al*, 2018; Vieira *et al*, 2017).

CRC arises through neoplastic transformations of epithelial cells in the mucosa of the colorectal compartment. The colon epithelium is formed by terminally differentiated cells originating from a population of multipotent stem cells. Due to the short life span of colon epithelial cells, these stem cells, resident at the basis of crypts, undergo a large number of cell cycles (Barker *et al*, 2008). This allows an increasing accumulation of somatic mutations in individual crypts ultimately leading to a malignant transformation (Siudeja *et al*, 2015). The development of colorectal adenocarcinoma is commonly divided in several stages. In 1990, Fearon and Vogelstein proposed a model, which describes the acquisition of more mutations in each developmental stage of CRC (Fearon & Vogelstein, 1990). The first step, regarded to as tumor initiation, leads to formation of desmoplastic crypts and is defined by a loss-of function mutation of the tumor suppressor gene *APC*, coding for the adenomatous polyposis coli protein. This common CRC mutation leads to an activation of Wnt/ β -catenin signaling, hence, allowing maintenance of stem cell properties and giving the transformed epithelial cell a selective growth advantage (Fodde, 2002; Testa *et al*, 2018). Indeed, patients with familial adenomatous, a rare genetic disorder in which patients harbor a heterozygous loss of function mutation in the *APC* gene, develop thousands of colorectal adenomas, a phenomenon called lynch syndrome (Half *et al*, 2009). However, only 5 % of diagnosed cases of CRC are related to lynch syndrome. Further development of desmoplastic crypts towards adenoma promotion and tumor progression is characterized by the acquisition of mutations favoring cell proliferation. Common mutations in this context are, among others, a gain-of-function

mutations of the Kirsten rat sarcoma virus gene (*KRAS*) and a gain of function mutation of *BRAF* at early stages as well as a loss of function or dysregulating mutations of the tumor suppressor gene *TP53* and loss of function mutation of *SMAD4* at later stages (Hussain *et al*, 2015; Huang *et al*, 2018). In general, about 65 % of CRC cases are the result of sporadic somatic mutations and only a minor fraction can be associated to genetically inherited genetic dispositions (Keum & Giovannucci, 2019).

According to the American Cancer Society, progression of CRC development is divided into five mayor stages. Stage 0: describes the earliest stage of cancer, in which the carcinoma has not grown beyond the mucosa layer of the colorectal area; stage I: is characterized by an invasion of the submucosa and muscularis propria; stage II: describes a CRC which has grown through all layers colon or rectum; stage III: CRC, which has spread into proximal lymph nodes and/or is attached to nearby organs; stage IV: This last stage is characterized by the presence of metastasis in distal organs (American Joint Committee on Cancer, 2017).

CRC is commonly divided into left-sided and right-sided CRC. This classification is dependent on the tumor site with right-sided CRC arising in the cecum, ascending colon, hepatic flexure or transverse colon and left-sided CRC occurring in the splenic flexure, descending colon, sigmoid colon or rectum (Mukund *et al*, 2020; Baran *et al*, 2018). The basis for this distinction can be found in their embryological origin. While the right-sided part of the colon is originated from the midgut, the left-sided colon and rectum are of hindgut origin (Iacopetta, 2002). Thereby, the 5-year survival rate for right-sided CRC is significantly lower compared left sided CRC with 74.0 % and 70.4 %, respectively (Nakagawa-Senda *et al*, 2019). Molecular analysis revealed a higher incidence of mismatch repair impaired CRC for right-sided CRC (about 20 % of cases) compared to left-sided CRC (5 % of cases) leading to a microsatellite instable phenotype (Iacopetta *et al*, 2010; Baran *et al*, 2018). Mismatch repair impaired CRC is characterized by a rapid accumulation of mutations leading to a poor differentiation status but also accumulation of neoantigens. In line with this, higher infiltration of lymphocytes has been observed in microsatellite instable CRC (Saeterdal *et al*; Iacopetta *et al*, 2010). However, as mentioned before, the majority of CRC cases (about 80 %) are characterized as microsatellite stable, hence, having no dysfunction in the mismatch repair machinery (Nojadeh *et al*, 2018).

1.2.2 High frequency of liver metastasis in colorectal carcinoma

While primary CRC can be surgically removed in most of the cases and has a 5-year survival rate of 64 %, the appearance of distant metastasis dramatically changes the predicted outcome with a 5-year survival rate of only 12 % (Siegel *et al*, 2019; Tomlinson *et al*, 2007). CRC is considered a highly metastatic carcinoma. Thereby, the liver is considered the most frequent site of CRC metastasis. The occurrence rate of hepatic metastasis in the life span of a patient diagnosed with CRC is about 50 % (Tomlinson *et al*, 2007). Other prominent metastatic sites for CRC are the lung with an incidence rate of 10-15 % (Pihl *et al*, 1987; Manfredi *et al*, 2006) and peritoneum in about 5 % of the patients (Lemmens *et al*, 2011; Vatandoust *et al*, 2015). In general, about 95 % of metastatic CRC cases display a microsatellite stable and therefore not immunogenic phenotype (Gholami *et al*, 2021).

1.2.3 Formation of liver metastasis

Formation of metastasis can be in general divided into five key steps, namely invasion, intravasation, circulation, extravasation and colonization (Fares *et al*, 2020). Invasion describes the process of a cancer cell to detach from the primary tumor and invade the healthy surrounding tissue. Epithelial cells are conventionally immobile and highly dependent on survival signals from neighboring cells (Fouad & Aanei, 2017). Therefore, acquisition of capabilities like mobility, resistance to stress and independent survival is crucial. This process of trans-differentiation is called epithelial-mesenchymal-transition (EMT) (Ye & Weinberg, 2015). The mesenchymal phenotype is achieved by activation of several signaling pathways as tumor growth factor beta (TGF β)-signaling and Wnt-signaling as well as epigenetic changes triggered by external influences as hypoxia (Craene & Berx, 2013; Nieto & Cano, 2012; Fares *et al*, 2020). The second step, invasion and intravasation, is the process of cancer cells entering the vasculature structure. Wong *et al*. has described a process in which cancer cells partially disrupt the endothelium surrounding the blood vessel and detach into the blood stream, a process mainly driven by the expression of several integrins as E-cadherin (Wong & Searson, 2017; Padmanaban *et al*, 2019). Circulation describes the travelling of cancer cells through the blood stream, in which cancer cells are subject to high mechanic stress. Most cancer cells circulate as single cells, but also clusters of circulating cancer cells have been observed in the blood stream. In general, engraftment of a single circulating cancer cell can lead to

successful formation of metastasis. However, a recent study by Taftaf et al has shown, that the efficiency metastasis formation is increased for circulating clusters of cancer cells (Taftaf *et al*, 2021). Extravasation is based on trapping of circulating cancer cells in the microvascular structure. Extravasation is based on trapping of circulating cancer cells in the microvascular structure. Also, for the process of trespassing through the blood vessel endothelium into the metastatic organ integrins play a crucial role (Massagué & Obenauf, 2016). Efficiency of extravasation is highly dependent on the structure of vessels in different organs. Blood vessels in the liver are characterized by a high level of permissiveness, hence, facilitating the process of extravasation (Fouad & Aanei, 2017). A recent study showed that trapping of metastatic CRC clones leads to the formation of a fibrotic niche in sinusoids, which increases extravasation efficiency and allows engraftment even of less metastatic clones (Kok *et al*, 2021). The last step in the process of metastasis formation, colonization, describes the process homing of cancer cells into the site of metastasis. Normally, the environment in the target organ is suboptimal and does not allow survival of cancer cells, as they are poorly adapted to this particular environment (Valastyan & Weinberg, 2011). Therefore, formation of a premetastatic niche is of importance. Formation of a premetastatic niche describes the remodeling of the microenvironment in the metastatic target organ to be more submissive to the engraftment of circulating cancer cells. Premetastatic niche formation is based on the release of systemic signals from the primary tumor, such as vesicles carrying tumor derived mRNA and other signaling molecules. These are taken up by different cells at the target site such as fibroblasts ultimately triggering a remodeling of extracellular matrix towards a more cancer cell submissive state (Zomer *et al*, 2015). Myeloid-derived suppressor cells (MDSCs) are discussed to play a role in the formation of a premetastatic niche as they have been shown to be accumulated in the premetastatic liver in a murine model of CRC as well as in the circulation of stage I to III diagnosed CRC patients (Zeng *et al*, 2021).

1.2.3.1 The liver favors metastasis formation

The high incidence of liver metastasis in the context of CRC is related to several reasons. One is the direct blood flow pattern from the colon towards the liver. In human, blood from the right sided colon flows through the superior mesenteric vein while blood from the left sided colon is collected in the inferior mesenteric vein. Merging of both

veins gives rise to the portal vein, which directly flows towards the liver (Rhu *et al*, 2017). Hence, cancer cells which underwent successful intravasation arrive directly to the liver as first potential metastatic organ. Another reason is the previously described permissiveness of the sinusoids in the liver, which is characterized by the presence of open pores and fenestrae in the wall. These openings in the sinusoidal wall, lack a physical barrier underneath the epithelium as a basal lamina, hence, providing a direct path for extravasation of cancer cells into the parenchymal hepatic tissue (Braet & Wisse, 2002). A third reason is the immunosuppressive microenvironment in the liver which has been described before. This hepatic environment favors metastatic colonialization by inhibiting potential immune reaction. Taken together, the liver milieu possesses characteristics supporting metastasis formation in the steps of extravasation as well as cancer cell seeding.

1.2.3.2 Liver metastasis formation is supported by acquisition of driver mutations

The potential of cancer cells to successfully perform the previously described steps for metastasis formation is supported by acquisition of different mutations. To identify driver mutations involved in metastasis formation, Oga *et al* compared by RNA- and whole exome sequencing a CRC cohort of 16 patients with a high primary tumor burden without distant metastasis to a cohort of 12 patients with small primary tumor that developed liver metastasis. While common CRC driver mutations as *KRAS* and *APC* were present in both cohorts, 987 mutated genes were identified exclusively in the metastatic cohort, suggesting their involvement in liver metastasis formation. Strikingly, these genes were enriched in pathways for extracellular matrix receptor interaction and focal adhesion (Oga *et al*, 2019). A more focused study by Sakai *et al* analyzed the role of five common CRC driver mutations in metastasizing towards the liver, namely *Apc*, *Kras*, tumor growth factor receptor 2 gene (*Tgfbr2*), *p53* and f-box and wd-40 domain-containing protein 7 gene (*Fbxw7*). In mouse models, they confirmed that presence of mutations in *Apc*, *Kras* and *Tgfbr2* is of main importance for development of liver metastasis confirming the requirement of efficient EMT (Sakai *et al*, 2018). Next to cell survival, deregulation of the cell cycle leading to enhanced cell proliferation is key in metastasis formation as well. While mutation of one allele of the cell cycle regulatory tumor suppressor gene *p53* is sufficient for enhanced primary CRC formation, Nakayama *et al* describes that the metastatic potential of CRC clones is strongly increased when the *p53* gene is mutated in

both alleles, as can result from loss of heterozygosity (Kok *et al*, 2021). Especially, the loss of function mutation commonly observed in *Tgfbr2* is of interest. Studies by Eduard Batlle and collaborators have highlighted the importance of TGF β signaling in the tumor microenvironment (TME) of primary and metastatic CRC as driving force for immune evasion by the promotion of T cell exhaustion (Tauriello *et al*, 2018). However, TGF β signaling in epithelial cell of the skin and colon has an antitumoral effect. Indeed, TGF β regulates growth of epithelial cell structures in homeostatic conditions prevents transformation and proliferation (Tauriello *et al*, 2022). Therefore, loss of TGF β signaling of epithelial cells is a crucial step in tumor formation of metastatic CRC.

1.2.3.3 The ambiguous role of Kupffer cells in metastasis formation

KCs are believed to play an ambivalent role in the process of LMS formation. In the initial phase of metastatic seeding, KCs have the ability to clear circulating cancer cells by phagocytosis (Gül *et al*, 2014). During growth of LMS the effect of KCs is dependent on the stage of growth progression. In a mouse model of CRC-derived LMS, Wen *et al* show that depletion of KCs at an early phase leads to an increased tumor growth whereas depletion of KCs at a late stage had a tumor inhibitory effect, therefore revealing an early inhibitory and a late tumor promoting effect of KCs (Wen *et al*, 2013).

1.2.4 Effective treatment options of metastatic CRC, an unmet clinical need

Treatment options are highly dependent on tumor progression at time of diagnosis. For CRC diagnosed at stages I-III treatment for the vast majority of patients (about 98 %) is based on resection of the primary tumor. For stage II and especially stage III CRC, this is surgery is supported by pre and/or postoperative chemotherapeutic or radio therapeutic treatment. With a 5-year survival rate of about 95 %, 90 % and 65 % in stage I, II and III CRC, respectively, this strategy has proven to be quite successful (Brouwer *et al*, 2018). For CRC diagnosed at stage IV, hence in the presence of distant metastasis, treatment options are more limited. The only potentially curative treatment option for stage IV CRC patients with liver metastasis is a surgical resection of the metastasis. This results in an increased 5-year overall survival to a comparable level of stage III diagnosed CRC patients (Morris *et al*, 2010). Despite a tremendous investigation of new treatment options as immunotherapeutic and targeted approaches only limited success has been observed. In fact, Brouwer *et al* observed only a mild improvement of the 5-year survival rate

between the patient cohorts diagnosed with stage IV CRC in the Netherlands between 1989 and 1994 (5 year survival rate of about 5 %) and between 2010 and 2014 (5 year survival rate of about 15 %)(Brouwer *et al*, 2018).

Therefore, up to now CRC prevention and early detection is believed to be one of the most effective strategies against CRC (Marcuello *et al*, 2019). However, despite improved screening methods and more close CRC detection programs, still about 25 % of CRC are diagnosed at an advanced metastatic stage (Xie *et al*, 2020b; Brouwer *et al*, 2018).

1.3 Preclinical models of CRC-LMS

As previously discussed, metastasis formation is a complex multistep process during which cancer cells are shaped and selected upon their potential to survive throughout these steps and their efficiency to give rise to metastasis. Furthermore, there is a distinct interplay between cancer cells, parenchymal cells and cells of the immune system giving rise to the tumor microenvironment which will be further discussed. Animal models can provide mechanistic insights into tumor development and provide a platform for development of new treatment options. In this context, however, it is an enormous challenge to provide animal models that proficiently and accurately recapitulate the human disease (Oh *et al*, 2017; Heijstek *et al*, 2005). Animal models of liver metastasis turn out to be particularly challenging due to their multifocal characteristics and the fact that the hepatic environment is a crucial factor.

Rodents, especially mice, are preferably used in preclinical studies due to their biological, anatomical and immunological similarities to human as well as the comparably simple handling requirements, fast and high breeding capacity and the possibility for genetic engineering (Vandamme, 2014). Early models of CRC were based on spontaneous tumor development in tumor prone mice and rats reaching a CRC incidence of about 40 %. (Miyamoto & Takizawa, 1975; Kobaek-Larsen *et al*, 2000). To increase the probability of tumor development, these models have been further developed by exposure of the mice to cancerogenic agents such as dimethylhydrazine leading to a tumor incidence of up to 100 % (Heijstek *et al*, 2005). Spontaneous models have the advantage that tumor development and establishment of metastasis is subject to the same process as in naturally occurring diseases. Therefore, these models are believed to harbor

the most accurate reconstitution of naturally occurring TME (Saito *et al*, 2020). On the other hand, these models lead to a broad variation of tumor size and especially incidence of metastasis in the liver. Reason for that is the fast uncontrolled acquisition of tumor driver mutations in these models leading to a high mutational burden compared to human disease and a low reproducibility between different animals. Recent advances in genome editing technologies and the development of inducible systems have simplified the generation of transgenic mice with a defined and tissue specific set of mutations. This has increased the reproducibility in terms of tumorigenic mutations. Control of tumor growth as well as level and organ-specificity of metastasis formation, however, remains a major challenge for accurate CRC-LMS modelling. Hence, while these models are of high interest for the investigation of tumor development, they are rather less suitable for translational research aiming at drug development (Saito *et al*, 2020; Bürtin *et al*, 2020).

In order to overcome this issue, new models have been developed which are based on the implantation of CRC-derived cell lines. These cell lines can be implanted orthotopically into the liver of mice and, due to the controlled genetic background, lead to a reproducible formation of CRC derived tumors in the hepatic environment. Heterotopic implantation, for example subcutaneous injection, of CRC-LMS cells is possible as well. Due to the critical influence of the hepatic environment onto the development of liver metastasis, heterotopic models are considered less valuable for the investigation of CRC-LMS (Bürtin *et al*, 2020; Saito *et al*, 2020). Implantation-based tumor models are commonly divided into different categories: xenograft models and syngeneic models. This division is based on the genetic background of the implanted tumor cells and the recipient mice.

Xenograft models describes a set up in which the genetic background of the implanted tumor cells and the recipient mouse strain are different. The most valuable advantage of xenograft models is the possibility to use patient-derived material, which can be transplanted into mice. Therefore, a precise recapitulation of the genetic alterations of specific patients as well as the presence of heterogeneity of tumor cells is given (Inoue *et al*, 2017). This allows drug screening even in a patient specific manner (Bertotti *et al*, 2011). The disadvantage, however, is the restriction to the usage of immunosuppressed mouse strains as transplantation of human material into immunocompetent mice would lead to an immediate rejection. Due to the absence of a functional immune system,

accurate recapitulation of the TME is not possible and neither antitumor nor protumor immune reactions can be established to full extent. This, in turn, excludes these models as tool for investigation of immunotherapies which are based on the activation of the host immune system (Bürtin *et al*, 2020). Development of humanized mouse models, in which the hematopoiesis is of human origin, can overcome the hurdle only partially.

Syngeneic mouse models are based on the transplantation of mouse CRC-LMS cells into mice of the same genetic background. The match of the major histocompatibility complex (MHC) on graft and recipient prevents tumor rejection and allows usage of immunocompetent mice. Hence, development of a TME with its immunosuppressive characteristics as well as antitumor immune reactions are enabled. Therefore, syngeneic mouse models are the most commonly used strategy in translational research for the development of immunotherapies (Bürtin *et al*, 2020).

One of the most commonly used murine CRC cell lines in this context are MC38 cells. They were isolated from primary stage III CRC of C57Bl6 mice that were exposed over a period of seven month to the carcinogen 1,2-dimethylhydrazine dihydrochloride (Corbett *et al*, 1975). Due to their strong cancerogenic potential, MC38 are capable of growing in the vast majority of organs and sites in the mice. This includes the liver, hence, giving rise to liver metastasis with origin of colorectal carcinoma. In this context, MC38 cells can be seeded to the liver in different ways. Orthotopic transplantation of MC38 cells into the colon leads to formation of a primary tumor but only with a low level of metastasis formation in the liver (Zigmond *et al*, 2011). For generation of liver metastasis, MC38 cells are most commonly injected intrasplenic. MC38 cell are disseminated from the spleen, travel through the bloodstream and enter the liver through the portal vein, hence mimicking the natural process of metastasizing. Accordingly, this model leads to the formation of multifocal metastasis in the liver. The major limitation of this model is the requirement of a splenectomy after tumor cell injection as otherwise a tumor would grow in the spleen as well (Dupaul-Chicoine *et al*, 2015; Catarinella *et al*, 2016). This is especially problematic for the investigation of treatment options involving the host immune system as the spleen is a central organ of the adaptive immune system. To overcome this, MC38 cells can be alternatively transplanted by direct intrahepatic injection. This leads to formation of a single experimental CRC-derived metastasis in the liver (Bustos *et al*, 2012). Intrahepatic injection, however, is a surgically challenging

method often leading to tumor development in the peritoneum (Sugase *et al*, 2020). Furthermore, the absence of crucial steps of the natural metastasis formation is considered a major disadvantage as natural selection of metastatic clones and the formation of a premetastatic niche influence the characteristics of LMS such as angiogenesis and tumor related immunosuppression (Liu & Cao, 2016). In general, MC38 cells provide a good tool for preliminary experimental murine models of CRC-LMS. However, there are certain limitations. MC38 cells are considered microsatellite instable hence are characterized by a rapid acquisition of mutations (Efremova *et al*, 2018). This results in a rapid and aggressive tumor growth pattern. As previously mentioned, this is the case only for a small fraction of human disease. Furthermore, cell line-based tumor models, including MC38-based liver metastasis, can in many cases only partially recapitulate the natural structure and complexity of the TME (Saito *et al*, 2020).

In recent years many studies have described intratumor heterogeneity and the presence of cancer stem cells which are crucial for tumor evasion mechanisms and drug resistance (Prasetyanti & Medema, 2017; Fan *et al*, 2019). Intratumor heterogeneity enables immune evasion through mechanisms as antigenic variations and loss of antigenicity (Vinay *et al*, 2015; Beatty & Gladney, 2015). The concept of cancer stem cells describes the presence of a small number of cells within the cancer cell population, which contains a high proliferative potential and ultimately fuel the tumor growth, much alike the homeostasis and self-renewal of many healthy tissues (Clevers, 2013; Batlle & Clevers, 2017). This concept appears to be especially relevant for epithelial cell-derived tumors such as primary and metastatic colorectal carcinoma (Ricci-Vitiani *et al*, 2007). Indeed, presence and persistence of cancer stem cells in a quiescent state are proposed to play a major role in the development of treatment resistance and the occurrence of relapse after successful chemotherapy and radiotherapy. In this context, cancer stem cells have been found to be enriched in the fraction of chemotherapy and radiotherapy resistant cells (Batlle & Clevers, 2017). To recapitulate these features in preclinical models, the presence of cancer stem cells is an important feature to increase the quality and potential to recapitulate the human disease. Both characteristics, the intratumor heterogeneity and presence of cancer stem cells, are only poorly represented in cell line-derived tumor models due to converging genetic and epigenetic drifts in long-term culture of cell lines (Torsvik *et al*, 2014). Cultivation of cancer organoids has raised a lot of attention in recent

years to overcome this issue. Indeed, organoid cultivation has been awarded as “Method of the year” in 2017 by the journal Nature Methods. This culture form allows formation of matrix embedded 3D-structures, hence permitting intrinsic self-organization, which, in turn, allows increased levels of heterogeneity and the presence of tumor stem cells (Fan *et al*, 2019). Among others, the team of Oshima established CRC organoids from C57BL6 mice harboring five defined mutations: (i) loss of function mutation in *Apc* (*APC^{Δ716}*); (ii) gain of function on *Kras* (*Kras^{G12D}*); (iii) gain of function in the p53 gene (*Trp53^{R270H}*); (iv) *Tgfbr2* knock out (*Tgfbr2^{-/-}*); (v) *Fbxw7* knock out (*Fbxw7^{-/-}*). These organoids, termed AKTPF organoids, contain a strong potential to form multifocal liver metastasis upon intrasplenic injection in C57Bl6 mice. These organoids overcome several of the previously mentioned obstacles. They are characterized as microsatellite stable and there is no requirement for splenectomy as these organoids do not form tumors in the spleen (Sakai *et al*, 2018). Therefore, the AKTP-organoid based syngeneic mouse model of CRC-LMS show promising characteristics. However, further investigation of tumor model must be performed for example with regards to its histopathologic features.

1.4 Identification and targeting of Hallmarks of cancer biology

Cancer development is subject to a highly complex multistep process during which many hurdles have to be overcome, such as space restraints, apoptotic signals and antitumoral immune reactions. Countless different genetic alterations and pathways have been described in this context. Variability in the mutational burden between different types of tumors as well as interpatient diversity suffering from the same type of cancer is enormous. Therefore, identifying a “fit-for-all” concept of tumor development and cancer biology is challenging. The most famous attempt to categorize the complexity of cancer biology into major underlying principals was done by Hanahan and Weinberg. They developed the concept of 14 hallmarks, describing characteristics, which are crucial for survival and proliferation of cancer cells (Hanahan & Weinberg, 2000, 2011; Hanahan, 2022). This concept is now considered the basis for tumor biology. Namely, these hallmarks which are demonstrated in figure 2 are: (i) enabling replicative immortality; (ii) tumor promoting inflammation; (iii) polymorphic microbiomes; (iv) activating invasion & metastasis; (v) inducing or accessing vasculature (angiogenesis); (vi) senescent cells; (vii) genome instability & mutation; (viii) resisting cell death; (ix) deregulating cellular energetics; (x) unlocking phenotypic plasticity; (xi) sustained

proliferative signaling; (xii) evading growth suppressors; (xiii) nonmutational epigenetic reprogramming; (xiv) avoiding immune destruction.

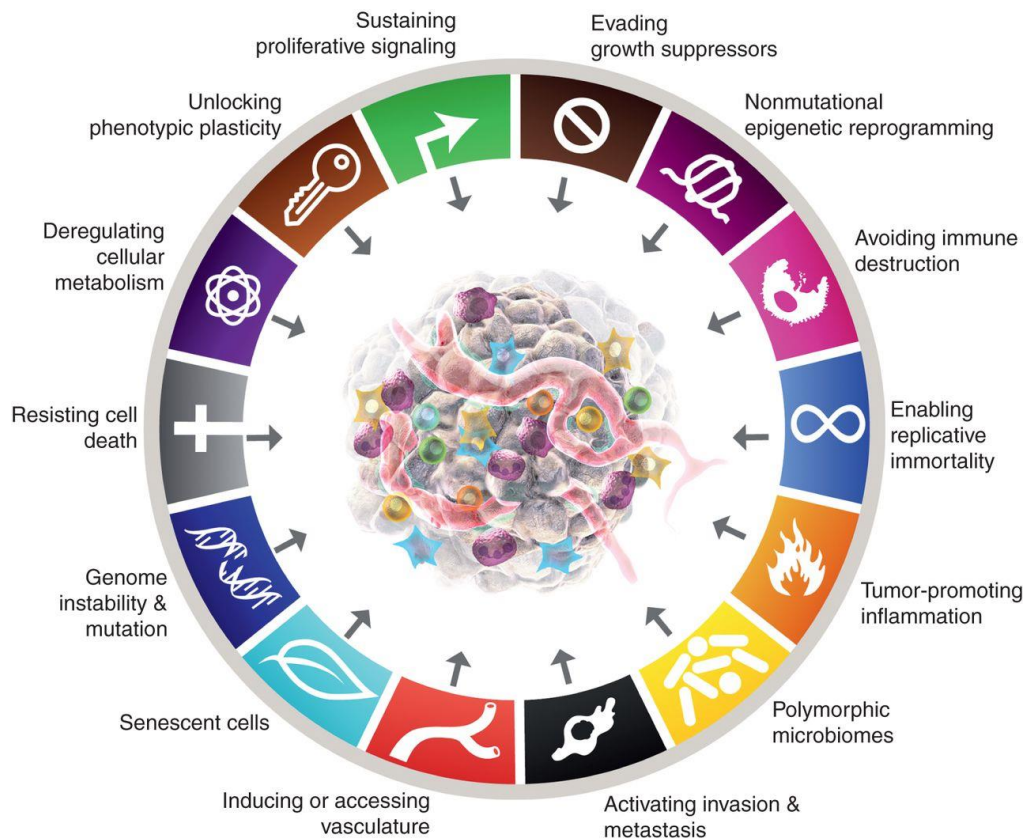


Figure 2: Hallmarks of cancer describing the characteristics a tumor has to acquire to sustain tumor growth and progression (Hanahan, 2022; permission to reproduce from the American Association for Cancer Research under the license number: 5264790271884).

Acquisition of the hallmarks during cancer development is driven by the appearance of different mutations of an epigenetic dysregulation in cancer cells. Therefore, genome instability & mutation and nonmutational epigenetic reprogramming can be considered as the driving force for gaining the other hallmarks (Hanahan, 2022; Hanahan & Weinberg, 2011). While the mutations and epigenetic changes leading to these hallmarks can differ between tumors, the concept is believed to be universal for all tumor types and separates them from healthy tissue (Hanahan & Weinberg, 2011). In this context, tumor progression is subject to an evolutionary process. Genome instability leads to the appearance of random mutations in the genome of single cancer cells, which will determine their phenotype. If a certain mutation leads to the acquisition or enhancement of one of the previously mentioned hallmarks, this cancer cell will have an advantage in terms of survival or proliferation compared to the other cells. Therefore, selective

pressure will lead to selection of most cancerogenic cells during tumor development in a Darwinian-like evolution process (Gaillard *et al*, 2015).

Historically, besides surgical interventions, chemotherapeutic and radiotherapeutic regimens were the most commonly used approaches for cancer treatments. Both are based on targeting and eliminating strongly proliferating cells. These treatments, however, do not allow distinguishing between homeostatic proliferating cells and cancer cells and lead to several severe side effects caused by normal tissue injury (Huang & Zhou, 2021).

Identification of these cancer cell-specific hallmarks enabled a new field for potential cancer treatments called targeted cancer therapy. The principal behind targeted cancer therapy is based on the interference with the previously described tumor specific hallmarks. This can be accomplished by selective targeting and functional inhibition of tumor associated proteins driving one or more hallmark. Small molecules and monoclonal antibodies are most used in targeted cancer therapy (Seebacher *et al*, 2019). Both rely on specific binding and thereby functional inhibition of the target protein (Sawyers, 2004). Among others, the most targeted protein family is the family of kinase proteins, which are involved in several signaling cascades. Inhibition of specific kinase proteins such as endothelial growth factor receptor or B-Raf proto-oncogene serine/threonine kinase (BRAF) can lead to disruption of the signaling cascade crucial for proliferation, migration and survival of cancer cells (Bhullar *et al*, 2018).

A highly targeted tumor characteristic is the hallmark of avoiding immune destruction. In this context, several strategies have been developed to either enhance the antitumoral immune reaction or prevent tumor immune evasion mechanisms. These strategies, which are summarized under the category of immune therapies, will be further discussed.

A total of about 89 small molecule-based and 65 monoclonal antibody-based targeted cancer therapeutics have reached U.S. Food and Drug Administration (FDA) approval (Seebacher *et al*, 2019; Zhong *et al*, 2021). For certain types of tumors, targeted cancer therapy has achieved remarkable clinical success. For example, Imatinib, a small molecule inhibiting the kinase function of the oncogene BCR-Abl, has shown a complete response rate over 5 years follow-up in 98 % of patients treated for BCR-Abl positive chronic myelogenous leukemia (Eck & Manley, 2009; Seebacher *et al*, 2019). Following

these overwhelmingly positive results, high expectations were raised for the usage of targeted therapy in cancer treatment and has therefore been considered the “magic bullet” to cure cancer (Keefe & Bateman, 2019). Subsequent observations, however, revealed only modest clinical benefit for several other targets as with a high interpatient variability. For example, only 30 % of HER2 high breast cancer patients respond to Trastuzumab treatment, a monoclonal antibody directed against HER2 (Esteva *et al*, 2010). In the context of liver metastasis with CRC origin, mostly epidermal growth factor receptor (EGFR) inhibitors as Cetuximab and Panitumumab and BRAF directed agents such as Encorafenib are under preclinical and clinical investigation (Osei-Bordom *et al*, 2021). Especially EGFR is a favorable target due to its high expression in CRC-LMS. The main aim of these studies is to transform initially unresectable LMS into surgically removable LMS. Response rate, however, is reported to be rather low (de Palma & Hanahan, 2012). A combination of anti-EGFR agents such as Cetuximab plus the chemotherapeutic regimen oxaliplatin increased the conversion rate from non-resectable to resectable LMS to 10 % compared to 4 % in patients only treated with oxaliplatin (Chen *et al*, 2018). Taken together, the clinical success in metastatic CRC appears to be limited (Osei-Bordom *et al*, 2021).

The reason for many tested targets failing to reach the expected clinical benefit can be found in the acquisition of resistance. Targeted therapy aims at inhibiting a central player in a cancer cell. Disrupting this central player should lead to the loss of at least one of the previously defined hallmarks crucial for tumor progression, hence, abolishing tumor growth. In turn, if the cancer cells develop a compensatory mechanism to sustain the targeted hallmark, the targeted therapy will render inefficient (de Palma & Hanahan, 2012). In this context, two categories of resistance have been defined. The first describes preexisting resistance. As previously discussed, cetuximab shows only limited success for treatment of metastatic CRC despite EGFR being a central player. Studies have found that mutations in *KRAS* can compensate inhibition of EGFR leading to resistance to the EGFR-targeted therapy in patients with a *KRAS* mutation (de Roock *et al*, 2010). The second mechanism of resistance describes the emergence of resistance following the treatment. For example, majority of patients with non-small cell lung carcinoma with a mutated endothelial growth factor receptor tyrosine kinase gene initially respond to tyrosine kinase inhibitor treatment but display a subsequent relapse due to the appearance

of secondary mutations in the endothelial growth factor receptor tyrosine kinase gene (Workman & Clarke, 2011). Hence, usage of targeted therapy creates a selective pressure towards cancer cell clones harboring mutations that allow to either compensate or revert the inhibition of the targeted protein. In general, the genetic intertumoral and intratumoral heterogeneity create a big challenge for targeted therapy, which remains to be overcome. Despite several combinatory approaches, in most cases, patients respond to targeted therapy only limited in time and rarely complete.

1.5 Antitumor immunity and immune evasion mechanisms

As previously discussed, genome instability is considered to be the driving force of tumor progression by enabling the acquisition of the remaining hallmarks (Hanahan & Weinberg, 2011). This accumulation leads to the occurrence of a high number of mutated genes and subsequently to the appearance of tumor antigens (TAs). TAs can be classified as either neoantigens, antigens which do not exist in health cells, or tumor associated antigens, antigens which are overexpressed in tumor cells compared to healthy tissue. These TAs can elicit a cancer cell specific antitumoral immune reaction by the patient's immune system leading to tumor rejection. In 1909, Paul Ehrlich suggested a mechanism in which the host defense prevents tumor development from transformed neoplastic cells (Ehrlich, 1909). This theory was further developed towards the so called "cancer immune surveillance hypothesis" by Burnet which describes a process in which transformed cells constantly appear in the human body. Due to the presence of TAs, cells of the adaptive immune system are capable of recognizing and eliminating these clones, hence, preventing subsequent tumor development in the majority of cases (Burnet, 1957, 1964, 1971). In 2011, Schreiber dissected the process of immune surveillance of neoplastic cells into different steps. The first step describes the elimination of transformed cells by the immune system upon recognition of TAs. This elimination process can be complete or incomplete. Mostly, a complete elimination is observed when all transformed cells are removed and no further tumor development is observed. In more rare events, however, an incomplete elimination takes place, in which some transformed cells escape the elimination, persist, and enter the equilibrium phase. In this phase, transformed cells are described to either enter a type of tumor dormancy state or continue to proliferate but extensive outgrowth is controlled mainly by the adaptive immune system. The length of this phase can vary and potentially last up to live long. At this stage, there is a strong

selective pressure for less immunogenic clones leading to a process called immunoediting which describes a directed evolution towards clones that can evade immune reactions. Once tumor cells have acquired the capacity to avoid immune recognition, the escape phase starts. In this phase tumor growth cannot be controlled by the immune system anymore and tumor progression is observed (Schreiber *et al*, 2011; Vinay *et al*, 2015).

1.5.1 Cancer immunity cycle

Mounting an effective antitumor immune response, which leads to elimination of cancer cells requires a number of steps to take place, known as the “cancer immunity cycle” defined by Chen and Mellman (Chen & Mellman, 2013). The first step describes the release of neoantigens by cancer cells and its uptake by DCs or other APCs. APCs migrate to lymphoid organs such as lymph nodes, spleen or bone marrow and present the neoantigens in an either MHCI or MHCII dependent manner. This leads to priming and activation of antigen specific T cells. These T cells traffic to and infiltrate the tumor. They encounter cancer cells, which are recognized by their MHCI dependent presentation of the antigen with the antigen specific TCR. Downstream signaling of the activated TCR leads to active killing of the cancer cells. The release of neoantigens by killed cancer cells closes the cancer immunity cycle.

Inhibition of one or more of the previously described steps would lead to immune escape by the tumor cells. There are several different strategies for tumors to interfere with the cancer immunity cycle at different steps and evade the immune system. They are summarized in the hallmark “Avoiding immune destruction” described by Hanahan and Weinberg in 2011 (Hanahan & Weinberg, 2011).

1.5.2 Antigenic variations

The major deterrent about the antigen related immunogenicity of cancer cells, called antigenicity, is the presence of MHCI-presented TAs. TAs arise from accumulation of mutations in cancer cells. Genome instability, the driving force for the occurrence of mutations, leads to acquisition of the hallmarks of cancer.

There are several strategies for tumors to reduce TA-related immunogenicity. One is the loss of antigens. Mutations correlated with increased oncogenicity are called driver mutations. Genome instability, however, also leads to an accumulation of so-called bystander mutations. These are mutations that do not enhance oncogenicity but can still

give rise to immunogenic TAs. Throughout the process of tumor growth, especially during the equilibrium phase, there is a selective pressure for less immunogenic cells forced by immune surveillance. Hence, a clone harboring a mutation causing highly immunogenic antigen would be rapidly removed by TA-specific T cells. This is especially true for clones in which bystander mutations cause the TA as this particular mutation does not give the cell any growth advantage. This leads to selection of clones harboring less immunogenic versions of mutated oncogenic proteins and a low number of immunogenic bystander mutations (Vinay *et al*, 2015; Beatty & Gladney, 2015).

A second strategy is the prevention of MHC I-dependent presentation of antigens at the surface of cancer cells. CD8 T cells are believed to be the key player in the elimination of cancer cells. In order to trigger target cell killing, CD8 T cells bind with their TA specific TCR to antigenic peptide presented on MHC I on the surface of target cells. Hence, downregulation of MHC I expression on the surface of cancer cells prevents recognition by CD8 T cells. Indeed, about 40 – 90 % of human tumors were reported to be MHC I deficient (Cornel *et al*, 2020). NK cells, however, recognize and kill cells that do not express MHC I on their surface. In response to that, several tumors have been observed to develop counter mechanisms to prevent NK cell killing for example by expressing cytokines impairing NK cell function or temporarily regulated expression of MHC I to prevent NK cell recognition (Jonges *et al*, 2000; Anfossi *et al*, 2006). Alternatively, several tumors have shown to possess defects in the loading process of peptides onto MHC I. Under normal conditions, proteins are degraded by the proteasome and resulting peptides of about nine amino acids are loaded onto MHC I and presented on the surface of cells. The transport associated with antigen processing protein (TAP), consisting of the subunits TAP1 and TAP2, plays a central role in the process of loading peptides onto MHC I molecules. Defects or absence of TAP effectively prevents MHC I dependent presentation of antigens, hence, impairs cancer cell recognition by CD8 T cells (Cornel *et al*, 2020; Vinay *et al*, 2015). Kaklamanis has shown that loss of TAP1 is observed in 14% of CRC patients (Kaklamanis *et al*, 1994).

1.5.3 Loss of immunogenicity

Next to avoiding the MHC I dependent presentation of TAs either by reducing the amount of TAs or by preventing their presentation, tumor cells can develop strategies to specifically inhibit the function of T cells. For that purpose, mainly immune checkpoints

are exploited by the malignant cells. Immune checkpoints in the context of T cells describes a number of inhibitory immunoreceptors expressed on the surface of T lymphocytes. The most known examples are programmed cell death protein 1 (PD1), lymphocyte-activation gene 3 (LAG3), T cell immunoglobulin and mucin protein 3 (TIM3) and T lymphocyte-associated protein 4 (CTLA4) (He & Xu, 2020). These immune checkpoints increase in expression with the level of activation of T cells. Indeed, high levels of immune checkpoint expression on the surface of T cells is considered to be a marker of exhaustion, which will be discussed below. Upon engagement of their ligands, downstream signaling induces dysfunction and apoptosis of T cells. Naturally, these mechanisms play a role in maintenance of immune homeostasis and prevention of autoimmune reactions. Cancer cells, however, can exploit that mechanism to prevent killing activity of tumor reactive T and NK cells by upregulation of immune checkpoint ligand expression on their surface, such as programmed death-ligand 1 (PDL1), the ligand of PD1 (He & Xu, 2020; Beatty & Gladney, 2015). Furthermore, T cell function can be directly inhibited by the expression of inhibitory cytokines such as IL-10 and TGF β by cancer cells (Itakura *et al*, 2011; Thomas & Massagué, 2005).

1.5.4 Suppression of immune response by modulation of the tumor microenvironment

In close relation to the previously discussed strategy of loss of immunogenicity is the strategy of avoiding tumor directed immune reactions by controlling and influencing the immune system through the TME. Two major principles are proposed in this context. First, the immune system can be locally impaired by for example inhibiting the infiltration of immune cells into the tumor. A second strategy is based on modulating the tumor directed immune reaction towards a tolerogenic and protumoral response by controlling the phenotype of tumor infiltrating immune cells towards a tolerogenic phenotype (Duan *et al*, 2020; Tang *et al*, 2021).

1.5.4.1 Tumor microenvironment

The tumor microenvironment describes the characteristics and cellular composition of the tumor site. It is composed not only of cancer cells, but also of a variety of other cell types such as vascular endothelial cell, cancer associated fibroblasts (CAFs), and a variety of different immune cells. This highly complex structure and interplay between different

cell types and cytokines creates a unique environment favoring tumor growth and inhibiting immune reaction (Tang *et al*, 2021). Interestingly, the TME has early been described to be functionally analogous to the microenvironment of some immune-privileged healthy organs as the eye, confirming that tumors leverage host-derived immune regulatory mechanisms to suppress the antitumoral immune reaction (Medawar, 1948; Joyce & Fearon, 2015).

Oxygen and nutrition supply through vascularization is crucial for tumors to sustain tumor growth. Therefore, a rapid and continuous reshaping of the vascularization structure is required leading to disorganized and uneven network of blood vessels. Together with the high demand of oxygen and nutrients by tumor cells, which mainly rely on aerobic glycolysis for their energy supply, this creates an environment characterized by hypoxia and a low pH in the TME (Petrova *et al*, 2018). These conditions do not favor antitumoral activity of immune cells as hypoxia negatively impacts the innate and adaptive immune response. For example, macrophages are polarized towards an alternatively activated M2-like phenotype, which will be discussed in more detail below. Furthermore, T cells, which require a high nutrient supply, are forced to compete with cancer cells for the available oxygen and nutrition. The resulting lack of nutrients lead to reduced functionality of T cells (Colegio *et al*, 2014; Chang *et al*, 2015).

CAFs which can represent up to 80 % of the cells within the TME and are characterized by their high expression of the Ca²⁺-binding protein S100A4 are believed to exert a protumoral effect by the secretion of different cytokines and chemokines (Petrova *et al*, 2018). For example, expression of CXCL12 and vascular endothelial growth factor (VEGF) A lead to a direct beneficial effect on tumor growth as well as stimulates angiogenesis (Orimo *et al*, 2005; Han *et al*, 2020). Furthermore, CAFs play a crucial role in the remodeling of the extracellular matrix, which can serve as storage for TGFβ, which in turn promotes EMT and highly influences the infiltration and the spatial distribution of immune cells in the TME (Gordon-Weeks & Yuzhalin, 2020; Petrova *et al*, 2018). In several tumor types, including CRC, the distribution of immune cells appears to be heterogeneous (Salmon *et al*, 2012; Petrova *et al*, 2018). As the extracellular matrix is thicker inside the tumor compared to the tumor surrounding area, mobility of immune cells is reduced inside the tumor. Therefore, infiltration and interaction between immune

cells and cancer cells is impaired. This leads to an accumulation of immune cells in the stroma and especially tumor surrounding area compared to the cancer cell nests in several tumor types, including CRC-derived LMS (Salmon *et al*, 2012; Berthel *et al*, 2017).

Studies have shown that certain features such as infiltration of cytotoxic T cells and the presence of immune suppressive cell types and cytokines can predict patient's clinical outcome (Giraldo *et al*, 2019). Within the TME there are several different bone marrow-derived immune cells which can be shaped towards a protumoral or tolerogenic phenotype. In particular, myeloid-derived suppressor cells, tumor-associated macrophages (TAMs) and T cells with a regulatory phenotype are described to be the main players for reshaping the TME towards its immunosuppressive state and limiting the cancer cell-eliminating activity of T cells (Joyce & Fearon, 2015).

In general, a balance between myeloid and lymphoid responses is required for immune homeostasis. In situations of chronic inflammation as present in the TME, this balance is lost and shifted towards a deregulated myelopoiesis leading to an accumulation of dysfunctional myeloid progenitor cells with immunosuppressive functions such as MDSCs and TAMs while effective lymphoid responses are suppressed. These induces a local and systemic antigen specific tumor tolerance with a strong tumor enhancing effect (Strauss *et al*, 2021).

1.5.4.2 Myeloid-derived suppressor cells

MDSCs describe a heterogeneous population of cells with a remarkable potential to suppress T cell effector functions (Gabrilovich & Nagaraj, 2009). They consist of bone marrow-derived myeloid progenitor cells that in healthy conditions further differentiate towards DCs, macrophages or granulocytes. In certain circumstances, such as cancer, there is a block in the differentiation process leading to an expansion of this immunosuppressive cell type. Their immunosuppressive activity is exerted through the expression of immunoinhibitory enzymes such as Arginase 1 and iNOS leading to degradation of arginine and accumulation of nitric oxide and reactive oxygen species, all of which have an immunosuppressive effect on T cells. Furthermore, MDSCs are a major source for reactive oxygen species (Rodríguez & Ochoa, 2008). Importantly, the presence of increased numbers of MDSCs in the TME of liver metastasis has been established as

a negative prognostic factor. Therefore, MDSCs may provide a potential target for liver cancer treatment (Ma *et al*, 2021).

1.5.4.3 Tumor-associated macrophages

Macrophages are a central part of the innate immune system and characterized by their high plasticity and their different functions in homeostatic as well as pathologic circumstances. They are present in nearly every part of the human body and can appear as tissue resident macrophages such as KCs or circulating macrophages of bone marrow origin. Next to their function in tissue homeostasis and elimination of pathogens and toxic substances, they have also been described to infiltrate the TME in form of TAMs. TAMs even constitute the dominant fraction of immune infiltrating cells in the TME (Long & Beatty, 2013).

Macrophages are capable to rapidly respond to distinct external stimuli and adjust their transcriptional profile and effect accordingly. In this context two major polarization states have been described, classically activated M1-like polarization and alternatively M2-like polarization (Squadrito & de Palma, 2016). M1-like macrophages polarization is triggered by a variety of proinflammatory stimuli such as lipopolysaccharide mimicking the presence of gram-negative bacteria, and inflammatory cytokine like IFN γ (Orecchioni *et al*, 2019b). Additionally, interferon alpha (IFN α) has been shown to drive macrophage polarization towards an M1-like phenotype (Müller *et al*, 2018). Accordingly, M1-like macrophages are characterized by enhanced Janus kinase and signal transduced and activator of transcription (JAK/STAT) signaling which is triggered by type I interferon such as IFN α and IFN γ (Horvath, 2004; Hu *et al*, 2002). JAK/STAT is a key regulator of several proinflammatory programs, which subsequently lead to secretion of proinflammatory cytokines and chemokines like TNF α , IL-12 and C-X-C motif chemokine ligand 9 and 10 (CXCL9/CXCL10) which triggers T cell infiltration and responses (McWhorter *et al*, 2013; Tokunaga *et al*, 2018). Furthermore, M1 polarization leads to upregulation of the costimulatory molecules CD86 on their surface enhancing T cell functions in a direct manner (Orecchioni *et al*, 2019b). With these properties, macrophages can have antitumoral functions especially in the initial state of tumor development and the inhibition of metastatic lesions by their capacity to eliminate

malignant cells by phagocytosis, inhibition of angiogenesis and depletion of fibrosis (Long & Beatty, 2013).

Due to the anti-inflammatory signals present in the TME, however, most of the TAMs are polarized towards an alternative activation (M2-like) state. M2-like macrophages are induced by immunoinhibitory cytokines as IL-4, IL-10, TGF β and prostaglandins, which are frequently found to be abundant in the TME of several tumors (Hind *et al*, 2016; Zhang *et al*, 2016). Upregulation of the scavenger receptor MRC1 is a common characteristic for the identification of M2-like macrophages. M2-macrophages have a direct beneficial effect on tumor cell proliferation by the secretion of several tumor growth stimulating factors such as EGF (Yin *et al*, 2016). However, M2-like TAMs promote tumor growth also in an indirect manner, i.e. expression of VEGF, which enhances angiogenesis. Furthermore, T cell functions are suppressed by the expression of Arginase 1 and iNOS in M2-like macrophages, similar to MDSCs, and the recruitment of regulatory T cells is enhanced by the expression of C₂C motif chemokine ligand (CCL) 22 (CCL22) (Curiel *et al*, 2004). Alternatively activated macrophages further support tissue and extracellular matrix remodeling by the expression of several different matrix metalloproteinases, which facilitates EMT and invasion, the first and second steps in the process of metastasis formation (Pan *et al*, 2020; Fares *et al*, 2020).

Dependent on the polarization state, macrophages adjust their metabolism. M1-like macrophages, much like other proinflammatory cells, mainly depend on glycolysis and the pentose phosphate pathway, pathways which allow fast energy supply to fuel acute inflammatory reactions. Instead, alternatively activated macrophages upregulate oxidative phosphorylation and fatty acid oxidation for their energy supply which are more efficient but more time consuming and oxygen dependent (Strauss *et al*, 2021; Soto-Herederó *et al*, 2020).

The model of macrophages polarizing either towards an M1-like or M2-like phenotype is a simplification of the situation *in vivo*, which arise from *in vitro* polarization studies. Indeed, there is a continuum of intermediate phenotypes especially in the TME with such a complex interplay of pro- and anti-inflammatory signals (Mantovani *et al*, 2017).

1.5.4.4 T cells

CD8 T cells are considered to be the effector cells of the adaptive immune system responsible for the elimination of target cells. In order to mount an efficient antitumoral immune reaction leading to tumor rejection, generation and engagement of tumor specific CD8 T cells is crucial. TCR-dependent recognition of MHC I dependent antigen presentation on the surface of target cells, such as cancer cells, triggers their cytotoxic immune functions. Release of death inducing granules by containing cytotoxic proteins such as granzymes and perforin induce apoptosis or lead to direct cell killing by the creation of holes in the membrane of targeted cells, respectively. Furthermore, CD8 T cells can express Fas ligand (FasL) on their surface inducing apoptosis of target cells by the engagement of Fas receptor expressed on target cells (Raskov *et al*, 2021).

In general, tumors are categorized into “hot” and “cold” tumors. While hot tumors are characterized by a high infiltration of CD8⁺ T cells, in cold tumors CD8 T cells are rather sparse. Interestingly, the vasculature of cold tumors is characterized by a high expression of the apoptosis inducing factor FasL, which induces apoptosis in CD8 T cells during the process of extravasation (Motz *et al*, 2014). While the CD8 T cell-based immune reaction in cold tumors is suppressed by the physical inhibition of CD8 T cells to encounter cancer cells, in hot tumors CD8 T cells function can be inhibited by one or more of the previously discussed strategies. Loss of antigenicity prevents the generation of tumor specific CD8 T cells in general. Loss of immunogenicity and the immunosuppressive influence of the TME, however, mostly aims at rendering CD8 T cells towards a dysfunctional state (Gao *et al*, 2021). Generally, CD8 T cells can take several different phenotypes during their maturation process with the so-called effector phenotype being the most efficient phenotype in executing their cytolytic function. However, there are also several CD8 T cells phenotypes exhibiting a dysfunctional state preventing cytolytic activity such as exhaustion. Indeed, the majority of tumor infiltrating CD8 T cells exhibits an exhausted phenotype (Zhang *et al*, 2020). Exhaustion describes a dysfunctional state of T cells, which can be triggered by several different factors such as chronic antigen encounter or cytokine-based overstimulation. It is characterized by a decreased effector function such as reduced cytokine production and reduced cytolytic activity. Exhausted T cells express high levels of immune checkpoint receptors such as PD1, LAG3 and TIM3 and have a low proliferative capacity (Blank *et al*, 2019). The phenotype of CD8 T cells can be

influenced by a variety of factors. Important factors are activation through TCR stimulation and/or engagement of co-stimulatory receptors such as CD28 or 4-1BB as well as presence of immune activating and immune inhibitory cytokines (Barber, 2014; Maimela *et al*, 2019).

The role of CD4 T cells, however, is more ambiguous. Similar to CD8 T cells, CD4 T cells can obtain a wide spectrum of phenotypes with activator or inhibitory effects on the immune reaction. In an effective antitumoral immune reaction, upon activation CD4 T cells proved help to CD8 cytotoxic T lymphocytes by secreting immune activating cytokines such as IFN γ and TNF α (Tay *et al*, 2021). There is, however, also a number of CD4 T cell phenotypes, which actively suppress antigen specific immune reactions. The most commonly known phenotype in this context are regulatory T cells (Tregs) with their characteristic expression of the key transcription factor forkhead box p3 (FoxP3) (Fontenot *et al*, 2003). Tregs are an important player in the maintenance of immune tolerance against specific antigens, thus, preventing autoimmune reactions as well as chronic inflammations (Vignali *et al*, 2008). Several mechanisms have been described for the immunosuppressive effect of Tregs. The expression of anti-inflammatory cytokines by Tregs such as IL-10 and TGF β as well as sequestration of inflammatory cytokines induces an immunoinhibitory environment (Vignali *et al*, 2008). Tregs can also function in a more direct manner by their high expression of CTLA4 on the surface. This immune checkpoint receptor binds to B7 (CD80/CD86) expressed on the surface of several myeloid cell types such as macrophages and DCs and thereby inhibits the engagement of B7 and the costimulatory molecule CD28 on the surface of effector T cells (Vasilevko *et al*, 2002). Interestingly, in patients increased amounts of Tregs in the TME is correlated with a worse prognosis for several different types of cancer including CRC (Saito *et al*, 2016).

1.5.4.5 T regulatory type 1 cells

More recently, a second type of CD4 regulatory T cells has been discovered, which is called T regulatory type 1 (Tr1) cells. Tr1 cells have been first identified in the context of a SCID patients undergoing hematopoietic stem cell transplant from a human leukocyte antigen (HLA) mismatched donor. This patient developed immunological tolerance driven by the presence of highly expanded host antigen specific CD4 T cell clone, which

successfully prevented graft versus host disease (Roncarolo *et al*, 1988). Later on, they have been described in the context of prevention of different immune-related disease such as allergic disease and autoimmune diseases, hence, confirming their role in the induction of antigen specific tolerance (Petrich de Marquesini *et al*, 2010; Xu *et al*, 2010). Tr1 cells can be identified by a high surface expression of the immune checkpoint receptors LAG3, PD1, TIM3 and CTLA4. Furthermore, in contrast to conventional Tregs, Tr1 cells are independent of the key transcription factor Foxp3 but depend on a number of other transcription factors such as Eomesodermin (EOMES), c-Maf, Aryl hydrocarbon receptors (Ahr) clearly separating the two populations (Quintana *et al*, 2008; Pot *et al*, 2009; Imbratta *et al*, 2020).

IL-10 in combination with antigen specific TCR dependent activation plays a key role in the development of Tr1 cells. Interestingly, presence of IFN α and TGF β has proven to further enhance Tr1 development in vitro (Levings *et al*, 2001; Roncarolo *et al*, 2018b). The mechanism and pathway towards Tr1 cell development, however, remains unclear. Several different CD4 T cell populations have been proposed as potential origin such as Th1 cells, Th2 cells, Th17 cells and memory T cells. Similarly, it is not clear, whether Tr1 cells are capable of further developing into other phenotypes or if the Tr1 phenotype is a terminal state. Tr1 cells, however, have proven to be stable and long lasting for more than seven years. (Roncarolo *et al*, 2018b; Bacchetta *et al*, 2014).

While the induction of Tr1 cells is antigen specific, the immunosuppressive effect is antigen independent. Interestingly, they function mainly by secretion of the immunosuppressive cytokine IL-10 which in turn can trigger expansion of Tr1 cells leading to a positive feedback loop. In line with this, the Tr1 key transcription factors EOMES, Ahr and c-Maf have been described to drive IL-10 expression. IL-10 modulates both the innate and adaptive immune response. It mainly functions through the inhibition of antigen presentation on APCs by downregulating expression of MHCII as well the costimulatory molecules reducing effector functions of T cells (Trinchieri, 2007). Furthermore, the group of John Wherry has shown that exhaustion of T cells is reduced in mouse models upon blockage of the IL-10 signaling (Blackburn & Wherry, 2007). Furthermore, Tr1 cells express TGF β , which similarly inhibits antigen presentation function in APC but also reduced proliferation and cytokine secretion of T cells and

further induces development of regulatory T cells (Batlle & Massagué, 2019; Levings *et al.*, 2002). Next to these indirect mechanisms of immunosuppression, also a more direct effect of TR1 cells has been described. Secretion of perforin, granzyme B (GZMB) and granzyme K (GZMK) by Tr1 cells leads to selective killing of APCs further abolishing T cell-based immune reactions (Solé & Santamaria, 2021; Gruarin *et al.*, 2019).

It has been long established that FoxP3 Tregs are the main regulatory T cell phenotype induction tumor tolerance, while Tr1 cells have been mostly described in the context of immune related disease. Recently, however, Pagani and collaborators have reported Tr1 cells in a variety of solid tumors, including CRC LMS. Interestingly, they describe a clonal relation between antitumoral effector cells and Tr1 cells, but not FoxP3 Tregs, which confirms the antigen specific function of Tr1 cell. Furthermore, a worse prognosis for patients with increased numbers of Tr1 cells in the tumor infiltrate was observed confirming the importance of Tr 1 cells in the context of cancer (Bonnal *et al.*, 2021).

1.5.4.6 Immunosuppressive tumor microenvironment in liver metastasis

The tumor microenvironment is a complex system influenced by its cellular composition and their phenotypes as well as the presence of different cytokines affecting the immune environment as well as the parenchymal cells and cancer cells. Therefore, especially for solid tumors, the TME is highly influenced by the environment of the host organ, as organ resident cells may infiltrate and host organ-derived cytokines might reshape the TME. This is particularly evident for primary tumors in the liver such as hepatocellular carcinoma and liver metastasis like CRC-LMS (Eggert & Greten, 2017; Zhou *et al.*, 2021).

The liver hosts an immune privileged environment implied by high levels of cytokines with immunosuppressive functions such as IL-10, prostaglandins and TGF β , all of which play a crucial role in reshaping the TME towards an immunosuppressive state. Sources of these cytokines are liver tissue resident immune cells and other cells with immune function such as KCs and LSECs colonizing the liver at high number. (Knoll *et al.*, 1995; Knolle *et al.*, 1998; Callery *et al.*, 1991; Roth *et al.*, 1998; Robinson *et al.*, 2016). These liver sourced immunoinhibitory cytokines exhibit their effect in the TME leading to a further increased suppression of immune functions (Brodt, 2016). The increased immune suppression in CRC LMS compared to the primary tumor is especially evident by the fact

that several treatments directed at enhancing antitumoral immune reactions have proven to be inefficient in the presence of LMS while being effective against primary nonmetastatic CRC. Indeed, the authors observed in mouse models that the presence of liver metastasis leads to a sequestration of TA-reactive CD8 T cells in the liver where proapoptotic signals drive them towards apoptosis. This leads to a removal of circulating TA specific CD8 T cells creating a systemic immune desert against the TA. Hence, the immune suppressive features of the TME of LMS does not only affect the LMS itself but also impacts and suppresses immune reactions against the primary CRC (Yu *et al*, 2021). LMS also leverage the previously discussed unique tolerogenic capacity of the liver to establish TA specific tolerance mediated by the recruitment of Tregs and TR1s (Lau, 2003; Levings *et al*, 2002). In this context, recent studies have shown that TAs released by the tumor are taken up and presented by liver resident APCs triggering a tolerogenic immune reaction (Lee *et al*, 2020).

The hepatic environment also leads to a reshaping of the TME towards a state favoring tumor growth in an immune independent manner. For example, LSECs have been demonstrated to favor angiogenesis by the secretion of VEGF (Yang & Zhang, 2021). Another cell type favoring tumor growth in the hepatic environment are hepatic stellate cells (HSCs). These cells, which are resident in the space of Disse, are activated upon tissue damage response triggered by tumor growth. Activated HSCs produce high amounts of extracellular matrix and thereby increase fibrosis in hepatic tumors (Yang *et al*, 2011).

1.6 Cancer Immunotherapy, a new promising strategy for cancer treatment

Even though tumors derive from host cells, they are not invisible to the immune system. As previously described, the accumulation of mutations leads to the appearance of TAs, which can be recognized by the immune system and lead to the elimination of cancer cells. This tumor directed immune reaction, however, is actively suppressed by several different strategies mentioned above summarized in the hallmark of “avoiding immune destruction”. Following this discovery, new therapeutic strategies have been developed which aim targeting this hallmark by either impairing the tumor immune evasion strategies or by actively supporting one or more steps of the cancer immunity

circle, hence, enabling antitumoral immune responses. These strategies are summarized as cancer immunotherapies.

Indeed, recent studies have shown that also conventional cancer treatment options as chemotherapy and radiotherapy function at least in part by enhancing antitumoral immune reactions. Radiotherapy has been shown to lead to the appearance of TAs, which increases antigenicity of cancer cells (Lhuillier *et al*, 2019; Zitvogel *et al*, 2013). Tumor cell killing induced by these treatments leads to an enhanced inflammation through the release of immune activating factors such as HMGB1, which triggers DC activation (Coffelt & de Visser, 2015). Furthermore, tumor cell death leads to release of TAs, which can be taken up and presented by professional APCs, the first step of the cancer immunity circle (Zitvogel *et al*, 2013). Similarly, several targeted therapy approaches trigger immune related antitumoral effects additionally to the inhibition of the oncogene. Marking of cancer cells with an antibody can result in antibody-dependent cellular toxicity, a mechanism, which induces NK cell dependent target cell killing (Ochoa *et al*, 2017).

Immunotherapy has revolutionized the field of oncology and is considered a breakthrough for the treatment of several different types of tumors (Zhang & Zhang, 2020).

1.6.1 Checkpoint inhibitors

Despite the presence of immunogenic TAs being presented at the surface of cancer cells in an MHCII dependent manner and the presence TA reactive T cells, T cell activity can be inhibited by the engagement of immune checkpoint receptors. This concept aims at reducing the risk to develop autoimmune reactions but can be hijacked by the tumor to prevent antitumoral immune reactions. Engagement of immune checkpoint receptors on the surface of T cells leads to immune inhibitory signaling and suppresses the immune functions of T cells (He & Xu, 2020).

Immune checkpoint inhibitors aim at interrupting the interaction of immune checkpoint receptors and their ligands expressed on either cancer cells or other cells in the TME. For that purpose, mostly monoclonal antibodies are exploited with a specificity to either the immune checkpoint receptor on the surface of the T cell, or its ligand. Binding of checkpoint inhibitor will then sterically prevent interaction of the immune

checkpoint receptor and the ligand, hence preventing immunoinhibitory signaling of immune checkpoint receptor in the T cells. This strategy has been shown to effectively increase effector functions and reduce exhaustion of T cells (Rotte *et al*, 2018).

Several immune checkpoints have been identified so far. Targeting of PD1 and CTLA4 by checkpoint inhibitors, however, has proven to be most successful so far (Marin-Acevedo *et al*, 2021). PD1 can be found on the surface of different lymphocytes as T cells, B cells, Tregs, natural killer (NK) cells and natural killer T (NKT) cells (Rotte *et al*, 2018). PD1 expression on the surface of T cells is tightly bound to their activation status and level of antigen encounter. While naive T cells express PD1 only at low levels, immune challenges leading to activation of T cells also trigger upregulation of PD1 expression, especially during chronic immune stimulation (Bally *et al*, 2016). Accordingly, especially TA specific tumor infiltrating T cells are characterized by a high expression of PD1 (Fernandez-Poma *et al*, 2017). PDL1 and PDL2, the ligands of PD1, are expressed on a variety of immune cells including macrophages, DCs, and T cells themselves, but also cells of nonhematopoietic origin such as endothelial cells including LSECs, fibroblasts (Rotte *et al*, 2018). As described previously, the expression level of PDL1 on several cells within the TME is high. Additionally, cancer cells have been observed to upregulate PDL1 expression to actively suppress T cells functions (He & Xu, 2020). Downstream signaling of PD1 upon ligand binding strongly counteracts TCR signal transduction and signal transduction of other costimulatory receptors such as CD28. Concordantly, secretion of immune stimulatory cytokines is reduced, and T cell survival and proliferation is impaired (Arasanz *et al*, 2017).

Disruption of the PD1-PDL1 interaction achieved by PD1 or PDL1-targeted immune checkpoint inhibitors has proven to be a clinically relevant therapeutic strategy for different type of tumors. Tumor regression and prolonged overall survival in combination with low side effects in patients with metastatic melanoma have led to FDA market approval of the first two PD1-targeted checkpoint inhibitors Pembrolizumab and Nivolumab in 2014 (Hazarika *et al*, 2017; Raedler, 2015). Following these promising results, beneficial effects of PD1/PDL1 targeted immune checkpoint inhibitor treatment have also been observed for further types of cancer as non-small-cell lung cancer and neck squamous cell carcinoma (Wu *et al*, 2019).

Next to the PD1/PDL1 axis, also CTLA4 is highly targeted by checkpoint inhibitors. Similarly to PD1, expression of CTLA4 is found to be upregulated upon T cell activation (Perkins *et al*, 1996). As previously discussed, T cell activation is triggered by TCR engagement, but also by the interaction of costimulatory molecules with its ligand such as CD28 with CD80 and CD86, respectively. CD80 and CD86 are expressed on the surface of APC in immunostimulatory conditions. Similar to CD28, also CTLA4 can interact to CD80 and CD86 but with a higher affinity. While CD28 engagement leads to an activator signaling, CTLA4 triggers immunoinhibitory pathways in T cells. Therefore, CTLA4 inhibits T cell functions in two ways: by dampening TCR signaling through blocking the engagement of the costimulatory molecule CD28 and by direct inhibitory signaling (Walker & Sansom, 2015; Wei *et al*, 2018). These immunoinhibitory mechanisms are also leveraged by regulatory T cells such as Tregs and TR1s, which contain a high expression of CTLA4 (Vasilevko *et al*, 2002; Roncarolo *et al*, 2018b).

In 2011, the first CTLA4-directed immune checkpoint inhibitor, Ipilimumab, was granted FDA marked approval for the treatment of advanced melanoma followed by applications in the treatment of renal cell carcinoma and non-small-cell lung cancer (Cameron *et al*, 2011; Sheng & Ornstein, 2020; Vellanki *et al*, 2021).

Despite these promising results, a high number of patients are refractory to immune checkpoint inhibitor treatment. While initial resistance may be explained by the complexity and variability in the characteristics of human tumors, the mechanism for the acquisition of resistance remains unclear (Jenkins *et al*, 2018; Schoenfeld & Hellmann, 2020). Immune checkpoint inhibitors rely on the presence of TA specific T cells, which are suppressed in their function and rescued by the treatment (Barrueto *et al*, 2020). Accordingly, the density of T cells in the TME can be used as a predictive factor for the efficacy of an immune checkpoint inhibitor-based treatment (Li *et al*, 2021). In line with this, the application of immune checkpoint inhibitors has shown some success especially in patients with mismatch repair deficient microsatellite instable CRC. Mismatch repair deficient CRC is characterized by a higher T cell infiltration compared to mismatch repair sufficient CRC due to the accumulation of mutations and TAs, thus, providing attack points for T cells (Morse *et al*, 2020). In general, however, the response rate of CRC patients to immune checkpoint inhibitor treatment have been described as far from satisfactory (Yu *et al*, 2020). Accordingly, the effect of immune checkpoint inhibitor

treatment of CRC with liver metastasis is limited. While patients with a microsatellite instable disease, with 5 % the minority of the cases, show an objective response rate of 40 % to treatment with pembrolizumab, it drops to 0 % in microsatellite stable CRC LMS patients (Yu *et al*, 2020; Gholami *et al*, 2021). Several attempts were done targeting different immune checkpoints including combinatory approaches. The results, however, remain unsatisfactory (Gholami *et al*, 2021). In general, presence of liver metastasis is a negative predictive factor for immune checkpoint inhibitor treatment outcome (Chen *et al*, 2021a). Reason for that is the strong immune suppressive TME in LMS, which highly suppress the antitumoral immune reaction not only locally at the site of metastasis but systemically including the primary tumor (Yu *et al*, 2021). The immune activating functions of immune checkpoint inhibitors appear to be not strong enough to overcome the obstacle of the immune suppressive TME in LMS to allow antitumoral T cell responses.

1.6.2 Reshaping the cytokine composition in the tumor microenvironment

The antitumoral immunity is highly influenced by the interplay of immunostimulatory and immunoinhibitory cytokines. As the TME is dominated by the presence of immunoinhibitory cytokines such as IL10 and TGF β , antitumoral immune reactions are commonly suppressed, as described above. Reshaping of the cytokine landscape within the TME, however, may provide a valid strategy to reshape the TME towards an immune reactive state, hence, enabling antitumoral immune reactions (Chulpanova *et al*, 2020). Two main strategies have been developed for that purpose: (i) prevention of signaling of inhibitory cytokines to prevent immune inhibition; (ii) supplementation with immune stimulatory cytokines to activate immune functions (Berraondo *et al*, 2019). Prevention of signaling of inhibitory cytokines can be achieved by removing the cytokines from the TME using neutralizing antibodies. For example, TNF α , which under certain circumstances can promote tumor progression through mediation of activation induced cell death of effector lymphocytes, can be targeted and removed from the TME with the antagonistic antibodies infliximab and adalimumab (Palladino *et al*, 2003; van Horssen *et al*, 2006). Similarly, TGF β can be neutralized by monoclonal antibodies such as Fresolimumab (Morris *et al*, 2014). Another option is inhibiting the interaction between the cytokine and its receptor by targeting of the receptor leading steric inhibition of cytokine binding. In this direction, Cabiralizumab, a monoclonal antibody targeting the

macrophage colony-stimulating factor 1 receptor is being tested in clinical trials for the treatment of advanced pancreatic cancer (NCT03336216, <https://clinicaltrials.gov/>). Additionally, IL10 receptor targeting antibodies are currently under investigation (Ni *et al*, 2020). The strategy of prevention of signaling of inhibitory cytokines, however, is considered challenging due to the ambivalent effect of many of those inhibitory cytokines dependent on the current state of the TME (Berraondo *et al*, 2019). For example, while IL10 is believed to play a crucial role in maintaining the immune suppressive state in the TME, recent preclinical and clinical studies have demonstrated that IL10 treatment can mediate tumor regression and enhanced CD8 T cell infiltration in solid tumors (Ni *et al*, 2020).

Supplementing of the TME with pro-inflammatory cytokines has proven to be a more promising approach. Proinflammatory cytokines are involved in every step of the cancer immunity circle and therefore provide a valuable tool to not only enhance but also trigger antitumoral immune reactions. Accordingly, cytokine-based cancer treatments are believed to have the capability of overcoming the resistance mechanisms to immune checkpoint inhibitor treatments (Berraondo *et al*, 2019). Several different cytokines have been tested in clinical trial such as the interleukins IL2, IL10, IL12, IL15 and IL21, the granulocyte-macrophage colony stimulating factor (GM-CSF) and different type I interferons including IFN α . Each of those cytokines exhibits its immune stimulatory function in a different manner. Due to the substantial differences of the TME of different patients and tumor types, the clinical beneficial effect varies. In this perspective, cytokines with a more pleiotropic immune activating effect may provide a better tool as this allows overcoming of different immune evasion strategies by simultaneously enhancing several steps of the cancer immunity circle. Accordingly, tumors are also less prone to develop resistance against pleiotropic cytokine-based treatments.

1.6.3 IFN α -based therapies in oncology

IFN α is a pleiotropic cytokine belonging to the family of type I interferons. Type I interferons are widely known for their crucial role in antiviral immune responses. Indeed, treatment regimens of patients harboring viral infections with hepatitis B and hepatitis C or human papilloma virus are based on systemic application of IFN α (Finter *et al*, 1991).

IFN α , however, also plays an emerging role in the antitumoral immune response (Ferrantini *et al*, 2007).

Naturally, plasmacytoid DCs are believed to have the highest contribution in secretion of IFN α in the event of an antiviral response, even if its expression can be triggered in every white blood cell (Colantonio *et al*, 2011). Its effect on target cells is triggered through the engagement of the IFN α receptor (IFN α R). It consists of two subunits, IFN α R1 and IFN α R2. Both of them contain a ligand binding site with a low and high binding affinity to IFN α , respectively. Ligand binding in any of the subunits triggers dimerization, which is fundamental for signal transduction (Short, 2015). Upon dimerization, the intracellular JAK- and tyrosine kinase 2 subunits are activated which in turn leads to activation of the JAK/STAT pathway triggering the expression of IFN α -stimulated genes (ISGs) (Pattyn *et al*, 1999).

Due to its pleiotropic characteristics, the antitumoral effect of IFN α is composed by several different mechanisms. In cancer cells, IFN α triggers the expression of proapoptotic factors such as FasL, different caspases and TNF-related apoptosis-inducing ligand (Chawla-Sarkar, 2003; Kotredes & Gamero, 2013). Furthermore, IFN α elicit a strong antiangiogenic effect (Indraccolo, 2010). Migration and proliferation of endothelial cells is reduced, and the angiogenic effect VEGF is suppressed due to the expression of antiangiogenic ISG upon IFN α signaling such as CXCL10 (Cicarese *et al*, 2020).

The main antitumoral effect of IFN α , however, is its capability to enhance antitumoral immune reactions. As previously discussed, a main strategy of cancer cells to evade immune reactions is based on the loss of immunogenicity by suppression of MHCII-dependent antigen presentation on their surface. IFN α directly counteracts this mechanism by stimulating antigen presentation in cancer cells, thus, making them more visible to the immune system (de Charette *et al*, 2016). Furthermore, IFN α activates immune cells of the adaptive as well as the innate immune system. In this context, antigen presentation is not only enhanced in cancer cells but also in the myeloid compartment. *In vitro* studies have shown that IFN α in combination with GM-CSF drives differentiation of myeloid progenitor cells towards DCs, which exhibit the most efficient antigen cross

presentation and T cell priming capability (Gessani *et al*, 2014). Furthermore, similarly to cancer cells, APCs are enhanced in their antigen presentation and cross presentation functions by direct IFN α -dependent upregulation of genes involved in antigen presentation such as genes coding for MHCI, MHCII and TAP (Gessani *et al*, 2014). Also, upregulation of costimulatory molecules like CD80 and CD86 have been observed on APCs upon IFN α induction, thus, enhancing T cell functions (Schiavoni *et al*, 2013). Cytotoxic functions of T cells and NK cells are further increased by the secretion of IL15 triggered in DCs upon IFN α stimulation (Mattei *et al*, 2001). The positive effect on the T cell compartment, however, is not only indirect through the reshaping of the myeloid compartment but also through a direct effect. Improved effector functions and more effective target cell killing by CD8 T cells has been observed upon IFN α stimulation (Dickow *et al*, 2019). Next to these immune activation effects, also inhibition of immunosuppressive mechanisms has been observed in the context of IFN α . For example, IFN α triggered a reduction in the amounts and impairment of the inhibitory functions of MDSCs in the TME (Fan *et al*, 2021). Moreover, decreased amounts of Tregs were observed in the TME in a murine model of CRC upon IFN α treatment (Hashimoto *et al*, 2014).

Taken together, IFN α provides a valid strategy to efficiently reshape the immune suppressive TME and enable antitumoral immune reactions. Indeed, Katlinski *et al*. has observed that downregulation of IFN α R in human CRC plays a key role in the establishment of the immune-privileged tumor niche. Accordingly, reduced expression of IFN α R constitutes a negative prognostic factor for patient outcome in CRC (Katlinski *et al*, 2017).

Despite the clear immune activator function of IFN α , also immunoinhibitory effects have been described in the context of IFN α signaling, such as Treg expansion as discussed above. Furthermore, breast cancer tumors expressing a high amount of IFNs-responsive genes are more prone to metastasis (Provance & Lewis-Wambi, 2019). However, this stands in strong contrast with preclinical and clinical observations of IFN α -based antitumor treatments.

The beneficial effect of IFN α -based strategies for cancer treatment was first demonstrated by Ion Gresser in 1969 who observed reduced tumor growth in mice (Gresser & Bourali, 1969). Clinically, IFN α treatment was first applied for the treatment mainly of hematologic malignancies and some solid tumors such as melanoma and renal cancer (Aricò *et al*, 2019). After initial clinical success, the euphoria in the field about IFN α -based cancer treatments decreased. Reason for that was mainly the observation of severe side effects in treated patients spanning coupled with an unsatisfactory clinical response. IFN α was commonly administered systemically leading to an unfavorable biodistribution. Furthermore, IFN α has a relatively short half-live time (García-García *et al*, 2016). Therefore, in order to reach therapeutically significant levels in the TME, high levels of IFN α had to be given to patients at a short interval.

This triggered a number of acute and chronic side effects, which were observed in a dose dependent manner (Sleijfer *et al*, 2005; Aricò *et al*, 2019). In this context, Flu-like symptoms, including fever, chills and headache have been observed in an acute manner in nearly all treated patients. Severity, however, correlated with the treatment dose. These acute severe side effects normally only last for a few hours and can be managed pharmacologically. In the subacute and chronic phase, however, other more severe adverse events were reported. Hematological adverse events of grade 3-4 have been observed in about 26 % - 60 % of patients treated with a high dose. These hematologic side effects manifested in anemia, thrombopenia and leucopenia, especially in the neutrophil compartment (Soza *et al*, 2002). Additionally, in about 60 % of patients treated with a high dose of IFN α , hepatotoxicity at grade 3-4 was noted. Similar observations were made for gastrointestinal disorders manifested in nausea, loss of appetite, vomiting and diarrhea (Sleijfer *et al*, 2005). Also, psychiatric side effects such as depression was observed in 21 % - 58 % of patients (Raison *et al*, 2005). IFN α treatment was further associated in the context of autoimmune disorders. Occurrence of autoimmune disorders during IFN α -based immunotherapy approaches have even been considered as reporter for favorable treatment outcome (Sleijfer *et al*, 2005). Other side effects like cardiovascular, pulmonary, and endocrine disorders have been reported as well.

Similarly, to other targeted therapy and immunotherapy approaches, occurrence of resistance to IFN α treatment has been observed in several cases. This can be triggered by

downregulation of INFaR expression or dysregulation of the IFNaR signaling pathway in cancer cells (Zhang *et al*, 2010). Furthermore, chronic exposure to suboptimal doses of IFN α can lead to desensitization through ligand-induced receptor degradation also in immune cells (Hardy *et al*, 2009). The unfavorable pharmacodynamic availability of IFN α due to the systemic administration may further manifest this, as has been seen for other systemically applied drugs (Naldini, 2019).

Lately, new strategies have been developed to improve bioavailability of IFN α in the TME and reduce side effects (Aricò *et al*, 2019). This includes gene-based delivery approaches as further discussed below. This approach, which will be discussed in detail below, has shown to efficiently reduce tumor growth remodel the TME in prophylactic settings of murine models of CRC-LMS, thus, validating IFN α based treatments as valid strategy to overcome the immune suppressive TME in LMS and enable immune reactions (Escobar *et al*, 2014a, 2014b, 2018; Catarinella *et al*, 2016). The full potential of IFN α -based cancer treatments, however, remains to be realized.

1.7 Gene therapy

In the recent decade, gene therapy has gained a lot of attention as a new and innovative tool for the intervention of numerous different disease and conditions. It is based on the transfer of genetic material into target cells allowing replacement or reparation of defective genes or equipment target cells with new functions. Compared to the historical approach of conventional pharmacological interventions, which are based on the sometimes life-long repetitive administration of biological or chemical compounds with a direct effect, gene therapy provides revolutionary possibilities for the treatment of several different disease. Most prominent is the ability to permanently cure genetic disorders, which cause a variety of severe and life-long disease (Naldini, 2015). Recently, gene therapy has also been extensively exploited for the purpose of reprogramming target cells and equipping them with new functions. The most prominent example is Chimeric antigen receptor expressing T cells (CAR T cells) which provide a promising strategy in cancer treatment and have proven to be highly efficient in leukemic disease. One of the main advantages of gene therapy is that it allows exploitation of naturally occurring regulation mechanisms in order to specially and temporally regulate the expression biological agents.

Gene therapy is mostly divided into two different approaches. One is based on engineering of patient cells *ex-vivo*. For that purpose, cells are collected from the patient, cultured and engineered *ex-vivo* and afterwards reinfused into the patient. This approach has proven to be safe and very effective for engineering of several cell types as T cells or hematopoietic stem and progenitor cells (HSPCs) in bone marrow transplantation setting. *Ex-vivo* gene therapy however has certain restriction: target cells have to be cultivable *ex-vivo* and *ex-vivo* gene therapy is restricted to personalized approaches, hence time and cost intensive (Naldini, 2011; Elverum & Whitman, 2020). The second strategy relies on genetic engineering of target cells *in vivo*. This approach allows circumvention of some of the disadvantages for *ex vivo* gene therapy as it allows targeting of virtually every cell in the human body and *in vivo* gene therapy enables an off-the-shelf treatment hence is less time consuming. *In vivo* gene therapy, however, requires a close spatial and temporal regulation in order to ensure safe and selective genetic engineering of the target cells and prevent adverse events (van Haasteren *et al*, 2018).

1.7.1 Lentiviral vectors allow stable gene transfer in dividing and non-dividing cells

Several platforms have been developed to efficiently transfer genetic material into target cells and are commonly divided into viral and non-viral strategies. While non-viral delivery systems, which are mainly based of the usage of lipid nanoparticles, have proven to have a low immunogenicity, viral strategies are still more commonly used in clinical gene therapy approaches. The reason for that is their high gene transfer efficiency as well as their flexibility (Patil *et al*, 2019; Bulcha *et al*, 2021). Viral vector exploit the intrinsic capability of viruses to deliver genetic material into host cells. The large variety of viruses with their different characteristics and cell tropisms grants the flexibility of viral vector-based delivery systems. The choice of viral vector depends direct on the requirement of the gene transfer. If a transient gene transfer is required, hence the transferred gene is not required to be present in daughter cells, the most commonly used system is based adeno associated viral vectors (AAV). This system is capable of delivering DNA into the target cell, but not integrate it into the host genome which consequently means that it is not replicated upon cell division (Bulcha *et al*, 2021). For a stable gene transfer Human Immunodeficiency 1 (HIV)-based lentiviral vectors are most commonly used (Bulcha *et al*, 2021). HIV is an enveloped virus, which belongs to the family of Retroviridae and is

characterized by a single strand RNA genome. The main advantage of LVs compared to other Retroviridae-based viral vectors such as retroviral vectors is their capability to efficiently transduce non-dividing cells. This enables genetic engineering of HSPCs, hepatocytes, neurons and several other commonly non-dividing cells (Naldini *et al*, 1996). During the process of infection, the viral genome is reverse-transcribed into double-stranded DNA and integrated into the host genome. Integration appears to be random with a bias for benign integration sites confirming its safety (Biffi *et al*, 2011).

The most important modification to create a viral vector from a virus is the deletion of its capability to replicate. For LVs the most successful strategy relies on separation of *trans*- and *cis*-acting elements. *Trans*-acting elements are necessary for the formation of LVs but are not required for efficient transduction of target cells. This includes viral structural proteins giving rise to the viral envelope as well as the retro transcriptase which is co-packaged into the LV. *Cis*-acting elements describe the parts of the LV genome which are necessary for efficient genome packaging into the LV and gene transfer into the target cells (Verma & Weitzman, 2005). Only viral particles that contain the genome coding for all *trans*- and *cis*-acting elements give rise to replication competent viruses. In order to prevent production of replication competent viruses during the production of LVs, *trans*- and *cis*-acting elements are separated into different plasmids. In third generation LVs, the *trans*-acting elements are divided into three separate plasmids, namely pMDL, pRev and pEnv. The pMDL contains group-specific antigen sequence (Gag), which encodes for structural proteins, and the DNA polymerase sequence (Pol) encoding for enzymes as reverse transcriptase and integrase. The pRev encodes for rev protein, which is required for the nuclear export of the full-length viral RNA. Finally, the pEnv encodes for the viral envelope protein. The viral envelope protein determines the tropism of the viral vector as it induces attachment as well as entry to a cell. Most commonly, LVs are pseudotyped with the envelop of vesicular stomatitis virus glycoprotein (VSVG) which gives rise to a broad tropism (Hastie *et al*, 2013). However, pseudotyping with other viral glycoproteins as well as engineering of the envelop protein is a valid strategy to generate LVs with a desired tropism (Frank & Buchholz, 2019; Hastie *et al*, 2013). The transgene, which is supposed to be delivered by the LV is flanked by the *cis*-acting elements on the so-called transfer vector ensuring efficient packaging into the LV. This strategy of dividing the viral genes into four separate plasmids ensures

that the chance of generating a replication competent virus is reduced to a minimum, even considering potential recombination events (Verma & Weitzman, 2005). Packaging capacity of LVs, is considered to be about 10 kb (Sweeney & Vink, 2021). For LV production, these plasmids are transfected into producer cells, which will consequently release LV particles into the culture supernatant. Several steps of purification ensure generation of high-quality LV stocks and a high concentration of functional viral particles which is pivotal importance especially for *in vivo* gene therapy approaches (Soldi *et al*, 2020).

In general, LVs provide a favorable safety profile for *in vivo* gene therapy. This is mostly due to the low level of pre-existing immunity in humans. Pre-existing immunity against the viral vector of choice is a major problem for the implication of *in vivo* gene therapy for many types of viral vectors. Even the presence of low amounts of viral vector specific neutralizing antibodies can dramatically decrease the gene transfer efficiency due to rapid clearance of viral vector from the bloodstream mediated by neutralizing antibodies (Aronson *et al*, 2019). While levels of preexisting immunity for several viral vectors tested for *in vivo* gene therapy is substantial, rendering a high number of patients not eligible, only about 20 % of HIV infected people develop neutralizing antibodies which is a total of 0.16 % of the human population (Doria-Rose *et al*, 2010; Cantore & Naldini, 2021).

Due to their high safety and efficiency profile, LVs are investigated as potential tools for the treatment of numerous genetic disorders, leading to several preclinical and clinical trials ongoing. Currently, there are about 315 LV-based clinical trials ongoing worldwide targeting different genetic disorders (Bulcha *et al*, 2021). These trials include β -thalassemia (Cavazzana-Calvo *et al*, 2010; Markt *et al*, 2019), X-linked severe combined immunodeficiency (de Ravin *et al*, 2016) and Wiskott–Aldrich syndrome (Bosticardo *et al*, 2014). Recently after intensive preclinical and clinical studies, a new LV based gene therapy approach for metachromatic leukodystrophy called Libmeldy has reached marked approval by the European commission, further confirming the successful journey of LVs (Sessa *et al*, 2016; Biffi *et al*, 2013, 2006).

1.7.2 Regulatory elements in gene therapy

As previously discussed, LVs allow insertion of genetic material into the host cell DNA leading to expression of the delivered transgene. One of the challenges of gene therapy is insuring that transgene expression is restricted to target cells in a spatial and temporal manner. In order to prevent undesired transgene expression in off target cell types or differentiation status, a tight regulation is required. The first layer of regulation is based on the restriction of transduction to certain target cells. This is especially important for *in vivo* gene therapy strategies and can be achieved by pseudo typing, as discussed previously (Hastie *et al*, 2013; Frank & Buchholz, 2019). Advanced engineering of the viral capsid, however, often leads to decreased transduction efficiency on target cells as well. A second layer of regulation is achieved by controlling the transgene expression on a transcriptional and posttranscriptional level. Naturally occurring regulatory mechanisms can be explored. For the transcriptional control, enhancer and promotor regulatory elements with a desired expression profile are used (Poletti & Mavilio, 2021). For posttranslational control, mircoRNA (miRNA) target sites (miRT) can be incorporated downstream to the transgene to prevent its expression in certain cell types. miRNAs are small RNAs that prevent expression of messenger RNA (mRNA) based on RNA interference. To harness miRNAs as a tool to regulate gene expression, miRTs can be incorporated in tandem into the LV design. Hence, transgene expression will be suppressed in cell types expressing the miRNA (Geisler & Fechner, 2016). Examples for successful exploitation of miRT sites for controlling transgene output in LV-based gene therapy strategies is exploitation of the miRT-122a for suppression of transgene expression in hepatocytes (Annoni *et al*, 2009). Furthermore, in the setting of transplantation of genetically engineered HSPCs, the miRT-126 has been incorporated to the LV design for the suppression of transgene expression in HSPCs (Gentner *et al*, 2010). Indeed, a clinical study for the treatment of glioblastoma multiforme has been initiated which is based on targeted IFN α expression in in tumor infiltrating cells derived from engineered HSPCs (NCT03866109, <https://clinicaltrials.gov/>). The LV design for HSPC engineering also exploits the miRT-126 to avoid transgene expression in progenitor cells (Escobar *et al*, 2014b; de Palma *et al*, 2008; Escobar *et al*, 2018; Catarinella *et al*, 2016; Escobar *et al*, 2014a).

1.8 Gene therapy approaches in oncology

Gene therapy has been largely exploited for gene repair and gene replacements strategies. Recently, however, gene therapy has also gained increasing attention in the field of oncology with remarkable clinical success for some tumor types. Different strategies for cancer gene therapy have been developed which can either aim at a direct effect on the cancer cells or on a remodeling of the microenvironment to enable immune reactions. Direct targeting of cancer cells often relies on delivering and expressing suicide genes in cancer cells such as TNF-related apoptosis-inducing ligand (Jeong & Yoo, 2020; Jia *et al*, 2012). Another approach is based on reduction of tumorigenicity by either expression of a tumor suppressor gene or suppression of an oncogene by siRNA or microRNA. A third strategy describes the overexpression of highly immunogenic antigens in cancer cells in order to increase immunogenicity of tumor cells and hence increase the antitumoral immune response (Das *et al*, 2015). Direct targeting of cancer cells is achieved by using oncolytic viruses. They are replication competent viral particles that have a strong and selective tropism for cancer cells. Several different strategies exist to restrict their infection and replication to cancer cells. Despite a high number of clinical trials being performed, clinical success of these strategies, however, is limited so far, mainly due to safety concerns (Lawler *et al*, 2017; Santos Apolonio *et al*, 2021).

The second strategy consists of combining targeted cancer immunotherapy with gene therapy. Here, gene therapy is exploited to modulate the immune system to enable antitumoral immunity. This approach allows direct armoring of the immune system in order to induce or strengthen an antitumor immune reaction. Chimeric antigen receptor (CAR) T cells represent the most famous and clinically most advanced product in this context and will be discussed in further detail below. However, also engineering of other cells such as macrophages and natural killer cells (NK cells) are being investigated (Chen *et al*, 2021b; Xie *et al*, 2020a). Boosting of the antitumor immune reaction can also be achieved by expression of immune modulatory molecules at the site of the tumor, such as immune activating cytokines or checkpoint inhibitors to circumvent immune evasion mechanisms.

1.8.1 CAR T cell therapy

Introduction and development of CAR T cells are considered a major breakthrough for cancer therapy. CAR T cells are characterized by the expression of a chimeric antigen receptor which is an artificial transmembrane protein comprised by an extracellular binding domain, a transmembrane domain and an intracellular signaling domain. The mechanism of action of a CAR is the similar to an endogenous T cell receptor (TCR). Target cells as cancer cells are recognized by the extracellular domain. Upon target binding by the extracellular domain, an intracellular signaling cascade is activated leading to activated effector function of the T cell.

For the extracellular binding domain, commonly tumor antigen specific single-chain variable fragments (scFv) are used and determine the specificity of the CAR to tumor cells. The main advantage of scFv usage as extracellular domain compared to conventional TCRs is the independence of MHC presentations. While for recognition of tumor antigens by TCRs, presentation by MHCI or MHCII is required, the scFv of a CAR can bind any protein expressed on the surface of a target cell. On the other hand, the CAR-based approach is restrictive to surface proteins (Zhao *et al*, 2021; Hartmann *et al*, 2017; June *et al*, 2018). The intracellular signaling domain is derived from CD3 ζ , the intracellular signaling domain of a TCR. Over the years, the intracellular signaling domain has been further developed and equipped with costimulatory molecules such as CD28 or 4-1BB to increase effectiveness of CAR T cells in terms of proliferation, cytokine release, resistance to paracrine and endocrine inhibitory signaling and decreased exhaustion profile (June *et al*, 2018).

CAR T cells are normally applied in an autologous T cell transfer setting. T cells are collected from patient derived peripheral blood, genetically engineered and infused back into the patient. For genetic engineering viral vectors allowing stable integration of the CAR-encoding sequence into the T cell genome, such as LVs, are used (Levine *et al*, 2017). In order to improve time and cost effectiveness, several attempts have been made to allow selective LV-based genetic engineering of T cells *in vivo*. Despite initial success, further development of these technologies are required to improve the safety and efficiency profile (Frank *et al*, 2020; Pfeiffer *et al*, 2018; Zhou *et al*, 2015).

Especially for CD19 positive B cell lymphoma, CAR T cells have led to an overwhelming clinical success. Treatment of patients with CAR T cells directed against the B cell surface marker CD19 induced effective and long-lasting clinical responses. About 51 % of patients showed a complete response duration of at least 3 years (Cappell *et al*, 2020). This success has ultimately led to marked approval by the FDA in 2017 (Anagnostou *et al*, 2020). As CD19 is expressed by the majority of circulating B cells, treatment with a CD19 directed CAR T cell product induced live-long depleting of B cells in patients which can be considered a tolerable adverse event. However, it underlines the importance of the choice of the target antigen (Cappell *et al*, 2020).

Despite the success observed in hematologic malignancy, there are many challenges remaining for CAR T cells. The biggest challenge is the ineffectiveness of CAR T cells in solid tumors. Regardless of many attempts to improve their efficiency, clinical success for solid tumors remains poor. The major challenge is the low infiltration of CAR T cells into solid tumors as well as the strong immunoinhibitory signaling in the TME leading to an exhausted phenotype of CAR T cells (Marofi *et al*, 2021). This applies as well for the treatment of liver metastasis. Burga *et al* have shown that intrahepatic administration of CAR T cells increases the amount of CAR T cells present in the LMS, efficiency, however, remains low (Burga *et al*, 2015). The previously discussed immune suppressive environment provides an additional barrier. Engagement of systemically administered cytokines such as IL-12 have shown an increase efficacy of CAR T cells in some solid tumors by reprogramming the TME (Chi *et al*, 2019). Therefore, development of new and innovative strategies to reprogram the TME towards an immune activating milieu might provide a valid strategy to enable CAR T cell therapy for solid tumors.

1.8.2 Tie2.IFN α -based gene therapy

An interesting example for application of gene therapy to modify the tumor microenvironment has been developed over the recent years by the group of Naldini. It is based on the usage of tumor infiltrating macrophages and TAMs to be used as vehicles for delivering of the immune activating cytokine IFN α to the tumor. In 2003 De Palma *et al* discovered a population of monocytes which is characterized by the expression of Tie2 (Tie2-expressing monocytes/TEMs). Interestingly, TEMs were exclusively found in the TME but not in other tissues and Tie2 expression in hematopoietic cells was mainly

restricted to TEMs hence allowing exploitation of TEMs as vehicles to the tumor. For that purpose, HSPCs are transduced *ex vivo* with a LV delivering a cDNA coding for IFN α under the control of the Tie2-promotor and enhancer regulatory element and the mirT. Mice transplanted with these engineered HSPCs showed a selective release of IFN α in the TME of different tumor types (de Palma *et al*, 2003). This strategy has been further developed by integration of the miRT-126 and mirT-130a to further restrict transgene expression to TEMs and has been shown to effectively reduce tumor growth in several different murine tumor models, including an experimental model of CRC derived liver metastasis. Reduced tumor growth was combined with an efficient reprogramming of the TME. Among others, the authors observed a polarization of the macrophage compartment towards a proinflammatory M1-like phenotype as well as a reduced exhaustion profile in the T cell compartment. This was manifested by reduced expression of the exhaustion markers PD1, Lag3, Tim3 and others (de Palma *et al*, 2008; Escobar *et al*, 2014a, 2014b; Catarinella *et al*, 2016). Interestingly, this strategy has been shown to synergize with the tumor specific CAR T cell and TCR-engineered T cells hence overcoming the immune inhibitory signaling of the TME in a murine model of leukemia. Thus, this provides further evidence that delivery of immune activating cytokines to the TME is a valid strategy for efficient reprogramming of the TME towards an immune activating state, which allows effective antitumor immune reactions (Escobar *et al*, 2018). Based on these promising results, an open label phase I/IIa clinical trial has been initiated by for the treatment of glioblastoma multiforme patients (NCT03866109, <https://clinicaltrials.gov/>).

1.9 Liver directed *in vivo* gene therapy

Due to its central role in metabolism, a high number of inherited metabolic disorders has its origin in the liver. Therefore, the liver has been intensively investigated as a target for gene therapy. One of many promising examples for that is the gene therapy-based treatment of patients with ornithine transcarbamylase deficiency, a rare genetic disorder with an estimated frequency of about 1 in 50.000 to 80.000. DTX301, an AAV8-based gene therapy product conveying an ornithine transcarbamylase encoding cDNA to hepatocytes which has shown promising results in phase I/II clinical trials (Wang *et al*, 2012, NCT02991144, NCT03636438, NCT04717453, <https://clinicaltrials.gov/>). The liver is not only a valid target for gene replacement strategies for the treatment of genetic disorders with hepatic origins. With their high abundance and efficiency in producing and

secreting proteins, hepatocytes can be used as factories for protein replacement strategies in plasma protein deficiencies or protein deficiencies in distant organs (Naldini, 2015). In this context, liver directed gene therapy is also intensely investigated as replacement strategy for hemophilic disease with several ongoing clinical trials (Perrin *et al*, 2019; Leebeek & Miesbach, 2021). Interestingly, AAV8 mediated expression of glycine N-methyltransferase in the liver has shown to delay progression of hepatocellular carcinoma, confirming the applicability of liver directed gene therapy for hepatic cancer treatment (Fang *et al*, 2018).

1.9.1 Lentiviral vector-based liver targeting

The vast majority of liver-directed gene therapy strategies are based on AAV derived viral vectors (Cantore & Naldini, 2021; Naldini, 2015). Transgene expression is however lost during liver growth, regeneration or homeostatic turnover of liver cell populations. Additionally, preexisting immunity is a challenge, as previously discussed. To overcome these obstacles, lentiviral vector-based liver gene therapy has been suggested. Stable integration of the transgene would no longer exclude treatment of pediatric patients, in which hepatocytes still undergo a high number of replication cycles (Cantore & Naldini, 2021). To that end, biodistribution studies in mice and non-human primates have shown a strong transduction bias towards the liver and, in part, the spleen upon systemic administration of VSVG-pseudo typed lentiviral vectors (Peng *et al*, 2001; Milani *et al*, 2019). Liver targeting is mostly provided by the high expression of the low-density lipoprotein receptor in hepatocytes, which serves as entry receptor of VSVG pseudo typed LVs, as well as active phagocytosis of LVs in the sinusoids by KCs and LSECs (Tao *et al*, 2001; Cantore & Naldini, 2021). Accordingly, more detailed analysis of the liver revealed a high transduction rate of KCs, plasmacytoid DCs and, to lower extend, LSECs and hepatocytes. In the same study, the authors revealed a strong involvement of the phagocytosis-shielding protein CD47 in the process. When CD47 is present to high amounts on the surface of LVs, transduction rate of hepatic macrophages was found to be reduced whereas absence of CD47 increased uptake of LVs by KCs in the liver (Milani *et al*, 2019). Importantly, integration events in the liver were found to be safe and no signs of genotoxicity or enhanced hepatic tumor formation in tumor-prone mice models were observed (Cantore *et al*, 2015). Clinical relevance of LV mediated liver directed gene transfer is provided by successful treatment of hemophilic mice with a systemic injection

of factor IX-conveying VSVG-LV which led to long-term curation reflected by persistence of viral particles in the liver, increased levels of factor XI in the plasma and reduced bleeding events (Cantore *et al*, 2015). Due to their safety and biodistribution profile, LVs represent a valid tool for liver-directed *in vivo* gene therapy with promising prospects for clinical translation.

2 Aim of this work

Despite recent advances in cancer treatment based on immunotherapy approaches, complete and durable responses are observed only in a small fraction of patients (Sambi *et al*, 2019). The main reasons for the underperformance of immunotherapies especially in solid tumors are the strongly immunosuppressive tumor microenvironment and the intratumor heterogeneity which in combination allow development of treatment resistance mechanisms. This is especially true for liver metastasis due to the intrinsically immunosuppressive hepatic environment (Yu *et al*, 2021). Indeed, up to now there is no promising and effective treatment for unresectable liver metastasis (Gholami *et al*, 2021; Brouwer *et al*, 2018). Therefore, overcoming the immunosuppressive microenvironment to enable antitumoral immune reactions may be key for opening the field of immunotherapies to the treatment of LMS and ultimately develop effective therapeutic strategies.

Several studies have shown that immunostimulatory cytokines such as IFN α contain the potential to reprogram the TME and foster antitumoral immune responses in several tumor types including CRC LMS (Catarinella *et al*, 2016; Ferrantini *et al*, 2007). However, applicability of such cytokines in clinical settings is strongly reduced due to the occurrence of severe adverse events upon systemic administration (Sleijfer *et al*, 2005). However, tumor-specific delivery may overcome this obstacle enabling high local concentration of immunostimulatory cytokines while sparing side effects. A valid strategy consists of controlled local release of cytokines using tumor infiltrating cells as a trojan horse (Escobar *et al*, 2018).

Here, we aim to develop a LV-based platform that allows selective genetic engineering of Kupffer cells *in vivo*. By further exploiting the distinct transcriptional phenotype of tumor-associated macrophages, this allows the usage of KCs as vehicles to selectively deliver IFN α to the TME of LMS. Furthermore, we aim to investigate the safety and efficiency of such approaches in preclinical models. For a better understanding of what may drive resistance mechanisms in this approach as well as immunotherapies triggering stimulation of IFN α -responsive genes, we further intend to study the mechanism underlying the therapeutic effect as well as the resistance. For that purpose, we are

planning to intensively characterize the reprogramming of the TME triggered by the tumor specific IFN α delivery.

3 Results

The liver hosts an immune suppressive environment favoring metastatic seeding and proliferation of cancer cells. Pharmacological treatments, including immunotherapies, fail in the presence of liver metastases (LMS). Here we target the unmet need of developing a potent immunotherapy, which is capable of overcoming the strongly immunosuppressive liver environment and enable immune responses against liver metastasis. The strategy relies on gene-based delivery of immune activating cytokines to LMS exploiting Kupffer cells as vehicles.

3.1 Development of a KC specific *in vivo* gene delivery platform

First, we aimed on the development of a lentiviral vector-based platform that enables selective engineering of Kupffer cells *in vivo*. Previous reports, including from our own group, have shown that KCs are highly transduced upon systemic delivery of VSVG-pseudo typed LVs. Building on these premises we set out to restrict transgene output to KCs by inserting regulatory elements to the LV design such as cell-type specific promoters and microRNA target sites.

3.1.1 Engagement and characterization of the MRC1 promoter

MRC1 is a type 1 transmembrane protein which is expressed in macrophages, including tissue resident macrophages as Kupffer cells. Importantly, it is upregulated in alternatively activated M2-like macrophages, hence it is preferentially expressed in tumor-associated macrophages (TAMs) (Squadrito *et al*, 2012). In order to restrict transgene expression of the KC-LV to Kupffer cells with preferential expression at the tumor site, we are aiming at leveraging the spatiotemporal transcription profile of *Mrc1* gene by controlling transgene expression with an *Mrc1* promoter.

In order to generate a murine *Mrc1* promoter a region of 1.8 kb length upstream to the *Mrc1* open reading frame was identified using the USCS murine gene browser. It contains a 284 bp sequence with promoter like signatures and shows high conservation compared to the same locus in human as well as other vertebrates. This sequence was incorporated in an LV-transfer vector upstream to a green fluorescent protein (GFP) coding sequence originating the *Mrc1*.GFP LV. We then transduced bone marrow-derived macrophages (BMDMs) obtained from C57BL6 mice with either the *Mrc1*.GFP LV or an LV driving GFP expression under the control of the constitutively expressed human PGK promoter

(*PGK.GFP LV*). Upon stimulation of transduced BMDMs with either LPS in combination with $IFN\gamma$ (M1 polarization) or IL4 (M2 polarization)

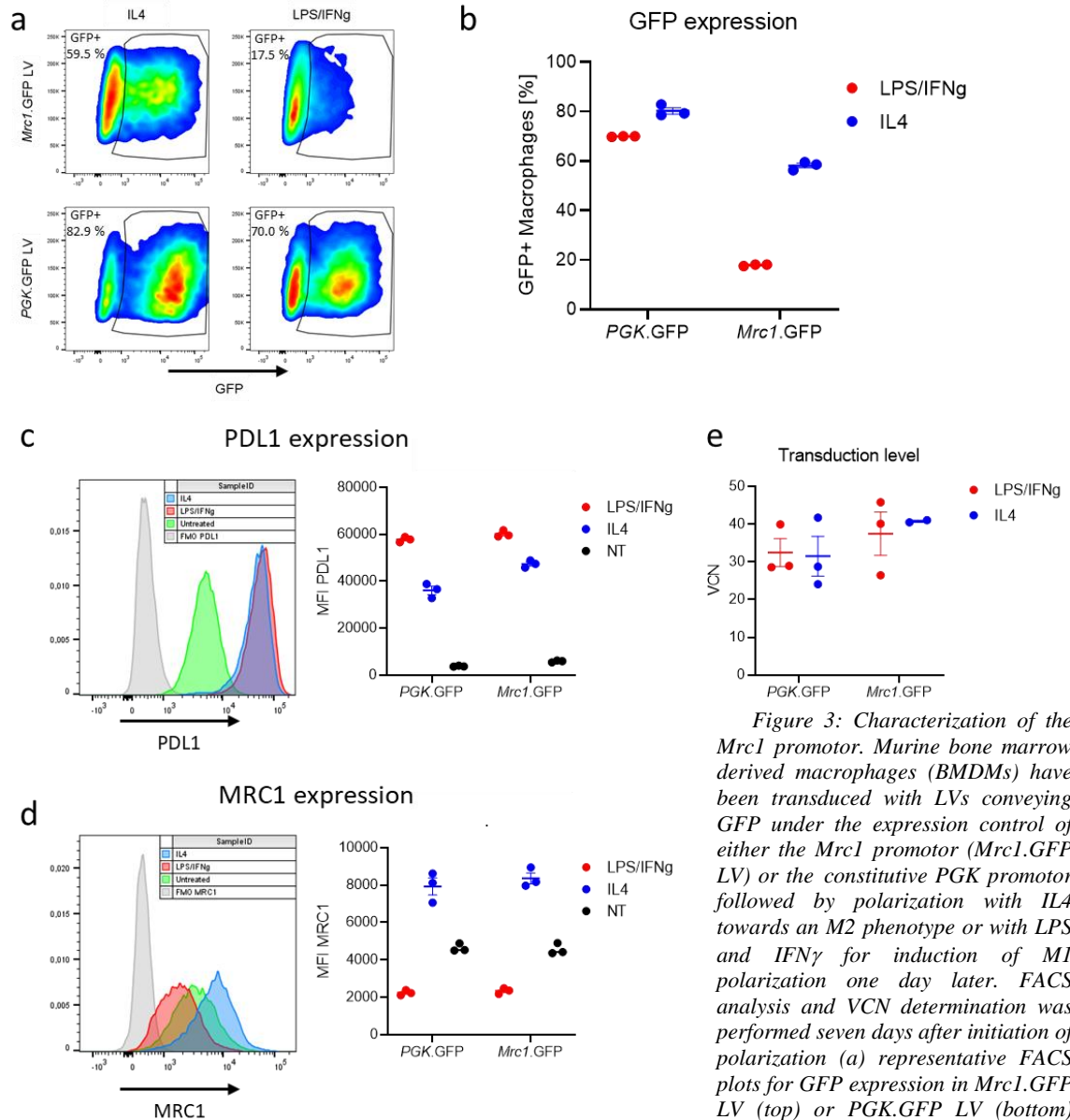


Figure 3: Characterization of the *Mrc1* promoter. Murine bone marrow derived macrophages (BMDMs) have been transduced with LVs conveying GFP under the expression control of either the *Mrc1* promoter (*Mrc1.GFP LV*) or the constitutive *PGK* promoter followed by polarization with IL4 towards an M2 phenotype or with LPS and $IFN\gamma$ for induction of M1 polarization one day later. FACS analysis and VCN determination was performed seven days after initiation of polarization (a) representative FACS plots for GFP expression in *Mrc1.GFP LV* (top) or *PGK.GFP LV* (bottom) transduced BMDMs polarized with IL4 (left) or LPS plus $IFN\gamma$ (right).

(b) Quantification of GFP expression in the flow cytometry analysis. (c-d) PDL1 and MRC1 expression on polarized and untreated BMDMs, respectively. Left, representative histogram and right quantification of the mean fluorescence intensity (MFI). (e) Transduction level (VCN) in the different conditions ($n = 3$ biological replicates).

we found that the *Mrc1.GFP LV* drove transgene expression in M2, but not in M1 BMDMs (Figure 3a and b), whereas the *PGK.GFP LV* drove transgene expression independently of BMDM polarization status. Efficient polarization has been confirmed by increased PDL1 expression in both M1 and M2 polarized macrophages compared to unstimulated macrophages. Furthermore, M2 polarized macrophages showed increased

expression of MRC1, a typical marker of alternatively activated macrophages (Figure 3c and d). By determination of the vector copy number (VCN), we confirmed that all cells have been transduced to a high extent with an average 40 to 60 vector copies per cell in all conditions (Figure 3d).

Taken together, these data confirm functionality of the *Mrc1* promoter in macrophages as well as its capability to restrict transgene expression to alternatively activated M2-like macrophages.

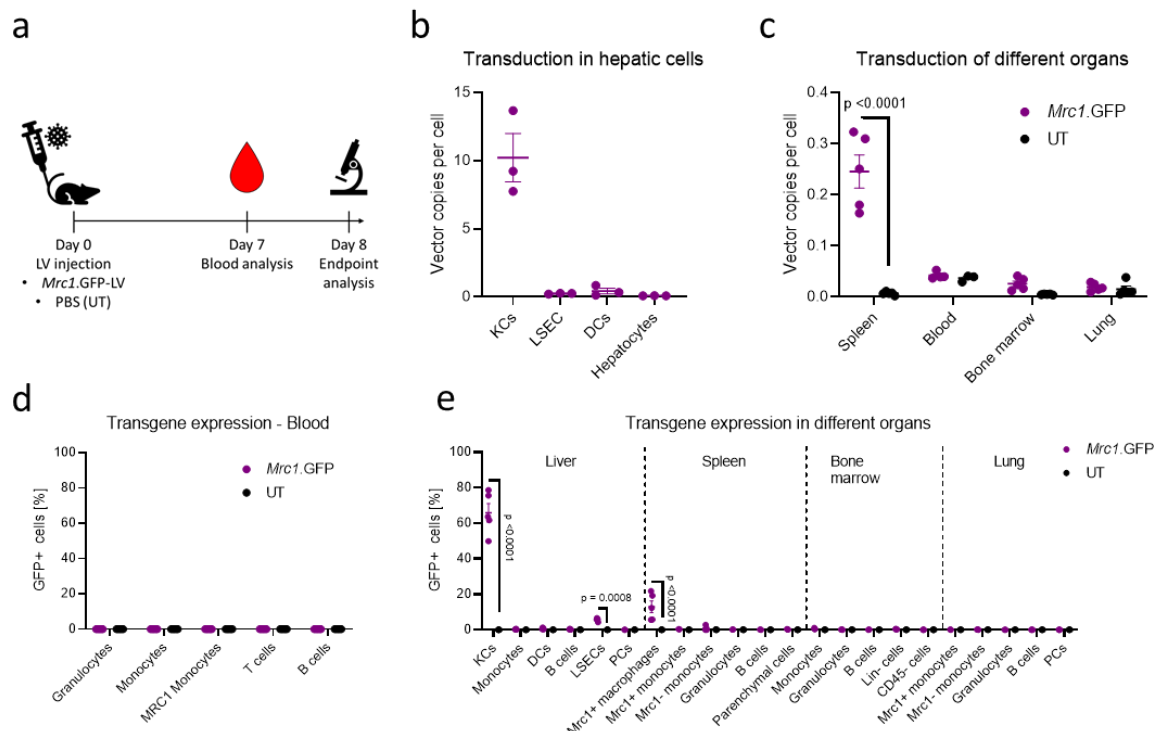


Figure 4: In vivo biodistribution analysis of the MRC1 LV. NUDE mice were injected with either 3×10^8 TU *Mrc1.GFP* LV diluted in PBS (*Mrc1.GFP*) or PBS only as control (UT) by tail vein injection. (a) Time line of the experiment. (b) VCN analysis performed by ddPCR on DNA extracted from sorted liver populations ($n=3$ biological replicates). (c) VCN analysis on different organs ($n=5$ biological replicates/2way Anova with Sidak correction). (d) GFP expression in different blood cell populations by flow cytometry analysis ($n=5$ biological replicates). (e) GFP expression in different blood cell populations in liver, spleen bone marrow and lung by flow cytometry analysis ($n=5$ biological replicates; Statistics: 2way Anova with Sidak correction).

3.1.2 In vivo bio distribution analysis of the MRC1 LV

After confirmation of the capability of the *Mrc1* promoter to drive transgene expression in M2-polarized macrophages, we delivered the *Mrc1.GFP* LV systemically to mice in order to determine the *in vivo* biodistribution and transgene expression of this construct. For that purpose, we employed immune suppressed NUDE mice, which cannot generate mature T lymphocytes due to a deletion in the *FOXN1* gene, hence avoiding potential GFP-directed immune reactions. Mice were treated with an intravenous

injection of 3×10^8 transducing units (TU) per mouse of the *Mrc1*.GFP LV in PBS, while control mice were injected with only PBS (Figure 4a). As previously shown, the liver is highly transduced upon systemic LV delivery. To determine which cellular compartments in the liver were transduced, we isolated by flow cytometry-based sorting Kupffer cells, hepatocytes, LSECs and DCs and determined the VCN in each compartment individually. In KCs we found a high transduction rate with about ten copies per cells, whereas LSECs, DCs and hepatocytes were transduced only to a low extent at this dose (VCN of 0.2, 0.35 and 0.09 respectively, Figure 2b). Regarding other biological compartments, we only observed vector copies in the spleen, but not in blood, bone marrow or lungs (Figure 4c). To address transgene expression more in detail, we analyzed GFP expression in distinct biological compartments by using flow cytometry. In the liver, we found high transgene expression in about 70 % of Kupffer cells whereas no transgene output was observed in monocytes, DCs, B cells and other parenchymal cells. Only in LSECs GFP expression was observed in about 5 % of cells. In the spleen, which was identified as the only other organ actively transduced upon systemic LV injection, we observed transgene expression only in about 13 % of MRC1-expressing macrophages, while all other cell types were GFP negative. In line with the observation of VCN in different organs, we did not observe transgene expression in any cell type in the blood, bone marrow and lung (Figure 4d and e).

Taken together, controlling transgene expression with the *Mrc1* promoter allows to restrict transgene expression to KCs, LSECs and splenic macrophages.

3.1.3 Integration of miRT sites fine-tunes transgene expression to Kupffer cells

To increase the specificity of the *Mrc1*-driven LV in macrophages, we incorporated miRNA target sequences (miRTs) in the LV design that suppress transgene expression in off target cell types. Besides KCs, the target cell type of our LV platform, transgene expression was observed in LSECs as well as in MRC1-expressing splenic macrophages as previously described. As previously shown by our group, hepatocytes can be transduced efficiently upon systemic delivery of LVs in non-human primates (Milani *et al.*, 2019). Therefore, we also identified hepatocytes as a potential off target cell type due to its high abundance in the liver. We assess the ability of the miRTs to abate transgene expression in the target cells by employing a bidirectional LV, which drives the expression of two independent transcripts, i.e., a truncated low affinity nerve growth

factor receptor (dLNGFR, an inert membrane protein used as normalizer), and the GFP. Downstream to the GFP sequence in the bidirectional LV, we incorporated four copies of microRNA target sequences for miR-126-3p (miRT126 LV), expressed by LSECs (Li *et al*, 2022), miR-122-5p (miRT122 LV), expressed by hepatocytes (Annoni *et al*, 2009) or miR-451 (miRT451 LV), expressed by splenic macrophages (Rose *et al*, 2021) (Figure 5a).

The miRT LVs were delivered systemically to immune deficient mice (NUDE mice) at a dose of 3×10^8 TU per mouse and six days after treatment GFP expression was evaluated by flow cytometry for KCs, LSECs and splenic macrophages, and by immune fluorescence for hepatocytes. VCN of around 0.2 in the liver of individuals of all treatment confirmed efficient transduction of the liver. Furthermore, similar expression level of LNGFR in different cell types in the animals from all treatment groups confirmed that incorporation of miRTs did not alter the bio distribution by itself (Figure 5b-d). As depicted in Figure 5e, incorporation of the miRT-126 was able to efficiently suppress GFP expression about 17-fold in LSECs while controlling transgene expression by miRT-122 and miRT-451 did not induce any changes in transgene output in LSECs. In a similar way, miRT-122 significantly suppressed the expression of GFP in hepatocytes, represented by the amount of GFP expressing hepatocyte per frame in an immunofluorescence analysis (Figure 5f and g). Incorporation of miRT-451 did not have any effect on GFP expression in splenic macrophages or any other cell type analyzed in this setting. Of note, transgene expression in KCs was preserved independent of incorporation of miRTs.

These results indicate that addition of the miRT-122 and miRT-126 to the LV design efficiently de-target transgene expression from LSECs and hepatocytes. Building on this result, we incorporated four copies of the miRT122 and four copies of the miRT126 sequences to the *Mrc1*.GFP LV design downstream to the woodchuck hepatitis virus posttranscriptional regulatory element (WPRE) originating the *Mrc1*.GFP.miRT LV.

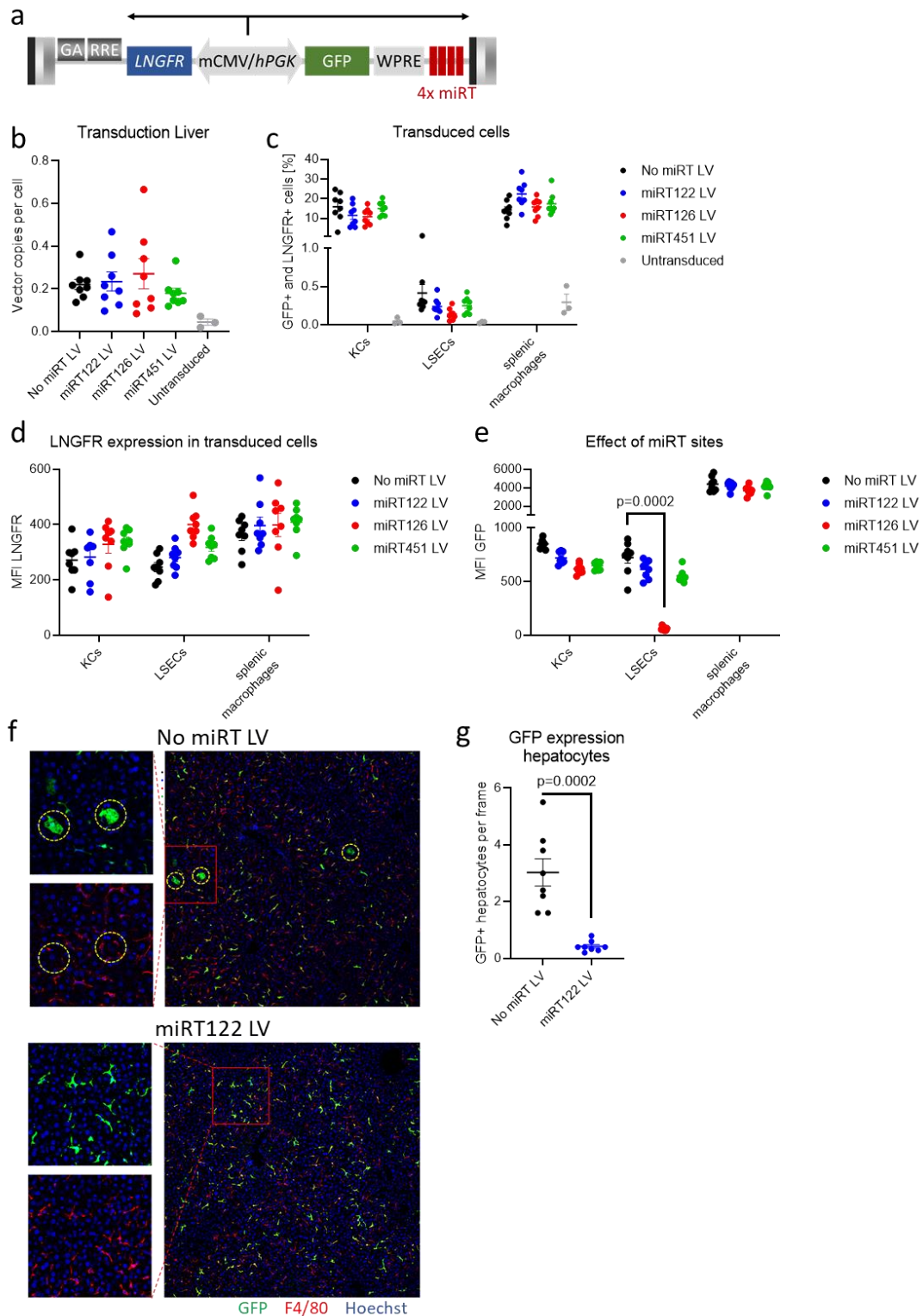


Figure 5: Screening of miRT sites. (a) vector design used for the assessment of miRT activity in different populations. NUDE mice were injected with a dosis of 3×10^8 TU diluted in PBS of the LV containing the indicated miRT sequences. Endpoint analysis was performed seven days after LV injection. (b) VCN analysis of the liver tissue. (c) Frequency of transduced cells (GFP+ and LNGFR+ cells) within KCs, LSECs and splenic macrophages addressed by flow cytometry analysis. (d) Flow cytometric assessment of MFI of LNGFR expression on transduced cells within the individual populations. (e) MFI of GFP expression on transduced cells by flow cytometry. (f)

representative immunofluorescence images of the liver of mice treated with the LV not containing any miRT site (top) and the miRT122 LV (bottom) stained for GFP (green), F4/80 (red) and Hoechst (blue). The image on the right shows a merge of all channels while the left shows a zoom into of the indicated zone (red line) with the overly of GFP and Hoechst (upper) and F4/80 and Hoechst (lower). (g) quantification of the amount of transgene positive hepatocytes per frame. Each dot represents the average of 5-6 images per mouse acquired at a 10X magnification (n=8 biological replicates; Statistics: nonparametric T test (Mann-Whitney test)).

3.1.4 Transgene expression is enhanced in close proximity to liver metastasis

Next, we investigated transgene product expression driven by the *Mrc1*.GFP.miRT LV in the presence of experimental liver metastasis.

To this aim, we employed a MC38-based mouse tumor model. MC38 cells are a murine colorectal carcinoma cell line with a background in the C57BL6 mouse strain. We engineered this cell line to express a membrane-bound version of the fluorescent protein mCherry in order to facilitate identification of tumor cells by immunofluorescence. For that purpose, we transduced MC38 cells with a lentiviral vector conveying a sequence for mCherry fused to the N terminus of the transmembrane protein CD81 under the control of the constitutively expressed human PGK promoter.

NUDE mice were injected with 3×10^8 TU/mouse of either the *Mrc1*.GFP LV or the *Mrc1*.GFP.miRT LV in order to allow a direct analysis of the influence of the incorporation of the miRT sites. Ten days after LV injection, we transplanted 500.000 MC38-mCherry cells per mouse by intrahepatic injection in a surgical procedure, which lead to efficient development of LMS in all animals. Two weeks after tumor transplant, we performed an endpoint analysis.

We found integrated vector copies only in the liver (VCN of ~0.3) and the spleen (VCN of ~0.1) in both treatment groups. Inguinal lymph nodes, small intestine and brain remained untransduced (Figure 6a). To exclude even rare events of tissue resident macrophages with phagocytic activity in these tissues, we performed immunofluorescence analysis. No GFP positive events have been observed in treated animals in any of these tissues (data not shown).

Highest level of GFP expression for the *Mrc1*.GFP LV as well as the *Mrc1*.GFP.miRT LV was observed in KCs. Importantly, transgene produce expression was abated in LSECs upon incorporation of the miRT (5 % for *Mrc1*.GFP LV and 0.5 % for *Mrc1*.GFP.miRT LV treated animals) confirming the functionality of the miRT-126 (Figure 6b). In all other cell types, namely B cells, cDCs and pDCs, no transgene

expression was observed. FACS analysis of the spleen revealed transgene expression in about 15 % of splenic macrophages, independent of the incorporation of the miRT sites.

In order to determine if a certain population of splenic macrophages is transduced to a higher extent, we performed an immunofluorescence analysis of the spleen with a co-staining for CD31, expressed by endothelial cells, F4/80, a marker for macrophages with high expression in tissue resident macrophages, and GFP. Analysis revealed that exclusively macrophages in the red pulp and the marginal zone express the transgene whereas no GFP positive events can be observed in the white pulp. This observation is consistent across both treatment groups (Figure 6c and d).

Next, we addressed transgene expression in the liver with regards to the tumor by immunofluorescence analysis. By the mCherry signal, tumor sites can be clearly defined and are characterized by high amounts of F4/80 positive macrophages present inside the tumor. Interestingly, some tumor associated macrophages close to the boarder of the tumor are GFP positive. In agreement with previous results, in the hepatic region co-staining for GFP, F4/80 and mCherry revealed high numbers of GFP and F4/80 double positive cells confirming robust transgene expression by KCs. Importantly, we found that transgene product expression, measured as GFP positive area, was statistically significantly increased in regions located in close proximity to liver metastases (distance to the tumor less than 200 μm) than in tumor distant hepatic regions (distance to the tumor more than 200 μm) (Figure 6e and f). This was evident not only for the *Mrc1*.GFP.miRT LV but also for *Mrc1*.GFP LV- injected mice confirming that the tumor specificity is conveyed by the *Mrc1* promotor and not by the miRT sites.

In summary, we generated an LV-based *in vivo* gene delivery platform, called KC-LV, which allows selective transgene expression in Kupffer cells. Remarkably, transgene expression is significantly increased in close proximity to the tumor site confirming the ability of this platform to deliver molecules to LMS.

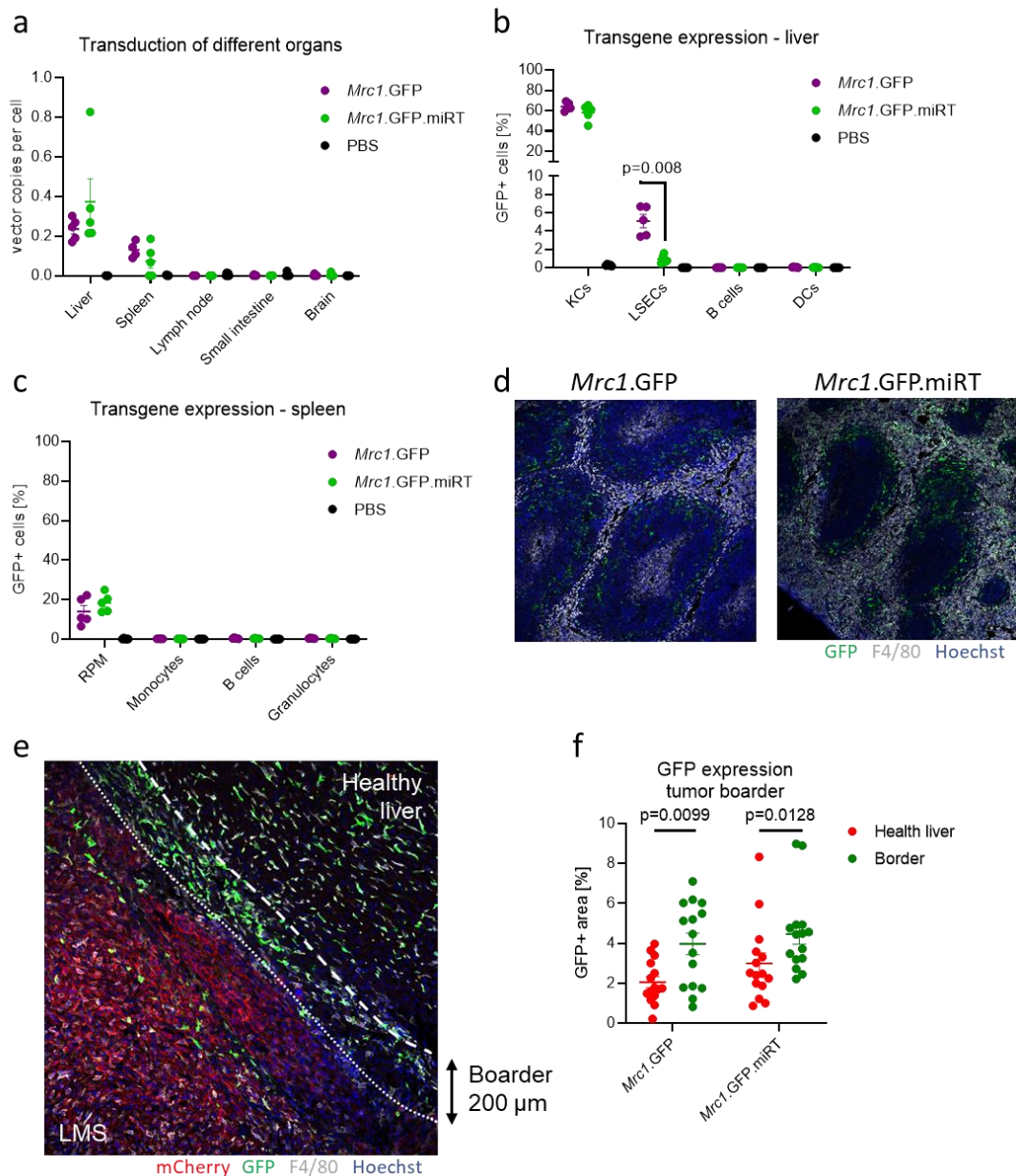


Figure 6: Biodistribution analysis of the *Mrc1.GFP.miRT* LV in the presence of MC38-based LMS. Immunosuppressive NUDE mice have been injected with a dose of 6×10^8 TU of the indicated LV diluted in PBS or PBS only as control. Ten days later, 500000 mCherry expressing MC38 cells have been injected intrahepatic. Endpoint analysis has been performed 24 days after LV injection. (a) VCN detected in different tissues ($n=5$ biological replicates). (b-c) Fraction of transgene expressing (GFP+) cells within the indicated populations in liver and spleen, respectively, in flow cytometry analysis ($n=5$ biological replicates, statistics: Mann-Whitney test). (d) Representative immunofluorescence image of the spleen of a *Mrc1.GFP* LV (left) and a *Mrc1.GFP.miRT* LV injected mouse. Slides were stained for GFP (green), F4/80 (grey) and Hoechst (blue). (e) Representative image of the liver with LMS of a *Mrc1.GFP.miRT* LV injected mouse with the signal of mCherry in red, GFP in green, F4/80 in grey and Hoechst in blue. The interface between the tumor covering area (LMS) and the area of liver (healthy liver) is indicated by a dotted white line and the tumor boarder, defined as area within 200 μ m surrounding the LMS, is shown by a dashed white line. (f) Quantification of the transgene expression represented by the GFP+ fraction within the tumor boarder and the healthy liver area. Each dot represents the quantification of an image with five mice per group and three images per mouse (statistics: Mann-Whitney test).

3.2 IFN α delivery to LMS leveraging the KC LV

In order to validate the *Mrc1*/miRT-driven LV platform as a tool to express proteins of interest in the liver, we aimed at delivering molecules with anti-tumor activity to liver metastases. As molecule with anti-tumor activity, we employed interferon- α (IFN α), a cytokine that can drive anti-tumor immune and angiostatic effects. Here, we generated an LV hosting a mouse type I IFN α encoding cDNA under the control of the *Mrc1* promoter and miRT-122/miRT-126, originating the *Mrc1*.IFN α .miRT LV. As control LV, we generated a lentiviral vector containing the regulatory features of the *Mrc1*.IFN α .miRT LV (*i.e.* *Mrc1* promoter and miRT-122/miRT-126), but lacking IFN α cDNA, originating the ORFless LV (Figure 7a).

3.2.1 Dynamics and long-term systemic effects of *in vivo* IFN α deliver

In order to characterize the *in vivo* behavior of the *Mrc1*.IFN α .miRT LV in terms of practicability for clinical translation, we investigated its potential to express IFN α *in vivo* and the appearance of treatment-related adverse events.

3.2.1.1 Robust IFN α expression decays over a period of one year

In this context C57Bl6 mice were injected with $1 \cdot 10^8$ TU of either the *Mrc1*.IFN α .miRT or the ORFless LV. Efficient transgene expression was followed by investigation of IFN α levels in the plasma. We observed that IFN α was expressed robustly in *Mrc1*.IFN α .miRT LV treated mice while IFN α remained undetectable in ORFless LV and untreated (PBS injected) mice (Figure 7b). As a potential counter selection of engineered KC can be expected, we followed these mice over a period of one year to evaluate dynamics of IFN α expression. IFN α levels in the plasma of *Mrc1*.IFN α .miRT LV treated mice reached a maximum of 500 to 1200 pg/mL about 23 days after LV administration. In the following period, we observed a sharp decrease of IFN α levels up to day 50 after LV administration with a subsequent stabilization of 200 to 600 pg/mL till day 150. In the time frame up to day 359 after LV injection, IFN α levels in the plasma dropped to a low or undetectable levels in all animals. Accordingly, at the end of the experiment 367 days after LV injection, no integrated copies of the LV were detected in the liver of *Mrc1*.IFN α .miRT LV-treated mice. In Orfless LV treated mice instead we observed about 0.22 vector copies per cell, suggesting a counter selection KCs engineered to overexpress IFN α , but not of LV-transduced KCs in general (Figure 7c).

These data confirm that the KC-LV allows robust and sustained expression of immune-activating molecules in vivo over a period of approximately one year for IFN α . Moreover, dynamics and decay of transgene expression is reproducible allowing a good dose control as well as offering the definition of a window in which the treatment is active.

3.2.1.2 Mrc1.IFN α .miRT LV treatment is well tolerated and does not induce adverse events

As demonstrated in previous studies, systemic treatment with recombinant IFN α is accompanied by severe side effects as neutropenia and autoimmunity (Sleijfer *et al*, 2005).

To investigate whether similar effects are triggered during the liver-directed treatment with the *Mrc1.IFN α .miRT LV*, we monitored the mice for one year after treatment. No macroscopic and behavioral abnormalities have been observed. Blood analysis revealed no changes in number of platelets and red blood cells or the amount of hemoglobin, confirming that no chronic anemic condition is triggered by the treatment (Figure 7d). We observed a mild reduction in the number of white blood cells (WBCs). Detailed analysis of the white blood cell compartment revealed a reduction in the B cell count of about 50 %. In a similar way, we observed a partial depletion of eosinophils. Interestingly, both effects, the decrease in the B cells as well as the shrinking of eosinophils was in close correlation with decreasing levels of IFN α in the plasma, confirming that these effects are transient and IFN α -related. Other compartments as CD4+ and CD8+ T cells, inflammatory and resident monocytes, as well as neutrophils remained unchanged (Figure 7e).

IFN α has a strong inflammatory effect and leads to counter selection of engineered KCs. In order to evaluate whether expression of IFN α in the liver induces chronic hepatotoxicity we monitored levels of alanine aminotransferase (ALT) and aspartate aminotransferase (AST) in the plasma, two enzymes, which are commonly observed to be elevated in the context of hepatotoxicity. At 126 days after treatment, both, the *Mrc1.IFN α .miRT* and the ORFless LV treated animals showed normal levels of ALT and AST compared to PBS treated mice confirming the absence of chronic hepatotoxicity (Figure 7f).

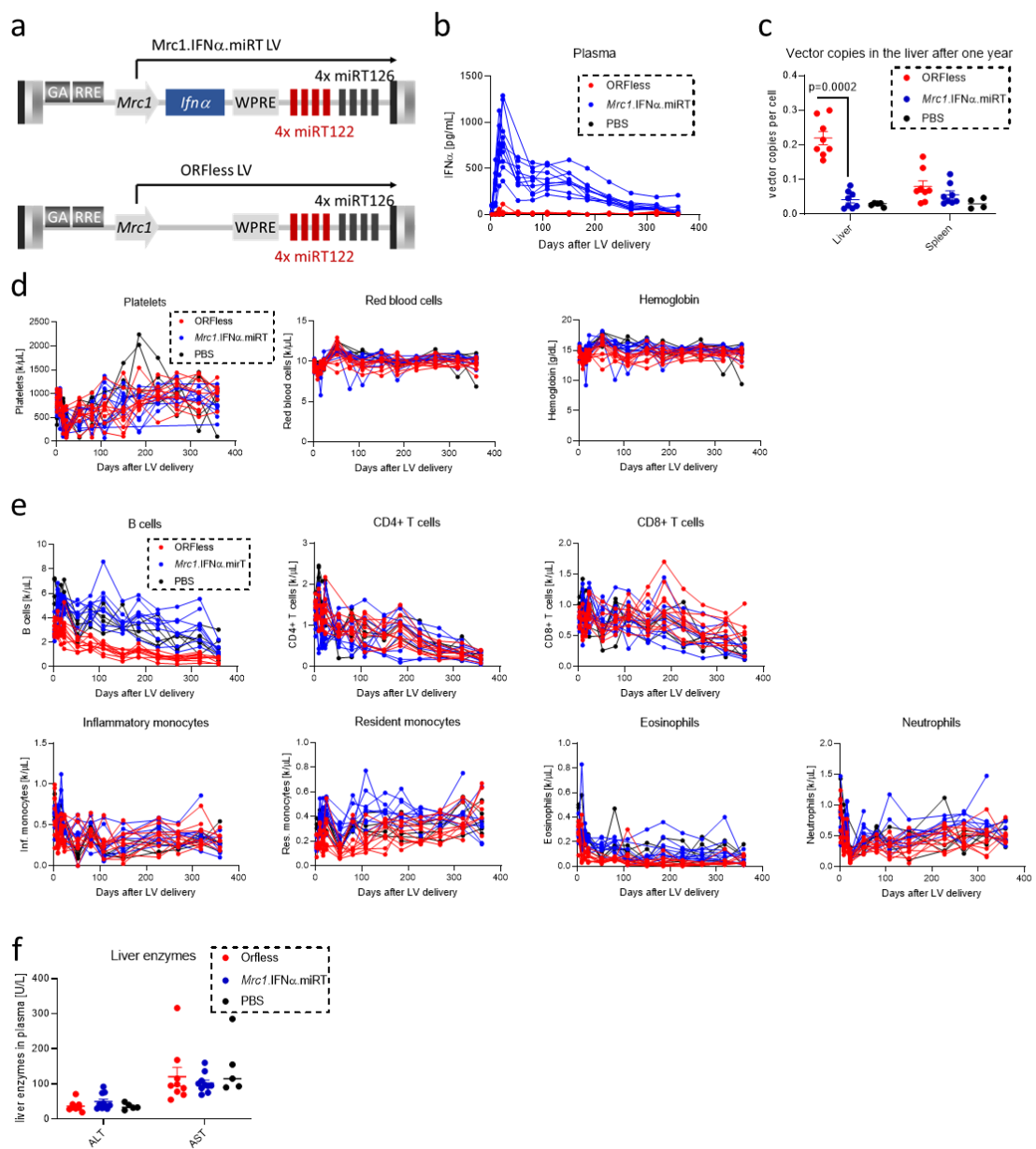


Figure 7: Assessment of the long-term dynamics of IFN α expression and adverse events in the blood parameters and liver enzymes. Immunocompetent C57Bl6 mice have been injected with 1×10^8 TU of either the Mrc1.IFN α .miRT LV or ORFless LV or only PBS. Blood analysis has been performed over a period of 1 year following injection and endpoint analysis was done 367 days after LV injection. (a) schematic representation of the LV constructs Mrc1.IFN α .miRT LV (top) and ORFless LV (bottom). (b) Level of IFN α detected in the blood plasma by IFN α ELISA over a period of one year following LV injection. (c) VCN detected in liver and spleen at the endpoint analysis (statistics: Mann-Whitney test). (d) Amounts of platelets (left), red blood cells (middle) and hemoglobin levels (right) measured by hemocytometer analysis over the period of one year following LV injection. (e) Amounts of different white blood cell populations in the blood, namely, B cells (upper left), CD4+ T cells (upper middle), CD8+ T cells (upper right), inflammatory monocytes (lower left), resident monocytes (lower middle left), eosinophils (lower middle right) and neutrophils (lower right). Amounts were determined by normalizing the fraction of cells within CD45+ cells measured by flow cytometry by the amount of white blood cells measured by hemocytometer, except for eosinophils, which have been determined directly by hemocytometer. (f) Levels of the liver enzymes ALT and AST in the plasma at day 126 after LV injection.

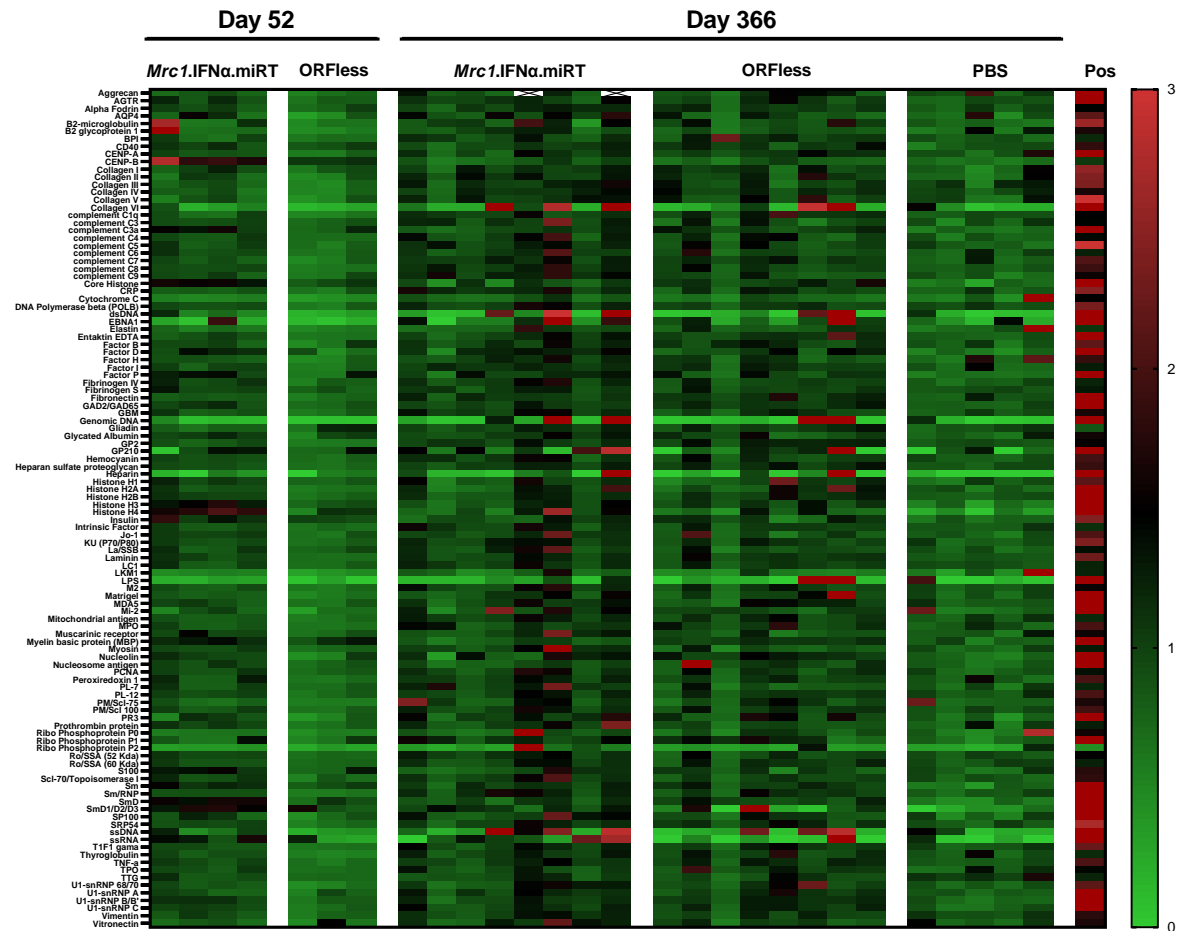


Figure 8: No induction of autoreactive antibodies in treated mice. Presence of autoreactive antibodies in the plasma against a broad panel of autoantigens was assessed at day 52 in *Mrc1.IFN α .miRT* LV (n=4) and *ORFless* LV (n=3) treated mice as well as at day 366 after LV injection in in *Mrc1.IFN α .miRT* LV (n=8), *ORFless* LV (n=8) and *PBS* (n=5) treated mice. As positive control, plasma from a lupus mouse (18-week-old female NZB/NZW mouse) was included. For experimental set up, see description of figure 5.

Elevated systemic levels of IFN α may have a systemic immune activating effect, which could lead to induction of autoimmune reactions. We addressed that risk by testing the serum of *Mrc1.IFN α .miRT*, *ORFless* LV-treated and untreated mice collected at day 52 and day 366 for the presence of autoreactive IgG-type antibodies. In this assay, we included wide array of 110 different potential autoantigens. As positive control, we included serum collected from a NZB/NZW mouse, a common mouse model for lupus displaying high levels of autoreactive IgGs (Dubois, 1966; Ono *et al*, 2000). As expected, strongly elevated levels of autoreactive IgGs have been observed in the serum of the mouse suffering from lupus compared to all animals in the experimental group. Furthermore, even though we observed presence of autoreactive antibodies against some antigens in single animals, we could not observe a trend of increased autoimmunity in

Mrc1.IFN α .miRT LV-treated animals compared to control animals. Hence, no autoimmunity has been induced by the treatment with the *Mrc1*.IFN α .miRT (Figure 8).

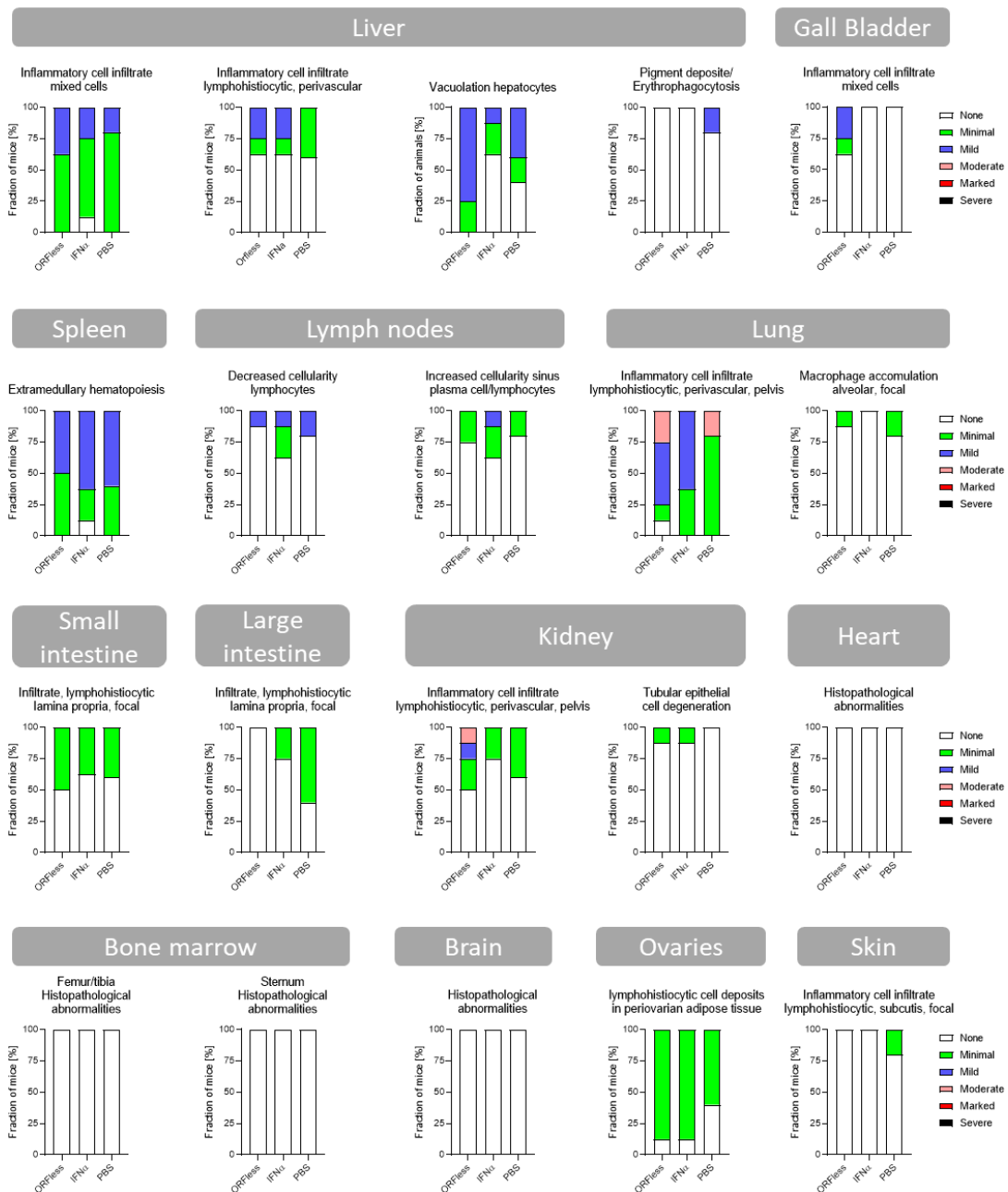


Figure 9: Histopathologic assessment of adverse events in different organs collected during endpoint analysis. Adressed histopathologic features were scored as not present (non), minimal, mild, moderate, marked and severe. Investigated organs were liver, gall bladder, spleen, lymph nodes, lung, small intestine, large intestine, kidney, heart, bone marrow, brain, ovaries and skin.

At endpoint analysis 366 days after LV injection, no macroscopic abnormalities other than age related skin irritations were observed independently of the treatment group. Histopathological analysis of the liver, gall bladder, spleen, lymph nodes, lung, small and

large intestine, kidney, heart, bone marrow from femur, tibia and sternum, brain, ovaries and skin revealed no treatment-related toxicity. Histopathologic abnormalities observed were classified as age related and no difference in frequency or severity has been observed between the treatment groups (Figure 9).

Taken together, treatment with the *Mrc1*.IFN α .miRT at doses of 1×10^8 TU per mouse is well tolerated with only modest and transient side effects observed in the B cell and eosinophil compartment. Importantly, commonly observed adverse events correlated with systemic IFN α treatment as neutropenia and induction of autoimmunity have not been observed. These data support that the KC LV composes a safe and robust platform to deliver IFN α *in vivo*.

3.2.2 Therapeutic intervention leads to reduced tumor growth in an MC38 based murine tumor model

After establishing an efficient platform to deliver IFN α to LMS in a safe manner without inducing severe side effects, we applied our LV-based IFN α delivery platform for a therapeutic intervention in an experimental CRC-LMS mouse model.

3.2.2.1 Intervention with high dose of Mrc1.IFN α .miRT LV reveals its therapeutic potential

We performed an intrahepatic injection of MC38 cells in immunocompetent mice giving rise to a commonly used syngeneic mouse model of CRC-LMS and treated them six days post tumor placement with 3×10^8 TU of the *Mrc1*.IFN α .miRT LV (Figure 10a). In the plasma of treated animals robust IFN α levels of up to 2000 pg/mL were observed, following the previously described dynamics (Figure 10b) which confirms transduction and transgene expression. In control (ORFless LV)-treated animal, we detected increased IFN α levels (~300 pg/mL) two days after LV injection that decayed to undetectable levels within one week, while PBS-treated mice did not show detectable levels of IFN α at any time point. Reason for that is a naturally occurring antiviral response upon systemic delivery of the LV (Soldi *et al*, 2020; Grandvaux *et al*, 2002). In accordance with previous experiments, we observed a reduction in the white blood cell compartment caused by a partial B cell depletion (Figure 10d). Tumor growth was followed by magnetic resonance imaging (MRI). Remarkably, we observed a significantly reduced tumor size in the treated animals compared to control-treated animals (Figure 10e). Of note, while in all

control mice tumor progression was observed, one *Mrc1*.IFN α .miRT LV-treated mice rejected the tumor entirely after initial tumor growth onset and remained tumor free until the end of the experiment 55 days after tumor placement.

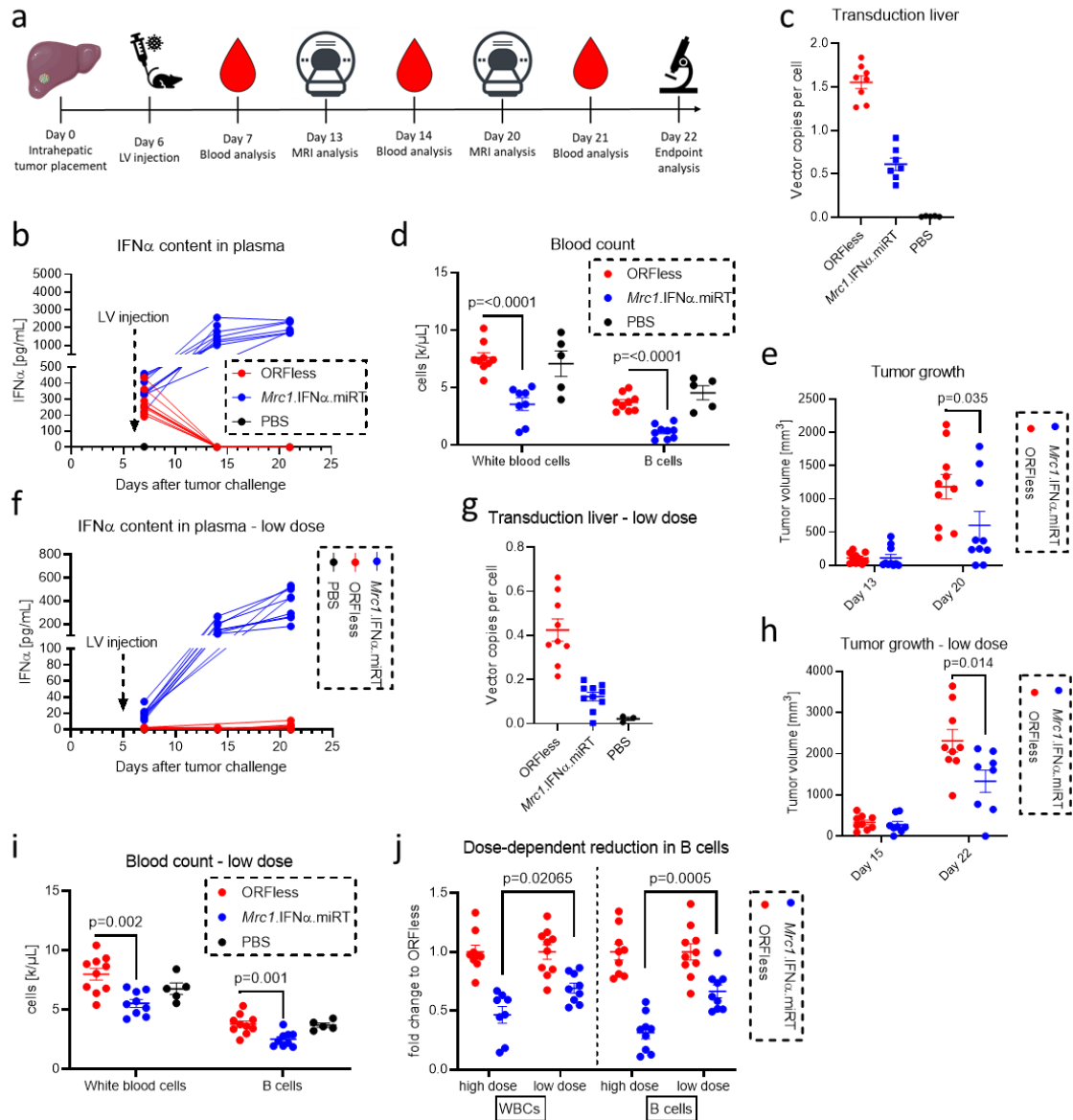


Figure 10: Therapeutic efficacy of the *Mrc1*.IFN α .miRT LV treatment in a murine MC38 cell-based tumor model. MC38 cells were transplanted in the liver of female C57Bl6 mice by intrahepatic injection followed by treatment with 3×10^8 TU of either the *Mrc1*.IFN α .miRT LV ($n = 10$) or the ORFless LV ($n = 10$). Tumor growth was addressed by MRI and adverse events as well as treatment activity was followed by blood analysis. As control mice did not undergo MC38 cell transplantation and were injected with PBS only (PBS, $n = 5$) (a) schematic timeline of the experiment. (b) IFN α content measured in the plasma of mice. The timepoint of LV injection is indicated by an arrow. (c) VCN analysis in the liver. (d) Number of white blood cells and in particular B cells in the blood measured by flowcytometry analysis and hemocytometer (statistics: Mann-Whitney test). (e) tumor volume measured by MRI at day 13 and 20 after tumor transplant (statistics: Mann-Whitney test). In a second experiment annotated as “low dose” with a similar timeline, LV doses was reduced to 3×10^7 TU per mice. (f) IFN α content measured in the plasma of mice. The timepoint of LV injection is indicated by an arrow. (g) VCN in the liver of mice from the low dose experiment. (h) Volume of LMS measured at day 15 and day 22 after tumor placement by MRI (statistics: Mann-Whitney test). (i) Number of white blood cells and in particular B cells in the blood of mice from the low dose experiment measured by flowcytometry

analysis and hemocytometer (statistics: Mann-Whitney test). (j) Fold reduction of WBCs and B cells upon treatment in the high dose experiment (mice treated with an LV dose of 3×10^8 TU) and the low dose experiment (mice treated with an LV dose of 3×10^7 TU). Absolute amounts of WBCs and B cells were normalized by the average amount of WBCs and B cells in the ORFless group with matched treatment doses, respectively (statistics: Mann-Whitney test).

3.2.2.2 Lowering the dose maintains the antitumor effect while reducing side effects

In mouse models of acute inflammation, IFN α levels in the plasma of mice can rise up to 300 pg/mL (Hickerson *et al*, 2020). In order to investigate whether we can also observe a therapeutic effect at a dose leading to IFN α levels in the plasma within a physiological range, we repeated the previously described experiment with a 10-fold decrease dose of 3×10^7 TU per mouse. In accordance with the applied dose, we observed concentrations of IFN α in the plasma of about 400 pg/mL (Figure 10f), underlining the direct correlation between dosing and transgene output of the *Mrc1*.IFN α .miRT LV. In terms of tumor growth, similar results as in the high dose have been observed. Tumor burden was significantly reduced in treated animals. Also in this setting, one mouse cleared the tumor (Figure 10h). The reduction in the B cell compartment however is less evident at this dose (Figure 10i and j).

Taken together, the *Mrc1*.IFN α .miRT LV shows a strong therapeutic effect in this experimental model of CRC-derived liver metastasis. Importantly, the antitumor effect is evident not only at doses leading to supra physiological also at levels of IFN α in the plasma which can be reached during physiological immune reactions. Furthermore, these data also confirm the direct controllability of effective dose by dosing of the vector.

3.2.2.3 Complete responding mice are refractory to re-challenge with matched cancer cells

In order to investigate whether a protective and systemically active tumor immunity was triggered mice that rejected the tumor following to *Mrc1*.IFN α .miRT LV treatment, we performed a re-challenging experiment by transplanting MC38 cells subcutaneously into the flank of these mice. While control mice showed a rapid onset and progression of tumor growth, the mice that previously rejected the LMS showed a delayed growth progression (mouse from low dose setting, Figure 11a) up to a complete rejection of the tumor (mouse from high dose setting, Figure 11b).

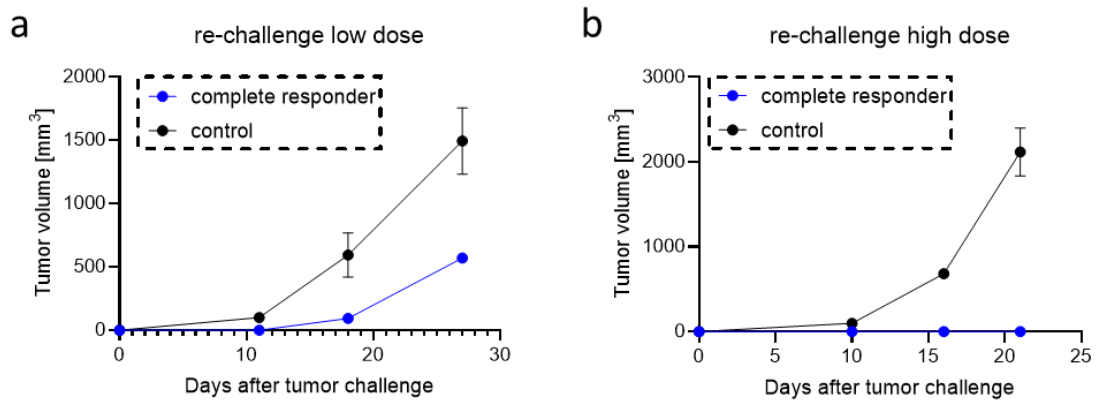


Figure 11: Re-challenge shows partial protection of complete responding mice. Mice that completely cleared the tumor in low dose ($n=1$) and high dose ($n=2$) experiment were challenged with a subcutaneous injection of 1×10^6 MC38 cells together with the PBS control mice of the respective experiment (low dose: $n=4$; high dose: $n=5$). Here the tumor growth is shown for the low dose experiment (a) and the high dose experiment (b).

In sum, we could show that treatment with the *Mrc1*.IFN α .miRT LV does not only elucidate an antitumor effect but is also capable to induce an immunological memory in mice preventing potential tumor reoccurrence.

3.2.2.4 IFN α treatment leads to induction of tumor antigen specific CD8 T cells

IFN α is an immune activating cytokine with a pleotropic effect engaging the lymphoid as well as the myeloid compartment. Furthermore, a direct effect of IFN α on cancer cells leading to increased apoptosis has been suggested as well (Chawla-Sarkar, 2003; Kotredes & Gamero, 2013; Gessani *et al*, 2014; Dickow *et al*, 2019). In this set of experiments, we wanted to investigate the phenotypic alterations in the TME, triggered upon LV-based IFN α delivery to the liver ultimately leading to decreased tumor growth. We employed MC38 cells expressing the surrogate tumor antigen chicken ovalbumin (OVA). To express OVA in cancer cells is common tool in the field of cancer research for modelling the presence a strong tumor antigen (TA). It allows detailed assessment of a TA specific immune reaction.

OVA-expressing MC38 cells were generated by transducing MC38 cells with an LV conveying an OVA encoding cDNA under the control of a PGK promotor. The bulk-transduced MC38-OVA cells showed an average of 2.8 VCN per cell which results in about 96 % cells being transduced with at least one LV copy. The presence of a small number of cells not expressing the model TA is desired as it resembles human disease

quite well in which not all cells harbor the same TAs due to continuous acquisition of new mutations.

We transplanted MC38-OVA cells by intrahepatic injection into immunocompetent mice and treated them with the *Mrc1*.IFN α .miRT LV which resulted in IFN α levels of about 650 pg/mL in the plasma eight days after treatment initiation (Figure 12a). In line with the observation in previously described therapeutic experiments, we observed a significantly reduced tumor growth in treated animals including two mice in which treatment lead to complete rejection of the tumor (Figure 12b).

In order to understand the mechanism of action of the treatment, we first investigated the activity of the treatment by assessing the expression of the IFN α - responsive genes in tumor, liver as well as spleen (Figure 12c). In liver and spleen, the identified sites of transgene expression, we observed strong upregulation of the IFN α - responsive genes *Irf7*, *Ifit1* and *Oas1a* confirming IFN α activity. In the tumor instead, we observed only a mild upregulation of *Irf7* expression, whereas *Ifit1* and *Oas1a* remained unaltered. Interestingly, basal levels of *Ifit1* and *Oas1a* expression in the tumor of untreated animals are higher than in the liver and spleen, hinting towards an increased basal IFN α signaling inside the tumor. To address unresponsiveness of the tumor we also examined the expression of the IFN α receptor. While the expression level of *Ifnar1* is comparable between tumor, liver and spleen, *Ifnar2* expression is strongly reduced in the tumor in both, the *Mrc1*.IFN α .miRT LV and Orfless treated group (Figure 12d). Of note, for efficient intracellular IFN α signaling presence and dimerization of the subunits IFN α R1 and IFN α R2 is of crucial importance (Short, 2015).

Next, we investigated the antitumor immune reaction on a cellular basis by applying flow cytometer analysis on the tumor infiltrate. Despite the absence of increased IFN α signaling in the tumor, we observed a skewing of TAMs towards a pro-inflammatory state, manifested by a trend towards a decrease in M2-like macrophages and increase in M1-like polarized TAMs (Figure 12f). Furthermore, we also saw an enhanced engagement of the adaptive immunity. Strikingly, in the *Mrc1*.IFN α .miRT LV treated group the number of OVA reactive and therefore cancer specific CD8⁺ T cells was significantly increased (Figure 12e).

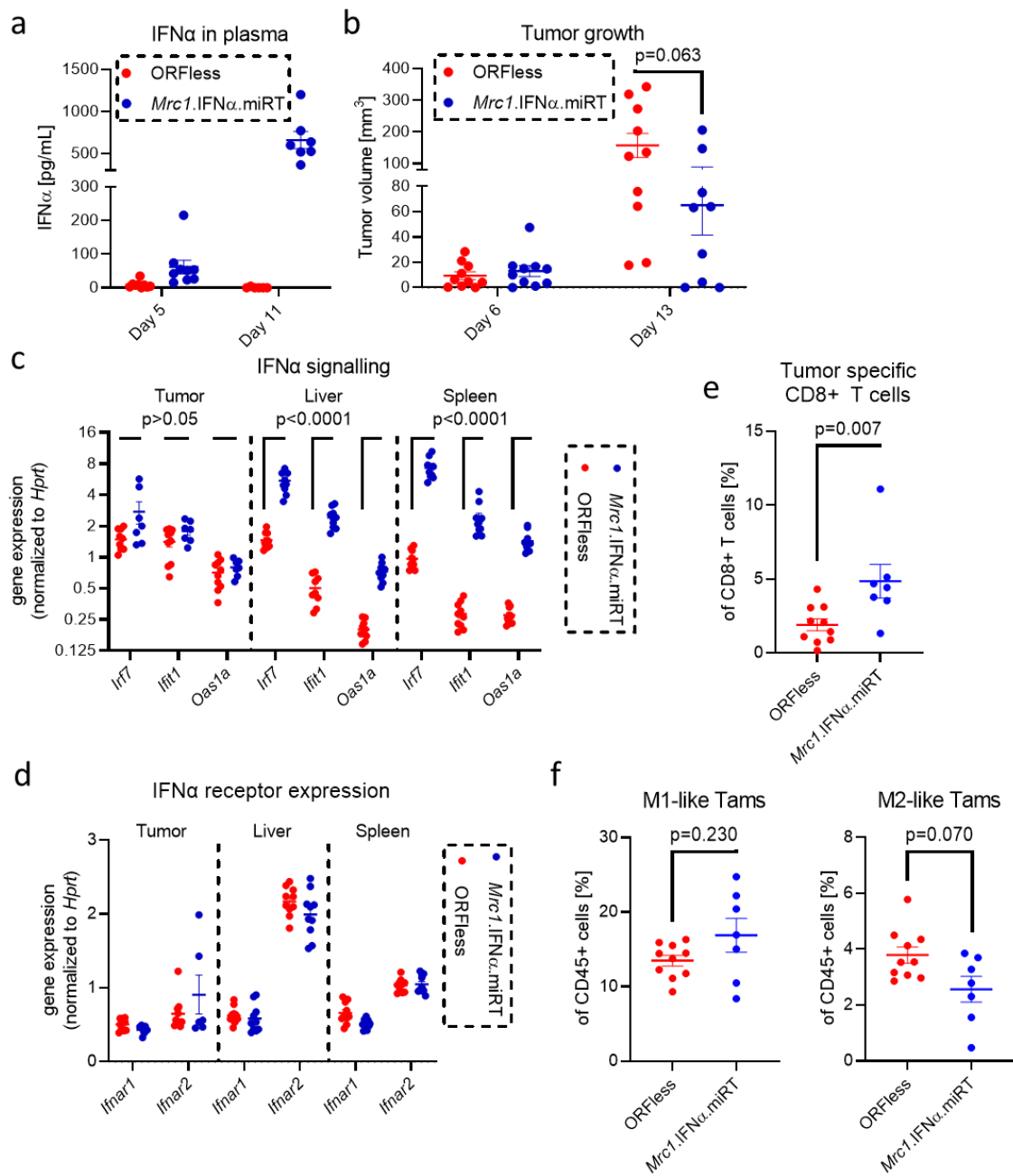


Figure 12: Remodelling of the TME upon treatment in MC38-OVA derived LMS. Female C57Bl6 mice were challenged with an intrahepatic injection of 500000 MC38-OVA cells followed by treatment with 3×10^8 TU of the Mrc1.IFN α .miRT LV or ORFless LV three days after tumor placement. (a) IFN α level measured in the plasma of mice at day 5 and day 11 after tumor placement ($n=6-9$ mice per group). (b) Tumor volume measured by MRI at day 6 and day 13 after tumor placement ($n=9, 10$ mice per group; Statistics: Mann-Whitney test). (c) Gene expression by digital droplet PCR (ddPCR) of the IFN α -responsive genes *Irf7*, *Ifit1* and *Oas1a* normalized to the expression of *Hprt* in the tumor (left), liver (middle) and spleen (right). Only mice with considerable tumor volume were included in the tumor gene expression analysis as well as all following analysis on tumor tissue ($n=7, 10$ mice per group; statistics: Mann-Whitney test, p -value indicates statistical significance for all indicated comparisons within tumor, liver and spleen). (d) Gene expression by ddPCR of the interferon alpha receptor subunits *Ifnar1* and *Ifnar2* normalized to the expression of *Hprt* in the tumor (left), liver (middle) and spleen (right) ($n=7, 10$ mice per group). (e) Frequency of OVA-reactive CD8 T cells within CD8+ T cells assessed by flow cytometry ($n=7, 10$ mice per group; statistics: Mann-Whitney test). (f) Frequency of M1-like ($CD11b^+ F4/80^+ CD11c^+ Ly6C^-$) and M2-like cells ($CD11b^+ F4/80^+ CD11c^-$) of CD45+ cells ($n=7, 10$ mice per group; statistics: Mann-Whitney test).

Coherent with the inhibited tumor growth in treated animals, these data confirm a reprogramming in terms of cellular composition of the TME towards an antitumor state upon treatment with the *Mrc1*.IFN α .miRT LV. This includes the myeloid as well as the lymphoid compartment. This is the case in spite of the apparent absence of a direct increase of IFN α signaling in the TME upon treatment in this tumor model. However, the effect of the *Mrc1*.IFN α .miRT LV treatment on individual cell types within the TME remains to be investigated.

3.3 Evaluation of therapeutic effect in a more relevant tumor model

Delivery of MC38 cells to the liver of C57Bl6 mice is a commonly used murine model for experimental CRC-derived LMS. It has, however, certain limitations and does not fully recapitulate human disease and accordingly the response to the therapy. MC38 cells harbor mutations in the DNA mismatch repair machinery. Hence, they are characterized as microsatellite instable, which leads to rapid acquisition of new mutations. However, in the majority of human disease CRC-LMS are described as microsatellite stable. Furthermore, direct intrahepatic seeding of MC38 cells leads to formation of a single bulky tumor characterized by a virtually homogeneous cellular mass without the typical histopathological features of human CRC LMS (Figure 6e). Natural occurring processes during metastasizing of human CRC as migration through the blood stream followed by extravasation and seeding into the liver are not required. In order to overcome these limitations, we attempted to employ an innovative murine model of CRC-LMS, which better recapitulates human disease and allows a more accurate assessment of therapeutic efficiency and mechanism of action of the *Mrc1*.IFN α .miRT LV treatment.

3.3.1 Organoid based tumor model closely resembles human disease

For the murine model of CRC-LMS we employed CRC-derived organoids with a C57Bl6 background harboring a distinct and well-defined set of driver mutations, which are frequently observed in human CRC-LMS. Namely, they are characterized by a loss of function mutation in the adenomatous polyposis coli protein gene, the Kirsten rat sarcoma virus gene and the p53 gene (*APC* ^{Δ 716}; *Kras*^{G12D}; *Trp53*^{R270H}) as well as the bi-allelic knockout of genes for tumor growth factor receptor 2 (*Tgfr2*^{-/-}) and F-box/WD repeat-containing protein 7 (*Fbxw7*^{-/-}) giving rise to AKTPF-organoids. The organoids were established by the usage of mice with C57Bl6y background that harbor a monoallelic

constitutive *APC*^{A716} mutation and inducible versions of the mutations *Kras*^{G12D} (monoallelic), *Trp53*^{R270} (monoallelic), *Tgfr2*^{-/-} and *Fbxw7*^{-/-} exploiting the Flox-CreERT system (Jackson *et al*, 2001; Olive *et al*, 2004; Chytil *et al*, 2002; Oshima *et al*, 1995; Onoyama *et al*, 2007). Mice were treated by four consecutive intraperitoneal tamoxifen injections to activate the Cre-recombinase and allow the induction of all mutations in the epithelial cell which form the crypts in the large intestine and colon. Five to eight weeks after the initial tamoxifen injection, organoid cultures were established from the CRC tumor cell found in these mice intestinal crypt (Sakai *et al*, 2018). By seeding of the organoids into the spleen or by portal vein injection, CRC cells enter and migrate through the blood stream and enter the liver through the portal vein, which is in close accordance with the migration route of human CRC cells towards the liver (Kok *et al*, 2021). Extravasation and seeding of the organoid-derived CRC cells into the liver completes the naturally occurring process of LMS formation in human disease. This model of spontaneous LMS seeding into the liver leads to formation of multifocal metastases widely distributed through all liver lobules (Figure 13a).

To confirm that this organoid-based murine model closely recapitulates human CRC-LMS in terms of cellular structure we performed a pathological analysis of murine and human CRC-LMS. Side-by-side comparison revealed extensively overlapping features, emphasizing the relevance of this tumor model. Namely, we observed dilated neoplastic gland formations, which are characterized by central dirty necrosis and neoplastic epithelium without mucus secretion composed of atypical cells with pleomorphic nuclei (Figure 13b). This compartmentalization inside the LMS could not be observed in MC38-based tumor models, underlining the value of the AKTPF-organoid based LMS model.

Furthermore, immunofluorescence analysis revealed the presence infiltrating immune cells in the tumor microenvironment of the AKTPF-organoid based LMS-bearing mice. Namely, TAMs (F4/80 positive cells), dendritic cells (CD11c positive cells), CD4+ and CD8+ T cells have been identified. In line with human disease, infiltrating cells have been mainly observed in the surrounding of tumor cell nests and the stroma of tumors. Only some macrophages have been observed also in the necrotic area of the tumor inside the glands. Furthermore, fibroblasts (α -SMA positive cells) and the presence of endothelial

cells (CD31+ cells) have been observed in the TME hinting towards angiogenesis and fibrosis (Figure 13c-e).

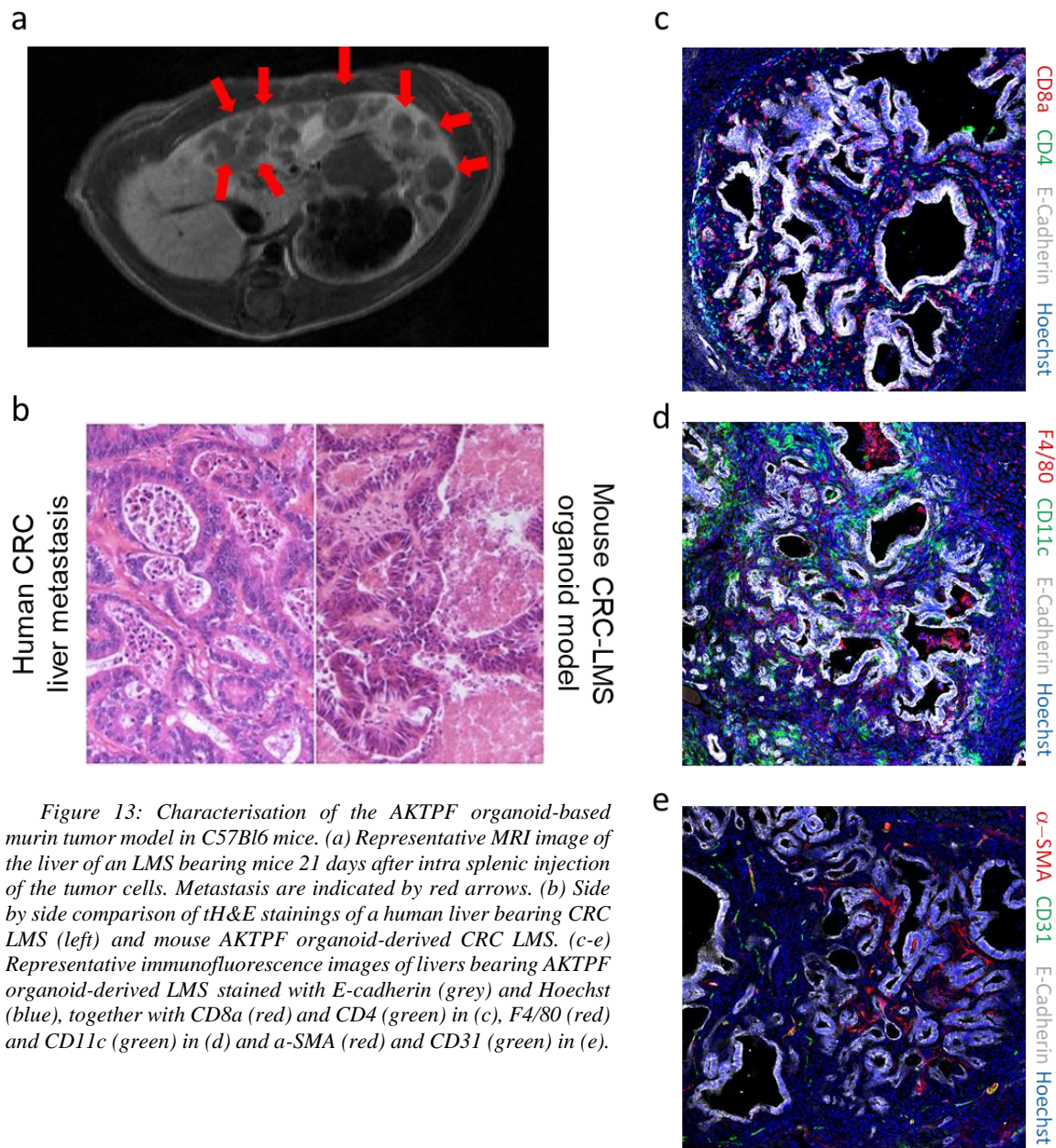


Figure 13: Characterisation of the AKTPF organoid-based murin tumor model in C57Bl6 mice. (a) Representative MRI image of the liver of an LMS bearing mice 21 days after intra splenic injection of the tumor cells. Metastasis are indicated by red arrows. (b) Side by side comparison of tH&E stainings of a human liver bearing CRC LMS (left) and mouse AKTPF organoid-derived CRC LMS. (c-e) Representative immunofluorescence images of livers bearing AKTPF organoid-derived LMS stained with E-cadherin (grey) and Hoechst (blue), together with CD8a (red) and CD4 (green) in (c), F4/80 (red) and CD11c (green) in (d) and α-SMA (red) and CD31 (green) in (e).

Collectively, the AKTPF-organoid murine tumor model closely recapitulates human disease in terms of metastasis formation and distribution as well as pathological characterization of the metastasis. This model of CRC-LMS allows us to better investigate the therapeutic effect as well as the underlying mechanism of action, especially in terms of translatability to humans.

3.3.2 Enhanced tumor infiltration of transgene expressing cells in the organoid based tumor model

Since we observed dramatic differences in the structure and the distribution of the AKTPF organoid-based LMS compared to the MC38 based tumor model, we suspected potential changes in transgene expression upon KC-LV treatment with regards to the tumor.

To address this question, we used the immune-suppressed NSG mouse strain, which is lacking functional NK cells. In contrast to C57BL6 mice, NSG mice, however, recognize the human “don’t eat me” signal CD47 which can be found on the surface of LVs produced in the human cell line HEK293T. As previously shown, presence of CD47 on the LV surface alters the biodistribution of systemically injected LV into NSG mice, especially the transduction efficiency of KCs is reduced. To circumvent this, we used an *Mrc1*.GFP.miRT LV lacking CD47 on its surface as previously described by our group (Milani *et al*, 2019).

Seven days after tumor placement by intrasplenic injection of AKTPF organoids, we treated mice with 1×10^8 TU per mice of the CD47 free *Mrc1*.GFP.miRT LV. Coherent with previous analysis, by immunofluorescence analysis we found high amounts of transgene expressing KCs in close proximity to the tumor site. Interestingly, in this model the number of GFP+ macrophages inside the tumor area, which was identified by E-cadherin staining, is increased compared to the MC38-based tumor model. These transgene expressing cells can be mostly found in the areas between the neoplastic epithelium (Figure 14a and b).

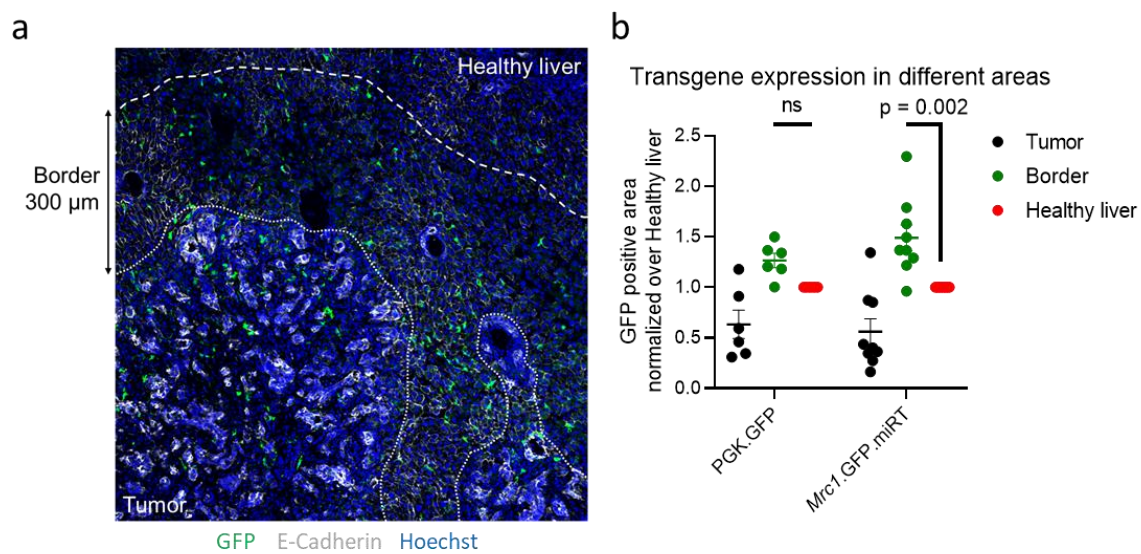


Figure 14: Biodistribution of transgene expression of the *Mrc1.GFP.miRT* LV. AKTPF organoids have been transplanted into NSG mice, followed by the injection of 1×10^8 TU of *MRC1.GFP.mirT* LV 7 days after tumor placement. Endpoint analysis has been performed 28 days after tumor placement. (a) A representative immunofluorescence image of an LMS bearing liver stained for GFP (green), E-Cadherin (grey) and Hoechst (blue). The tumor area is indicated by the dotted white line and the border area defined as the area within 300 μ m surrounding the tumor is indicated with a white dashed line. (b) Quantification of the GFP positive area within the indicated zones (tumor, border and healthy liver) normalized to the GFP positive area in the healthy liver detected in each individual image. Each dot represents the average detected for a mouse while 4 to 5 images per mouse were analyzed ($n = 6-9$ mice per group; statistics: 2way Anova (Turkey test)).

These data confirm the possibility of the KC LV platform to deliver transgenes to LMS also in a more relevant murine model. Increased presence of transgene expressing cells in the TME of AKTPF organoid-derived LMS suggests that the MC38 cell-based analysis may even have underestimated the potential of the KC LV platform.

3.3.3 *Mrc1*.IFN α .miRT LV substantially inhibits tumor growth

Demonstration of a therapeutic effect in this more relevant murine model of CRC-LMS would severely enhance the value of the *Mrc1*.IFN α .miRT LV especially with regards to its translational potential. Furthermore, biodistribution experiments suggest that IFN α delivery in this tumor model is more efficient than in the more basic MC38 based tumor model, thus, potentially enhancing the therapeutic effect.

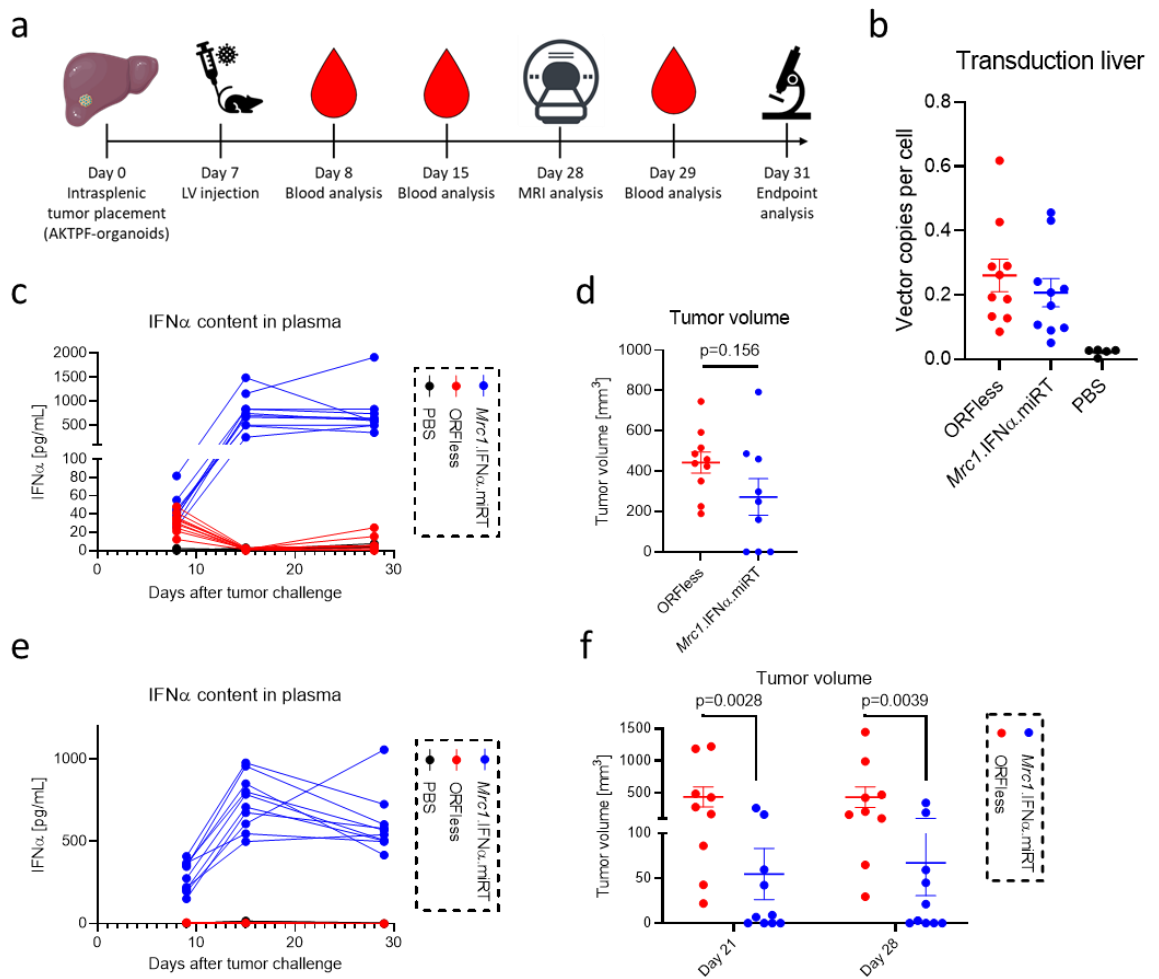


Figure 15: Therapeutic efficacy of the *Mrc1.IFN α .miRT* LV in the AKTPF organoid-based tumor model. To that aim, AKTPF organoids have been transplanted into C57B16 mice by intra splenic injection. Seven days after tumor placement, mice have been injected by 1×10^8 TU of either the *Mrc1.IFN α .miRT* LV or the ORFless LV. Control mice did not receive AKTPF organoids and were injected with PBS only (PBS). Tumor growth has been assessed by MRI. (a) Schematic experimental timeline. (b) VCN detected in tumor-free liver tissue. (c) IFN α levels in the plasma at indicated timepoints after tumor challenge. (d) Cumulative tumor volume 28 days after tumor placement ($n=9, 10$ mice per group; statistics: Mann-Whitney test). A second experiment with a similar set up has been performed with the same treatment groups and experimental timelines with an additional MRI analysis at day 21 after tumor placement. (e) IFN α content in the plasma ($n=10$). (f) Cumulative tumor volume detected by MRI at days 21 and 28 after tumor placement ($n=10$; statistics: Mann-Whitney test).

To proof this hypothesis, we treated AKTPF-organoid derived LMS bearing C57B16 mice with the *Mrc1.IFN α .miRT* LV seven days after tumor placement (Figure 15a). Treated animals showed substantial amounts of integrated LV copies in liver and spleen and of IFN α levels of about 700 pg/mL eight days after LV injection, which is in line with previously observed levels at this dose- (Figure 15c). Despite substantial variability within the treatment groups, we observed a reduced tumor growth in *Mrc1.IFN α .miRT* LV treated mice compared to the Orfless LV control group which was close to statistical significance (Figure 15d). Strikingly, the complete response rate in treated animals was

30 % while all control mice showed robust LMS growth, hinting towards an increase therapeutic efficiency of the *Mrc1*.IFN α .miRT LV in this tumor model.

In order to further establish the therapeutic efficiency of the *Mrc1*.IFN α .miRT LV by increasing the number of mice per group, we repeated the previously described experiment. Parameters as IFN α levels in the plasma were analogous with previous observations confirming activity of the treatment (Figure 15e). In this experiment we observed strong therapeutic effect manifested by a statistically significant reduction in tumor growth with a complete response rate of 40 % and overall response rate of about 80 % (Figure 15f).

Taken together, these data further confirm the therapeutic potential of *Mrc1*.IFN α .miRT LV treatment for LMS in a second and clinically highly relevant murine model of LMS. In line with our expectations based on the previously performed biodistribution experiment, the therapeutic effect was indeed enhanced in this organoid-based tumor model compared to the MC38-based tumor model.

3.4 Enhanced IFN α signaling in treated LMS leads to substantial reprogramming of the TME

Understanding the mechanistic of a treatment is of crucial importance for clinical translation. It may allow identification of targets for further improvement and engagement of combinatorial treatments as well as prediction of efficiency and risk assessment for potential adverse events dependent on the patient anamnesis.

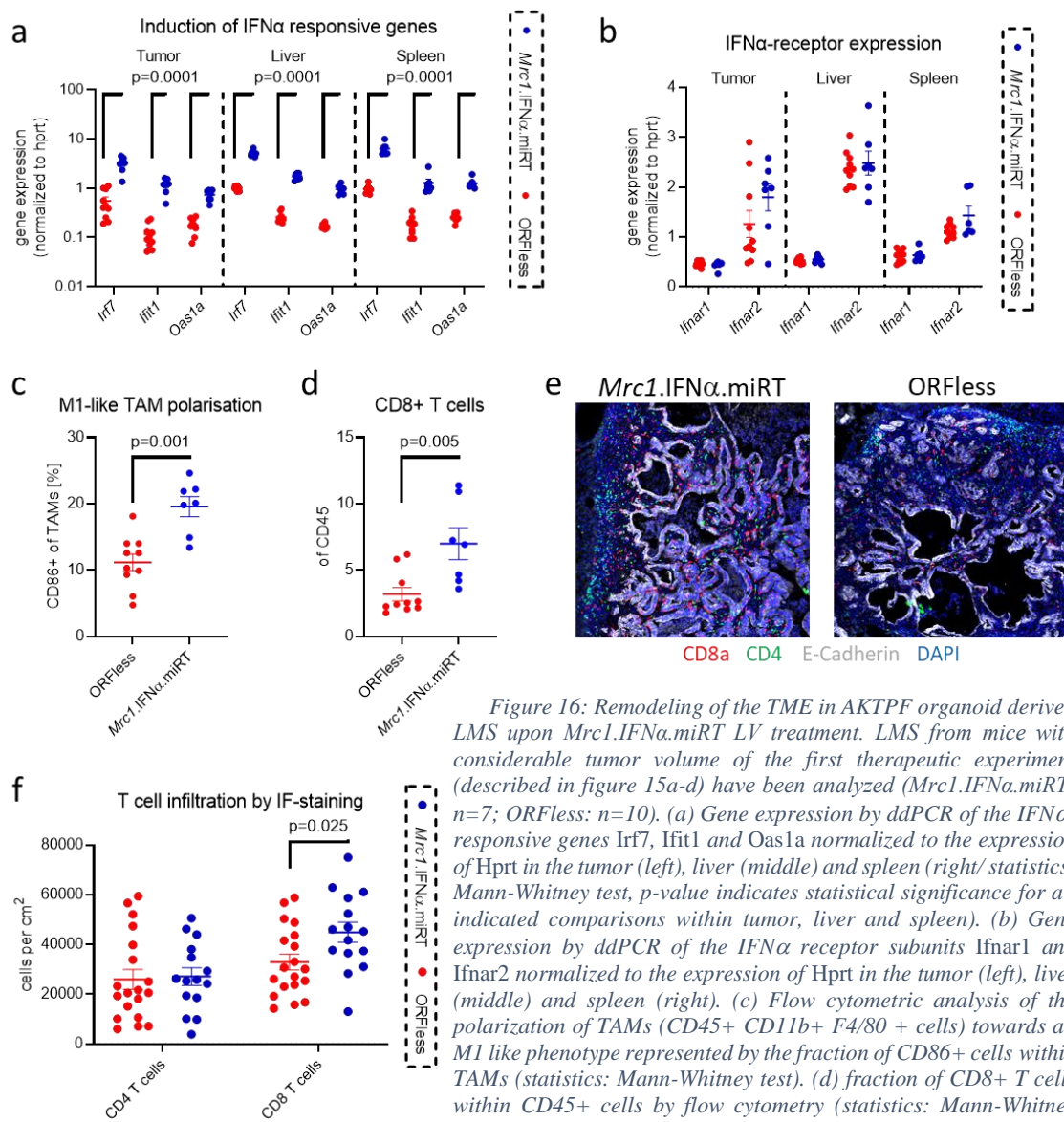


Figure 16: Remodeling of the TME in AKTPF organoid derived LMS upon *Mrc1.IFN α .miRT* LV treatment. LMS from mice with considerable tumor volume of the first therapeutic experiment (described in figure 15a-d) have been analyzed (*Mrc1.IFN α .miRT*: $n=7$; ORFless: $n=10$). (a) Gene expression by ddPCR of the IFN α -responsive genes *Irf7*, *Ifit1* and *Oas1a* normalized to the expression of Hprt in the tumor (left), liver (middle) and spleen (right/ statistics: Mann-Whitney test, p -value indicates statistical significance for all indicated comparisons within tumor, liver and spleen). (b) Gene expression by ddPCR of the IFN α receptor subunits *Ifnar1* and *Ifnar2* normalized to the expression of Hprt in the tumor (left), liver (middle) and spleen (right). (c) Flow cytometric analysis of the polarization of TAMs (CD45 $^{+}$ CD11b $^{+}$ F4/80 $^{+}$ cells) towards an M1 like phenotype represented by the fraction of CD86 $^{+}$ cells within TAMs (statistics: Mann-Whitney test). (d) fraction of CD8 $^{+}$ T cells within CD45 $^{+}$ cells by flow cytometry (statistics: Mann-Whitney test). (e) Representative image of an immunofluorescence staining of liver sections containing LMS from an *Mrc1.IFN α .miRT* LV (left) and ORFless treated mouse (right). Sections were stained for CD8a (red), CD4 (green), E-Cadherin (grey) and Hoechst (blue). (f) quantification of CD4 $^{+}$ and CD8 $^{+}$ cells per cm 2 within LMS. Each data point represents an image taken from *Mrc1.IFN α .miRT* LV ($n=7$) and ORFless LV treated mice ($n=10$) with 1-2 images taken per mouse (statistics: Mann-Whitney test)

3.4.1 Upregulation of IFN α responsive genes confirms activity of the treatment in LMS

First, we addressed the site of activity of the *Mrc1.IFN α .miRT* LV treatment represented by the expression of IFN α - responsive genes in the tumor as well as liver and spleen. Expression of *Irf7*, *Ifit1* and *Oas1a* in liver and spleen is increased to comparable levels as in previous experiment. Interestingly, however, the expression level of these IFN α - responsive genes in AKTPF organoid-derived LMS is strongly increased as well in *Mrc1.IFN α .miRT* LV-treated mice which stands in contrast to what has been observed

in the MC38 cell-based tumor model (Figure 16a). However, this is in line with the more efficient transgene expression inside the tumor in the AKTPF organoid based tumor model as witnessed in the bio distribution experiments. An important observation with this regard is that the basal expression level of IFN α -responsive genes is not increased compared to liver and spleen tissue, hence, there does not seem to be an increased IFN α signaling present in the tumor. A second difference we observed compared to the MC38 model is a robust expression of the *Ifnar2* inside the tumor, similar to *Ifnar2* expression in the liver and spleen, thus enabling efficient IFN α signaling (Figure 16b).

3.4.2 Effective reprogramming of the TME in cellular composition and spatial distribution

Enhanced IFN α signaling also correlated with an enhanced remodeling of the tumor microenvironment. FACS analysis of the tumor infiltrate revealed a tendency towards an increased polarization towards an M1-like phenotype. This is especially evident by the increased CD86 expression, a typical M1-macrophage marker (Figure 16c). Furthermore, the number of CD8⁺ T cells is significantly increased (Figure 16d). Importantly, complete responding mice could not be analyzed due to the absence of LMS. The polarization of the macrophage compartment towards pro-inflammatory phenotypes as well as the increased infiltration of cytotoxic T cells was confirmed by increased expression of the genes *Cd86* and granzyme beta (*Gzmb*).

Previous studies have shown that the interface between the tumor and liver parenchymal tissue is crucial for initiation of an antitumor immune reaction (Berthel *et al*, 2017). According to our bio-distribution analysis transgene expression of the KC LV is increased in this area (Figure 14a and b). To further investigate the restructuring of the tumor microenvironment focusing on special differences, we performed immunofluorescence analysis focusing on the T cell, dendritic cell and macrophage compartment. In the T cell compartment, we detected an increased infiltration of CD8⁺ but not of CD4⁺ T cells. This is in accordance with previous results obtained by flow cytometry.

These data reveal that enhanced IFN α signaling in the tumor is accompanied by a substantial reprogramming of the innate and adaptive component of the TME towards an antitumoral state upon *Mrc1*.IFN α .miRT LV treatment.

3.5 Single cell omics gives mechanistic insight into therapeutic effect and reveals a compensatory mechanism

Our previous data have demonstrated a reprogramming of the cellular composition of the TME upon IFN α treatment. To assess the impact of the *Mrc1*.IFN α .miRT LV treatment on the different cellular compartments in more detail, we performed single-cell RNA sequencing (scRNA-seq) on sorted LMS-derived viable cells. For that purpose, we took advantage of LMS from *Mrc1*.IFN α .miRT LV and ORFless LV treated mice of the second organoids-based therapeutic experiment described in section 4.3.3. Based on their tumor volume, we divided the mice into three cohorts, namely, partial responders (n=3) characterized by a reduced tumor growth, resistant mice (n=2) showing a tumor growth of similar extent as control mice and ORFless LV treated animals (n=3) with an average tumor burden. Of note, complete responding mice were excluded from this study as there was no tumor present that could be investigated (Figure 17a).

All viable cells were sorted from the dissociated LMS and processed for scRNA-seq. Quality analysis revealed capturing of 6000 to 12000 cells per sample with a coverage of 46000 to 80000 reads per cell and about 17000 different genes detected which is in line with expectations and historic data. Based on unsupervised clustering we identified ten different cell populations, namely, APCs, B cells, B1a cells, cancer cells, erythroblasts, hepatocytes, LSECs, mast cells, neutrophils and T and NK cells (Figure 17b). These populations were identified by the characteristic expression of populations specific genes such as *Cd79a* in B cells and B1a cells, the TCRbeta chain (*Trbc2*) in the majority of cells of the T and NK cell compartment, *Csf1r* expression in APCs and to lesser extent in neutrophils, *Cd33* on neutrophils, the Tie2 gene (*Tek*) on LSECs and the epithelial cell marker *Epcam* on cancer cells (Figure 17c). Umap representation of the individual cohorts reveals an extensive overlap of the populations between different treatment groups (Figure 17d). Accordingly, the cellular composition within the different treatment groups is similar. LSECs are detected nearly exclusively in the cohort of partial responders, exclusively in the cohort of partial responders, T and NK cells are enriched

clustering. (c) Level of gene expression in of the genes Cd79a (upper left), Trbc2 (upper right), Csf1r (middle left), Cd33 (middle right), Tek (lower left) and Epcam (lower right) in a umap representation (d) Umap representation of samples split into the three cohorts control (left) partial responders (middle) and resistant (right). (e) Percentage fraction of cells belonging to the identified populations within each sample. (f) Heatmap showing expression of the top 20 upregulated genes for each population identified in (b). Manually selected genes are annotated.

in both *Mrc1*.IFN α .miRT LV-treated cohorts and the TME of the control cohort shows a trend of enriched in neutrophil contents (Figure 17e). Expression analysis of the top 20 upregulated genes in each cluster confirms the individuality of each population demonstrated by the low overlap of gene expression patterns between the different clusters identified. Furthermore, the top 20 upregulated genes of each cluster contained common genes associated to each particular population, further confirming their identity (Figure 17f).

3.5.1 Strong reprogramming of the APC compartment upon IFN α treatment

After the identification of these distinct cell populations, we performed an individual analysis focusing on the APC compartment. Upon gene set enrichment analysis (GSEA) comparing the APC compartment from the LMS of the different cohorts we observed a strong upregulation of IFN α response, represented by the gene set Hallmark_Interferon_Alpha_Response, in both *Mrc1*.IFN α .miRT LV treated cohorts compared to ORFless LV treated LMS, thus confirming the efficient IFN α delivery to LMS upon treatment. This was accompanied by an increased IFN γ signaling. Furthermore, positive regulation of cell killing, regulation of the innate immune response and regulation of T cell mediated cytotoxicity was enhanced in IFN α -treated cohorts. Moreover, GSEA shows increased antigen presentation in IFN α -treated cohorts and upregulation of MHC expression in responding mice. Interestingly, antigen processing and presentation and MHC expression in particular was increased in partial responding LMS compared to the resistant cohort.

To further address the polarization state of the APC compartment, we took advantage of gene sets derived from the group of Renato Ostuni who characterized BMDMs stimulated with different immune activating and immunosuppressive cytokines, including IFN α , LPS for M1-like polarization, and IL10, PGE2 and IL4 for M2-like polarization (Cilenti *et al.*, 2021). The gene sets for IFN α and LPS-stimulated macrophages (IFN α _RO and LPS_RO) were enriched in partial responders as well as resistant LMS compared to the control, confirming activation of the APC compartment towards an

immunostimulatory state. However, comparison of the partial responder and resistant cohort showed an enhanced IFN α and LPS stimulation in resistant mice. Interestingly, the signatures of IL10, PGE2 and IL4 stimulated BMDMs were enriched in APCs derived from LMS of treatment resistant mice. This holds true for the comparison with responders as well as the control cohort, thus, hinting towards an immunosuppressive polarization phenotype of the APCs in the resistant mice (Figure 18a).

For better understanding of the cellular composition of the APC compartment we performed sub clustering and identified ten different populations. Based on the expression of characteristic markers, we identified the following populations: Ccr7 DCs expressing *Fscn1* and *Ccr7*; CD8 cDC1 characterized by expression of *Xcr1* and MHCII related genes such as *H2-Ab1* and *H2-AB1*; *Cd209a* and *Bcl11a* positive common dendritic cell progenitors (CDPs); The two TAM populations IFN α TAMs and TAMs expressing TAM markers such as *Chil3*, *Fn1* and *Vcan*; KCs expressing the common resident macrophage marker genes *C1qa* and *C1qb*; monocyte dendritic cells (Mo DCs) which express genes related to MHCII dependent antigen presentation such as *Ciita*, *H2-Ab1* and *H2-AB*; monocytes expressing *CD300e* and *Eno3*; pDCs with phenotypic expression of *Siglech* and *Ccr9*; and pre DCs expressing the cell cycle related genes *Stmn1* and *Mki6*. Their identity was confirmed by the expression analysis of the top 20 upregulated genes in each cluster confirming their individuality and identity (Figure 18b and c). The compartment of tumor-associated macrophages appears to be strongly reshaped by the *Mrc1*.IFN α .miRT LV. This is evident by the fact that TAMs from both *Mrc1*.IFN α .miRT LV treated groups form a separate cluster in the umap representation, annotated as IFN α TAMs (Figure 18b). Indeed, quantification of the cellular composition demonstrated that all TAMs of the *Mrc1*.IFN α .miRT LV treatment groups can be found in this cluster while the vast majority of TAMs from the control group can be found in the cluster of conventional TAMs (Figure 18d). However, expression analysis of the top 20 markers of each cluster revealed an extensive overlap between TAMs and IFN α TAMs and the expression of characteristic genes expressed in tumor associated macrophages in both clusters such as *Chil3*. IFN α TAMs showed an increased expression of IFN α responsive genes such as *Ifi204* and *Ifi2712a*. To better understand the difference between IFN α TAMs and TAMs we performed a GSEA directly comparing the two clusters (Figure 18e). As expected, we observed an enrichment of genes associated with response to IFN α

in IFN α TAMs. However, enrichment of genes responsive to other immune activation cytokines such as IFN γ , LPS and TNF α as well as a general enrichment in the cytokine mediated signaling pathway demonstrates an increase proinflammatory phenotype of IFN α TAMs compared to TAMs. In accordance, IFN α TAMs are characterized by increased immune functions such as production of immune related cytokines, regulation of immune effector functions and antigen presentation. TAMs, instead, are enriched in protein synthesis programs which is a feature observed in alternatively activated M2-like macrophages with protumoral functions (Shay *et al*, 2017).

Furthermore, assessment of the cellular distribution of the APCs to the different identified clusters revealed an accumulation of CD8 cDC1 and Mo DCs, two cell types which are characterized by high antigen presenting activity (Figure 18d). This confirms the previously observed enhancement in antigen presentation activity in APCs of the responder cohort.

Taken together, treatment with the *Mrc1*.IFN α .miRT LV leads to a strong remodeling of the APC compartment towards a proinflammatory state. This is especially evident in the population of tumor-associated macrophages. However, in resistant mice antigen presentation appears to be impaired compared to the partial responding LMS and the APC compartment seems to be influenced by the presence of immune suppressive cytokines such as IL10.

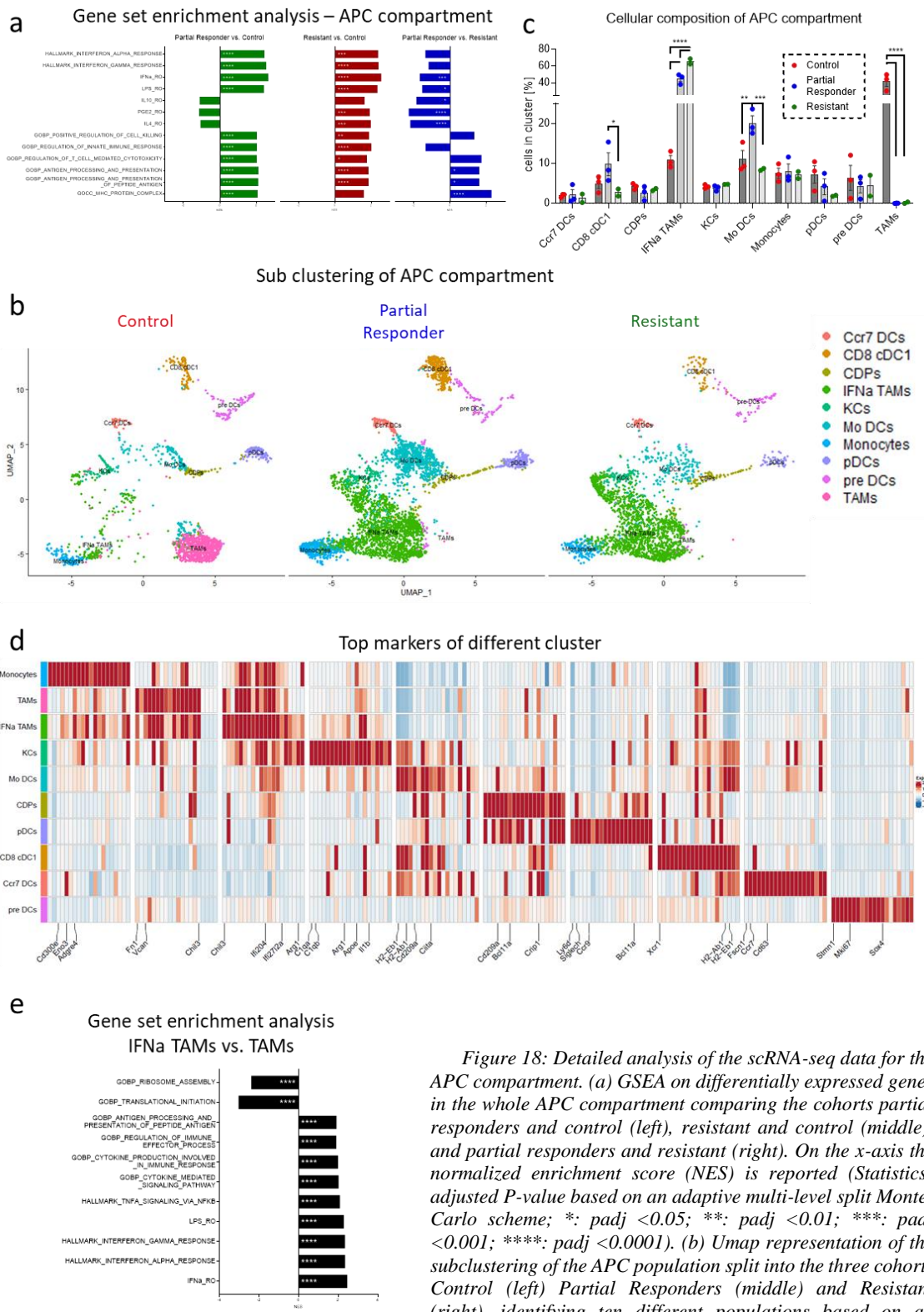


Figure 18: Detailed analysis of the scRNA-seq data for the APC compartment. (a) GSEA on differentially expressed genes in the whole APC compartment comparing the cohorts partial responders and control (left), resistant and control (middle), and partial responders and resistant (right). On the x-axis the normalized enrichment score (NES) is reported (Statistics: adjusted P-value based on an adaptive multi-level split Monte-Carlo scheme; *: padj <0.05; **: padj <0.01; ***: padj <0.001; ****: padj <0.0001). (b) Umap representation of the subclustering of the APC population split into the three cohorts Control (left) Partial Responders (middle) and Resistant (right), identifying ten different populations based on an unbiased clustering approach. (c) Fraction of cells in percent belonging to the identified populations within each sample (statistics: 2way Anova (Fisher's LSD test); *: p<0.05; **: p<0.01; ***: p<0.001; ****: p<0.0001). (d) Heatmap showing expression of the top 20 upregulated genes for each population identified in (b) with annotation of manually selected genes. (e) GSEA analysis on differentially expressed genes comparing the populations IFNα TAMs and TAMs. On the x-axes the normalised enrichment score (NES) is reported (Statistics: adjusted P-value based on an adaptive multi-level split Monte-Carlo scheme; *: padj <0.05; **: padj <0.01; ***: padj <0.001; ****: padj <0.0001).

3.5.2 Composition of T and NK cell compartment determines antitumoral immune response

Similarly to the APC compartment, we performed an isolated analysis of the compartment of adaptive immune response represented by the T and NK cell compartment. GSEA revealed that also in the T and NK cell compartment sensing of IFN α is evident by an enrichment of interferon alpha responsive genes in LMS of *Mrc1*.IFN α .miRT LV treated animals. Interestingly and in contrast to the APC compartment IFN α signaling is increased in partial responding mice compared to resistant mice. This IFN α signaling is accompanied by a general immune activation of T and NK cells evident by an enrichment of the gene sets Interferon_Gamma_Response, Response_To_Type_I_Interferon, Response_To_Virus and Cytokine_Mediated_Signaling_Pathway. Remarkably, effector functions such as T cell mediated cytotoxicity, natural killer cell activation and regulation of cell killing is found to be upregulated only in the group of partial responders, but not in resistant animals (Figure 19a).

Subsequent clustering of the T and NK cell compartment revealed a variety of different phenotypes of CD8 T cells, CD4 T cells as well as NK and NKT cells. T and NKT cells were characterized by the expression of *Cd3e*. Among the CD4 positive cell we identified stem cell memory like cells (CD4 Tsm-like cells) expressing *Lef1*, *Tcf7* and *Sell*, effector-like cells (CD4 Teff-like cells) which show upregulated expression of *Cd40lg* and *Rora*, *Pdcd1* expressing exhausted cells (CD4 Tex cells), *Foxp3*-expressing regulatory T cells (CD4 Treg cells) and *Eomes* positive T regulatory type 1-like cells (CD4 Tr1-like cells). The CD8 T cell compartment was subdivided into stem cell memory-like cells (CD8 Tsm-like cells) based on the expression of *Lef1*, *Tcf7* and *Sell*, memory T cells (CD8 Tm cells), two different cluster of effector cells (CD8 Teff1 cells and CD8 Teff2 cells), which express *Rora* and *Tnf* or *Gzma*, *Gzmb* and *Gzmk*, respectively, and exhausted T cells (CD8 Tex cells) showing increased expression of *Lag3* and *Pdcd1*. Furthermore, we identified a cluster of proliferating T cells (T prol cells) expressing several genes related to cell cycle progression such as *Stemn1* and *Mki67*, as well as gamma-delta T cells (gd T cells) expressing the TCR gamma and delta chain (*Tcr γ -C1* and *Trdc*, respectively). Within the NK and NKT cells compartment with their characteristic expression of *Fcer1g*, we subdivided into innate lymphocytic cells (ILCs), MAIT cells, invariant NKT cells

As expected, we observed similarities majorly between the different NK and NKT cell populations in the expression analysis of the tow 20 marker genes of each cluster (Figure 19c and d). Also in the T cell compartment we observed overlap between certain cell types such as the CD4 Tsm-like cells and CD8 Tsm-like cells as well as the CD8 Teff1 cells and CD8 Teff2 cells. Interestingly, the similarity between CD4 Treg cells and CD4 TR1-like cells was minor. Instead, CD4 TR1-like cells showed similarities to CD8 Tex cells and the two CD8 Teff populations.

Side by side comparison of the T and NK cell compartment of the different cohorts in a umap visualization demonstrate extensive overlap for most of the populations (Figure 20a). However, quantification of the cellular composition shows differences in the abundance of several cell populations (Figure 20b). In the NK and NK T cell compartment, we observed a higher abundance of ILCs in partial responding mice compared to the control and resistant cohort. This is in line with the increased NK cell activation in partial responders observed in the GSEA analysis. In the CD8 T cell compartment, we observed an accumulation of CD8 Teff1 cells in partial responders (between 6 and 20 % of all T and KN cells), a population which is spars in the resistant and control cohort (below 3 %). At the same time, we observe a trend towards reduced amounts of exhausted CD8 T cells (CD8 Tex cells) in partial responders, even though not significant. To further investigate this, we performed GSEA analysis comparing the different treatment cohorts focusing taking into account all CD8 T cell populations (Figure 20c). In line with previous observations, we observed an increased $IFN\alpha$ and $INF\gamma$ signaling in all *Mrc1*. $IFN\alpha$.miRT LV treated cohorts. However, direct comparison between partial responders and resistant mice revealed an enhanced $IFN\alpha$ and $INF\gamma$ signaling in partial responders. Gene sets focusing on the immunologic activity of CD8 T cells such as positive regulation of adaptive immune response, positive regulation of T cell mediated immunity and positive regulation of T cell mediated cytotoxicity where significantly enriched in the partial responders, suggesting enhanced effector functions in this cohort. To address exhaustion in the CD8 T cell compartment we took advantage of a gene set which has been published by Wherry and collaborators (Wherry *et al*, 2007). Indeed, we observe that the signature score for the expression of the genes in this gene set largely overlaps with the population of exhausted CD8 T cells (Figure 20d). Strikingly, exhaustion was reduced in CD8 T cells derived from LMS of the partial

responder cohort compared to control LMS. In contrast, we found strongly increase exhaustion in resistant mice compared to control as well as partial responder mice. This indicates that treatment with the *Mrc1*.IFN α .miRT LV in general leads to increased CD8 T cell activation. However, in responding mice this leads to a reduced exhaustion profile of CD8 T cells while in resistant mice a T cell exhaustion is triggered, hence, rendering the CD8 T cell response unfunctional in this cohort.

The CD4 T cell compartment reveals major differences in the regulatory T cell compartments. *Foxp3* positive conventional Tregs appear to be reduced in number in responders compared to control animals. More strikingly, we observe large amounts of Tr1-like T cell almost exclusively in treatment-resistant mice. Indeed, about 38 % of all T and NK cells belong to the cluster of CD4 Tr1-like cells compared to only 1 % and 5 % in partial responders and control mice, respectively. To further confirm the identity of Tr1-like cells we addressed the expression of Tr1 cell-related genes comparing the population of CD4 Tr1-like cells to all other T and NK cells. Indeed, we found that several genes which have been described to be highly expressed or downregulated in Tr1 cells to be upregulated and downregulated in the population annotated as CD4 Tr1-like cells, respectively, (Figure 20e). This hints towards the appearance of an antigen specific tolerogenic mechanism leading to resistance against the treatment. Of note, Tr1 cells can be induced by TCR engagement of CD4 T cells plus stimulation with IFN α and IL10, two cytokines, which appear to be abundant in *Mrc1*.IFN α .miRT LV treated but resistant mice.

Taken together, we observed effective IFN α signaling in the T and NK cell compartment in LMS of *Mrc1*.IFN α .miRT LV treated mice. While this leads to increased effector functions and reduced exhaustion in partial responders, in resistant mice a tolerogenic mechanism is triggered evident by increased exhaustion in CD8 T cells and the appearance of high amounts of Tr1-like cells.

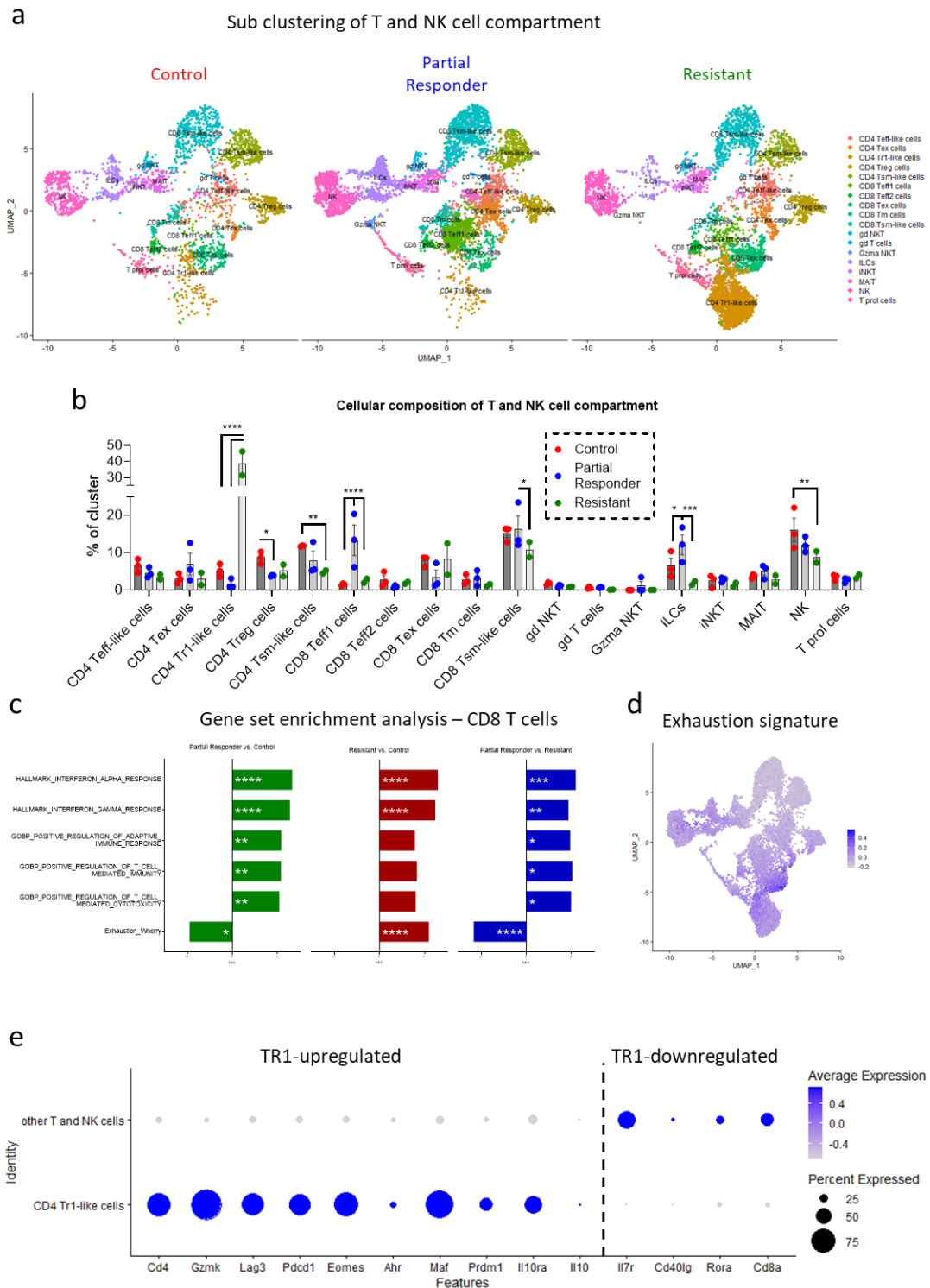


Figure 20: Focused analysis of the T and NK cell compartment in the scRNA-seq data. (a) Umap representation of the subclustering of the T and NK cell population split into the three cohorts control (left) partial responders (middle) and resistant (right). (b) Fraction of cells in percent belonging to the identified populations within each sample (statistics: 2way Anova (Fisher's LSD test); *: $p < 0.05$; **: $p < 0.01$; ***: $p < 0.001$; ****: $p < 0.0001$). (c) GSEA on differentially expressed genes in all CD8 T cells comparing the cohorts partial responders and control (left), resistant and control (middle), and partial responders and resistant (right). On the x-axis the normalized enrichment score (NES) is reported (statistics: adjusted p-value based on an adaptive multi-level split Monte-Carlo scheme; *: $\text{padj} < 0.05$; **: $\text{padj} < 0.01$; ***: $\text{padj} < 0.001$; ****: $\text{padj} < 0.0001$). (d) Expression level score of the gene set Exhaustion_Wherry

derived from Wherry *et al.* in a umap representation (Wherry *et al.*, 2007). (e) Expression level of Tr1-associated genes (left) and genes commonly downregulated in Tr1 cells (right) in the population of CD4 Tr1-like cells and other T and NK cells. The color describes the expression level (blue representing a high expression and grey a low expression) while the size of the dot represents the percent of cells in the population expressing the gene.

In general, we observed an effective delivery of IFN α to LMS upon *Mrc1*.IFN α .miRT LV. Its immunologic activity is evident in all cellular compartments of the TME. The APC as well as the T and NK cell compartments are strongly reshaped towards an immune stimulatory state with enhanced antitumoral effector functions. This is evident by increased antigen presentation on APCs and improved effector functions in the CD8 T cells. In resistant mice, however, an immune evasion mechanism is triggered leading to resistance to *Mrc1*.IFN α .miRT LV treatment. Most evident is the appearance of tolerogenic CD4 Tr1-like T cells in resistant mice. This is accompanied by partially impaired antigen presentation in the APC compartment and increased exhaustion in the T cell compartment.

3.6 Spatial transcriptomics analysis reveals importance of the tumor border

To gain further insights into the mechanism of the *Mrc1*.IFN α .miRT LV treatment and to better understand the reshaping of the TME also with regards to the spatial component we performed spatial transcriptomic analysis. To this aim, we took advantage of the Visium technology developed by 10X genomics. It allows transcriptomic profiling of individual spots of 55 μ m diameter in an area of 6.5x6.5 mm. From each dot we can retrieve whole transcriptome information, enabling assessment of gene expression patterns and pathways. Transcriptional profiling from each spot can then be mapped based on their coordinates and used to reconstruct the piece of tissue. Furthermore, a hematoxylin/eosin image is produced in parallel from the same piece of tissue, thus enabling perfect spatial positioning of analyzed dots.

To be able to match results obtained by scRNA-seq we process pieces of the liver containing LMS of the same mice and cohorts as described above (Figure 17a). Quality control revealed an average of 1365 spots under tissue, 198653 reads per spot, 4566 genes per spot and 18361 genes per sample.

3.6.1 Unbiased determination of spatial zones with regards to the tumor

Several studies have shown that the tumor boarder and peritumoral tissue are of high importance for the tumor immune landscape (Berthel *et al.*, 2017). Therefore, we decided

to focus our analysis on the assessment of differences between areas inside the tumor, the tumor boarder, peritumoral tissue and healthy liver tissue. In order to enable integration and comparative analysis of different samples, we developed a method to assign each spot to a zone dependent on its position relative to the tumor. To this aim, we integrated the results from all samples treating each spot as an independent entity. We performed unsupervised clustering, which resulted into eight clusters (Figure 21a). To identify clusters resembling spots that cover tumor areas we addressed the expression of genes in the different clusters which are either commonly upregulated CRC-derived LMS such as *Epcam*, *SI00a6* or *Saa3* (Tumor specific genes) or liver-associated like *Alb*, *Fabp1* and *Apob*. Following this analysis, we found upregulation of tumor specific genes and downregulation of liver specific genes in the cluster 1 and cluster 6 while the other clusters showed increased expression of hepatic genes and reduced expression of tumor specific genes (Figure 21b). Indeed, spots of the clusters 1 and 6 largely covered tumor spanning areas while the other spots are originated from liver tissue. Exemplary assessment of a sample from the resistant cohort confirms this as can be seen by the representation of the H&E staining allowing histopathologic identification of tumor areas (Figure 21c) and the mapping of the spots from the different cluster on the tissue (Figure 21d). Based on these results we annotated the entities of cluster 1 and 6 as tumor-derived (LMS) and the entities of cluster 0, 2, 3, 4, 5 and 7 as liver-derived, which led to a precise and unbiased identification of the tumor-derived spots (Figure 21e). Next, we took advantage of a moving average-based approach to further subdivide the spots on the tissue into eight different zones based on their location with respect to the tumor-liver interface. For that classification, the density of spots in the surrounding of each spot annotated as tumor was taken as measure to divide the tumor spanning spots into four zones called zone A, zone B, zone C and zone D, whereas zone A resembles spots that are surrounded mainly by spots classified as LMS and zone D classified as spots that are surrounded by fewer spots annotated as LMS. In a similar fashion, the spots annotated as liver-derived were divided into the Zones E to H, in which spots of zone E have a lower density of liver spots in their surroundings.

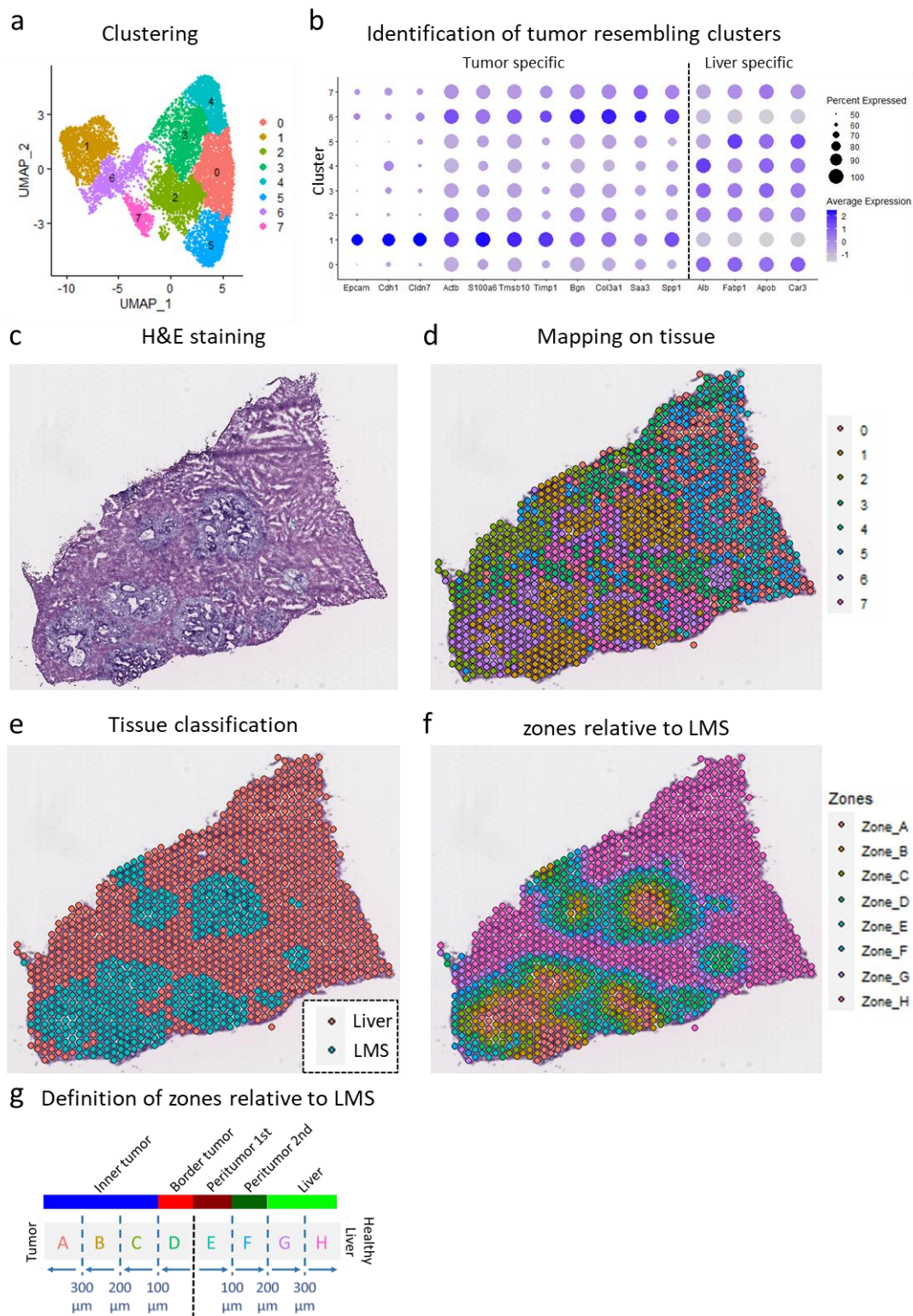


Figure 21: Development of a method to determine zones based on distance to the tumor-liver interface in spatial transcriptomic analysis. (a) Umap representation of the entire dataset after integration of all samples treating every spot as independent entity. Clusters are determined by unsupervised clustering. (b) Expression level of LMS-related genes (left) and healthy liver-related genes (right) in the different clusters identified in (a). The color describes the expression level (blue representing a high expression and grey a low expression) while the size of the dot represents the percent of spots in the cluster expressing the gene. (c) H&E staining of the section processed for spatial transcriptomics of a representative sample. (d) Annotation of the spots with the previously defined clusters in (a) on

the same section shown in (c). (e) Classification as LMS or Liver of each spot on the tissue section based on the identification of tumor resembling clusters in (b) and the cluster annotation in (d). (f) Division of spots into eight zones based on the surrounding environment in terms of density of LMS and liver annotated spots. (g) Determination of the estimated distance of the zones to the tumor-liver interface and classification of the zones into the areas inner tumor, tumor border, peritumoral 1st, peritumoral 2nd and liver.

By this approach we created a gradient from the center of the tumor, which is annotated as zone A spanning the interface between tumor and liver between zone D and E towards areas of healthy liver annotated as zone H (Figure 21f). Taking the dimensions of the analyzed tissue into account, we estimated the distance of each zone to the tumor boarder. Zone D resembles spots inside the tumor within 100 μm to the boarder, zone C between 100 μm and 200 μm , zone B between 200 μm and 300 μm and zone A resembling the center of the tumor with more than 300 μm distance from the tumor-liver interface. In this manner, zone A, B and C were classified as inner tumor and zone D and border tumor. Similarly, zone E describes spots in the hepatic area within 100 μm to the tumor, zone F within 100 μm to 200 μm , zone G 200 μm to 300 μm and zone H resembles spots covering healthy liver at a minimum distance of 300 μm to LMS. Zone E and F were annotated as peritumor 1st and 2nd, respectively, and zones G and H as liver (Figure 21g).

3.6.2 Multiple comparison of the zones by GSEA

The previously described division of the tissue into different zones allows analysis based on a GSEA comparing different dimension (Figure 22a). To address spatial differences within each cohort, a comparison between zones within each treatment group can be performed. To that end, we determined differentially expressed genes comparing each zone to all other zones combined. Focusing on the control cohort, we observed an enrichment of tumor related gene sets such as the hallmark epithelial-mesenchymal-transition, hallmark p53 pathway and hallmark angiogenesis in the tumor spanning zones A, B, C and D while liver related gene sets like hallmark peroxisome and hallmark adipogenesis were enriched in the liver spanning zones E, F, G and H. This confirms the precision of the zone-classification approach. Addressing the immune landscape, we observed a strong intrinsic IFN α and IFN γ response in the inner tumor and the tumor border compared to the peritumor and liver zones. Interestingly, antigen presentation seems to be specifically enriched in the zone C and D, hence in the tumor boarder, supporting the hypothesis of the tumor-liver interface being an immunologically important site (Figure 22b).

In the *Mrc1*.IFN α .miRT LV-treated cohorts we observe a similar pattern. Tumor related gene sets were found to be enriched in the inner tumor and tumor boarder, while liver related gene sets were enriched in the liver-spanning zones. Interestingly, the interface between LMS and liver appears to be less sharp especially in the partial responders as there is no significant downregulation of the tumor specific gene sets and no significant enrichment of hepatic gene sets in the peritumoral areas. Furthermore, the increased IFN α and IFN γ signaling is not only evident in the inner tumor and tumor boarder, but also in the peritumoral zones. In contrast to resistant mice, this spans not only the first peritumoral zone, but also the second peritumoral zone as well as the zone G in the partial responder cohort. This is overlapping with the transgene expression pattern observed in the biodistribution analysis (Figure 14a and b). Interestingly, *Mrc1*.IFN α .miRT LV treatment seems to trigger IL-10 signaling in LMS which is not observed in control mice (Figure 22b).

To better evaluate the effect of the treatment on each individual zone, we also performed an analysis comparing the different cohorts focusing on each zone individually. To that end, we determined the differentially expressed genes within each zone comparing the cohorts with each other. GSEA revealed a strongly increased IFN α and IFN γ response in both *Mrc1*.IFN α .miRT LV-treated cohorts compared to control mice in all zones. Interestingly, comparison between partial responders and resistant mice revealed enhanced IFN α and IFN γ signaling in resistant mice in the inner tumor, the tumor boarder and the first peritumoral area but not in the second peritumoral area and the liver area. Furthermore, triggering of IL-10 signaling is observed in resistant mice. This holds true for all zones in comparison to partial responder mice, but only the tumoral area and the first peritumoral area in comparison to animals. Indeed, we observe a decreased IL-10 signaling in the liver area of *Mrc1*.IFN α .miRT LV-treated animals compared to control animals. Moreover, antigen presentation is strongly increased in the inner tumor and the peritumoral area in partial responder mice, but not resistant mice, compared to control mice. In terms of immune unrelated effects, we observed striking changes in angiogenesis. Angiogenesis is decreased in the center of the tumor of partial responding mice, but not in resistant mice compared to control mice. Indeed, angiogenesis is slightly increased in the tumor and the first peritumoral area compared to control mice. The direct comparison between the partial responder and resistant cohort showed a

decreased angiogenesis in in the tumor and peritumor area in partial responders (Figure 22c).

Taken together, spatial transcriptomics revealed an endogenous inflammatory program activated in AKTPF organoid-derived murine LMS. Treatment with *Mrc1*.IFN α .miRT LV triggered an expansion of the inflammatory reaction towards the peritumor area. In line with observations from the scRNA-seq antigen presentation was enhanced only in partial responders and especially in the peritumoral area, the major side IFN α expression. In contrast, resistant mice are characterized by a strongly enhanced IL-10 signaling program, which is in accordance with the immune evasion mechanism observed in the scRNA-seq analysis.

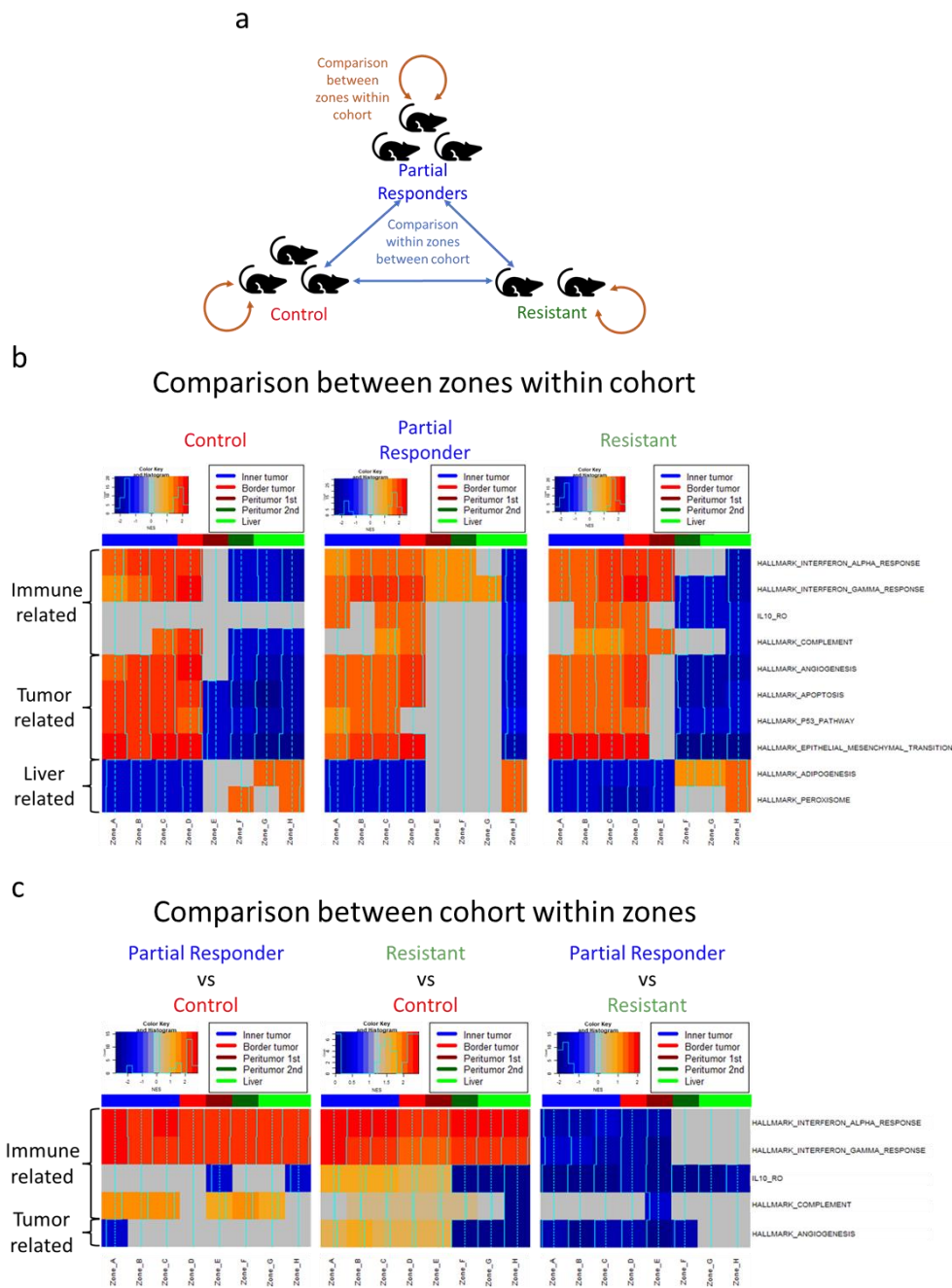


Figure 22: Spatial transcriptomics differential analysis of the previously defined zones. Sections from LMS bearing liver of the same mice processed for scRNA-seq were processed for spatial transcriptomics using the Visium technology from 10X Genomics. (a) Schematic description of the comparisons performed. (b) GSEA analysis for comparison between zones within the cohorts control (left), partial responders (middle) and resistant (right). Differentially expressed genes were calculated comparing each zone to all other zones within each cohort, ranked and processed for GSEA. The heatmap shows the NES for the different gene sets within each zone. The upper left shows a histogram with the detected NES describing the color scale with a positive NES in red and a negative NES in blue. For more detailed indication of the NES, the NES is plotted as a solid lightblue line each cell of the heatmap considering the same scale as the histogram on the x-axis and the dotted lightblue line indicating an NES of 0. If the GSEA analysis of a gene set led to a not significant result (adjusted p -value > 0.05) the NES was determined as 0 (Statistics: adjusted p -value based on an adaptive multi-level split Monte-Carlo scheme). The color bar above the plot indicates the area classification defined in figure 21g. (c) Comparison between cohorts within the same zone. For this comparison, differentially expressed genes were calculated within each zone comparing partial responders and control (left), resistant and control (middle) and partial responder and resistant. The heatmap representation is the same as in (b).

4 Discussion

Recent advances in the understanding of tumor biology as the definition of the tumor hallmarks has allowed development of new therapeutic strategies like targeted therapy and immunotherapy (Hanahan, 2022; Hanahan & Weinberg, 2011, 2000). However, durable and complete clinical response rates especially for solid tumors remain limited (Sambi *et al*, 2019). One of the reasons for the underperformance of these strategies in solid tumors is the powerful immune suppressive microenvironment, which does not allow establishment of antitumoral immune reactions rendering most immunotherapies ineffective (Yu *et al*, 2021; Schoenfeld & Hellmann, 2020; Jenkins *et al*, 2018). Consequently, CRC patients diagnosed with liver metastasis, which are characterized by an extraordinarily strong immunosuppressive environment, do not benefit from novel treatment approaches such as CAR T cells or checkpoint inhibitors (Burga *et al*, 2015; Yu *et al*, 2021).

To overcome this obstacle, it is of crucial importance to remodel the TME towards an immune activating state to allow antitumoral immune reactions. In this context, specific targeting of the tumor while sparing healthy tissue has been considered the “holy grail”. For example, IFN α has demonstrated an antitumoral effect in several different tumor types including liver metastasis arising from CRC which was accompanied by the remodeling of the TME towards a proinflammatory and antitumoral state (Catarinella *et al*, 2016; Escobar *et al*, 2014a). However, clinical application remains challenging due to severe side effects observed upon systemic application of relevant doses (Sleijfer *et al*, 2005).

In this regard, the strategy to employ cells, which locate in close proximity to the tumor, as trojan horses to convey the immune activating cytokine IFN α may prove a valid strategy to overcome this hurdle. Indeed, recent studies exploring Tie2-expressing monocytes for expression of IFN α in the TME has shown encouraging results in preclinical studies and has led to the initiation of a clinical trial for the treatment of glioblastoma multiforme (Escobar *et al*, 2014a, 2014b, 2018; Catarinella *et al*, 2016). However, the requirement of hematopoietic stem cell transplantation and the variation in the number of Tie2-expressing monocytes in the TME of different patients provides challenges for this approach.

Here, we present a new strategy based on *in vivo* gene therapy to specifically deliver IFN α to CRC LMS, which allows increase of the number of transgene-expressing cells and without the requirement of a hematopoietic stem cell transplantation. The intrinsic capability of lentiviral vectors to transduce KCs *in vivo* upon systemic injection in combination with the regulatory elements *Mrc1* promoter and miRT-122 and miRT-126 provides a tool to selectively engineer a highly abundant liver resident cell type, which is closely associated to LMS. Indeed, with a single intravenous injection of the KC-LV, a high fraction of KCs can be converted into vehicles to express IFN α in the liver of LMS bearing mice. Following the intrinsic properties of *Mrc1* promoter and the increased M2-like polarization state of tumor-associated KCs, the transgene expression is strikingly increased in areas surrounding LMS, hence allowing not only specific targeting of the tumor bearing organ but also an increased IFN α expression at the tumor site inside the liver. Tumor infiltrating macrophages express the transgene only to a lower extent. This is most likely due to the origin of TAMs, which are conventionally bone marrow-derived and therefore not targeted by the KC-LV platform. It is unclear if bone marrow-derived TAMs in the TME at the moment of LV injection cannot be reached and engineered by the KC-LV platform or if a fast turnover of TAMs leads to a rapid removal of engineered TAMs from the TME. However, we believe that expression of IFN α at the border area of the tumor is more desired than inside the tumor as several studies have identified the peritumoral area as major site for the initiation of immune reactions. Indeed, the result of our spatial transcriptomic analysis supports this hypothesis as we observe an increased inflammatory signaling and antigen presentation in this area even in control-treated animals. Next to KCs we only observed off target expression in splenic red pulp and marginal zone macrophages. Tissue resident splenic macrophages are characterized by a similar function and transcriptional profile as KCs. Further characterization and miRNA profiling of these two populations will be necessary to efficiently remove off target expression in splenic macrophages. However, the spleen is part of the lymphatic system and plays a central role in the initiation of T cell-based immune reaction. Therefore, an immunologic stimulation by IFN α expression in the spleen may have a beneficial effect and further support the initiation of antitumor immune reactions. Importantly, no chronic tissue damage has been observed in the spleen.

The appearance of severe adverse events in context of systemic IFN α treatment is believed to be caused by the bioavailability. Repeated systemic IFN α injection leads to the typical peak-and-drop in systemic levels of IFN α in which the level of IFN α reaches toxic levels immediately after injection and drops below the therapeutic window after the injection. This leads to the induction of side effect as well as low therapeutic efficiency due to desensitization and only a short period in which the level of IFN α is within the optimal therapeutic window (Budhwani *et al*, 2018). With the gene-based approach presented in this project, we are able to overcome this obstacle. Indeed, we observe sustained IFN α expression over the period of one year, which is directly dependent on the injected LV dose, thus allowing a good dose control. The initial drop as well as the slow decay of the transgene expression most likely reflects counter selection of the highly transduced IFN α expressing KCs followed by a slow decay of the less transduced KCs, respectively. A counter selection of IFN α expressing KCs in general can be expected due to autocrine IFN α signaling, which may alter the activation status and reduce the proliferative potential of these KCs. Importantly, the counter selection is not dependent on the LV transduction itself as the transduction level in control-treated mice is maintained. In general, the observed decay can be considered beneficial as this allows a natural termination of the treatment. Alternatively, if the treatment has to be terminated at earlier time points due to unforeseen events, a temporal KC depletion could be considered.

Indeed, the sustained IFN α expression at the tumor side led to an accumulation of IFN α in the plasma of treated mice which can be considered close to physiological as similar amounts of IFN α can be observed during acute viral infections (Hickerson *et al*, 2020). The prolonged exposure to these levels of IFN α did not induce any severe side effects other than a reduction in the absolute number of B cells. The severity of the reduction in B cell counts was directly correlating with the amount of IFN α in the plasma of the mice. Whether the reduction is a result of overactivation of B cells in circulation or an impairment in B cell development leading to a reduced B cell clonality remains to be elucidated. However, the reduction of B cells can be evaluated as tolerable considering the complete lifelong B cell depletion in B cell lymphoma patients treated with a CD19-directed CAR T cell therapy (Schuster *et al*, 2017). Importantly, common IFN α -related

side effects such as neutropenia, induction of autoimmune responses or chronic inflammation have not been observed in treated animals (Sleijfer *et al*, 2005). This is of crucial importance for clinical translation of this treatment approach.

In the field of cancer research, the choice of an appropriate tumor model is of crucial importance for the accurate prediction of the therapeutic potential as well as investigation of mode of action of new treatment options. Here, we used two distinct murine models of CRC-LMS, both based on 5- to 8-week-old female C57Bl6 mice. The gender and age selectivity were introduced for practical reasons as young female mice allow facilitated mouse handling and display reduced fighting between individuals. However, the selectivity of mice used in this study may give rise to a bias as gender and age are well established risk factors for the developments of metastatic CRC with an increased incidence in male individuals and an amplified risk at high age (Abancens *et al*, 2020; Siegel *et al*, 2020). While the MC38 cell-based tumor model is characterized as microsatellite instable, the AKTPF organoids are microsatellite stable, hence investigating two distinct subtypes of CRC harboring a different degree of immunogenicity. Importantly, we were able to demonstrate a clear therapeutic effect demonstrated in a reduced tumor growth in mice treated with the *Mrc1*.IFN α .miRT LV. The therapeutic efficiency is evident for all doses tested in the range between $3 \cdot 10^7$ TU up to $3 \cdot 10^8$ TU per mouse. Indeed, we observed a complete response in up to 50 % of treated animals. In general, the therapeutic efficiency seems to be enhanced in the AKTPF organoid tumor model. There are several reasons that can explain this observation. First, the MC38 cell-based tumor model leads to the development of a single bulky metastasis while the AKTPF organoid tumor model is characterized by the presence of multifocal metastasis of smaller size. Therefore, the border area is strongly increased in the AKTPF organoid tumor model in comparison to the cumulative tumor volume. The biodistribution studies have shown that the peritumoral area is the main area of IFN α expression and is most likely the site of initiation of an antitumor immune reaction. Furthermore, we observed an increased amount of transgene expressing cells in the TME of AKTPF organoid-derived tumors compared to MC38 cell-derived tumors. Therefore, the IFN α delivery to LMS may be more efficient in the AKTPF organoid tumor model. Moreover, AKTPF organoid-derived tumors show a more differentiated TME including tumor gland formation, necrotic areas and infiltration of immune cells while MC38 cell-

derived tumors appear to be less structured and more like a cellular mass. One might speculate that the presence of a distinct tumor microenvironment might favor the immune activating effect of IFN α . Indeed, the reprogramming of the TME towards an immune stimulating state appears to be more evident in the AKTPF organoid-based tumor model. Importantly, as previously demonstrated, the AKTPF organoid tumor model closely recapitulates the human disease, more than the MC38-based tumor model. Therefore, we can speculate that the therapeutic effect observed in the MC38-based tumor model is rather underestimating the clinical potential while results obtained from the AKTPF organoid tumor model more accurately predicts the clinical potential as well as the mechanistic.

In line with the more efficient IFN α delivery in AKTPF organoid tumor model, we observed an increase in expression of IFN α responsive genes only in AKTPF organoid-derived tumors but not in MC38-based tumors. However, baseline expression especially of *Ifit1* and *Oas1a* in MC38 tumors was highly increased compared to liver, spleen and AKTPF tumors. The expression of the IFN α receptor appears unaltered between both tumor models, which excludes potential differences in the capability of sensing IFN α . This suggests that there is an intrinsic IFN α signaling program activated in MC38 cell tumors, which is less evident in AKTPF organoid-derived tumors. As additional supply of IFN α still leads to a beneficial effect in the MC38 cell tumor model, the intrinsic IFN α signaling program is most likely independent from the presence of IFN α in the TME but rather triggered by a dysregulation of intrinsic signaling cascades such as the cGAS-STING or MAVS pathway, which both act through NF κ b (Schneider *et al*, 2014). The role of the cGAS-STING pathway in cancer cells has been described as ambivalent. While cGAS-STING pathway activation can lead to the expression of IFN α which exerts an anti-tumoral role, chronic stimulation of the cGAS-STING pathway has been reported to induce inflammation-driven carcinogenesis (Khoo & Chen, 2018). Indeed, tumors with high and chronic intrinsic IFN α signaling have been described to be more prone to resistance to checkpoint inhibitor treatment through upregulation of PDL-1 expression on the surface of cancer cells (Budhwani *et al*, 2018). However, more detailed analysis focusing on this aspect are required to proof this hypothesis. Importantly, these resistance mechanisms appear to be dependent on cancer cell intrinsic IFN α signaling and not

necessarily dependent on the presence of IFN α in the TME. Evidently, the beneficial effect of IFN α delivery clearly exceeds the potential triggering of these resistance mechanisms.

The remodeling of the TME towards an immune activating state is evident in both tumor models. We observed increased CD8 T cell infiltration and polarization of tumor-associated macrophages towards an antitumoral M1-like phenotype, two characteristics which are commonly seen as positive prognostic markers (Brummelman *et al*, 2018; Lin *et al*, 2019; Peng *et al*, 2019; Lalos *et al*, 2021). However, to predict potential improvements of the therapy and to evaluate the possibility of synergistic effects for prospective combinatory treatment approaches such as a combination of the *Mrc1*.IFN α .miRT LV with CAR or TCR-engineered T cells or Immune checkpoint inhibitors, more detailed in the mechanistic function of the treatment is required. To that end, we focused on the AKTPF organoid tumor model for further mechanistic characterization as the predictive accuracy for clinical translation of this tumor model is increased. For that purpose, we analyzed control-treated, treatment resistant and partial responding mice. Of note, analysis of liver metastases from complete responding mice was not possible due to the absence of tumors. Therefore, the presented results may underestimate the effect present in complete responding mice.

In this work we aim at targeting not only the TME in general, but especially the immune privileged niche at the interface between tumor and parenchymal tissue, the peritumor area (Brück *et al*, 2021). To further support the importance of the peritumor area as well as investigate the effects of the treatment in a spatially resolved manner we performed spatial transcriptomic analysis. To enable integrative analysis and comparison between the different treatment cohorts, we developed an unbiased method to divide the tissue sections into eight areas dependent on their location relative to the tumor-liver interface. Accordingly, we observed enrichment of tumor specific pathways in zones inside the tumor and liver related pathways in the hepatic area for all treatment cohorts. This confirms the accuracy of the method to divide the sections into zones as well as further proves the value of the AKTPF organoid tumor model. The division between tumor area and hepatic area appears very sharp in control animals. In *Mrc1*.IFN α .miRT LV-treated animals, especially in treatment responsive mice, the division is less sharp

hinting on an enlargement of the immune privileged peritumoral area. This is especially evident looking at inflammatory responses. Furthermore, we observed an increased antigen presentation in the areas surrounding the tumor boarder, confirming the importance of the peritumoral area for the establishment of antitumor immune reactions. In line with expectations, we observed an enrichment of IFN α responses in the entire tissue of treated animals.

Single cell transcriptomic analysis confirms a treatment-related effect in all cellular compartments of the tumor infiltrate represented by the enrichment in IFN α response. Accordingly, the increased IFN α reshapes all immune cell compartments in the TME. Reprogramming is especially evident in the TAM compartment, in which TAMs of *Mrc1*.IFN α .miRT LV-treated animals appear transcriptionally distinct to those of untreated animals and characterized by increased antigen presentation and immune activation signatures. Importantly, they are enhanced in secretion of immune related cytokines. Strong reshaping of the macrophage compartment is in line with the high plasticity of macrophages and their capability to respond to external stimuli including IFN α (Squadrino *et al*, 2012; Cilenti *et al*, 2021). Furthermore, the cell types that are highly active in antigen presentations such as MonoDCs and cDCs are enriched in their number in the tumor microenvironment of treatment responsive animals. Several studies have shown that the polarization state of TAMs highly impact the overall state of the TME and therefore the appearance of antitumoral immune reactions (Yang *et al*, 2020). The increased antigen presentation in TAMs and APCs in general in combination with the expression of immune activating cytokines and chemokines and the increased levels of IFN α may then trigger T cell responses and enable increased infiltration and improved function of T and NK cells. Fittingly, we observed not only an increased CD8 T cell infiltration but also an improved effector function in the T and NK cell compartment in general and in CD8 T cell compartment in particular. One might think that the strong immunologic stimulus that T cells experience in the TME due to the high levels of IFN α might lead to overactivation and exhaustion of CD8 T cells. However, we observe the opposite, *Mrc1*.IFN α .miRT LV responsive mice showed a decreased exhaustion profile in the CD8 T cells compartment. Furthermore, we observe a unique population of CD8 effector T cells in treatment responding mice. Based on the increased expression of *Rora*

and *Tnf* they seem to be characterized by a high mobility and effector function. Experiments in the presence of a surrogate tumor antigen have confirmed that *Mrc1*.IFN α .miRT LV treatment triggers an accumulation of tumor specific CD8 T cells in the TME. Based on that finding, one may speculate whether these CD8 T effector cells are indeed tumor reactive T cells. However, further phenotypic characterization of this population is required to confirm this hypothesis. Furthermore, we observed at least a partial systemic protection from secondary subcutaneous tumor growth with matched tumor cells in mice that rejected the tumor after primary LMS challenge after treatment. This suggests the establishment of a systemic antigen specific immunity against the tumor cells. The appearance of a delayed tumor growth in one of the three rechallenged complete responder mice may be explained by immune escape mechanisms. MC38 cells are microsatellite instable and therefore subject to rapid accumulation of mutations. Loss of antigen as resistance mechanism to an antigen specific immunity may therefore be favored in these cells. It has to be taken into account that there were still elevated levels of IFN α in the plasma of the complete responder mice and an antitumoral effect manifested by delayed tumor growth due to IFN α cannot be excluded. However, the observed protection from secondary tumor growth in the complete responder mice clearly exceeds the expected effect of IFN α on the tumor growth.

In all therapeutic experiments, we observe a fraction of mice which appears refractory to the treatment with *Mrc1*.IFN α .miRT LV and display a tumor volume similar to control animals. Indeed, this observation has been made in the context with other IFN α -based treatment approaches as well (Escobar *et al.*, 2018, 2014b). However, the mechanism driving the resistance to IFN α -based treatments remain unclear. To shed light on what determines the responsiveness to the treatment we included treatment resistant mice in this analysis. The most evident characteristic of the TME from treatment resistant mice is the accumulation of Tr1-like cells. Tr1 cells are induced *in vitro* upon TCR engagement in the presence of IL10 and IFN α . IFN α is highly abundant in the TME of *Mrc1*.IFN α .miRT LV treated mice. IL10 is a cytokine, which plays a major role in the establishment of the immunosuppressive niche in the liver. Furthermore, the spatial transcriptomic analysis as well as the GSEA on the APC compartment reveals an upregulated IL10 response specifically in resistant mice hinting towards increased levels

of IL10 in the TME of resistant mice. The source of IL10 in this setting remains to be identified. However, it is evident that all the signals required for induction of Tr1 cells are present in the TME of resistant mice. While the polarization of CD4 T cells towards Tr1 cells is described as antigen specific, the effect is mainly antigen independent. Indeed, Tr1 cells exert their immunoinhibitory function mainly by the secretion of IL10 and Tgfb (Levings *et al*, 2002). This establishes a positive feedback loop for the polarization of CD4 T cells towards a Tr1-like phenotype. The increased levels of IL10 induce a reduction of antigen presentation in APCs. Indeed, we observe a reduced antigen presentation in the APC compartment of treatment resistant compared to responder mice. Indeed, the APC compartment of resistant mice is characterized by an M2-like phenotype, which may be induced by the increased levels of IL10. Furthermore, Tr1 cells have been reported to kill APCs in an antigen specific manner by the secretion of granzyme B and perforin upon TCR-MHCII interaction (Solé & Santamaria, 2021; Gruarin *et al*, 2019). Accordingly, we saw reduced amounts MoDCs and cDCs in the TME of resistant mice compared to responding mice. Similarly, we observed reduced effector functions and strongly increased exhaustion in the CD8 T cell compartment in resistant mice, two characteristics which were described in the context of IL10 secreting Tr1 cells (Blackburn & Wherry, 2007; Levings *et al*, 2002). Therefore, we did not only confirm the presence of an environment favoring Tr1 cell development in this setting and the presence of Tr1-like cells in the TME of resistant mice, but also observed the tolerogenic effects commonly correlated with Tr1 cells. Therefore, there is strong evidence that Tr1 cells play a central role in the resistance mechanism to the *Mrc1*.IFN α .miRT LV treatment. Whether this is a resistance mechanism specific for this setting or a universal concept for treatment resistance in immunotherapies that establish IFN α -based responses remains to be elucidated. However, recent work of the group of Max Pagani and coworkers underlines the importance of Tr1 cells in the TME of different tumor types as negative prognostic factor in general (Bonnal *et al*, 2021).

Taken together, we hypothesis a mode of action in which the APC compartment in the TME gets reshaped by the presence of IFN α which in turn triggers CD8 T cell responses by the secretion of proinflammatory cytokines and the increased antigen presentation especially in the peritumor area. In this stage, an antitumor immune reaction can be established. However, the presence of IFN α and IL10 in the TME, triggers the induction

and accumulation of Tr1-like cells. These, in turn, suppress the establishment and the effectiveness of antitumoral T cell responses, hence, establishing resistance against the *Mrc1*.IFN α .miRT LV treatment as well as tumor tolerance in general. To proof this hypothesis, we will have to perform further studies in which Tr1-like cell development is either forced or inhibited to confirm the Tr1 cells are indeed the major discriminant between treatment response and resistance.

It remains to be investigated what determines the outcome in individual mice. Of note, no differences in the levels of IFN α in the plasma or the induction of IFN α responses in the TME were observed comparing responding and resistant mice. We speculate that the discriminant between responding mice and resistant mice is the stochastic appearance of tumor specific CD8 T cell clones. If there is a strong induction of a CD8 T cell response prior to the appearance of Tr1-like cells, an antitumor immune reaction may be established and the tumor will be rejected. After the appearance of significant numbers of Tr1-like cells, antitumor immune reactions will be suppressed due to their tolerogenic function.

Based on this hypothesis, we would expect a strong synergistic effect when combining the *Mrc1*.IFN α .miRT LV treatment with the transplantation of tumor specific T cell products such CAR T cells or TCR engineered T cells. This would provide an immediate source for tumor reactive CD8 T cell responses prior to the induction of Tr1 like cells. Furthermore, the observation of increased CD8 T cell infiltration in LMS of treated animals further suggests this combinatory approach. However, it is unclear if such tumor reactive T cell products could give rise to Tr1 cells as well. Furthermore, blockage of IL10 signaling by the application of IL10-receptor directed antibodies, which are currently under clinical investigation, might prevent the induction of Tr1-like cells. In general, the strong reshaping of the TME towards an immunostimulatory state enables antitumoral immune reactions thus increasing the effectiveness of immunotherapy, which so far has shown little success for the treatment of CRC-LMS patients which.

Collectively, we developed a new gene therapy tool for therapeutic intervention in patients with CRC LMS. The good safety profile and strong therapeutic effect upon a single well tolerated injection proof its applicability and suggest *Mrc1*.IFN α .miRT LV treatment as a strong candidate for clinical translation. Further testing of combinatory

treatment approaches will be necessary to identify its full therapeutic potential. Furthermore, we identified a new Tr1 cell-based mechanism, which induces tumor tolerance and treatment resistance potentially not only in the setting of *Mrc1*.IFN α .miRT LV treatment but also in other immunotherapies triggering IFN α responses. Furthermore, the scRNA-seq data as well as the spatial transcriptomic data produced in this work may provide a rich source of information for further studies.

5 Material and Methods

5.1 Molecular Biology

5.1.1 Plasmid design, cloning and amplification

The *Mrc1*.GFP LV transfer vector plasmid (unpublished), the *PGK*.GFP LV transfer vector plasmid (Genovese *et al*, 2014) as well as the empty mirT reporter (No moRT) LV transfer vector plasmid (Amendola *et al*, 2005) were already present in the lab.

To originate the miRT 122 LV, miRT 126 LV and miRT451 we cloned four copies of the indicated miRT sequences, respectively, with randomized linker sequences separating the single miRT sites were inserted downstream to the WPRE sequence. The *Mrc1*.GFP.mirT LV was created by inserting four copies of the miRT 122 and the miRT 126 with randomized linker sequences downstream to the WPRE of the *Mrc1*.GFP LV transfer vector plasmid. The *Mrc1*.IFN α .miRT LV transfer vector plasmid was created by replacing the GFP sequence of the *Mrc1*.GFP LV transfer vector plasmid with an IFN α encoding sequence and inserting four copies of the miRT 122 and the miRT 126 with randomized linker sequences downstream to the WPRE. The ORFless LV transfer vector plasmid was generated by depleting the GFP sequence of the *Mrc1*.GFP LV transfer vector plasmid followed by insertion of 4 copies of the miRT 122 and the miRT 126 with randomized linker sequences downstream to the WPRE.

Ligation products were transformed in bacteria by adding about 100 ng of ligation product to 50 μ L of competent bacteria (Top10 cells/Invitrogen). The retransformation mix was carefully mixed, incubated for 30 minutes on ice, transferred to 42 °C for 30 seconds followed by two additional minutes incubation on ice. 500 μ L of Luria-Bertani (LB) medium was add and incubated for 1h at 37 °C. Bacteria were plated onto LB agar plates containing 100 μ g/mL ampicillin and incubated over night at 37 °C. Afterwards, single colonies were picked and transferred into 5 mL LB medium containing 100 μ g/mL of carbenicillin and incubated at for at least 12 h at 37 °C shaking at 180 rotations per minute (rpm). DNA was extracted from 3 mL of the bacteria culture using the Wizard® Plus SV Minipreps DNA Purification System kit (Promega/A1330).

Plasmids derived from different clones were screened by analytical digest as well as sangar sequencing to confirm correctness of the sequence.

The following restriction enzymes were used:

Table 2: Restriction enzymes.

Restriction enzyme	Provider	Catalogue number
SmaI	New England Biolabs	R0141S
Sall-HF	New England Biolabs	R3138S
AgeI-HF	New England Biolabs	R3552S
NcoI-HF	New England Biolabs	R3193
KpnI-HF	New England Biolabs	R3142
PmeI	New England Biolabs	R0560
XbaI	New England Biolabs	R0145
ScaI	New England Biolabs	R3122
AgeI-HF	New England Biolabs	R3552L

To further amplify the plasmids, the remaining 2 mL of the bacteria culture from clones containing plasmids with the correct sequence were used to inoculate 500 mL of LB medium containing 100 µg/mL of carbenicillin. This was incubated over night at 37 °C shaking at 180 rpm. DNA extraction was performed using Nucleobond® Xtra Maxi EF (Macherey- Nagel/ 740424.50). The plasmid was resuspended in endotoxin-free water.

5.2 Cell culture

5.2.1 Human embryonic kidney 293T (HEK-293T) cells

HEK cells were cultured in adherent cell culture at 37 °C at a density of 20-90 % confluency in Iscove's Modification of Dulbecco's Modified Eagle Medium (IMDM) medium (Corning/ 10-016-CV) supplemented with 10 % fetal bovine serum (FBS; HyClone™/ SH30066.03), penicillin (100 IU/mL) and streptomycin (100 µg/mL). For splitting, the medium was removed, cells were washed with Phosphate Buffered Saline (PBS; Corning/ 21-031-CVR), detached using a solution of 0.05% trypsin and EDTA (4mM) in PBS (ATV), resuspended in fresh medium and transferred into a new plate.

5.2.2 MC38 cells

The murine colorectal cancer cell line MC38 cells were cultured in the same way as described for HEK-293T cells. For generation of the MC38-mCherry cells, MC38 cells were transduced with an LV conveying a sequence encoding a fusion protein of the CD81 transmembrane with mCherry fused to its C terminus under the control of a PGK promotor. Similarly, MC38 cells were transduced with an LV conveying the sequence of chicken ovalbumin (OVA) under the control of a PGK promotor. For that purpose, 200000 MC38 cells were plated into a six-well plate. For the generation of the MC38-mCherry cells, a mixture of 50 % fresh medium and 50 % unconcentrated LV stock was added. Seven days after transduction, mCherry expression was determined by flowcytometry, identifying 99.97 % mCherry positive cells. For the generation of MC38-OVA cells, 0.1 μ L of concentrated vector stock was added to 1 mL of culture medium. Ten days after transduction, DNA was extracted and a VCN of 2.86 was detected.

5.2.3 AKTPF Organoids

AKTPF-Organoids were cultured at 37 °C in 30 μ L of phenol-red free and growth factor reduced matrigel (BD Biosciences/ 356231) in a 48-well surrounded by 300 μ L Advanced DMEM/F-12 medium supplemented with 2 % GlutaMAX™ Supplement (Gibco/ A1286001), penicillin (100 IU/mL), streptomycin (100 μ g/mL), 1 % HEPES buffer solution (Gibco/ 15630056), 1 % N-2 supplement (Gibco/ 17502-048), 2 % B-27 supplement (Gibco/ 12587-010), 1 mM N-acetylcysteine- (Sigma-Aldrich/ A9165) and 50 ng/mL murine epidermal growth factor (rmEGF; Gibco/ PMG8041). For splitting, the medium was removed and 500 μ L ice-cold cell recovery solution (Corning/ 354253) was added and carefully pipetted. The mix was incubated on ice for 20 minutes. Cells were pelleted by centrifuging at 4 °C and 300 xg for 6 minutes. The supernatant was removed, and the cells were washed and signaled by pipetting with 30 mL of ice-cold PBS. Cells were pelleted by centrifuging at 4 °C and 300 xg for 6 minutes, the supernatant was removed, and the cells were resuspended in fresh matrigel. New droplets were placed in the center of 48 wells and placed to 37 °C for 15 minutes to allow the matrigel to solidify. Afterwards, the matrigel droplet was covered with 300 μ L of fresh medium.

5.2.4 Bone marrow derived macrophages

Bone marrow was harvested from C57Bl6 mice by flashing the femur and tibia with 10 mL autoMACS running buffer (Miltenyi Biotec/ 130-091-221). Bone marrow cells were pelleted by centrifuging at room temperature (RT) and 1500 rpm for 5 minutes. For red blood cell lysis, 1 mL of desalt water was added to the cell pellet and 50 mL autoMACS running buffer were added. Cells were pelleted by centrifuging at room temperature and 1500 rpm for 5 minutes. The cell pellet was resuspended in RPMI medium (Corning/ 15-040-CV) supplemented with 10 % FBS, 2 % GlutaMAX™ Supplement (Gibco/ A1286001), penicillin (100 IU/mL), streptomycin (100 µg/mL) and 100 ng/mL of Mouse M-CSF (Miltenyi Biotec/ 130-101-704). After seven days, cells were differentiated into bone marrow derived macrophages (BMDM).

For transduction, 1×10^6 BMDMs were seeded into a 24 well plate and transduced with the indicated vector at an MOI of ten. The following day, fresh medium was added containing the required cytokines in the culture medium inducing polarization. For M2-polarisation: 50 ng/mL of mouse IL-4 (Miltenyi / 130-097-757) and for M1-polarisation: 100 ng of lipopolysaccharides from Escherichia coli O55:B5 (LPS; Sigma-Aldrich/ L6529-1MG) and 5 ng/mL of mouse IFN γ (Miltenyi/ 130-105-778). Six days after induction of polarization, FACS analysis was performed using the following antibodies:

Table 3: Antibodies used for flow cytometry analysis

Antibody	Supplier	Catalogue No.
CD206(MRC1)	Biolegend	141712
CD11b	Biolegend	101224
CD274 (PD-L1)	Biolegend	124308
F4/80	Biolegend	123118
CD16/CD32 (Fc Block)	BD Pharmagen	553142

5.2.5 LV-Production

5.2.5.1 Plasmids used for LV production

In this study, third-generation VSV-G pseudotyped LVs were used. Production of these LVs was based on the transfection of five plasmids into HEK-293T cells. The pMDLg/pRRE encoding for the enzymes and proteins necessary for the vector core (gag

and pol genes of the HIV-1) plus the RRE which is required for export of the viral mRNA from the nucleus. The pCMV-Rev encodes for rev under the control of a CMV promoter. pMD2.VSV-G encodes for the VSV glycoprotein also under the control of a CMV promoter. The transfer vector plasmid contains the transfer vector sequence including the transgene cassette flanked by the HIV-1 derived minimal sequence required for encapsulation into the LV particles, reverse transcription, nuclear import and integration into the host genome. The pAdVantageTM vector (Promega/ E1711) inducing enhanced protein expression in transfected cells.

5.2.5.2 *Calcium phosphate transfection*

For LV production about 9×10^6 cells were plated into 15-cm dish 24 hours prior to transfection. A medium exchange was performed two hours before transfection to a final volume of 20 mL. For each plate a transfection reaction mix was prepared containing the pMDLg/pRRE (12.5 μ g), pCMV-Rev (6.25 μ g), pMD2.VSV-G (9 μ g), transfer vector plasmid (36 μ g) and pAdVantageTM vector (15 μ g) in a mix of 0.1x TE and water at a ratio of 1:2 to a final volume of 1125 μ L. 125 mL of a 2.5M CaCl₂ solution in water was added and the solution was mixed for 15 minutes using a spinning wheel. Immediately before transfection, 1250 μ L of a 2X HBS solution (281 mM NaCl, 100 mM HEPES, 1.5 mM Na₂HPO₄, pH 7.12) was added dropwise to the transfection reaction mix while vortexing at an intermediate speed. The reaction mix was immediately added to the cell culture medium. The medium was exchanged 14 to 16 hours after transfection to a final volume of 16 mL per plate. 30 hours later the supernatant was collected and filtered using a 0.22 μ m filter. If not indicated differently, concentrated LV stocks have been used in this project. For that purpose, the LV was centrifuged at 20000 xg for 2 hours at 20 °C. The supernatant was discarded and the LV pellet was resuspended in PBS for a 500X concentration. The LV stocks were aliquoted and stored at -80 °C.

5.2.5.3 *Titration*

The titer of the LV stocks was assessed by determination of the concentration of HEK 293T cell-transducing units (TU/mL). For that purpose, 200000 HEK 293T cells were seeded into a six-well plate. A serial dilution in medium of the concentrated vector stock was prepared with a factor 10, ranging from $1/10^3$ till $1/10^7$. 1 mL of the respective dilution was added on each well in the presence of the transduction enhancer polybrene

at a concentration of 16 µg/mL. The following day the medium was exchanged with normal medium. Transduction efficiency was assessed by ddPCR-based VCN determination. The titer was calculated based on the calculation:

$$\text{Titer} \left[\frac{\text{TU}}{\text{mL}} \right] = \text{VCN} * \frac{200000}{\text{dilution factor}}$$

5.3 ddPCR for vector copy determination and gene expression analysis

5.3.1 Vector copy number determination

From cell culture samples genomic DNA was extracted using with the Maxwell® 16 instrument (Promega) using the Maxwell® 16 DNA purification kit (Promega/ AS1030). For samples with a low cell number such as sorted cells the QIAamp® DNA micro kit (Qiagen/ 56304) was used while genomic DNA from whole tissue samples was extracted with the DNeasy Blood and Tissue Kit (Qiagen/ 69506). VCN was determined using the QX200 Droplet Digital PCR System (Biorad). The digital droplet PCR was performed according to the manufacturer's instructions; 5-20 ng of genomic DNA was added to the reaction, primers were used at a concentration of 900nM and the detection probes at 250 nM. Droplets were analyzed using the BioRad QX200 Droplet Reader and the QuantaSoft software (Biorad) was used for data analysis. For the detection of HIV genomes, the following primer and probe set was used: forward primer: 5'-TACTGACGCTCTCGACC -3'; reverse primer: 5'-TCTCGACGCAGGACTCG -3'; probe in the FAM detection channel: 5'-(FAM)-ATCTCTCTCCTTCTAGCCTC-(MGB)-3'. As normalizer for murine samples the *Sema3a* gene was used: forward primer: 5'-ACCGATTCCAGATGATTGGC -3'; reverse primer: 5'-TCCATATTAATGCAGTGCTTG -3'; detection probe in Hex channel: 5'-(HEX)-AGAGGCCTGTCCTGCAGCTCATGG -(BHQ-1)- 3'. For human samples, instead, the *GapDH* gene was used as normalizer (TaqMan™ Gene Expression Assay from Invitrogen; catalogue number: 4400291; Assay number: Hs00894322_cn). VCN was calculated by the formular:

$$\text{VCN} = \frac{\text{concentration}(\text{HIV})}{\text{concentration}(\text{Normalizer})} * 2$$

5.3.2 Gene expression

Gene expression analysis was performed based on digital droplet PCR as previously described as well. For that purpose, RNA was extracted from frozen tissue using the RNeasy® Plus Mini Kit (Qiagen/ 74134). Retro transcription was performed according to manufacturer's instruction with the SuperScript™ IV VILO (Invitrogen/ 11766500). 5-20 ng of generated cDNA was used as input for the gene expression analysis. TaqMan™ Gene Expression Assay from Invitrogen were used. The following primer/probe pairs were applied:

Table 4: TaqMan™ Gene Expression Assays used in this project.

Target	Detection channel	Reference number	Catalogue number
<i>Hprt</i>	VIC	4448491	Mm03024075_m1
<i>Irf7</i>	FAM	4331182	Mm00516788_m1
<i>Ifit1</i>	FAM	4331182	Mm00515153_m1
<i>Oas1a</i>	FAM	4331182	Mm00836412_m1
<i>Ifnar1</i>	FAM	4331182	Mm00439544_m1
<i>Ifnar2</i>	FAM	4331182	Mm00494916_m1

5.4 Flow cytometry analysis and fluorescence activated cell sorting

For flow cytometry analysis, cells from cell culture or tissues processed for flow cytometry analysis were incubated in 100 µL autoMACS running buffer containing the indicated antibodies at the indicated concentrations for 15 minutes on ice. Afterwards cells were washed twice by addition of autoMACS running buffer followed by centrifugation at 1500 rpm for 5 minutes and discarding of the supernatant. Then, cells were resuspended in 200 µL autoMACS running buffer containing a 1:50 dilution of 7AAD (BioLegend/ 420404). Samples were analyzed using either a FACSCanto II or a FACSymphony™ A5 Cell Analyzer (BDBiosciences). For fluorescence activated cell sorting a BD FACSAria Fusion was used.

5.5 In-vivo methods

5.5.1 Mouse strains

Female 6-week-old C57Bl/6N mice, NUDE mice or NSG mice were purchased from Charles River Laboratory.

5.5.2 LV Injection

For systemic LV injection, LVs were diluted in PBS to obtain the desired TU to be injected per mouse in a volume of 250 μ L. Mice were warmed up and the LV was injected by tail vein injection.

5.5.3 Intrahepatic injection of MC38 cells

For intrahepatic transplantation of MC38 cells, the fur of mice was removed in the stomach area one day prior to the surgical procedure by shaving followed by application of hair removal cream (Balea). Immediately prior to surgery, mice were injected with 50 μ L carprofen (2.5 mg/mL) for pain treatment. During surgery, mice were anesthetized using isoflurane (Iso-Vet) at a concentration of about 3 % in about 95 % to 98 % oxygen. A liver lobule was exposed by with a ventral cut up to the sternum opening the peritoneum. Either 500000 cells (MC38-mCherry and MC38-OVA) or 100000 cells (MC38-WT) resuspended in a volume of 5 μ L PBS were injected localized into the liver lobule. The peritoneum wall was closed by stiches while the skin was closed with clamps. Following surgery, mice were subjected to antibiotic treatment for one week by adding Baytril (Bayer) at a concentration of 0.5 mg/mL to the drinking water.

5.5.4 Subcutaneous injection of MC38 cells

For subcutaneous MC38-WT cell injection, $1 \cdot 10^6$ cells were injected in subcutaneously into the flank of mice in a volume of 100 μ L PBS. Tumor growth was followed by measuring the dimensions (diameter x and diameter y) and tumor volume was calculated with the formula:

$$Volume = \frac{3}{4} * \pi * (0.5 * diameter(x))^2 * 0.5 * diameter(y)$$

in which diameter(x) is the larger diameter.

5.5.5 Intrasplenic injection of AKTPF organoids

Intrasplenic transplantation of AKTPF organoids is based on a surgical procedure similarly to the intrahepatic injection. Organoids were split two days prior to the injection and an equivalent of organoids from three wells was injected per mouse which corresponds to an estimate of $3\text{-}4 \times 10^5$ cells. One day prior to the surgery, the fur of the mice was removed at the left flank of the mice by shaving followed by application of hair removal cream (Balea). Immediately prior to surgery, mice were injected with 50 μL carprofen (2.5 mg/mL) for pain treatment. Similar to the previously described procedure of intrasplenic injection, isoflurane (Iso-Vet) at a concentration of about 3 % in about 95 % to 98 % oxygen was used to anesthetize the mice during surgery. With a cut at left flank of the mice below the rib cage, the spleen was exposed. AKTPF-organoid cells were, resuspended in 50 μL matrigel (BD Biosciences/ 356231) and carefully injected into the spleen using a precooled syringe (29 G, U-100 INSULIN 0.5 mL/324892). The peritoneum wall was closed by stitches while the skin was closed with clamps. Following surgery, mice were subjected to antibiotic treatment for one week by adding Baytril (Bayer) at a concentration of 0.5 mg/mL to the drinking water.

5.5.6 Blood collection and analysis

Blood was retrieved either from the tail vein or retroorbital. Hemocytometer analysis was performed on whole blood using the ProCyte DX™ (IDEXX).

For flow cytometry analysis, in contrast to the procedure described above, the antibodies were directly added at the indicated concentrations to 70 μL blood and incubated at 15 min protected from light on ice. Afterwards, 2 mL of Red Blood Cell Lysis Buffer Hybri-Max™ (Sigma/R7757-100ML) was added and vortexed briefly. This was incubated for 10 minutes in the dark. Afterwards cells were washed twice by addition of autoMACS running buffer followed by centrifugation at 1500 rpm for 5 minutes and discarding of the supernatant. Then, cells were resuspended in 200 μL autoMACS running buffer containing a 1:50 dilution of 7AAD (BioLegend/ 420404). Samples were analyzed using the FACSymphony™ A5 Cell Analyzer (BDBiosciences). The following antibodies were used for blood analysis:

Table 5: Flow cytometry antibodies used for blood analysis.

Target	Color	Dilution	Provider	Article number
CD11b	Pacific Blue	1/70	Biolegend	101224
CD11b	Brilliant Violet 711	1/70	Biolegend	101242
CD206(MRC1)	Alexa Fluor 647	1/70	Biolegend	141712
CD223 (LAG3)	PE	1/70	BD	552380
CD279 (PD1)	PE/Cy7	1/70	BioLegend	135216
CD4	BUV737	1/70	BD Horizon	564933
CD44	BV605	1/70	BD	563058
CD45	Brilliant Violet 510	1/140	Biolegend	103138
CD45R/B220	APC/Cy7	1/70	Biolegend	103224
CD8a	FITC	1/140	BD Pharmagen	553030
Gr-1 (Ly6G7Ly6C)	APC	1/140	Biosciences	553129
LY6C	eFluor 450	1/70	eBioscience	48-5932-82
Ly6G	PE/Cy7	1/70	Biolegend	127618

Furthermore, plasma and serum were collected. For the collection of plasma, blood was collected initially collected in a Microvette[®] (Sarstedt/20.1341). The blood was centrifuged at 3000 xg for 10 minutes at room temperature and the fraction of clear supernatant was collected. For the collection of blood serum, blood was collected in a conventional Eppendorf tube. The blood was incubated at room temperature for 40 minutes. Afterwards, the blood was centrifuged at 3000 xg for ten minutes at room temperature and the fraction of clear supernatant was collected.

Quantification of IFN α content in the blood was performed on plasma. For that purpose, the plasma was diluted at an appropriate factor between 10-fold and 50-fold and the Mouse IFN Alpha All Subtypes ELISA KIT High Sensitivity (pbl Assay Science/ 42115-1) was used according to manufacturer's instruction.

The quantification of autoreactive antibodies was performed on blood serum and was performed by the UTSW Microarray Core facility (University of Texas, Southwestern Medical Center).

5.5.7 Magnetic resonance imaging analysis for liver metastasis volume assessment

For magnetic resonance imaging a 7T preclinical scanner (Bruker, BioSpec 70/30 USR, Paravision 6.0.1), equipped with 450/675 mT/m gradients (slew-rate: 3400-4500T/m/s; rise-time 140 μ s) and a circular polarized mouse body volume coil with an inner diameter of 40 mm was used. During acquisition, mice were kept in anesthesia by inhaling isoflurane (Iso-Vet) at a concentration of about 3 % in about 95 % to 98 % oxygen and mice were placed on a dedicated temperature control apparatus to prevent hypothermia. The breathing rate and the body temperature was continuously monitored (SA Instruments, Inc., Stony Brook, NY, USA). To display liver lesion, we used a hepatocyte-specific contrast agent, the Gd-EOB-DTPA (Bayer Schering Pharma, Berlin, Germany) known as gadoxetic acid (0.05 μ mol/g of body weight). Axial fat-saturated T2-weighted images (RARE-T2, Rapid Acquisition with Relaxation Enhancement, TR = 3000 ms, TE = 40 ms, voxel-size = 0.125 \times 0.100 \times 0.8 mm, averages = 4,) and axial fat-saturated T1-weighted sequences (RARE-T1: TR = 540 ms, TE = 7.2 ms, voxel size = 0.125 \times 0.100 \times 0.8 mm, averages = 4) were acquired during the hepatobiliary phase of Gd- EOB-DTPA enhancement (10 minutes after administration). Volume measurement was performed taking advantage of the Medical Image Processing, Analysis, and Visualization software (MIPAV).

5.5.8 Endpoint analysis

For endpoint analysis, mice were euthanized by cervical dislocation. The liver was perfused by injecting 10 mL PBS containing 5 mM EDTA (Invitrogen/ 15575-038) through the central vein and cutting the portal vein to allow exiting of the solution to achieve clearance from peripheral blood. When flow cytometry analysis but not immunofluorescence analysis is performed, 10 mL of IMDM (Corning/ 10-016-CV)

containing 0.35 mg/mL collagenase (Sigma-Aldrich/ C5138-16) was injected in the same way to initiate digestion of cell-to-cell interactions. Required organs were collected.

5.5.9 Processing of organs for flow cytometry analysis

For flowcytometry analysis, organs were cut into small piece and one mL IMEM (Conring/ 10-016-CV) supplemented with 0.35 mg/mL collagenase (Sigma-Aldrich/ C5138-16) was added. This was incubated at 37 °C while shaking at 350 rpm for ten minutes. Afterwards, the tissue was further dissociated by pipetting and filtered using a 0.4 µm cell strainer (Corning/ 352340). The cells were washed two times with autoMACS running buffer and further processed for flow cytometry analysis as described above. The following antibodies were used:

Table 6: Antibodies used for flow cytometry analysis on murine organs.

Target	Color	Dilution	Provider	Article number
CD11b	Brilliant Violet 711	1/200	Biolegend	101242
CD11c	PE/Cy7	1/100	Biolegend	117318
CD16/CD32 (Fc Block)	-	1/100	BD Pharmagen	553142
CD206(MRC1)	Alexa Fluor 647	1/100	Biolegend	141712
CD223 (LAG3)	BV421	1/100	BioLegend	125221
CD24	BV605	1/100	BioLegend	101827
CD271 (LNGFR)	APC	1/10	Miltenyi Biotec	130-113-418
CD274 (PD-L1)	PE	1/100	Biolegend	124308
CD279 (PD1)	PE/Cy7	1/100	BioLegend	135216
CD31	Alexa Fluor 647	1/100	Biolegend	102516
CD31	FITC	1/100	eBioscience	11-0311-82
CD4	BUV737	1/100	BD Horizon	564933
CD44	BV605	1/100	BD	563058
CD45	Brilliant Violet 510	1/100	Biolegend	103138
CD45R/B220	PE	1/100	Biosciences	553090
CD45R/B220	PB	1/100	BD Pharmagen	558108
CD45R/B220	APC/Cy7	1/100	Biolegend	103224
CD62L	BV786	1/100	Biosciences	564109
CD86	APC/Cy7	1/100	Biolegend	105030
CD8a	FITC	1/100	BD Pharmagen	553030
F4/80	APC/Cy7	1/100	Biolegend	123118
F4/80	FITC	1/100	Biolegend	123108
F4/80	PE	1/100	Biolegend	123110
Ly6C	APC/Cy7	1/100	BioLegend	128026
LY6C	eFluor 450	1/100	eBioscience	48-5932-82

Ly6G	PE/Cy7	1/100	Biolegend	127618
LY6G	BV605	1/100	Biosciences	563005
Ly6G	BUV737	1/100	Biosciences	741813
MHCII	Brilliant Violet 785	1/100	Biolegend	107645
TCRβ	BV711	1/100	Biosciences	563135

5.5.10 Processing of organs for IF analysis

For immune fluorescence, a piece of the respective organ was incubated in paraformaldehyde solution 4 % in PBS (PFA; ChemCruz®/ SC281692) for 4 hours at 4 °C. Afterwards, the PFA was exchanged for a solution of 10% sucrose (Sigma-Aldrich/ S0389) and 0,02% NaN₃ in H₂O. After an 8h incubation at room temperature, this was exchanged for a 20% sucrose solution containing 0,02% NaN₃ in H₂O. Finally, after further 8 h of incubation at room temperature, the organ was transferred into a 30% sucrose solution containing 0,02% NaN₃ in H₂O and incubated at 8 hours. The organ was embedded into Killik, O.C.T. Compound embedding medium for cryostat (Bio-Optica/ 05-9801). Sections of 20 μ m thickness were prepared and placed on glass slides using a cryostat. These sections dried for 30 minutes at room temperature. For antigen retrieval, slides were incubated for 20 minutes in a 95 °C preheated water bath in the following solution: for a low pH antigen retrieval: 10 mM citric acid in H₂O pH adjusted to pH 6; for high pH antigen retrieval: 10 mM Tris base and 1mM EDTA plus 0,05 % tween in H₂O with the pH adjusted to pH 9. Afterwards slides were cooled down in the indicated solution of 15 minutes at room temperature and then slides were washed with PBS three times by covering the glass slides completely and incubating for 5 minutes while mildly shaking with an orbital shaker. Blocking was performed by covering the sections with blocking buffer (5 % normal donkey serum, 1 % BSA (Sigma-Aldrich/ A9647), 0.3 % TritonTM X-100 (Sigma/ T8787)). For staining with a primary antibody with mouse origin, mouse on mouse Ig blocking solution (Vector Laboratories/ MKB-2213) was added according to manufacturer's instruction. This was incubated for 1h at room temperature and afterwards replaced by blocking buffer containing the indicated concentrations of primary antibody for an overnight incubation at 4 °C. The following day, the sections were washed with washing buffer (PBS containing 0.3 % TritonTM X-100) for five times. Sections were stained with the secondary antibody by covering them in their indicated concentrations in blocking buffer. An incubation for one hour at room

temperature in the dark was performed followed by six washing steps with washing buffer. For staining of the nuclei, sections were covered with a 1/2000 dilution of Hoechst 33342 solution (life technology/ H3570) in PBS for two minutes. Slides were washed additional three times with PBS and mounted using Fluoromount-G® (SouthernBiotech/ 0100-01). Images were acquired using an SP8 lightning confocal microscope (Leica Microsystems) at a 10x magnification. The following antibody combinations of primary and secondary antibodies were used:

Table 7: Antibodies and antibody combinations used for immunofluorescence staining.

Pane	target	Clone	Host	Cat/Provider	Dilution	2nd AB	Cat/Provider	label	Dilutio	Retrieva	Figure
1	E-Cadhering	Polyclonal	Goat	AF748/R&D Systems	1/50	Donkey-aGoat	A32849/Invitrogen	AF647	1/300		Figure 13c and 16e
	CD8a	4SM16	Rat	14-019-582e/Bioscience	1/100	Donkey-aRat	ab150154/abcam	AF555	1/300	high pH	
	CD4	EPR1951	Rabbit	ab183685/abcam	1/100	Donkey-	A11010/Invitrogen	AF488	1/300		
2	E-Cadhering	Polyclonal	Goat	AF748/R&D Systems	1/50	Donkey-aGoat	A32849/Invitrogen	AF647	1/300		Figure 13e
	α -SMA	1A4	Mouse	G6198-.2ML/Merck	1/100	-	-	Cy3	-	Low pH	
3	CD31	Polyclonal	Rabbit	ab28364/abcam	1/50	Donkey-	A11010/Invitrogen	AF488	1/300		Figure 13d
	E-Cadhering	Polyclonal	Goat	AF748/R&D Systems	1/50	Donkey-aGoat	A32849/Invitrogen	AF647	1/300		
	F4/80	CI:A3-1	Rat	ab6640/abcam	1/100	Donkey-aRat	ab150154/abcam	AF555	1/300	none	
4	CD11c	Polyclonal	Rabbit	97585S/Cell signalling	1/100	Donkey-	A11010/Invitrogen	AF488	1/300		Figure 14
	E-Cadhering	Polyclonal	Goat	AF748/R&D Systems	1/50	Donkey-aGoat	A32849/Invitrogen	AF647	1/00		
	F4/80	CI:A3-1	Rat	ab6640/abcam	1/500	Donkey-aRat-	A32849/Invitrogen	Tritc	1/500	none	
5	GFP	Polyclonal	Chicke	abcam/ab13970	1/500	Donkey-	703-545-155/Jackson	AF488	1/500		Figure 6e
	F4/80	CI:A3-1	Rat	ab6640/abcam	1/200	Goat-aRat	A21247/Invitrogen	AF647	1/500		
	mCherry	Polyclonal	Rabbit	ab167453/abcam	1/200	Goat-aRabbit	A11010/Invitrogen	AF546	1/500	none	
6	GFP	Polyclonal	Chicke	abcam/ab13970	1/500	Goat-aChicken	A-11039/Invitrogen	AF488	1/500		Figure 6d
	F4/80	CI:A3-1	Rat	ab6640/abcam	1/200	Goat-aRat	A21247/Invitrogen	AF647	1/500	none	
	GFP	Polyclonal	Chicke	abcam/ab13970	1/500	Goat-aChicken	A-11039/Invitrogen	AF488	1/500		
7	F4/80	CI:A3-1	Rat	ab6640/abcam	1/200	Goat-aRat	A21247/Invitrogen	AF647	1/500	none	Figure 5f
	GFP	Polyclonal	Chicke	abcam/ab13970	1/500	Goat-aChicken	A-11039/Invitrogen	AF488	1/1000		

5.5.11 Processing of organs for VCN and gene expression analysis

A small piece of the target organ was taken and frozen at -80 °C. Afterwards, it was processed for VCN analysis as described above.

5.6 Single-cell RNA sequencing

5.6.1 Sample processing and fluorescence activated cell sorting

Immediately after euthanizing the mice and perfusion with PBS containing 5 mM EDTA, liver metastases were isolated and dissociated into single cells as described above. No antibody staining was performed, single cells were resuspended in autoMACS running buffer containing 7AAD (BioLegend/ 420404) in a 1/50 dilution. Viable cells were sorted based on the gating strategy depicted below (Figure 23). A minimum of 100000 cells per sample were sorted.

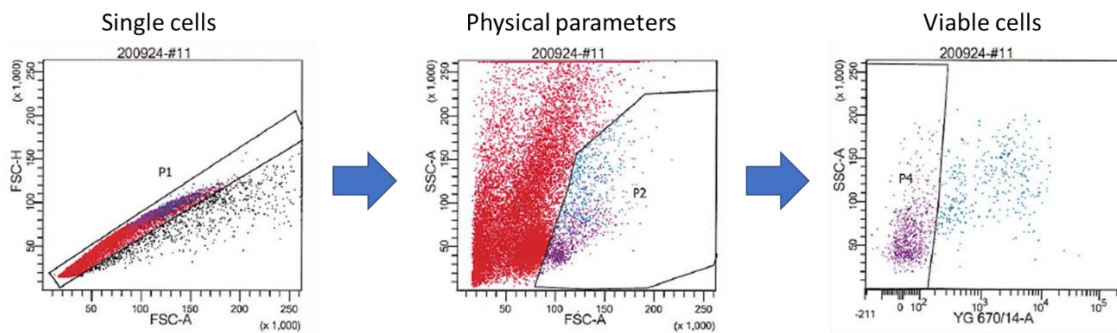


Figure 23: Gating strategy for sorting of all viable cells processed for scRNA-seq. P4 is the population which is sorted.

5.6.2 Library preparation

Sorted cells were further processed for single-cell RNA sequencing. ScRNA-seq was performed using the Next GEM Single Cell 3' GEM Kit v3.1 from Chromium 10X according to manufacturer's recommendation (User Guide Chromium Next GEM Single Cell 3' Reagent Kits v3.1/ CG000204). The target of cells loaded per sample was 10000.

5.6.3 scRNA-seq analysis

5.6.4 scRNA-seq analysis – data handling

Base call files obtained as result from the Illumina sequencing were converted into FASTQ files and processed with the *Cell Ranger* Single-Cell Software Suite (10X Chromium v3.1.0) using default setting. In details, the demultiplexed samples were aligned against the murine mm10 reference genome employing the STAR aligner

(producing alignment files in BAM format) and a UMI-count gene quantification was performed (based on the reference annotation). This latter gene-by-cell matrix was then imported into R and processed with the Seurat package (<http://satijalab.org/seurat> v4.0.3). As a first step of the analyses, doublets were assessed using the DoubletFinder (v3) software. More precisely, following the 'Best-Practices' suggested by the authors for scRNA-seq processing, the following parameters were selected to annotate doublets in each sample:

Table 8: Parameters used for the DoubletFinder v3.

Sample	Treatment group	nExp	pK
Sample 3	Control	0.07	0.005
Sample 4	Resistant	0.09	0.005
Sample 7	Control	0.07	0.005
Sample 10	Partial Responder	0.09	0.01
Sample 11	Partial Responder	0.07	0.005
Sample 14	Resistant	0.09	0.005
Sample 19	Control	0.05	0.005
Sample 22	Partial Responder	0.09	0.2

Samples were merged into a single Seurat dataset, keeping the information about the original sample as well as the corresponding treatment group. Then, the pre-processing step on the produced data started by removing cells with a low sequencing quality, those with a feature count below 1000 and above 6000, as well as cells with a fraction of mitochondrial genes higher than 10 %. Afterwards, cells annotated as doublets with the DoubletFinder were excluded as well from the analysis with Seurat. RNA UMI-counts were normalized using a global-scaling normalization method and the Variance Stabilizing Transformations (SCTransform) was performed to scale based on the percentage of mitochondrial genes, the absolute count of RNAs in each cell, and the difference between S and G2/M cell cycle scores computed for each cell. A principal component analysis with 50 principal components (PCs) was performed for dimensional reduction, and a UMAP-representation as well as clusters (with a resolution of 1.2) were computed on those reductions. Marker genes for each cluster were obtained using the *FindAllMarkers* Seurat function, and consequently clusters were annotated as indicated

in figure 17b as well as a small population of undefined cells (which was then removed from the dataset). Analysis of the subclusters “T and NK cells” and “APCs” was performed accordingly. First, T and NK cells were isolated using the subset function, then SCTransform based on the RNA-count matrix was performed, followed by a principal component analysis with 35 PCs, and cluster identification with a resolution of 0.8. At this resolution, CD4 T cells, CD8 T cells, gd T cells, NK cells, ILCs and NKT cells were identified, as well as a population of undefined cells. CD4, CD8 and NKT cells were further refined by a sub-clustering. The number of PCs used for sub-clustering in NKT cells, CD8 T cells and CD4 T cells were 30, 35, and 35, while the resolution was 0.6, 0.3 and 0.3, respectively. This led to the identification of the clusters as depicted in figure 19b. Similarly, a specific analysis was performed in the APC compartment with 35 PCs and a resolution of 1.2 which led to the identification of the clusters depicted in figure 18b as well as a population of undefined cells. Afterwards, cluster annotations were reintegrated into the full dataset and undefined cells were removed. SCTransform was repeated on the RNA slot and PC analysis was repeated on the full dataset as well as the subsets T and NK cells and APCs with the same parameters depicted before. Top upregulated markers of each population were calculated based on the *FindAllMarkers* function and a heatmap was generated based on the top 20 upregulated genes in each cluster to represent them. For the calculation of differentially expressed genes within individual clusters comparing the different treatment cohorts, namely control, partial responders and resistant, the *FindMarker* function was utilized. For GSEA, the gene sets from <https://www.gsea-msigdb.org/gsea/msigdb/genesets.jsp> were used, if not indicated differently.

5.7 Spatial transcriptomic analysis

5.7.1 Sample processing for spatial transcriptomics

Immediately after euthanizing the mice and perfusion of the liver with PBS containing 5 mM EDTA, small pieces of the liver containing metastasis from the mice were taken and shock-frozen in isopentane which was cooled down with liquid nitrogen. Afterwards, the samples were embedded in Killik, O.C.T. Compound embedding medium for cryostat (Bio-Optica/ 05-9801). The samples were stored at -80 °C.

5.7.2 Library preparation for Visium

To proceed the samples for Visium analysis, 10 μm sections of the previously prepared tissues were prepared using a cryostat and placed on the visium slides. For that purpose, the cryostat was cooled to 16 °C. Methanol fixation and Hematoxylin & Eosin (H&E) staining was performed according to the manual provided by 10x Genomics under the name Methanol Fixation, H&E Staining & Imaging for Visium Spatial Protocols (10x Genomics/ CG000160 Rev A) using a Aperio ePathology digital scanner (Leica Biosystems) for image acquisition. Afterwards, the samples were processed for Visium analysis according to the manual: User Guide Visium Spatial Gene Expression Reagent Kits (10X Genomics/ CG000239 Rev F).

5.7.3 Spatial transcriptomic sample analysis

Spatial transcriptomic samples obtained with the 10X Visium technology and sequenced on Illumina machines were initially processed with the *Space Ranger* software v1.2.2. More precisely, samples were demultiplexed using the *mkfastq* utility (which exploits the Illumina's *bcl2fastq* program) to produce initial FASTQ files. Then, starting from these latter input reads and the corresponding microscope slide image, the *count* step was run on each sample to perform alignment (exploiting STAR), tissue detection, fiducial detection, and barcode/UMI counting. This results in a spot-by-gene matrix, which was imported (with the corresponding tissue slide image) and analyzed with Seurat. It must be noted that the difference between scRNA-seq and Spatial scRNA-seq mainly consists of having spatial spots, in which (possibly) more than a single cell could be present (depending on the tissue and cell types). This means that UMI counts in each spot represent the expressions of multiple cells. For all samples separately a SCTransform and normalization was performed, and variable features were determined. Next, samples were integrated into one data set. For that purpose, the *IntegrateData* function was used in which the anchor set was previously determined by using the *FindIntegrationAnchors* function with anchor features being defined by the *SelectIntegrationFeatures* function. Data scaling was performed on the whole dataset followed by a principal component analysis. For the generation of a UMAP visualization as well as cluster determination, 25 PCs were employed and a resolution of 0.1 has been used. Clusters were further manually merged towards the 8 clusters depicted figure 21a based on their marker genes. Differentially expressed genes in each cluster were determined using the *FindMarker*

function. Individual spots belonging to clusters 1 and 6 were annotated as tumor, while all the remaining ones as liver (Figure 21e). Based on a moving average function, spots annotated as liver and tumor were divided into four zones each, leading to a classification of each spot dependent on the distance to the tumor-liver interface (Figure 21f). For that purpose, the geographic spot matrix was converted to a binary form based on tumor and liver annotation of the spot. To define the closeness to the tumor-liver interface, the moving average for each spot assigned as tumor and liver was determined separately for the tumor and liver area with the function *ma.matrix* using the following formular:

$$\text{moving average} = \text{ma.matrix}[\text{delta} = 3] + 2 * \text{ma.matrix}[\text{delta} = 2]$$

For the determination of the zones, the following thresholds were set: zone A: moving average (tumor) > 2.96; zone B: moving average (tumor) ≤ 2.96 and > 2.7; zone C: moving average (tumor) ≤ 2.7 and > 2.3; zone D: moving average (tumor) ≤ 2.3; zone E: moving average (liver) ≤ 1.7; zone F: moving average (liver) ≤ 1.91 and > 1.7; zone G: moving average (liver) ≤ 2.095 and > 1.91; zone H: moving average (liver) > 2.095. Differentially expressed genes comparing the different zones with each other within each treatment cohort as well as comparing the treatment cohorts within each zone were calculated using the *FindMarker* function. For GSEA the gene sets from <https://www.gsea-msigdb.org/gsea/msigdb/genesets.jsp> were used, if not indicated differently.

6 References

- Abancens M, Bustos V, Harvey H, McBryan J & Harvey BJ (2020) Sexual Dimorphism in Colon Cancer. *Frontiers in Oncology* 10
- Abar L, Vieira AR, Aune D, Sobiecki JG, Vingeliene S, Polemiti E, Stevens C, Greenwood DC, Chan DSM, Schlesinger S, *et al* (2018) Height and body fatness and colorectal cancer risk: an update of the WCRF–AICR systematic review of published prospective studies. *European Journal of Nutrition* 57: 1701–1720
- Alan R, Ezekowitz B, Hill M & Gordon S (1986) Interferon α/β selectively antagonises down-regulation of mannosyl-fucosyl receptors on activated macrophages by interferon γ . *Biochemical and Biophysical Research Communications* 136: 737–744
- Amendola M, Venneri MA, Biffi A, Vigna E & Naldini L (2005) Coordinate dual-gene transgenesis by lentiviral vectors carrying synthetic bidirectional promoters. *Nature Biotechnology* 23: 108–116
- American Joint Committee on Cancer (2017) AJCC Cancer Staging Manual 8th ed. New York: Springer
- Anagnostou T, Riaz IB, Hashmi SK, Murad MH & Kenderian SS (2020) Anti-CD19 chimeric antigen receptor T-cell therapy in acute lymphocytic leukaemia: a systematic review and meta-analysis. *The Lancet Haematology* 7: e816–e826
- Anfossi N, André P, Guia S, Falk CS, Roeytynck S, Stewart CA, Bresó V, Frassati C, Reviron D, Middleton D, *et al* (2006) Human NK Cell Education by Inhibitory Receptors for MHC Class I. *Immunity* 25: 331–342
- Annoni A, Brown BD, Cantore A, Sergi LS, Naldini L & Roncarolo M-G (2009) In vivo delivery of a microRNA-regulated transgene induces antigen-specific regulatory T cells and promotes immunologic tolerance. *Blood* 114: 5152–5161
- Arasanz H, Gato-Cañas M, Zuazo M, Ibañez-Vea M, Breckpot K, Kochan G & Escors D (2017) PD1 signal transduction pathways in T cells. *Oncotarget* 8: 51936–51945
- Aricò E, Castiello L, Capone I, Gabriele L & Belardelli F (2019) Type I Interferons and Cancer: An Evolving Story Demanding Novel Clinical Applications. *Cancers (Basel)* 11: 1943

- Aronson SJ, Veron P, Collaud F, Hubert A, Delahais V, Honnet G, de Knecht RJ, Junge N, Baumann U, di Giorgio A, *et al* (2019) Prevalence and Relevance of Pre-Existing Anti-Adeno-Associated Virus Immunity in the Context of Gene Therapy for Crigler–Najjar Syndrome. *Human Gene Therapy* 30: 1297–1305
- AYALA A (1992) Differential effects of hemorrhage on kupffer cells: decreased antigen presentation despite increased inflammatory cytokine (IL-1, IL-6 and TNF) release. *Cytokine* 4: 66–75
- Bacchetta R, Lucarelli B, Sartirana C, Gregori S, Lupo Stanghellini MT, Miqueu P, Tomiuk S, Hernandez-Fuentes M, Gianolini ME, Greco R, *et al* (2014) Immunological Outcome in Haploidentical-HSC Transplanted Patients Treated with IL-10-Anergized Donor T Cells. *Frontiers in Immunology* 5
- Bally APR, Austin JW & Boss JM (2016) Genetic and Epigenetic Regulation of PD-1 Expression. *The Journal of Immunology* 196: 2431–2437
- Baran B, Mert Ozupek N, Yerli Tetik N, Acar E, Bekcioglu O & Baskin Y (2018) Difference Between Left-Sided and Right-Sided Colorectal Cancer: A Focused Review of Literature. *Gastroenterology Research* 11: 264–273
- Barber A (2014) Costimulation of Effector CD8+ T Cells: Which Receptor is Optimal for Immunotherapy? *MOJ Immunology* 1
- Barker N, de Wetering M van & Clevers H (2008) The intestinal stem cell. *Genes and Development* 22: 1856–1864 doi:10.1101/gad.1674008 [PREPRINT]
- Barrueto L, Caminero F, Cash L, Makris C, Lamichhane P & Deshmukh RR (2020) Resistance to Checkpoint Inhibition in Cancer Immunotherapy. *Translational Oncology* 13: 100738
- Battle E & Clevers H (2017) Cancer stem cells revisited. *Nature Medicine* 23: 1124–1134
- Battle E & Massagué J (2019) Transforming Growth Factor- β Signaling in Immunity and Cancer. *Immunity* 50: 924–940
- Beatty GL & Gladney WL (2015) Immune Escape Mechanisms as a Guide for Cancer Immunotherapy. *Clinical Cancer Research* 21: 687–692

- Bénéchet AP, de Simone G, di Lucia P, Cilenti F, Barbiera G, le Bert N, Fumagalli V, Lusito E, Moalli F, Bianchessi V, *et al* (2019) Dynamics and genomic landscape of CD8+ T cells undergoing hepatic priming. *Nature* 574: 200–205
- Berraondo P, Sanmamed MF, Ochoa MC, Etxeberria I, Aznar MA, Pérez-Gracia JL, Rodríguez-Ruiz ME, Ponz-Sarvisé M, Castañón E & Melero I (2019) Cytokines in clinical cancer immunotherapy. *British Journal of Cancer* 120: 6–15
- Berthel A, Zoernig I, Valous NA, Kahlert C, Klupp F, Ulrich A, Weitz J, Jaeger D & Halama N (2017) Detailed resolution analysis reveals spatial T cell heterogeneity in the invasive margin of colorectal cancer liver metastases associated with improved survival. *OncoImmunology* 6: e1286436
- Bertotti A, Migliardi G, Galimi F, Sassi F, Torti D, Isella C, Corà D, di Nicolantonio F, Buscarino M, Petti C, *et al* (2011) A Molecularly Annotated Platform of Patient-Derived Xenografts (“Xenopatients”) Identifies HER2 as an Effective Therapeutic Target in Cetuximab-Resistant Colorectal Cancer. *Cancer Discovery* 1: 508–523
- Bhullar KS, Lagarón NO, McGowan EM, Parmar I, Jha A, Hubbard BP & Rupasinghe HPV (2018) Kinase-targeted cancer therapies: progress, challenges and future directions. *Molecular Cancer* 17: 48
- Biffi A, Bartolomae CC, Cesana D, Cartier N, Aubourg P, Ranzani M, Cesani M, Benedicenti F, Plati T, Rubagotti E, *et al* (2011) Lentiviral vector common integration sites in preclinical models and a clinical trial reflect a benign integration bias and not oncogenic selection. *Blood* 117: 5332–5339
- Biffi A, Capotondo A, Fasano S, Carro U del, Marchesini S, Azuma H, Malaguti MC, Amadio S, Brambilla R, Grompe M, *et al* (2006) Gene therapy of metachromatic leukodystrophy reverses neurological damage and deficits in mice. *Journal of Clinical Investigation* 116: 3070–3082
- Biffi A, Montini E, Lorioli L, Cesani M, Fumagalli F, Plati T, Baldoli C, Martino S, Calabria A, Canale S, *et al* (2013) Lentiviral Hematopoietic Stem Cell Gene Therapy Benefits Metachromatic Leukodystrophy. *Science (1979)* 341

- Blackburn SD & Wherry EJ (2007) IL-10, T cell exhaustion and viral persistence. *Trends in Microbiology* 15: 143–146
- Blank CU, Haining WN, Held W, Hogan PG, Kallies A, Lugli E, Lynn RC, Philip M, Rao A, Restifo NP, *et al* (2019) Defining ‘T cell exhaustion.’ *Nature Reviews Immunology* 19: 665–674
- Bonnal RJP, Rossetti G, Lugli E, de Simone M, Guarin P, Brummelman J, Drufulca L, Passaro M, Bason R, Gervasoni F, *et al* (2021) Clonally expanded EOMES+ Tr1-like cells in primary and metastatic tumors are associated with disease progression. *Nature Immunology* 22: 735–745
- Bosticardo M, Ferrua F, Cavazzana M & Aiuti A (2014) Gene Therapy for Wiskott-Aldrich Syndrome. *Current Gene Therapy* 14: 413–421
- Braet F & Wisse E (2002) Structural and functional aspects of liver sinusoidal endothelial cell fenestrae: a review. *Comparative Hepatology* 1: 1
- Brodth P (2016) Role of the Microenvironment in Liver Metastasis: From Pre- to Prometastatic Niches. *Clinical Cancer Research* 22: 5971–5982
- Brouwer NPM, Bos ACRK, Lemmens VEPP, Tanis PJ, Hugen N, Nagtegaal ID, de Wilt JHW & Verhoeven RHA (2018) An overview of 25 years of incidence, treatment and outcome of colorectal cancer patients. *International Journal of Cancer* 143: 2758–2766
- Brück O, Lee MH, Turkki R, Uski I, Penttilä P, Paavolainen L, Kovanen P, Järvinen P, Bono P, Pellinen T, *et al* (2021) Spatial immunoprofiling of the intratumoral and peritumoral tissue of renal cell carcinoma patients. *Modern Pathology* 34: 2229–2241
- Brummelman J, Mazza EMC, Alvisi G, Colombo FS, Grilli A, Mikulak J, Mavilio D, Alloisio M, Ferrari F, Lopci E, *et al* (2018) High-dimensional single cell analysis identifies stem-like cytotoxic CD8+ T cells infiltrating human tumors. *Journal of Experimental Medicine* 215: 2520–2535

- Budhwani M, Mazzieri R & Dolcetti R (2018) Plasticity of Type I Interferon-Mediated Responses in Cancer Therapy: From Anti-tumor Immunity to Resistance. *Frontiers in Oncology* 8
- Bulcha JT, Wang Y, Ma H, Tai PWL & Gao G (2021) Viral vector platforms within the gene therapy landscape. *Signal Transduction and Targeted Therapy* 6: 53
- Burga RA, Thorn M, Point GR, Guha P, Nguyen CT, Licata LA, DeMatteo RP, Ayala A, Joseph Espat N, Junghans RP, *et al* (2015) Liver myeloid-derived suppressor cells expand in response to liver metastases in mice and inhibit the anti-tumor efficacy of anti-CEA CAR-T. *Cancer Immunol Immunother* 64: 817–29
- Burnet FM (1971) Immunological Surveillance in Neoplasia. *Immunological Reviews* 7: 3–25
- Burnet M (1957) Cancer--A Biological Approach: III. Viruses Associated with Neoplastic Conditions. IV. Practical Applications. *BMJ* 1: 841–847
- Burnet M (1964) IMMUNOLOGICAL FACTORS IN THE PROCESS OF CARCINOGENESIS. *British Medical Bulletin* 20: 154–158
- Bürtin F, Mullins CS & Linnebacher M (2020) Mouse models of colorectal cancer: Past, present and future perspectives. *World Journal of Gastroenterology* 26: 1394–1426
- Bustos M, Dubrot J, Martinez-Anso E, Larequi E, Castaño D, Palazon A, Belza I, Sanmamed MF, Perez-Gracia JL, Ortiz de Solorzano C, *et al* (2012) Cardiotrophin-1 determines liver engraftment of syngenic colon carcinoma cells through an immune system-mediated mechanism. *OncImmunity* 1: 1527–1536
- Callery MP, Mangino MJ & Flye MW (1991) Kupffer cell prostaglandin-E2 production is amplified during hepatic regeneration. *Hepatology* 14: 368–72
- Cameron F, Whiteside G & Perry C (2011) Ipilimumab. *Drugs* 71: 1093–1104
- Cantore A & Naldini L (2021) WFH State-of-the-art paper 2020: In vivo lentiviral vector gene therapy for haemophilia. *Haemophilia* 27: 122–125

- Cantore A, Ranzani M, Bartholomae CC, Volpin M, Valle P della, Sanvito F, Sergi LS, Gallina P, Benedicenti F, Bellinger D, *et al* (2015) Liver-directed lentiviral gene therapy in a dog model of hemophilia B. *Science Translational Medicine* 7
- Cappell KM, Sherry RM, Yang JC, Goff SL, Vanasse DA, McIntyre L, Rosenberg SA & Kochenderfer JN (2020) Long-Term Follow-Up of Anti-CD19 Chimeric Antigen Receptor T-Cell Therapy. *Journal of Clinical Oncology* 38: 3805–3815
- Catarinella M, Monestiroli A, Escobar G, Fiocchi A, Tran NL, Aiolfi R, Marra P, Esposito A, Cipriani F, Aldrighetti L, *et al* (2016) IFN α gene/cell therapy curbs colorectal cancer colonization of the liver by acting on the hepatic microenvironment. *EMBO Molecular Medicine* 8: 155–170
- Cavazzana-Calvo M, Payen E, Negre O, Wang G, Hehir K, Fusil F, Down J, Denaro M, Brady T, Westerman K, *et al* (2010) Transfusion independence and HMGA2 activation after gene therapy of human β -thalassaemia. *Nature* 467: 318–322
- Chang C-H, Qiu J, O’Sullivan D, Buck MD, Noguchi T, Curtis JD, Chen Q, Gindin M, Gubin MM, van der Windt GJW, *et al* (2015) Metabolic Competition in the Tumor Microenvironment Is a Driver of Cancer Progression. *Cell* 162: 1229–1241
- de Charette M, Marabelle A & Houot R (2016) Turning tumour cells into antigen presenting cells: The next step to improve cancer immunotherapy? *European Journal of Cancer* 68: 134–147
- Chawla-Sarkar M (2003) Apoptosis and interferons: Role of interferon-stimulated genes as mediators of apoptosis. *Apoptosis* 8: 237–249
- Chen D, Li L, Zhang X, Gao G, Shen L, Hu J, Yang M, Liu B & Qian X (2018) FOLFOX plus anti-epidermal growth factor receptor (EGFR) monoclonal antibody (mAb) is an effective first-line treatment for patients with RAS-wild left-sided metastatic colorectal cancer. *Medicine* 97: e0097
- Chen DS & Mellman I (2013) Oncology Meets Immunology: The Cancer-Immunity Cycle. *Immunity* 39: 1–10

- Chen X-J, Ren A, Zheng L, Zheng E-D & Jiang T (2021a) Pan-Cancer Analysis Identifies Liver Metastases as Negative Predictive Factor for Immune Checkpoint Inhibitors Treatment Outcome. *Frontiers in Immunology* 12
- Chen Y, Yu Z, Tan X, Jiang H, Xu Z, Fang Y, Han D, Hong W, Wei W & Tu J (2021b) CAR-macrophage: A new immunotherapy candidate against solid tumors. *Biomedicine & Pharmacotherapy* 139: 111605
- Chi X, Yang P, Zhang E, Gu J, Xu H, Li M, Gao X, Li X, Zhang Y, Xu H, *et al* (2019) Significantly increased anti-tumor activity of carcinoembryonic antigen-specific chimeric antigen receptor T cells in combination with recombinant human IL-12. *Cancer Medicine* 8: 4753–4765
- Chulpanova DS, Kitaeva K v., Green AR, Rizvanov AA & Solovyeva V v. (2020) Molecular Aspects and Future Perspectives of Cytokine-Based Anti-cancer Immunotherapy. *Frontiers in Cell and Developmental Biology* 8
- Chytil A, Magnuson MA, Wright CVE & Moses HL (2002) Conditional inactivation of the TGF- β type II receptor using Cre:Lox. *genesis* 32: 73–75
- Ciccarese F, Grassi A, Pasqualini L, Rosano S, Noghero A, Montenegro F, Bussolino F, di Camillo B, Finesso L, Toffolo GM, *et al* (2020) Genetic perturbation of IFN- α transcriptional modulators in human endothelial cells uncovers pivotal regulators of angiogenesis. *Computational and Structural Biotechnology Journal* 18: 3977–3986
- Cilenti F, Barbiera G, Caronni N, Iodice D, Montaldo E, Barresi S, Lusito E, Cuzzola V, Vittoria FM, Mezzanzanica L, *et al* (2021) A PGE2-MEF2A axis enables context-dependent control of inflammatory gene expression. *Immunity* 54: 1665-1682.e14
- Clevers H (2013) The Intestinal Crypt, A Prototype Stem Cell Compartment. *Cell* 154: 274–284
- Coffelt SB & de Visser KE (2015) Immune-mediated mechanisms influencing the efficacy of anticancer therapies. *Trends in Immunology* 36: 198–216
- Colantonio AD, Epeldegui M, Jesiak M, Jachimowski L, Blom B & Uittenbogaart CH (2011) IFN- α Is Constitutively Expressed in the Human Thymus, but Not in Peripheral Lymphoid Organs. *PLoS ONE* 6: e24252

- Colegio OR, Chu N-Q, Szabo AL, Chu T, Rhebergen AM, Jairam V, Cyrus N, Brokowski CE, Eisenbarth SC, Phillips GM, *et al* (2014) Functional polarization of tumour-associated macrophages by tumour-derived lactic acid. *Nature* 513: 559–563
- Corbett TH, Griswold DP, Roberts BJ, Peckham JC & Schabel FM (1975) Tumor induction relationships in development of transplantable cancers of the colon in mice for chemotherapy assays, with a note on carcinogen structure. *Cancer Res* 35: 2434–9
- Cornel AM, Mimpfen IL & Nierkens S (2020) MHC Class I Downregulation in Cancer: Underlying Mechanisms and Potential Targets for Cancer Immunotherapy. *Cancers (Basel)* 12: 1760
- Craene B de & Berx G (2013) Regulatory networks defining EMT during cancer initiation and progression. *Nature Reviews Cancer* 13: 97–110
- Curiel TJ, Coukos G, Zou L, Alvarez X, Cheng P, Mottram P, Evdemon-Hogan M, Conejo-Garcia JR, Zhang L, Burow M, *et al* (2004) Specific recruitment of regulatory T cells in ovarian carcinoma fosters immune privilege and predicts reduced survival. *Nature Medicine* 10: 942–949
- Das SK, Menezes ME, Bhatia S, Wang X-Y, Emdad L, Sarkar D & Fisher PB (2015) Gene Therapies for Cancer: Strategies, Challenges and Successes. *J Cell Physiol* 230: 259–71
- Dickow J, Francois S, Kaiserling R-L, Malyskhina A, Drexler I, Westendorf AM, Lang KS, Santiago ML, Dittmer U & Sutter K (2019) Diverse Immunomodulatory Effects of Individual IFN α Subtypes on Virus-Specific CD8 $^{+}$ T Cell Responses. *Frontiers in Immunology* 10
- Diesselhoff-den Dulk MM, Crofton RW & van Furth R (1979) Origin and kinetics of Kupffer cells during an acute inflammatory response. *Immunology* 37: 7–14
- Doherty DG (2019) Antigen-specific immune tolerance in the liver. *Nature Biomedical Engineering* 3: 763–765
- Doria-Rose NA, Klein RM, Daniels MG, O'Dell S, Nason M, Lapedes A, Bhattacharya T, Migueles SA, Wyatt RT, Korber BT, *et al* (2010) Breadth of Human

- Immunodeficiency Virus-Specific Neutralizing Activity in Sera: Clustering Analysis and Association with Clinical Variables. *Journal of Virology* 84: 1631–1636
- Duan Q, Zhang H, Zheng J & Zhang L (2020) Turning Cold into Hot: Firing up the Tumor Microenvironment. *Trends in Cancer* 6: 605–618
- Dubois EL (1966) NZB/NZW Mice as a Model of Systemic Lupus Erythematosus. *JAMA: The Journal of the American Medical Association* 195: 285
- Dupaul-Chicoine J, Arabzadeh A, Dagenais M, Douglas T, Champagne C, Morizot A, Rodrigue-Gervais IG, Breton V, Colpitts SL, Beauchemin N, *et al* (2015) The Nlrp3 Inflammasome Suppresses Colorectal Cancer Metastatic Growth in the Liver by Promoting Natural Killer Cell Tumoricidal Activity. *Immunity* 43: 751–763
- Eck MJ & Manley PW (2009) The interplay of structural information and functional studies in kinase drug design: insights from BCR-Abl. *Current Opinion in Cell Biology* 21: 288–295
- Efremova M, Rieder D, Klepsch V, Charoentong P, Finotello F, Hackl H, Hermann-Kleiter N, Löwer M, Baier G, Krogsdam A, *et al* (2018) Targeting immune checkpoints potentiates immunoediting and changes the dynamics of tumor evolution. *Nature Communications* 9: 32
- Eggert T & Greten TF (2017) Tumor regulation of the tissue environment in the liver. *Pharmacology & Therapeutics* 173: 47–57
- Ehrlich P (1909) Ueber den jetzigen Stand der Karzinomforschung. *Nederlands Tijdschrift voor Geneeskunde* 5: 273–290
- Elverum K & Whitman M (2020) Delivering cellular and gene therapies to patients: solutions for realizing the potential of the next generation of medicine. *Gene Therapy* 27: 537–544
- Escobar G, Barbarossa L, Barbiera G, Norelli M, Genua M, Ranghetti A, Plati T, Camisa B, Brombin C, Cittaro D, *et al* (2018) Interferon gene therapy reprograms the leukemia microenvironment inducing protective immunity to multiple tumor antigens. *Nature Communications* 9: 2896

- Escobar G, Gentner B, Naldini L & Mazziere R (2014a) Engineered tumor-infiltrating macrophages as gene delivery vehicles for interferon- α activates immunity and inhibits breast cancer progression. *OncImmunity* 3: e28696
- Escobar G, Moi D, Ranghetti A, Ozkal-Baydin P, Squadrito ML, Kajaste-Rudnitski A, Bondanza A, Gentner B, de Palma M, Mazziere R, *et al* (2014b) Genetic Engineering of Hematopoiesis for Targeted IFN- α Delivery Inhibits Breast Cancer Progression. *Science Translational Medicine* 6
- Esteva FJ, Yu D, Hung M-C & Hortobagyi GN (2010) Molecular predictors of response to trastuzumab and lapatinib in breast cancer. *Nature Reviews Clinical Oncology* 7: 98–107
- Fan H, Demirci U & Chen P (2019) Emerging organoid models: leaping forward in cancer research. *Journal of Hematology & Oncology* 12: 142
- Fan L, Xu G, Cao J, Li M, Zhang H, Li F, Qi X, Zhang X, Li Z, Han P, *et al* (2021) Type I Interferon Promotes Antitumor T Cell Response in CRPC by Regulating MDSC. *Cancers (Basel)* 13: 5574
- Fang C-C, Wu C-F, Liao Y-J, Huang S-F, Chen M & Chen Y-MA (2018) AAV serotype 8-mediated liver specific GNMT expression delays progression of hepatocellular carcinoma and prevents carbon tetrachloride-induced liver damage. *Scientific Reports* 8: 13802
- Fares J, Fares MY, Khachfe HH, Salhab HA & Fares Y (2020) Molecular principles of metastasis: a hallmark of cancer revisited. *Signal Transduction and Targeted Therapy* 5 doi:10.1038/s41392-020-0134-x [PREPRINT]
- Fearon ER & Vogelstein B (1990) A genetic model for colorectal tumorigenesis. *Cell* 61: 759–767
- Feinberg H, Jégouzo SAF, Lasanajak Y, Smith DF, Drickamer K, Weis WI & Taylor ME (2021) Structural analysis of carbohydrate binding by the macrophage mannose receptor CD206. *Journal of Biological Chemistry* 296: 100368
- Fernandez-Poma SM, Salas-Benito D, Lozano T, Casares N, Riezu-Boj J-I, Mancheño U, Elizalde E, Alignani D, Zubeldia N, Otano I, *et al* (2017) Expansion of Tumor-

- Infiltrating CD8+ T cells Expressing PD-1 Improves the Efficacy of Adoptive T-cell Therapy. *Cancer Research* 77: 3672–3684
- Ferrantini M, Capone I & Belardelli F (2007) Interferon- α and cancer: Mechanisms of action and new perspectives of clinical use. *Biochimie* 89: 884–893
- Fidler MM, Soerjomataram I & Bray F (2016) A global view on cancer incidence and national levels of the human development index. *International Journal of Cancer* 139: 2436–2446
- Finter NB, Chapman S, Dowd P, Johnston JM, Manna V, Sarantis N, Sheron N, Scott G, Phua S & Tatum PB (1991) The Use of Interferon- α in Virus Infections. *Drugs* 42: 749–765
- Fodde R (2002) The APC gene in colorectal cancer. *European Journal of Cancer* 38: 867–871
- Fontenot JD, Gavin MA & Rudensky AY (2003) Foxp3 programs the development and function of CD4+CD25+ regulatory T cells. *Nature Immunology* 4: 330–336
- Fouad YA & Aanei C (2017) Revisiting the hallmarks of cancer. *Am J Cancer Res* 7: 1016–1036
- Frank AM, Braun AH, Scheib L, Agarwal S, Schneider IC, Fusil F, Perian S, Sahin U, Thalheimer FB, Verhoeyen E, *et al* (2020) Combining T-cell-specific activation and in vivo gene delivery through CD3-targeted lentiviral vectors. *Blood Adv* 4: 5702–5715
- Frank AM & Buchholz CJ (2019) Surface-Engineered Lentiviral Vectors for Selective Gene Transfer into Subtypes of Lymphocytes. *Molecular Therapy - Methods & Clinical Development* 12: 19–31
- Friedman SL (1997) Scarring in alcoholic liver disease: new insights and emerging therapies. *Alcohol Health Res World* 21: 310–6
- van Furth R (1980) Monocyte origin of Kupffer cells. *Blood Cells* 6: 87–92
- Gabrilovich DI & Nagaraj S (2009) Myeloid-derived suppressor cells as regulators of the immune system. *Nature Reviews Immunology* 9: 162–174

- Gaillard H, García-Muse T & Aguilera A (2015) Replication stress and cancer. *Nature Reviews Cancer* 15: 276–289
- Gao Y, Ouyang Z, Yang C, Song C, Jiang C, Song S, Shen M & Shi X (2021) Overcoming T Cell Exhaustion via Immune Checkpoint Modulation with a Dendrimer-Based Hybrid Nanocomplex. *Advanced Healthcare Materials* 10: 2100833
- García-García I, Hernández-González I, Díaz-Machado A, González-Delgado CA, Pérez-Rodríguez S, García-Vega Y, Campos-Mojena R, Tuero-Iglesias AD, Valenzuela-Silva CM, Cruz-Ramírez A, *et al* (2016) Pharmacokinetic and pharmacodynamic characterization of a novel formulation containing co-formulated interferons alpha-2b and gamma in healthy male volunteers. *BMC Pharmacology and Toxicology* 17: 58
- Geisler A & Fechner H (2016) MicroRNA-regulated viral vectors for gene therapy. *World Journal of Experimental Medicine* 6: 37
- Genovese P, Schirolli G, Escobar G, di Tomaso T, Firrito C, Calabria A, Moi D, Mazzieri R, Bonini C, Holmes MC, *et al* (2014) Targeted genome editing in human repopulating haematopoietic stem cells. *Nature* 510: 235–240
- Gentner B, Visigalli I, Hiramatsu H, Lechman E, Ungari S, Giustacchini A, Schira G, Amendola M, Quattrini A, Martino S, *et al* (2010) Identification of Hematopoietic Stem Cell-Specific miRNAs Enables Gene Therapy of Globoid Cell Leukodystrophy. *Science Translational Medicine* 2
- Gessani S, Conti L, del Cornò M & Belardelli F (2014) Type I Interferons as Regulators of Human Antigen Presenting Cell Functions. *Toxins (Basel)* 6: 1696–1723
- Gholami S, Grothey A & Lenz H-J (2021) Microsatellite Stable Colorectal Liver Metastases—Understanding the Mechanisms of Immune Resistance. *JAMA Network Open* 4: e2119025
- Gilgenkrantz H & Collin de l’Hortet A (2018) Understanding Liver Regeneration. *The American Journal of Pathology* 188: 1316–1327

- Giraldo NA, Sanchez-Salas R, Peske JD, Vano Y, Becht E, Petitprez F, Validire P, Ingels A, Cathelineau X, Fridman WH, *et al* (2019) The clinical role of the TME in solid cancer. *British Journal of Cancer* 120: 45–53
- Gordon-Weeks A & Yuzhalin A (2020) Cancer Extracellular Matrix Proteins Regulate Tumour Immunity. *Cancers (Basel)* 12: 3331
- Grandvaux N, tenOever BR, Servant MJ & Hiscott J (2002) The interferon antiviral response: from viral invasion to evasion. *Current Opinion in Infectious Diseases* 15: 259–267
- Gresser I & Bourali C (1969) Exogenous Interferon and Inducers of Interferon in the Treatment of Balb/c Mice inoculated with RC19 Tumour Cells. *Nature* 223: 844–845
- Gruarin P, Maglie S, Simone M, Häringer B, Vasco C, Ranzani V, Bosotti R, Noddings JS, Larghi P, Facciotti F, *et al* (2019) Eomesodermin controls a unique differentiation program in human IL-10 and IFN- γ coproducing regulatory T cells. *European Journal of Immunology* 49: 96–111
- Gül N, Babes L, Siegmund K, Korthouwer R, Bögels M, Braster R, Vidarsson G, ten Hagen TLM, Kubes P & van Egmond M (2014) Macrophages eliminate circulating tumor cells after monoclonal antibody therapy. *Journal of Clinical Investigation* 124: 812–823
- van Haasteren J, Hyde SC & Gill DR (2018) Lessons learned from lung and liver in-vivo gene therapy: implications for the future. *Expert Opinion on Biological Therapy* 18: 959–972
- Half E, Bercovich D & Rozen P (2009) Familial adenomatous polyposis. *Orphanet Journal of Rare Diseases* 4
- Han C, Liu T & Yin R (2020) Biomarkers for cancer-associated fibroblasts. *Biomarker Research* 8: 64
- Hanahan D (2022) Hallmarks of Cancer: New Dimensions. *Cancer Discovery* 12: 31–46
- Hanahan D & Weinberg RA (2000) The Hallmarks of Cancer. *Cell* 100: 57–70

- Hanahan D & Weinberg RA (2011) Hallmarks of Cancer: The Next Generation. *Cell* 144: 646–674
- Hardy GAD, Sieg SF, Rodriguez B, Jiang W, Asaad R, Lederman MM & Harding C v. (2009) Desensitization to type I interferon in HIV-1 infection correlates with markers of immune activation and disease progression. *Blood* 113: 5497–5505
- Hartmann J, Schüßler-Lenz M, Bondanza A & Buchholz CJ (2017) Clinical development of CAR T cells—challenges and opportunities in translating innovative treatment concepts. *EMBO Molecular Medicine* 9: 1183–1197
- Hashimoto H, Ueda R, Narumi K, Heike Y, Yoshida T & Aoki K (2014) Type I IFN gene delivery suppresses regulatory T cells within tumors. *Cancer Gene Therapy* 21: 532–541
- Hastie E, Cataldi M, Marriott I & Grzelishvili VZ (2013) Understanding and altering cell tropism of vesicular stomatitis virus. *Virus Res* 176: 16–32
- Hazarika M, Chuk MK, Theoret MR, Mushti S, He K, Weis SL, Putman AH, Helms WS, Cao X, Li H, *et al* (2017) U.S. FDA Approval Summary: Nivolumab for Treatment of Unresectable or Metastatic Melanoma Following Progression on Ipilimumab. *Clinical Cancer Research* 23: 3484–3488
- He X & Xu C (2020) Immune checkpoint signaling and cancer immunotherapy. *Cell Research* 30: 660–669
- Heijstek MW, Kranenburg O & Borel Rinkes IHM (2005) Mouse Models of Colorectal Cancer and Liver Metastases. *Digestive Surgery* 22: 16–25
- Hickerson BT, Sefing EJ, Bailey KW, van Wettere AJ, Penichet ML & Gowen BB (2020) Type I interferon underlies severe disease associated with Junín virus infection in mice. *Elife* 9
- Hind LE, Lurier EB, Dembo M, Spiller KL & Hammer DA (2016) Effect of M1–M2 Polarization on the Motility and Traction Stresses of Primary Human Macrophages. *Cellular and Molecular Bioengineering* 9: 455–465

- van Horssen R, ten Hagen TLM & Eggermont AMM (2006) TNF- α in Cancer Treatment: Molecular Insights, Antitumor Effects, and Clinical Utility. *The Oncologist* 11: 397–408
- Horvath CM (2004) The Jak-STAT Pathway Stimulated by Interferon α or Interferon β . *Science's STKE* 2004
- Hu X, Herrero C, Li W-P, Antoniv TT, Falck-Pedersen E, Koch AE, Woods JM, Haines GK & Ivashkiv LB (2002) Sensitization of IFN- γ Jak-STAT signaling during macrophage activation. *Nature Immunology* 3: 859–866
- Huang D, Sun W, Zhou Y, Li P, Chen F, Chen H, Xia D, Xu E, Lai M, Wu Y, *et al* (2018) Mutations of key driver genes in colorectal cancer progression and metastasis. *Cancer and Metastasis Reviews* 37: 173–187 doi:10.1007/s10555-017-9726-5 [PREPRINT]
- Huang R & Zhou P-K (2021) DNA damage repair: historical perspectives, mechanistic pathways and clinical translation for targeted cancer therapy. *Signal Transduction and Targeted Therapy* 6: 254
- Hussain MRM, Baig M, Mohamoud HSA, Ulhaq Z, Hoessli DC, Khogeer GS, Al-Sayed RR & Al-Aama JY (2015) BRAF gene: From human cancers to developmental syndromes. *Saudi Journal of Biological Sciences* 22: 359–373 doi:10.1016/j.sjbs.2014.10.002 [PREPRINT]
- Iacopetta B (2002) Are there two sides to colorectal cancer? *International Journal of Cancer* 101: 403–408
- Iacopetta B, Grieu F & Amanuel B (2010) Microsatellite instability in colorectal cancer. *Asia-Pacific Journal of Clinical Oncology* 6: 260–269 doi:10.1111/j.1743-7563.2010.01335.x [PREPRINT]
- Imbratta C, Hussein H, Andris F & Verdeil G (2020) c-MAF, a Swiss Army Knife for Tolerance in Lymphocytes. *Frontiers in Immunology* 11
- Indraccolo S (2010) Interferon- α as angiogenesis inhibitor: Learning from tumor models. *Autoimmunity* 43: 244–247

- Inoue T, Terada N, Kobayashi T & Ogawa O (2017) Patient-derived xenografts as in vivo models for research in urological malignancies. *Nature Reviews Urology* 14: 267–283
- Itakura E, Huang R-R, Wen D-R, Paul E, Wunsch PH & Cochran AJ (2011) IL-10 expression by primary tumor cells correlates with melanoma progression from radial to vertical growth phase and development of metastatic competence. *Modern Pathology* 24: 801–809
- Jackson EL, Willis N, Mercer K, Bronson RT, Crowley D, Montoya R, Jacks T & Tuveson DA (2001) Analysis of lung tumor initiation and progression using conditional expression of oncogenic *K-ras*. *Genes & Development* 15: 3243–3248
- Jenkins RW, Barbie DA & Flaherty KT (2018) Mechanisms of resistance to immune checkpoint inhibitors. *British Journal of Cancer* 118: 9–16
- Jeong S-N & Yoo SY (2020) Novel Oncolytic Virus Armed with Cancer Suicide Gene and Normal Vasculogenic Gene for Improved Anti-Tumor Activity. *Cancers (Basel)* 12
- Jia L-T, Chen S-Y & Yang A-G (2012) Cancer gene therapy targeting cellular apoptosis machinery. *Cancer Treatment Reviews* 38: 868–876
- Jonges LE, Giezeman-Smits KM, van Vlierberghe RLP, Ensink Ng, Hagens M, Joly étienne, Eggermont AMM, van de Velde CJH, Fleuren GJ & Kuppen PJK (2000) NK Cells Modulate MHC Class I Expression on Tumor Cells and their Susceptibility to Lysis. *Immunobiology* 202: 326–338
- Joyce JA & Fearon DT (2015) T cell exclusion, immune privilege, and the tumor microenvironment. *Science (1979)* 348: 74–80
- June CH, O'Connor RS, Kawalekar OU, Ghassemi S & Milone MC (2018) CAR T cell immunotherapy for human cancer. *Science (1979)* 359: 1361–1365
- Kakinuma Y, Kimura T & Watanabe Y (2017) Possible Involvement of Liver Resident Macrophages (Kupffer Cells) in the Pathogenesis of Both Intrahepatic and Extrahepatic Inflammation. *Can J Gastroenterol Hepatol* 2017: 2896809

- Kaklamanis L, Townsend A, Doussis-Anagnostopoulou IA, Mortensen N, Harris AL & Gatter KC (1994) Loss of major histocompatibility complex-encoded transporter associated with antigen presentation (TAP) in colorectal cancer. *Am J Pathol* 145: 505–9
- Katlinski K v., Gui J, Katlinskaya Y v., Ortiz A, Chakraborty R, Bhattacharya S, Carbone CJ, Beiting DP, Gironde MA, Peck AR, *et al* (2017) Inactivation of Interferon Receptor Promotes the Establishment of Immune Privileged Tumor Microenvironment. *Cancer Cell* 31: 194–207
- Keefe DMK & Bateman EH (2019) Potential Successes and Challenges of Targeted Cancer Therapies. *JNCI Monographs* 2019
- Keum N & Giovannucci E (2019) Global burden of colorectal cancer: emerging trends, risk factors and prevention strategies. *Nature Reviews Gastroenterology & Hepatology* 16: 713–732
- Khoo LT & Chen L (2018) Role of the cGAS–STING pathway in cancer development and oncotherapeutic approaches. *EMBO Rep* 19
- Knoll P, Schlaak J, Uhrig A, Kempf P, zum Büschenfelde K-HM & Gerken G (1995) Human Kupffer cells secrete IL-10 in response to lipopolysaccharide (LPS) challenge. *Journal of Hepatology* 22: 226–229
- Knolle PA, Uhrig A, Protzer U, Trippler M, Duchmann R, Meyer zum Büschenfelde K-H & Gerken G (1998) Interleukin-10 expression is autoregulated at the transcriptional level in human and murine kupffer cells. *Hepatology* 27: 93–99
- Knolle PA & Wöhlleber D (2016) Immunological functions of liver sinusoidal endothelial cells. *Cellular & Molecular Immunology* 13: 347–353
- Kobaek-Larsen M, Thorup I, Diederichsen A, Fenger C & Hoitinga MR (2000) Review of colorectal cancer and its metastases in rodent models: comparative aspects with those in humans. *Comp Med* 50: 16–26
- Kok SY, Oshima H, Takahashi K, Nakayama M, Murakami K, Ueda HR, Miyazono K & Oshima M (2021) Malignant subclone drives metastasis of genetically and

- phenotypically heterogenous cell clusters through fibrotic niche generation. *Nature Communications* 12: 863
- Kotredes KP & Gamero AM (2013) Interferons as Inducers of Apoptosis in Malignant Cells. *Journal of Interferon & Cytokine Research* 33: 162–170
- Kupffer C (1876) Ueber Sternzellen der Leber. *Archiv für Mikroskopische Anatomie* 12: 353–358
- Lalos A, Tülek A, Tosti N, Mechera R, Wilhelm A, Soysal S, Daester S, Kancherla V, Weixler B, Spagnoli GC, *et al* (2021) Prognostic significance of CD8+ T-cells density in stage III colorectal cancer depends on SDF-1 expression. *Scientific Reports* 11: 775
- Lau AH (2003) Liver tolerance mediated by antigen presenting cells: fact or fiction? *Gut* 52: 1075–1078
- Lawler SE, Speranza M-C, Cho C-F & Chiocca EA (2017) Oncolytic Viruses in Cancer Treatment. *JAMA Oncology* 3: 841
- Lee JC, Mehdizadeh S, Smith J, Young A, Mufazalov IA, Mowery CT, Daud A & Bluestone JA (2020) Regulatory T cell control of systemic immunity and immunotherapy response in liver metastasis. *Science Immunology* 5
- Lee MS & Kim Y-J (2007) Signaling Pathways Downstream of Pattern-Recognition Receptors and Their Cross Talk. *Annual Review of Biochemistry* 76: 447–480
- Lee SJ, Evers S, Roeder D, Parlow AF, Risteli J, Risteli L, Lee YC, Feizi T, Langen H & Nussenzweig MC (2002) Mannose Receptor-Mediated Regulation of Serum Glycoprotein Homeostasis. *Science (1979)* 295: 1898–1901
- Leebeek FWG & Miesbach W (2021) Gene therapy for hemophilia: a review on clinical benefit, limitations, and remaining issues. *Blood* 138: 923–931
- Lemmens VE, Klaver YL, Verwaal VJ, Rutten HJ, Coebergh JWW & de Hingh IH (2011) Predictors and survival of synchronous peritoneal carcinomatosis of colorectal origin: A population-based study. *International Journal of Cancer* 128: 2717–2725

- Levine BL, Miskin J, Wonnacott K & Keir C (2017) Global Manufacturing of CAR T Cell Therapy. *Molecular Therapy - Methods & Clinical Development* 4: 92–101
- Levings MK, Bacchetta R, Schulz U & Roncarolo MG (2002) The Role of IL-10 and TGF- β in the Differentiation and Effector Function of T Regulatory Cells. *International Archives of Allergy and Immunology* 129: 263–276
- Levings MK, Sangregorio R, Galbiati F, Squadrone S, de Waal Malefyt R & Roncarolo M-G (2001) IFN- α and IL-10 Induce the Differentiation of Human Type 1 T Regulatory Cells. *The Journal of Immunology* 166: 5530–5539
- Lhuillier C, Rudqvist N-P, Elemento O, Formenti SC & Demaria S (2019) Radiation therapy and anti-tumor immunity: exposing immunogenic mutations to the immune system. *Genome Medicine* 11: 40
- Li F, Deng Y, Zhang S, Zhu B, Wang J, Wang J, Wang X, Zhao Z, Deng W, Mao R, *et al* (2022) Human hepatocyte-enriched miRNA-192-3p promotes HBV replication through inhibiting Akt/mTOR signalling by targeting ZNF143 in hepatic cell lines. *Emerging Microbes & Infections* 11: 616–628
- Li F, Li C, Cai X, Xie Z, Zhou L, Cheng B, Zhong R, Xiong S, Li J, Chen Z, *et al* (2021) The association between CD8⁺ tumor-infiltrating lymphocytes and the clinical outcome of cancer immunotherapy: A systematic review and meta-analysis. *EClinicalMedicine* 41: 101134
- Lin Y, Xu J & Lan H (2019) Tumor-associated macrophages in tumor metastasis: biological roles and clinical therapeutic applications. *Journal of Hematology & Oncology* 12: 76
- Liu Y & Cao X (2016) Characteristics and Significance of the Pre-metastatic Niche. *Cancer Cell* 30: 668–681
- Londoño M-C, Rimola A, O’Grady J & Sanchez-Fueyo A (2013) Immunosuppression minimization vs. complete drug withdrawal in liver transplantation. *Journal of Hepatology* 59: 872–879
- Long KB & Beatty GL (2013) Harnessing the antitumor potential of macrophages for cancer immunotherapy. *OncImmunity* 2: e26860

- Ma C, Zhang Q & Greten TF (2021) MDSCs in liver cancer: A critical tumor-promoting player and a potential therapeutic target. *Cellular Immunology* 361: 104295
- Maimela NR, Liu S & Zhang Y (2019) Fates of CD8+ T cells in Tumor Microenvironment. *Computational and Structural Biotechnology Journal* 17: 1–13
- Manfredi S, Lepage C, Hatem C, Coatmeur O, Faivre J & Bouvier A-M (2006) Epidemiology and Management of Liver Metastases From Colorectal Cancer. *Annals of Surgery* 244: 254–259
- Mantovani A, Marchesi F, Malesci A, Laghi L & Allavena P (2017) Tumour-associated macrophages as treatment targets in oncology. *Nature Reviews Clinical Oncology* 14: 399–416
- Marcuello M, Vymetalkova V, Neves RPL, Duran-Sanchon S, Vedeld HM, Tham E, van Dalum G, Flügen G, Garcia-Barberan V, Fijneman RJA, *et al* (2019) Circulating biomarkers for early detection and clinical management of colorectal cancer. *Molecular Aspects of Medicine* 69: 107–122
- Marin-Acevedo JA, Kimbrough EO & Lou Y (2021) Next generation of immune checkpoint inhibitors and beyond. *Journal of Hematology & Oncology* 14: 45
- Marktel S, Scaramuzza S, Cicalese MP, Giglio F, Galimberti S, Lidonnici MR, Calbi V, Assanelli A, Bernardo ME, Rossi C, *et al* (2019) Intrabone hematopoietic stem cell gene therapy for adult and pediatric patients affected by transfusion-dependent β -thalassemia. *Nature Medicine* 25: 234–241
- Marofi F, Motavalli R, Safonov VA, Thangavelu L, Yumashev AV, Alexander M, Shomali N, Chartrand MS, Pathak Y, Jarahian M, *et al* (2021) CAR T cells in solid tumors: challenges and opportunities. *Stem Cell Research & Therapy* 12: 81
- Massagué J & Obenauf AC (2016) Metastatic colonization by circulating tumour cells. *Nature* 529: 298–306
- Mattei F, Schiavoni G, Belardelli F & Tough DF (2001) IL-15 Is Expressed by Dendritic Cells in Response to Type I IFN, Double-Stranded RNA, or Lipopolysaccharide and Promotes Dendritic Cell Activation. *The Journal of Immunology* 167: 1179–1187

- McWhorter FY, Wang T, Nguyen P, Chung T & Liu WF (2013) Modulation of macrophage phenotype by cell shape. *Proceedings of the National Academy of Sciences* 110: 17253–17258
- Medawar PB (1948) Immunity to homologous grafted skin; the fate of skin homografts transplanted to the brain, to subcutaneous tissue, and to the anterior chamber of the eye. *Br J Exp Pathol* 29: 58–69
- Milani M, Annoni A, Moalli F, Liu T, Cesana D, Calabria A, Bartolaccini S, Biffi M, Russo F, Visigalli I, *et al* (2019) Phagocytosis-shielded lentiviral vectors improve liver gene therapy in nonhuman primates. *Science Translational Medicine* 11
- Miyamoto M & Takizawa S (1975) Brief Communication: Colon Carcinoma of Highly Inbred Rats. *JNCI: Journal of the National Cancer Institute* 55: 1471–1472
- Morris EJA, Forman D, Thomas JD, Quirke P, Taylor EF, Fairley L, Cottier B & Poston G (2010) Surgical management and outcomes of colorectal cancer liver metastases. *British Journal of Surgery* 97: 1110–1118
- Morris JC, Tan AR, Olencki TE, Shapiro GI, Dezube BJ, Reiss M, Hsu FJ, Berzofsky JA & Lawrence DP (2014) Phase I Study of GC1008 (Fresolimumab): A Human Anti-Transforming Growth Factor-Beta (TGF β) Monoclonal Antibody in Patients with Advanced Malignant Melanoma or Renal Cell Carcinoma. *PLoS ONE* 9: e90353
- Morse MA, Hochster H & Benson A (2020) Perspectives on Treatment of Metastatic Colorectal Cancer with Immune Checkpoint Inhibitor Therapy. *The Oncologist* 25: 33–45
- Motz GT, Santoro SP, Wang L-P, Garrabrant T, Lastra RR, Hagemann IS, Lal P, Feldman MD, Benencia F & Coukos G (2014) Tumor endothelium FasL establishes a selective immune barrier promoting tolerance in tumors. *Nature Medicine* 20: 607–615
- Mukund K, Syulyukina N, Ramamoorthy S & Subramaniam S (2020) Right and left-sided colon cancers-specificity of molecular mechanisms in tumorigenesis and progression. *BMC Cancer* 20

- Müller E, Speth M, Christopoulos PF, Lunde A, Avdagic A, Øynebråten I & Corthay A (2018) Both Type I and Type II Interferons Can Activate Antitumor M1 Macrophages When Combined With TLR Stimulation. *Frontiers in Immunology* 9
- Naito M, Hasegawa G, Ebe Y & Yamamoto T (2004) Differentiation and function of Kupffer cells. *Medical Electron Microscopy* 37: 16–28
- Nakagawa-Senda H, Hori M, Matsuda T & Ito H (2019) Prognostic impact of tumor location in colon cancer: The Monitoring of Cancer Incidence in Japan (MCIJ) project. *BMC Cancer* 19
- Naldini L (2011) Ex vivo gene transfer and correction for cell-based therapies. *Nature Reviews Genetics* 12: 301–315
- Naldini L (2015) Gene therapy returns to centre stage. *Nature* 526: 351–360
- Naldini L (2019) Genetic engineering of hematopoiesis: current stage of clinical translation and future perspectives. *EMBO Molecular Medicine* 11
- Naldini L, Blömer U, Gallyat P, Ory D, Mulligan R, Gage FH, Verma IM & Trono D (1996) In Vivo Gene Delivery and Stable Transduction of Nondividing Cells by a Lentiviral Vector. *Science (1979)* 272: 263–267
- Nguyen-Lefebvre AT & Horuzsko A (2015) Kupffer Cell Metabolism and Function. *J Enzymol Metab* 1
- Ni G, Zhang L, Yang X, Li H, Ma B, Walton S, Wu X, Yuan J, Wang T & Liu X (2020) Targeting interleukin-10 signalling for cancer immunotherapy, a promising and complicated task. *Human Vaccines & Immunotherapeutics* 16: 2328–2332
- Nieto MA & Cano A (2012) The epithelial-mesenchymal transition under control: Global programs to regulate epithelial plasticity. *Seminars in Cancer Biology* 22: 361–368 doi:10.1016/j.semcancer.2012.05.003 [PREPRINT]
- Nojadeh JN, Behrouz Sharif S & Sakhinia E (2018) Microsatellite instability in colorectal cancer. *EXCLI J* 17: 159–168

- Ochoa MC, Minute L, Rodriguez I, Garasa S, Perez-Ruiz E, Inogés S, Melero I & Berraondo P (2017) Antibody-dependent cell cytotoxicity: immunotherapy strategies enhancing effector NK cells. *Immunology & Cell Biology* 95: 347–355
- Oga T, Yamashita Y, Soda M, Kojima S, Ueno T, Kawazu M, Suzuki N, Nagano H, Hazama S, Izumiya M, *et al* (2019) Genomic profiles of colorectal carcinoma with liver metastases and newly identified fusion genes. *Cancer Science* 110: 2973–2981
- Oh BY, Hong HK, Lee WY & Cho YB (2017) Animal models of colorectal cancer with liver metastasis. *Cancer Letters* 387: 114–120
- Olive KP, Tuveson DA, Ruhe ZC, Yin B, Willis NA, Bronson RT, Crowley D & Jacks T (2004) Mutant p53 Gain of Function in Two Mouse Models of Li-Fraumeni Syndrome. *Cell* 119: 847–860
- Ono S, Shao D-Z, Yamada S, Yang Y, Yamashita M & Hamaoka T (2000) A novel function of B lymphocytes from normal mice to suppress autoimmunity in (NZB × NZW)F₁ mice. *Immunology* 100: 99–109
- Onoyama I, Tsunematsu R, Matsumoto A, Kimura T, de Alborán IM, Nakayama K & Nakayama KI (2007) Conditional inactivation of Fbxw7 impairs cell-cycle exit during T cell differentiation and results in lymphomatogenesis. *Journal of Experimental Medicine* 204: 2875–2888
- Orecchioni M, Ghosheh Y, Pramod AB & Ley K (2019a) Macrophage Polarization: Different Gene Signatures in M1(LPS+) vs. Classically and M2(LPS-) vs. Alternatively Activated Macrophages. *Frontiers in Immunology* 10
- Orecchioni M, Ghosheh Y, Pramod AB & Ley K (2019b) Macrophage Polarization: Different Gene Signatures in M1(LPS+) vs. Classically and M2(LPS-) vs. Alternatively Activated Macrophages. *Frontiers in Immunology* 10
- Orimo A, Gupta PB, Sgroi DC, Arenzana-Seisdedos F, Delaunay T, Naeem R, Carey VJ, Richardson AL & Weinberg RA (2005) Stromal Fibroblasts Present in Invasive Human Breast Carcinomas Promote Tumor Growth and Angiogenesis through Elevated SDF-1/CXCL12 Secretion. *Cell* 121: 335–348

- Osei-Bordom D-C, Kamarajah S & Christou N (2021) Colorectal Cancer, Liver Metastases and Biotherapies. *Biomedicines* 9: 894
- Oshima M, Oshima H, Kitagawa K, Kobayashi M, Itakura C & Taketo M (1995) Loss of Apc heterozygosity and abnormal tissue building in nascent intestinal polyps in mice carrying a truncated Apc gene. *Proceedings of the National Academy of Sciences* 92: 4482–4486
- Padmanaban V, Krol I, Suhail Y, Szczerba BM, Aceto N, Bader JS & Ewald AJ (2019) E-cadherin is required for metastasis in multiple models of breast cancer. *Nature* 573: 439–444
- Palladino MA, Bahjat FR, Theodorakis EA & Moldawer LL (2003) Anti-TNF- α therapies: the next generation. *Nature Reviews Drug Discovery* 2: 736–746
- de Palma M & Hanahan D (2012) The biology of personalized cancer medicine: Facing individual complexities underlying hallmark capabilities. *Molecular Oncology* 6: 111–127
- de Palma M, Mazziere R, Politi LS, Pucci F, Zonari E, Sitia G, Mazzoleni S, Moi D, Venneri MA, Indraccolo S, *et al* (2008) Tumor-Targeted Interferon- α Delivery by Tie2-Expressing Monocytes Inhibits Tumor Growth and Metastasis. *Cancer Cell* 14: 299–311
- de Palma M, Venneri MA, Roca C & Naldini L (2003) Targeting exogenous genes to tumor angiogenesis by transplantation of genetically modified hematopoietic stem cells. *Nature Medicine* 9: 789–795
- Pan Y, Yu Y, Wang X & Zhang T (2020) Tumor-Associated Macrophages in Tumor Immunity. *Frontiers in Immunology* 11
- Patil, Gao, Lin, Li, Dang, Tian, Zhang, Jiang, Qadir & Qian (2019) The Development of Functional Non-Viral Vectors for Gene Delivery. *International Journal of Molecular Sciences* 20: 5491
- Pattyn E, van Ostade X, Schauvliege L, Verhee A, Kalai M, Vandekerckhove J & Tavernier J (1999) Dimerization of the Interferon Type I Receptor IFN α 2–2 Is

- Sufficient for Induction of Interferon Effector Genes but Not for Full Antiviral Activity. *Journal of Biological Chemistry* 274: 34838–34845
- Peng J, Wang Y, Zhang R, Deng Y, Xiao B, Ou Q, Sui Q, Xu J, Qin J, Lin J, *et al* (2019) Immune Cell Infiltration in the Microenvironment of Liver Oligometastasis from Colorectal Cancer: Intratumoural CD8/CD3 Ratio Is a Valuable Prognostic Index for Patients Undergoing Liver Metastasectomy. *Cancers (Basel)* 11: 1922
- Peng K-W, Pham L, Ye H, Zufferey R, Trono D, Cosset F-L & Russell S (2001) Organ distribution of gene expression after intravenous infusion of targeted and untargeted lentiviral vectors. *Gene Therapy* 8: 1456–1463
- Perkins D, Wang Z, Donovan C, He H, Mark D, Guan G, Wang Y, Walunas T, Bluestone J, Listman J, *et al* (1996) Regulation of CTLA-4 expression during T cell activation. *J Immunol* 156: 4154–9
- Perrin GQ, Herzog RW & Markusic DM (2019) Update on clinical gene therapy for hemophilia. *Blood* 133: 407–414
- Petrich de Marquesini LG, Fu J, Connor KJ, Bishop AJ, McLintock NE, Pope C, Wong FS & Dayan CM (2010) IFN- γ and IL-10 islet-antigen-specific T cell responses in autoantibody-negative first-degree relatives of patients with type 1 diabetes. *Diabetologia* 53: 1451–1460
- Petrova V, Annicchiarico-Petruzzelli M, Melino G & Amelio I (2018) The hypoxic tumour microenvironment. *Oncogenesis* 7: 10
- Pfeiffer A, Thalheimer FB, Hartmann S, Frank AM, Bender RR, Danisch S, Costa C, Wels WS, Modlich U, Stripecke R, *et al* (2018) In vivo generation of human CD19-CAR T cells results in B-cell depletion and signs of cytokine release syndrome. *EMBO Molecular Medicine* 10
- Pihl E, Hughes ESR, McDermott FT, Johnson WR & Katrivessis H (1987) Lung recurrence after curative surgery for colorectal cancer. *Diseases of the Colon & Rectum* 30: 417–419
- Poletti V & Mavilio F (2021) Designing Lentiviral Vectors for Gene Therapy of Genetic Diseases. *Viruses* 13: 1526

- Pot C, Jin H, Awasthi A, Liu SM, Lai C-Y, Madan R, Sharpe AH, Karp CL, Miaw S-C, Ho I-C, *et al* (2009) Cutting Edge: IL-27 Induces the Transcription Factor c-Maf, Cytokine IL-21, and the Costimulatory Receptor ICOS that Coordinately Act Together to Promote Differentiation of IL-10-Producing Tr1 Cells. *The Journal of Immunology* 183: 797–801
- Prasetyanti PR & Medema JP (2017) Intra-tumor heterogeneity from a cancer stem cell perspective. *Molecular Cancer* 16: 41
- Provance OK & Lewis-Wambi J (2019) Deciphering the role of interferon alpha signaling and microenvironment crosstalk in inflammatory breast cancer. *Breast Cancer Research* 21: 59
- Quintana FJ, Basso AS, Iglesias AH, Korn T, Farez MF, Bettelli E, Caccamo M, Oukka M & Weiner HL (2008) Control of Treg and TH17 cell differentiation by the aryl hydrocarbon receptor. *Nature* 453: 65–71
- Raedler LA (2015) Keytruda (Pembrolizumab): First PD-1 Inhibitor Approved for Previously Treated Unresectable or Metastatic Melanoma. *Am Health Drug Benefits* 8: 96–100
- Raichlin E, Daly RC, Rosen CB, McGregor CG, Charlton MR, Frantz RP, Clavell AL, Rodeheffer RJ, Pereira NL, Kremers WK, *et al* (2009) Combined Heart and Liver Transplantation: A Single-Center Experience. *Transplantation* 88: 219–225
- Raison CL, Demetrashvili M, Capuron L & Miller AH (2005) Neuropsychiatric Adverse Effects of Interferon-?? *CNS Drugs* 19: 105–123
- Raskov H, Orhan A, Christensen JP & Gögenur I (2021) Cytotoxic CD8+ T cells in cancer and cancer immunotherapy. *British Journal of Cancer* 124: 359–367
- de Ravin SS, Wu X, Moir S, Anaya-O'Brien S, Kwatema N, Littel P, Theobald N, Choi U, Su L, Marquesen M, *et al* (2016) Lentiviral hematopoietic stem cell gene therapy for X-linked severe combined immunodeficiency. *Sci Transl Med* 8: 335ra57
- Rhu J, Heo JS, Choi SH, Choi DW, Kim JM, Joh J-W & Kwon CHD (2017) Streamline flow of the portal vein affects the lobar distribution of colorectal liver metastases

- and has a clinical impact on survival. *Annals of Surgical Treatment and Research* 92: 348
- Ricci-Vitiani L, Lombardi DG, Pilozzi E, Biffoni M, Todaro M, Peschle C & de Maria R (2007) Identification and expansion of human colon-cancer-initiating cells. *Nature* 445: 111–115
- Richardson N, Ng STH & Wraith DC (2020) Antigen-Specific Immunotherapy for Treatment of Autoimmune Liver Diseases. *Frontiers in Immunology* 11
- Robinson MW, Harmon C & O'Farrelly C (2016) Liver immunology and its role in inflammation and homeostasis. *Cellular & Molecular Immunology* 13: 267–276
- Rodríguez PC & Ochoa AC (2008) Arginine regulation by myeloid derived suppressor cells and tolerance in cancer: mechanisms and therapeutic perspectives. *Immunological Reviews* 222: 180–191
- Roncarolo MG, Gregori S, Bacchetta R, Battaglia M & Gagliani N (2018a) The Biology of T Regulatory Type 1 Cells and Their Therapeutic Application in Immune-Mediated Diseases. *Immunity* 49: 1004–1019
- Roncarolo MG, Gregori S, Bacchetta R, Battaglia M & Gagliani N (2018b) The Biology of T Regulatory Type 1 Cells and Their Therapeutic Application in Immune-Mediated Diseases. *Immunity* 49: 1004–1019
- Roncarolo MG, Yssel H, Touraine JL, Betuel H, de Vries JE & Spits H (1988) Autoreactive T cell clones specific for class I and class II HLA antigens isolated from a human chimera. *Journal of Experimental Medicine* 167: 1523–1534
- de Roock W, Claes B, Bernasconi D, de Schutter J, Biesmans B, Fountzilias G, Kalogeras KT, Kotoula V, Papamichael D, Laurent-Puig P, *et al* (2010) Effects of KRAS, BRAF, NRAS, and PIK3CA mutations on the efficacy of cetuximab plus chemotherapy in chemotherapy-refractory metastatic colorectal cancer: a retrospective consortium analysis. *The Lancet Oncology* 11: 753–762
- Rose SA, Wroblewska A, Dhainaut M, Yoshida H, Shaffer JM, Bektesevic A, Ben-Zvi B, Rhoads A, Kim EY, Yu B, *et al* (2021) A microRNA expression and regulatory

- element activity atlas of the mouse immune system. *Nature Immunology* 22: 914–927
- Roth S, Gong W & Gressner AM (1998) Expression of different isoforms of TGF- β and the latent TGF- β binding protein (LTBP) by rat Kupffer cells. *Journal of Hepatology* 29: 915–922
- Rotte A, Jin JY & Lemaire V (2018) Mechanistic overview of immune checkpoints to support the rational design of their combinations in cancer immunotherapy. *Annals of Oncology* 29: 71–83
- Saeterdal I, Bjørheim J, Lislrud K, Gjertsen MK, Bukholm IK, Olsen OC, Nesland JM, Eriksen JA, Møller M, Lindblom A, *et al* Frameshift-mutation-derived peptides as tumor-specific antigens in inherited and spontaneous colorectal cancer
- Saito R, Kobayashi T, Kashima S, Matsumoto K & Ogawa O (2020) Faithful preclinical mouse models for better translation to bedside in the field of immuno-oncology. *International Journal of Clinical Oncology* 25: 831–841
- Saito T, Nishikawa H, Wada H, Nagano Y, Sugiyama D, Atarashi K, Maeda Y, Hamaguchi M, Ohkura N, Sato E, *et al* (2016) Two FOXP3+CD4+ T cell subpopulations distinctly control the prognosis of colorectal cancers. *Nature Medicine* 22: 679–684
- Sakai E, Nakayama M, Oshima H, Kouyama Y, Niida A, Fujii S, Ochiai A, Nakayama KI, Mimori K, Suzuki Y, *et al* (2018) Combined Mutation of Apc, Kras, and Tgfbr2 Effectively Drives Metastasis of Intestinal Cancer. *Cancer Research* 78: 1334–1346
- Salmon H, Franciszkievicz K, Damotte D, Dieu-Nosjean M-C, Validire P, Trautmann A, Mami-Chouaib F & Donnadieu E (2012) Matrix architecture defines the preferential localization and migration of T cells into the stroma of human lung tumors. *Journal of Clinical Investigation* 122: 899–910
- Sambi M, Bagheri L & Szewczuk MR (2019) Current Challenges in Cancer Immunotherapy: Multimodal Approaches to Improve Efficacy and Patient Response Rates. *Journal of Oncology* 2019: 1–12

- Santos Apolonio J, Lima de Souza Gonçalves V, Cordeiro Santos ML, Silva Luz M, Silva Souza JV, Rocha Pinheiro SL, de Souza WR, Sande Loureiro M & de Melo FF (2021) Oncolytic virus therapy in cancer: A current review. *World J Virol* 10: 229–255
- Sawyers C (2004) Targeted cancer therapy. *Nature* 432: 294–297
- Schiavoni G, Mattei F & Gabriele L (2013) Type I Interferons as Stimulators of DC-Mediated Cross-Priming: Impact on Anti-Tumor Response. *Frontiers in Immunology* 4
- Schneider WM, Chevillotte MD & Rice CM (2014) Interferon-Stimulated Genes: A Complex Web of Host Defenses. *Annual Review of Immunology* 32: 513–545
- Schoenfeld AJ & Hellmann MD (2020) Acquired Resistance to Immune Checkpoint Inhibitors. *Cancer Cell* 37: 443–455
- Schreiber RD, Old LJ & Smyth MJ (2011) Cancer Immunoediting: Integrating Immunity's Roles in Cancer Suppression and Promotion. *Science (1979)* 331: 1565–1570
- Schulze RJ, Schott MB, Casey CA, Tuma PL & McNiven MA (2019) The cell biology of the hepatocyte: A membrane trafficking machine. *J Cell Biol* 218: 2096–2112
- Schuster SJ, Svoboda J, Chong EA, Nasta SD, Mato AR, Anak Ö, Brogdon JL, Pruteanu-Malinici I, Bhoj V, Landsburg D, *et al* (2017) Chimeric Antigen Receptor T Cells in Refractory B-Cell Lymphomas. *New England Journal of Medicine* 377: 2545–2554
- Scodeller P, Simón-Gracia L, Kopanchuk S, Tobi A, Kilk K, Säälük P, Kurm K, Squadrito ML, Kotamraju VR, Rinken A, *et al* (2017) Precision Targeting of Tumor Macrophages with a CD206 Binding Peptide. *Scientific Reports* 7: 14655
- Seebacher NA, Stacy AE, Porter GM & Merlot AM (2019) Clinical development of targeted and immune based anti-cancer therapies. *Journal of Experimental & Clinical Cancer Research* 38: 156

- Sessa M, Lorioli L, Fumagalli F, Acquati S, Redaelli D, Baldoli C, Canale S, Lopez ID, Morena F, Calabria A, *et al* (2016) Lentiviral haemopoietic stem-cell gene therapy in early-onset metachromatic leukodystrophy: an ad-hoc analysis of a non-randomised, open-label, phase 1/2 trial. *The Lancet* 388: 476–487
- Shay AE, Diwakar BT, Guan B-J, Narayan V, Urban JF & Prabhu KS (2017) IL-4 up-regulates cyclooxygenase-1 expression in macrophages. *Journal of Biological Chemistry* 292: 14544–14555
- Sheng IY & Ornstein MC (2020) Ipilimumab and Nivolumab as First-Line Treatment of Patients with Renal Cell Carcinoma: The Evidence to Date. *Cancer Management and Research* Volume 12: 4871–4881
- Shepherd VL, Abdolrasulnia R, Garrett M & Cowan HB (1990) Down-regulation of mannose receptor activity in macrophages after treatment with lipopolysaccharide and phorbol esters. *J Immunol* 145: 1530–6
- Shepherd VL, Konish MG & Stahl P (1985) Dexamethasone increases expression of mannose receptors and decreases extracellular lysosomal enzyme accumulation in macrophages. *J Biol Chem* 260: 160–4
- Short B (2015) Dimerization dictates the message. *Journal of Cell Biology* 209: 471–471
- Siegel RL, Miller KD, Goding Sauer A, Fedewa SA, Butterly LF, Anderson JC, Cercek A, Smith RA & Jemal A (2020) Colorectal cancer statistics, 2020. *CA: A Cancer Journal for Clinicians* 70: 145–164
- Siegel RL, Miller KD & Jemal A (2019) Cancer statistics, 2019. *CA: A Cancer Journal for Clinicians* 69: 7–34
- Siudeja K, Nassari S, Gervais L, Skorski P, Lameiras S, Stolfa D, Zande M, Bernard V, Frio TR & Bardin AJ (2015) Frequent Somatic Mutation in Adult Intestinal Stem Cells Drives Neoplasia and Genetic Mosaicism during Aging. *Cell Stem Cell* 17: 663–674
- Sleijfer S, Bannink M, Gool AR, Kruit WHJ & Stoter G (2005) Side Effects of Interferon- α Therapy. *Pharmacy World & Science* 27: 423–431

- Soldi M, Sergi L, Unali G, Kerzel T, Cuccovillo I, Capasso P, Annoni A, Biffi M, Rancoita PMV, Cantore A, *et al* (2020) Laboratory-Scale Lentiviral Vector Production and Purification for Enhanced Ex Vivo and In Vivo Genetic Engineering. *Mol Ther Methods Clin Dev* 19: 411–425
- Solé P & Santamaria P (2021) Re-Programming Autoreactive T Cells Into T-Regulatory Type 1 Cells for the Treatment of Autoimmunity. *Frontiers in Immunology* 12
- Soto-Herederó G, Gómez de las Heras MM, Gabandé-Rodríguez E, Oller J & Mittelbrunn M (2020) Glycolysis – a key player in the inflammatory response. *The FEBS Journal* 287: 3350–3369
- Soza A, Everhart JE, Ghany MG, Doo E, Heller T, Promrat K, Park Y, Liang TJ & Hoofnagle JH (2002) Neutropenia during combination therapy of interferon alfa and ribavirin for chronic hepatitis C. *Hepatology* 36: 1273–1279
- Squadrito ML & de Palma M (2016) DICERing macrophages for reprogramming TAMs. *Cell Cycle* 15: 3149–3150
- Squadrito ML, Pucci F, Magri L, Moi D, Gilfillan GD, Ranghetti A, Casazza A, Mazzone M, Lyle R, Naldini L, *et al* (2012) miR-511-3p Modulates Genetic Programs of Tumor-Associated Macrophages. *Cell Reports* 1: 141–154
- Strauss L, Guarneri V, Gennari A & Sica A (2021) Implications of metabolism-driven myeloid dysfunctions in cancer therapy. *Cellular & Molecular Immunology* 18: 829–841
- Sugase T, Lam BQ, Danielson M, Terai M, Aplin AE, Gutkind JS & Sato T (2020) Development and optimization of orthotopic liver metastasis xenograft mouse models in uveal melanoma. *Journal of Translational Medicine* 18: 208
- Sung H, Ferlay J, Siegel RL, Laversanne M, Soerjomataram I, Jemal A & Bray F (2021) Global Cancer Statistics 2020: GLOBOCAN Estimates of Incidence and Mortality Worldwide for 36 Cancers in 185 Countries. *CA: A Cancer Journal for Clinicians* 71: 209–249

- Sweeney NP & Vink CA (2021) The impact of lentiviral vector genome size and producer cell genomic to gag-pol mRNA ratios on packaging efficiency and titre. *Molecular Therapy - Methods & Clinical Development* 21: 574–584
- Taftaf R, Liu X, Singh S, Jia Y, Dashzeveg NK, Hoffmann AD, El-Shennawy L, Ramos EK, Adorno-Cruz V, Schuster EJ, *et al* (2021) ICAM1 initiates CTC cluster formation and trans-endothelial migration in lung metastasis of breast cancer. *Nature Communications* 12: 4867
- Tang T, Huang X, Zhang G, Hong Z, Bai X & Liang T (2021) Advantages of targeting the tumor immune microenvironment over blocking immune checkpoint in cancer immunotherapy. *Signal Transduction and Targeted Therapy* 6: 72
- Tao N, Gao G-P, Parr M, Johnston J, Baradet T, Wilson JM, Barsoum J & Fawell SE (2001) Sequestration of Adenoviral Vector by Kupffer Cells Leads to a Nonlinear Dose Response of Transduction in Liver. *Molecular Therapy* 3: 28–35
- Tauriello DVF, Palomo-Ponce S, Stork D, Berenguer-Llergo A, Badia-Ramentol J, Iglesias M, Sevillano M, Ibiza S, Cañellas A, Hernando-Momblona X, *et al* (2018) TGF β drives immune evasion in genetically reconstituted colon cancer metastasis. *Nature* 554: 538–543
- Tauriello DVF, Sancho E & Batlle E (2022) Overcoming TGF β -mediated immune evasion in cancer. *Nature Reviews Cancer* 22: 25–44
- Tay RE, Richardson EK & Toh HC (2021) Revisiting the role of CD4+ T cells in cancer immunotherapy—new insights into old paradigms. *Cancer Gene Therapy* 28: 5–17
- Testa U, Pelosi E & Castelli G (2018) Colorectal Cancer: Genetic Abnormalities, Tumor Progression, Tumor Heterogeneity, Clonal Evolution and Tumor-Initiating Cells. *Medical Sciences* 6: 31
- Thomas DA & Massagué J (2005) TGF- β directly targets cytotoxic T cell functions during tumor evasion of immune surveillance. *Cancer Cell* 8: 369–380
- Ticho AL, Malhotra P, Dudeja PK, Gill RK & Alrefai WA (2019) Bile Acid Receptors and Gastrointestinal Functions. *Liver Res* 3: 31–39

- Tokunaga R, Zhang W, Naseem M, Puccini A, Berger MD, Soni S, McSkane M, Baba H & Lenz H-J (2018) CXCL9, CXCL10, CXCL11/CXCR3 axis for immune activation – A target for novel cancer therapy. *Cancer Treatment Reviews* 63: 40–47
- Tomlinson JS, Jarnagin WR, DeMatteo RP, Fong Y, Kornprat P, Gonen M, Kemeny N, Brennan MF, Blumgart LH & D’Angelica M (2007) Actual 10-year survival after resection of colorectal liver metastases defines cure. *Journal of Clinical Oncology* 25: 4575–4580
- Torsvik A, Stieber D, Enger PØ, Golebiewska A, Molven A, Svendsen A, Westermarck B, Niclou SP, Olsen TK, Chekenya Enger M, *et al* (2014) U-251 revisited: genetic drift and phenotypic consequences of long-term cultures of glioblastoma cells. *Cancer Medicine* 3: 812–824
- Trinchieri G (2007) Interleukin-10 production by effector T cells: Th1 cells show self control. *Journal of Experimental Medicine* 204: 239–243
- Valastyan S & Weinberg RA (2011) Tumor metastasis: Molecular insights and evolving paradigms. *Cell* 147: 275–292 doi:10.1016/j.cell.2011.09.024 [PREPRINT]
- Vandamme T (2014) Use of rodents as models of human diseases. *Journal of Pharmacy and Bioallied Sciences* 6: 2
- van de Laar L, Saelens W, De Prijck S, Martens L, Scott CL, Van Isterdael G, Hoffmann E, Beyaert R, Saeys Y, Lambrecht BN, *et al* (2016) Yolk Sac Macrophages, Fetal Liver, and Adult Monocytes Can Colonize an Empty Niche and Develop into Functional Tissue-Resident Macrophages. *Immunity* 44: 755–768
- Vasilevko V, Ghochikyan A, Holterman MJ & Agadjanyan MG (2002) CD80 (B7-1) and CD86 (B7-2) are Functionally Equivalent in the Initiation and Maintenance of CD4+ T-Cell Proliferation after Activation with Suboptimal Doses of PHA. *DNA and Cell Biology* 21: 137–149
- Vatandoust S, Price TJ & Karapetis CS (2015) Colorectal cancer: Metastases to a single organ. *World Journal of Gastroenterology* 21: 11767–11776
- Vauthey J-N, Chaoui A, Do K-A, Bilimoria MM, Fenstermacher MJ, Charnsangavej C, Hicks M, Alsfasser G, Lauwers G, Hawkins IF, *et al* (2000) Standardized

- measurement of the future liver remnant prior to extended liver resection: Methodology and clinical associations. *Surgery* 127: 512–519
- Vellanki PJ, Mulkey F, Jaigirdar AA, Rodriguez L, Wang Y, Xu Y, Zhao H, Liu J, Howe G, Wang J, *et al* (2021) FDA Approval Summary: Nivolumab with Ipilimumab and Chemotherapy for Metastatic Non–small Cell Lung Cancer, A Collaborative Project Orbis Review. *Clinical Cancer Research* 27: 3522–3527
- Verma IM & Weitzman MD (2005) GENE THERAPY: Twenty-First Century Medicine. *Annual Review of Biochemistry* 74: 711–738
- Vieira AR, Abar L, Chan DSM, Vingeliene S, Polemiti E, Stevens C, Greenwood D & Norat T (2017) Foods and beverages and colorectal cancer risk: a systematic review and meta-analysis of cohort studies, an update of the evidence of the WCRF-AICR Continuous Update Project. *Annals of Oncology* 28: 1788–1802
- Vignali DAA, Collison LW & Workman CJ (2008) How regulatory T cells work. *Nature Reviews Immunology* 8: 523–532
- Vinay DS, Ryan EP, Pawelec G, Talib WH, Stagg J, Elkord E, Lichtor T, Decker WK, Whelan RL, Kumara HMCS, *et al* (2015) Immune evasion in cancer: Mechanistic basis and therapeutic strategies. *Seminars in Cancer Biology* 35: S185–S198
- Walker LSK & Sansom DM (2015) Confusing signals: Recent progress in CTLA-4 biology. *Trends in Immunology* 36: 63–70
- Wang L, Morizono H, Lin J, Bell P, Jones D, McMenamin D, Yu H, Batshaw ML & Wilson JM (2012) Preclinical evaluation of a clinical candidate AAV8 vector for ornithine transcarbamylase (OTC) deficiency reveals functional enzyme from each persisting vector genome. *Molecular Genetics and Metabolism* 105: 203–211
- Wei SC, Duffy CR & Allison JP (2018) Fundamental Mechanisms of Immune Checkpoint Blockade Therapy. *Cancer Discovery* 8: 1069–1086
- Wen SW, Ager EI & Christophi C (2013) Bimodal role of Kupffer cells during colorectal cancer liver metastasis. *Cancer Biology & Therapy* 14: 606–613

- Weston CJ, Zimmermann HW & Adams DH (2019) The Role of Myeloid-Derived Cells in the Progression of Liver Disease. *Frontiers in Immunology* 10
- Wherry EJ, Ha S-J, Kaech SM, Haining WN, Sarkar S, Kalia V, Subramaniam S, Blattman JN, Barber DL & Ahmed R (2007) Molecular Signature of CD8+ T Cell Exhaustion during Chronic Viral Infection. *Immunity* 27: 670–684
- Wong AD & Searson PC (2017) Mitosis-mediated intravasation in a tissue-engineered tumor–microvessel platform. *Cancer Research* 77: 6453–6461
- Workman P & Clarke PA (2011) Resisting Targeted Therapy: Fifty Ways to Leave Your EGFR. *Cancer Cell* 19: 437–440
- Wu X, Gu Z, Chen Y, Chen B, Chen W, Weng L & Liu X (2019) Application of PD-1 Blockade in Cancer Immunotherapy. *Computational and Structural Biotechnology Journal* 17: 661–674
- Xie G, Dong H, Liang Y, Ham JD, Rizwan R & Chen J (2020a) CAR-NK cells: A promising cellular immunotherapy for cancer. *EBioMedicine* 59: 102975
- Xie YH, Chen YX & Fang JY (2020b) Comprehensive review of targeted therapy for colorectal cancer. *Signal Transduction and Targeted Therapy* 5 doi:10.1038/s41392-020-0116-z [PREPRINT]
- Xu Y-Q, Gao Y-D, Yang J & Guo W (2010) A Defect of CD4⁺ CD25⁺ Regulatory T Cells in Inducing Interleukin-10 Production From CD4⁺ T Cells Under CD46 Costimulation in Asthma Patients. *Journal of Asthma* 47: 367–373
- Yamamoto T, Naito M, Moriyama H, Umezu H, Matsuo H, Kiwada H & Arakawa M (1996) Repopulation of murine Kupffer cells after intravenous administration of liposome-encapsulated dichloromethylene diphosphonate. *Am J Pathol* 149: 1271–86
- Yang JD, Nakamura I & Roberts LR (2011) The tumor microenvironment in hepatocellular carcinoma: Current status and therapeutic targets. *Seminars in Cancer Biology* 21: 35–43

- Yang M & Zhang C (2021) The role of liver sinusoidal endothelial cells in cancer liver metastasis. *Am J Cancer Res* 11: 1845–1860
- Yang Q, Guo N, Zhou Y, Chen J, Wei Q & Han M (2020) The role of tumor-associated macrophages (TAMs) in tumor progression and relevant advance in targeted therapy. *Acta Pharmaceutica Sinica B* 10: 2156–2170
- Ye X & Weinberg RA (2015) Epithelial-Mesenchymal Plasticity: A Central Regulator of Cancer Progression. *Trends in Cell Biology* 25: 675–686
doi:10.1016/j.tcb.2015.07.012 [PREPRINT]
- Yin M, Li X, Tan S, Zhou HJ, Ji W, Bellone S, Xu X, Zhang H, Santin AD, Lou G, *et al* (2016) Tumor-associated macrophages drive spheroid formation during early transcoelomic metastasis of ovarian cancer. *Journal of Clinical Investigation* 126: 4157–4173
- Yu J, Green MD, Li S, Sun Y, Journey SN, Choi JE, Rizvi SM, Qin A, Waninger JJ, Lang X, *et al* (2021) Liver metastasis restrains immunotherapy efficacy via macrophage-mediated T cell elimination. *Nature Medicine* 27: 152–164
- Yu X, Zhu L, Liu J, Xie M, Chen J & Li J (2020) Emerging Role of Immunotherapy for Colorectal Cancer with Liver Metastasis. *OncoTargets and Therapy* Volume 13: 11645–11658
- Zeng D, Wang M, Wu J, Lin S, Ye Z, Zhou R, Wang G, Wu J, Sun H, Bin J, *et al* (2021) Immunosuppressive Microenvironment Revealed by Immune Cell Landscape in Pre-metastatic Liver of Colorectal Cancer. *Frontiers in Oncology* 11
- Zhang F, Wang H, Wang X, Jiang G, Liu H, Zhang G, Wang H, Fang R, Bu X, Cai S, *et al* (2016) TGF- β induces M2-like macrophage polarization via SNAIL-mediated suppression of a pro-inflammatory phenotype. *Oncotarget* 7: 52294–52306
- Zhang K, Matsui Y, Hadaschik BA, Lee C, Jia W, Bell JC, Fazli L, So AI & Rennie PS (2010) Down-regulation of type I interferon receptor sensitizes bladder cancer cells to vesicular stomatitis virus-induced cell death. *International Journal of Cancer*: NA-NA

- Zhang Y & Zhang Z (2020) The history and advances in cancer immunotherapy: understanding the characteristics of tumor-infiltrating immune cells and their therapeutic implications. *Cellular & Molecular Immunology* 17: 807–821
- Zhang Z, Liu S, Zhang B, Qiao L, Zhang Y & Zhang Y (2020) T Cell Dysfunction and Exhaustion in Cancer. *Frontiers in Cell and Developmental Biology* 8
- Zhao Q, Jiang Y, Xiang S, Kaboli PJ, Shen J, Zhao Y, Wu X, Du F, Li M, Cho CH, *et al* (2021) Engineered TCR-T Cell Immunotherapy in Anticancer Precision Medicine: Pros and Cons. *Frontiers in Immunology* 12
- Zhong L, Li Y, Xiong L, Wang W, Wu M, Yuan T, Yang W, Tian C, Miao Z, Wang T, *et al* (2021) Small molecules in targeted cancer therapy: advances, challenges, and future perspectives. *Signal Transduction and Targeted Therapy* 6: 201
- Zhou J, Wang W & Li Q (2021) Potential therapeutic targets in the tumor microenvironment of hepatocellular carcinoma: reversing the protumor effect of tumor-associated macrophages. *Journal of Experimental & Clinical Cancer Research* 40: 73
- Zhou Q, Uhlig KM, Muth A, Kimpel J, Lévy C, Münch RC, Seifried J, Pfeiffer A, Trkola A, Coulibaly C, *et al* (2015) Exclusive Transduction of Human CD4⁺ T Cells upon Systemic Delivery of CD4-Targeted Lentiviral Vectors. *The Journal of Immunology* 195: 2493–2501
- Zhou Z, Xu M-J & Gao B (2016) Hepatocytes: a key cell type for innate immunity. *Cellular & Molecular Immunology* 13: 301–315
- Zigmond E, Halpern Z, Elinav E, Brazowski E, Jung S & Varol C (2011) Utilization of Murine Colonoscopy for Orthotopic Implantation of Colorectal Cancer. *PLoS ONE* 6: e28858
- Zigmond E, Samia-Grinberg S, Pasmanik-Chor M, Brazowski E, Shibolet O, Halpern Z & Varol C (2014) Infiltrating Monocyte-Derived Macrophages and Resident Kupffer Cells Display Different Ontogeny and Functions in Acute Liver Injury. *The Journal of Immunology* 193: 344–353

Zitvogel L, Galluzzi L, Smyth MJ & Kroemer G (2013) Mechanism of Action of Conventional and Targeted Anticancer Therapies: Reinstating Immunosurveillance. *Immunity* 39: 74–88

Zomer A, Maynard C, Verweij FJ, Kamermans A, Schäfer R, Beerling E, Schiffelers RM, de Wit E, Berenguer J, Ellenbroek SIJ, *et al* (2015) In Vivo Imaging Reveals Extracellular Vesicle-Mediated Phenocopying of Metastatic Behavior. *Cell* 161: 1046–1057

T. Kerst